On 4-Dimensional Point Groups and on Realization Spaces of Polytopes

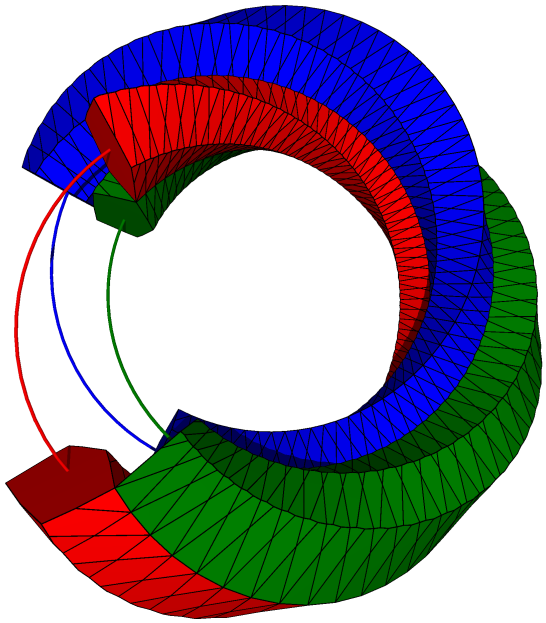

Dissertation zur Erlangung des Grades
eines Doktors der Naturwissenschaften (Dr. rer. nat.)
am Fachbereich Mathematik und Informatik
der Freien Universität Berlin

von

Laith Rastanawi

Berlin
May 2022

Supervisors:
Prof. Dr. Günter Rote
Prof. Dr. Rainer Sinn

Reviewers:
Prof. Dr. Günter Rote
Prof. Dr. Rainer Sinn
Prof. Dr. Jürgen Richter-Gebert

Day of thesis defense:
October 14, 2022

Acknowledgements

My sincere thanks go to

- my supervisor, **Günter Rote**, for his continuous support and guidance through all these years, for always finding time for my questions, and for his insightful comments and suggestions.
- my supervisor, **Rainer Sinn**, for all the interesting mathematical discussions, for his support and encouragement, and for offering directions to go further.
- **Günter M. Ziegler**, for introducing me to the world of polytopes, and for finding time for discussions.
- **Jürgen Richter-Gebert**, for spending time in reviewing this thesis.
- **Facets of Complexity**, for funding me during my doctoral studies, and to **Freie Universität Berlin**, for offering the outstanding environment for study and research.
- **people of the Villa**, for the nice time. Specially, **Jonathan Kliem** and **Jean-Philippe Labbé**.
- **my family and friends**, for their endless support and encouragement.
- my epsilon (**Janna**) and her mother (**Ahed**), for being in my life. This work is dedicated for you both.

Contents

List of Tables

Summary and Introduction

This dissertation consists of two parts. We highlight the main results from each part.

Part I. 4-Dimensional Point Groups.

(This part is based on a joint work with Günter Rote [55].)

We propose the following classification for the finite groups of orthogonal transformations in 4-space, the so-called 4-dimensional point groups.

Theorem A. The 4-dimensional point groups can be classified into

- 25 polyhedral groups (Table 5.1),
- 21 axial groups (7 pyramidal groups, 7 prismatic groups, and 7 hybrid groups, Table 6.3),
- 22 one-parameter families of tubical groups (11 left tubical groups and 11 right tubical groups, Table 3.1), and
- 25 infinite families of toroidal groups (Table 4.3), among them
  - 2 three-parameter families,
  - 19 two-parameter families, and
  - 4 one-parameter families.

In contrast to earlier classifications of these groups (notably by Du Val in 1962 [23] and by Conway and Smith in 2003 [14]), see Section 1.7), we emphasize a geometric viewpoint, trying to visualize and understand actions of these groups. Besides, we correct some omissions, duplications, and mistakes in these classifications.

Overview of the groups. The 25 *polyhedral* groups (Chapter 5) are related to the regular polytopes. The symmetries of the regular polytopes are well understood, because they are generated by reflections, and the classification of such groups as Coxeter groups is classic. We will deal with these groups only briefly, dwelling a little on just a few groups that come in enantiomorphic pairs (i.e., groups that are not equal to their own mirror.)

The 21 *axial* groups (Chapter 6) are those that keep one axis fixed. Thus, they essentially operate in the three dimensions perpendicular to this axis (possibly combined with a flip of the axis), and they are easy to handle, based on the well-known classification of the three-dimensional point groups.

The *tubical* groups (Chapter 3) are characterized as those that have (exactly) one Hopf bundle invariant. They come in left and right versions (which are mirrors of each other) depending on the Hopf bundle they keep invariant. They are so named because they arise with a decomposition of the 3-sphere into tube-like structures (discrete Hopf fibrations).

The *toroidal* groups (Chapter 4) are characterized as having an invariant torus. This class of groups is where our main contribution in terms of the completeness of the classification lies. We propose a new, geometric, classification of these groups. Essentially, it boils down to classifying the isometry groups of the two-dimensional square flat torus.

We emphasize that, regarding the completeness of the classification, in particular concerning the polyhedral and tubical groups, we rely on the classic approach (see Section 1.6). Only for the toroidal and axial groups, we supplant the classic approach by our geometric approach.

Hopf fibrations. We give a self-contained presentation of Hopf fibrations (Chapter 2). In many places in the literature, one particular Hopf map is introduced as "the Hopf map", either in terms of four real coordinates or two complex coordinates, leading to "the Hopf fibration". In some sense, this is justified, as all Hopf bundles are (mirror-)congruent. However, for our characterization, we require the full generality of Hopf bundles. As a tool for working with Hopf fibrations, we introduce a parameterization for great circles in S^3, which might be useful elsewhere.

Orbit polytope. Our main tool to understand tubical groups are polar orbit polytopes. (Chapter 1). In particular, we study the symmetries of a cell of the polar orbit polytope for different starting points.

Part II. Realization Spaces of Polytopes.

(This part is based on a joint work with Rainer Sinn and Günter M. Ziegler [56].)

Robertson in 1988 [59] suggested a model for the realization space of a d-dimensional polytope P, and an approach via the implicit function theorem to prove that the realization space is a smooth manifold of dimension $\mathrm{NG}(P) := d(f_0 + f_{d-1}) - f_{0,d-1}$. We call $\mathrm{NG}(P)$ the natural guess for (the dimension of the realization space of) P.

Combinatorial criteria. We build on Robertson's model and approach to study the realization spaces of higher-dimensional polytopes. We conclude combinatorial criteria (Sections 9.3.3 and 9.4.1) to decide if the realization space of the polytope in consideration is a smooth manifold of dimension given by the natural guess. As another application, we study the realization spaces of the second hypersimplices (Section 9.4.2).

Counter-examples. We apply these criteria on 4-polytopes with small number of vertices, and along the way, we analyze examples where Robertson's approach fails, identifying the three smallest examples of 4-polytopes, for which the realization space is still a smooth manifold, but its dimension is not given by the natural guess (Section 9.5).

The 24-cell. Finally, we investigate the realization space of the 24-cell (Section 9.5.2). We construct families of realizations of the 24-cell, and using them we show that the realization space of the 24-cell has points where it is not a smooth manifold. This provides the first known example of a polytope whose realization space is not a smooth manifold. We conclude by showing that the dimension of the realization space of the 24-cell is at least 48 and at most 52.

Part I.

4-Dimensional Point Groups

1 Orbit polytopes and point groups

1.1. Geometric understanding through orbit polytopes

A *d-dimensional point group* is a finite group of orthogonal transformations in $\mathbb{R}^d$, or in other words, a finite subgroup of $\mathrm{O}(d)$. One can try to visualize a point group $G \leqslant \mathrm{O}(d)$ by looking at the orbit of some point $0 \neq v \in \mathbb{R}^d$ and taking the convex hull. This is called the *G-orbit polytope* of v. For an in-depth study of orbit polytopes and their symmetries, refer to [26, 27].

The orbit polytope will usually depend on the choice of v, and it may have other symmetries in addition to those of G. For example, the C_n-orbit polytope in the plane is always a regular n-gon, and this orbit polytope has the larger dihedral group D_{2n} as its symmetry group.

We will illustrate the usefulness of orbit polytopes with a three-dimensional example. The pyritohedral group is perhaps the most interesting among the point groups in 3 dimensions. It is generated by a cyclic rotation of the coordinates $(x_1, x_2, x_3) \mapsto (x_2, x_3, x_1)$ and by the coordinate reflection $(x_1, x_2, x_3) \mapsto (-x_1, x_2, x_3)$. It has order 24. Figure 1.1 shows a few examples of orbit polytopes for this group, and their polars. The elements of the pyritohedral group are simultaneously symmetries of the octahedron (where it is an index-2 subgroup of the full symmetry group) and the icosahedron (an index-5 subgroup), and of course of their polars, the cube and the dodecahedron. The group contains reflections, but it is not generated by its reflections.

The orbit of the points $(1, 0, 0)$ and $(1, 1, 1)$ generate the regular octahedron and the cube, respectively. These are each other's polars, but they don't give any specific information about the pyritohedral group.

Figure 1.1a shows the orbit polytope (in yellow) of a generic point $(\frac{2}{3}, \frac{1}{2}, 1)$, and its polar (in orange). The symmetries of these polytopes are exactly the pyritohedral group. That orbit polytope has 6 rectangular faces (lying in planes of the faces of a cube), 8 equilateral triangles (lying in the faces of an octahedron), and 12 trapezoids (going through the edges of some cube, but not of some regular octahedron). The polar has 24 quadrilateral faces, corresponding to the 24 group elements. For any pair of faces, there is a unique symmetry of the polytope that maps one face to the other.[1]

If we choose one coordinate of the starting point to be 0, the rectangles shrink to line segments, and the trapezoids become isosceles triangles. See Figure 1.1b. The orbit polytope is an icosahedron with 20 triangular faces: 8 equilateral triangles and 12 isosceles triangles. The polar polytope is a *pyritohedron*, that is, a dodecahedron with 12 equal but not necessarily regular pentagons. For this choice, the orbit contains only 12 points, but the polytope gains no additional symmetries beyond the pyritohedral symmetries. However, for $(0, \frac{\sqrt{5}-1}{2}, 1)$, we get the regular icosahedron and the regular dodecahedron. For the specific choice $(0, \frac{1}{2}, 1)$, the polar orbit polytope is one of the crystal forms of the mineral pyrite, which gave the polytope and group its name, see Figure 1.1b. This polytope is also an *alternahedron* on 4 symbols [20]. An alternahedron can be constructed as the orbit of a generic point $(x_1, x_2, x_3, x_4) \in \mathbb{R}^4$ under all even permutations. Since

[1] In mineralogy, this shape is sometimes called a *diploid*, and *diploidal symmetry* is an alternative name for pyritohedral symmetry. In our context, the term diploid will show up in a different sense.

the points lie in a hyperplane $x_1 + x_2 + x_3 + x_4 = \text{const}$, this is a three-dimensional polytope. For the starting point $(0, 1, 2)$, we obtain the alternahedron that results from the canonical choice $(x_1, x_2, x_3, x_4) = (1, 2, 3, 4)$, a scaled copy of Figure 1.1b.[2]

The pyritohedral group differs from the symmetries of the cube (or the octahedron) by allowing only even permutations of the coordinates x_1, x_2, x_3. When two coordinates are equal, this distinction plays no role, and the resulting polyhedron will have all symmetries of the cube, see Figure 1.1f. (We mention that some special starting points of this form lead to Archimedean polytopes: The starting point $(1, 1, \sqrt{2} + 1)$ generates a rhombicuboctahedron with 8 regular triangles and 18 squares; $(0, 1, 1)$ generates the cuboctahedron with 8 regular triangles and 6 squares; with $(\frac{1}{\sqrt{2}+1}, 1, 1)$, we get the truncated cube with 8 regular triangles and 8 regular octagons, similar to the yellow polytope in Figure 1.1f.)

For the purpose of visualizing the pyritohedral group, we will try to keep the three coordinates distinct. By choosing the point close to $(1, 1, 1)$ or $(0, 0, 1)$, we can emphasize the cube-like or the octahedron-like appearance of the orbit polytope or its polar. For example, the polar orbit polytope for $(0, \frac{1}{10}, 1)$ resembles a cube whose squares are subdivided into rectangles, like the orange polytope in Figure 1.1c. (Actually, the mineral pyrite has sometimes a cubic crystal form in which the faces carry parallel thin grooves, so-called *striations*.[3]) See also Figure 1.1d for $(\frac{2}{10}, \frac{1}{10}, 1)$. The orbit polytope in Figure 1.1c appears like an octahedron whose edges have been shaved off, but in an asymmetric way that provides a direction for the edges (see Figure 5.4a on p. 83 in Section 5.6).

On the other hand, the polar orbit polytope for $(\frac{8}{10}, \frac{9}{10}, 1)$ resembles an octahedron, carrying a pinwheel-like structure on every face. See Figure 1.1e.

1.1.1. The pyritohedral group for flatlanders

We will be in the situation that we try to visualize 4-dimensional point groups through orbit polytopes or their polars. So let us go one dimension lower and imagine that we, as ordinary three-dimensional people, would like to explain the pyritohedral group to flatlanders. We will see that different options have different merits, and there may be no unique best way of visualizing a group.

Assuming that flatlanders accept the notions of a cube or an octahedron, we could tell them that we build a cube whose squares are striped in such a way that the patterns on adjacent squares never abut, similar to the orange polytope in Figure 1.1c. It is allowed to map any square to any other square (6 possibilities) in such a way that the stripes match (the dihedral group D_4 with 4 possibilities, for a total of 24 transformations).

Alternatively, we could tell them that the edges of an octahedron are oriented such that each triangle forms a directed cycle (Figure 5.4a on p. 83). It is allowed to map any triangle to any other triangle (8 possibilities) in such a way that edge directions are preserved (the cyclic group C_3 with 3 possibilities, for a total of 24 transformations).

Another option is the polar of $(c, 1, 1)$, where $c \notin \{0, 1\}$, see the orange polytope in Figure 1.1f. It has 24 isosceles triangles, one per group element, As c approaches 1 or 0, the polar orbit polytope converges to an octahedron or to a rhombic dodecahedron. As a shape, the triangle does not reveal much about the group, so we have to add the information that the base edge acts as a mirror, and the opposite vertex is a 3-fold *gyration point*, i.e., there are three rotated copies that fit together. (This is essentially what is expressed in the orbifold notation 3∗2.) We are not allowed to use the reflection

[2] The illustration of this polytope in [20, Fig. 1] may make the wrong impression of consisting of equilateral triangles only. However, its isosceles faces have base length 2 and two equal legs of length $\sqrt{6} \approx 2.45$.

[3] See http://www.mineralogische-sammlungen.de/Pyrit-gestreift-engl.html

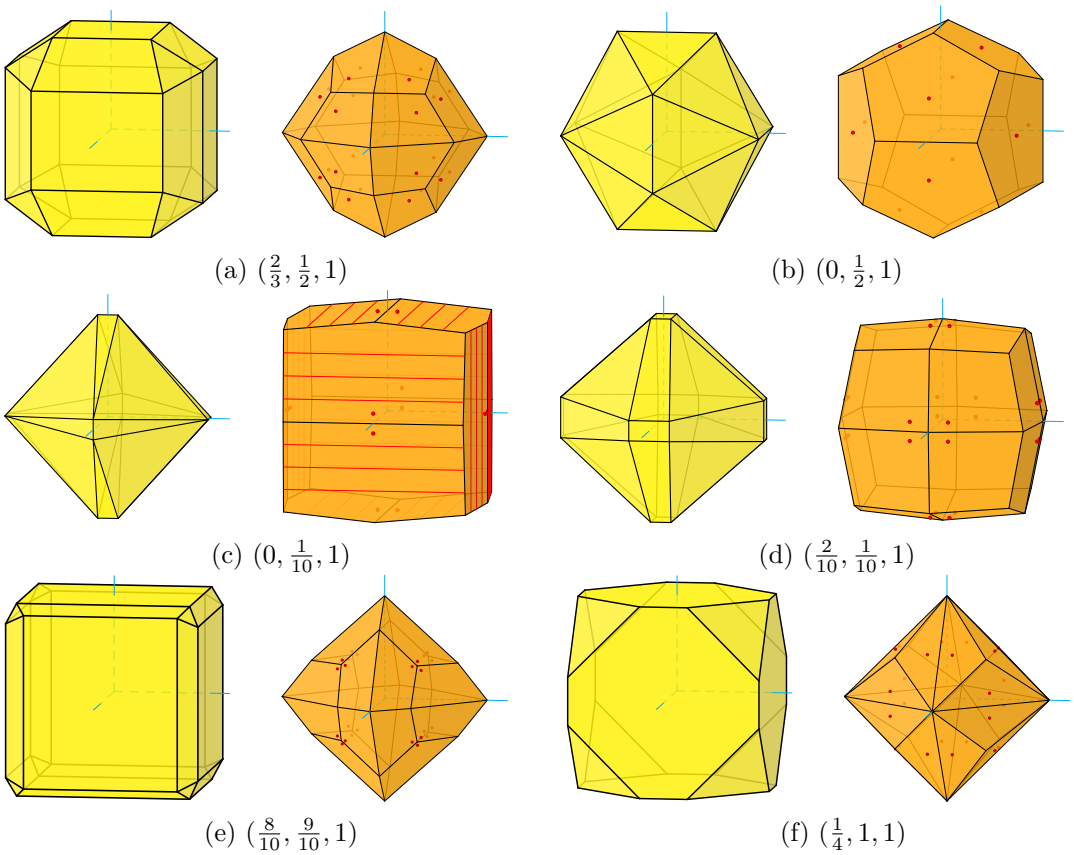

(a) $(\frac{2}{3}, \frac{1}{2}, 1)$ (b) $(0, \frac{1}{2}, 1)$

(c) $(0, \frac{1}{10}, 1)$ (d) $(\frac{2}{10}, \frac{1}{10}, 1)$

(e) $(\frac{8}{10}, \frac{9}{10}, 1)$ (f) $(\frac{1}{4}, 1, 1)$

Figure 1.1.: Orbit polytopes of the pyritohedral group (yellow, on the left) and their polar polytopes (orange, on the right) for various starting points. The pictures are rescaled to uniform size; the scale is not maintained between the pictures.

that maps the triangle to itself, and we might indicate this by placing an arrow along the base edge.

In most cases, it was advantageous to describe the group in terms of the polar orbit polytope: We have many copies of one shape, and any shape can be mapped to any other. It is not necessarily the best option to insist that all points of the orbit are distinct. Sometimes it is preferable to allow also symmetries within each face. In this case, the information, which of these symmetries are in the group must be conveyed as side information, for example by decorations or patterns that should be left invariant, such as the stripes in Figure 1.1c.

Figure 1.2 summarizes the relation between a polar orbit polytope and its group G. All cells are equal, and the cells correspond to the points of the orbit. We know that between any two cells, there is at least one transformation in G that carries one cell to the other. However, it is not directly apparent *which* transformations carry one cell to another cell, or to itself. If all symmetries of a cell belong to the group, the answer is clear; otherwise we have to discuss this question and describe the answer separately.

The bottom row of Figure 1.2 splits this question into two subproblems that are relevant only for tubical groups (Chapter 3), namely the relation between adjacent cells in a tube, and between cells of different tubes.

1.1.2. Polar orbit polytopes and Voronoi diagrams

There is a well-known connection between polar orbit polytopes and spherical Voronoi diagrams, or more generally, between polytopes whose facets are tangent to a sphere and spherical Voronoi diagrams: The central projection of the polytope to the sphere

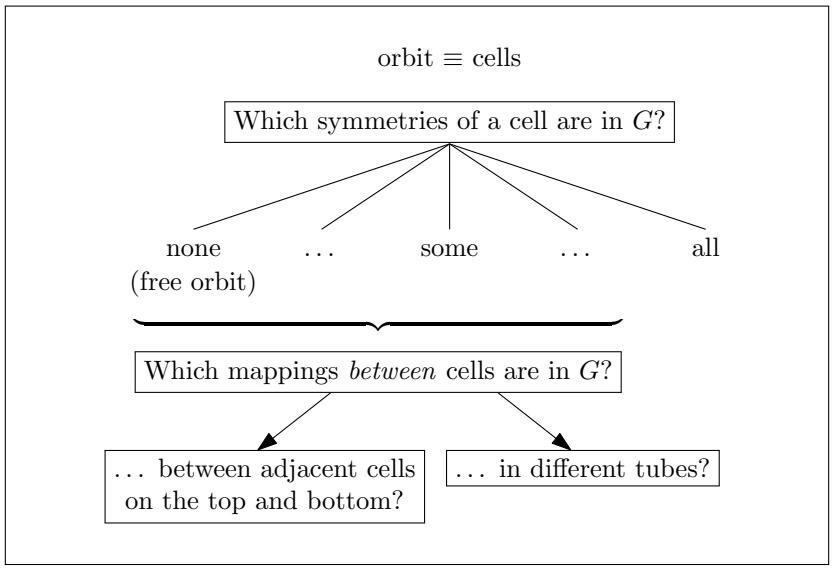

Figure 1.2.: Geometric understanding of a group G through is polar orbit polytope

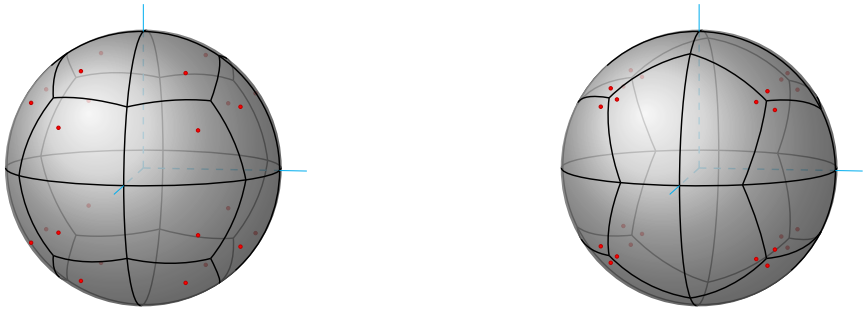

Figure 1.3.: Spherical Voronoi diagrams of the orbits in Figure 1.1a and Figure 1.1e.

gives the spherical Voronoi diagram of the tangency points (the orbit points). Figure 1.3 shows spherical Voronoi diagrams for two orbits of Figure 1.1.

Thus, when we look at polar orbit polytopes, we may think about partitioning the sphere according to the closest point from the orbit. The orbit polytope and the spherical Voronoi diagram have the same combinatorial structure, but the faces of the orbit polytope are true Euclidean polytopes, whereas the faces of the Voronoi diagram are spherical polytopes. The closer the orbit points are together, the smaller the distortion will be, and the more the orbit polytope will represent the true metric situation of the Voronoi diagram.

In our illustrations of 4-dimensional groups, we will prefer to show orbit polytopes, because these are easier to compute.

1.2. Fundamental domains and orbifolds

For comparison, we mention another way to characterize geometric groups, namely by showing a fundamental domain of the group, possibly extended by additional information that characterizes the type of rotations that fix an edge, such as in an orbifold. This is particularly appropriate for Coxeter groups, which are generated by reflections and for which the choice of fundamental domain is canonical.

Dunbar [24] studied orientation-preserving 4-dimensional point groups. He constructed fundamental domains for 10 out of the 14 orientation-preserving polyhedral groups (omitting $\pm[I \times T]$ and $\pm[I \times O]$ and their mirrors). For each of the 21 orientation-preserving

polyhedral and axial groups, he showed the structure of the singular set (fixpoints of some group elements) of the corresponding orbifold, which is a 3-valent graph where each edge is labeled with the order of the rotational symmetry around the edge.[4]

The fundamental domain, possibly enriched by additional information, is a concise way for representing some groups, but it does not have the immediate visual appeal of polar orbit polytopes. For example, the fundamental domain of every Coxeter group is a simplex, and the distinctions between different groups lies only in the dihedral angles at the edges.

1.3. Left or right orientation of projected images: view from outside

We will illustrate many situations in 4-space by three-dimensional graphics that are derived through projection. Just as a plane in space has no preferred orientation, a 3-dimensional hyperplane in 4-space has no intrinsic orientation. It depends on from which side we look at it. Hence, it is important to establish a convention about the orientation, in order to distinguish a situation from its mirror image.

Let us look at plane images of the familiar three-dimensional space "for orientation" in this matter. For a polytope or a sphere, we follow the convention that we want to look at it *from outside*, as for a map of some part of the Earth. Accordingly, when we interpret a plane picture with an x_1, x_2-coordinate system (with x_2 counterclockwise from x_1), the usual convention is to think of the third coordinate x_3 as the "vertical upward" direction that is facing us, leading to a right-handed coordinate system x_1, x_2, x_3.

Similarly, when we deal with a 4-polytope and want to show a picture of one of its facets, which is a three-dimensional polytope F, we use a right-handed orthonormal x_1, x_2, x_3-coordinate system in the space of F that can be extended to a positively oriented coordinate system x_1, x_2, x_3, x_4 of 4-space such that x_4 points outward from the 4-polytope.

We use the same convention when drawing a cluster of adjacent facets, or when illustrating situations in the 3-sphere, either through central projection or through parallel projection. For example, a small region in the 3-sphere can be visualized as 3-space, with some distortion, and we will be careful to ensure that this corresponds to a view on the sphere "from outside".

There are other contexts that favor the opposite convention. For example, stereographic projection is often done from the North Pole $(x_1, x_2, x_3, x_4) = (0, 0, 0, 1)$ of S^3, and this yields a view "from inside" in the (x_1, x_2, x_3)-hyperplane. See for example [67, §7], or also [24, p. 123] for a different ordering of the coordinates with the same effect.

1.4. Point groups

The 2-dimensional point groups are the cyclic groups C_n and the dihedral groups D_{2n}, for $n \geq 1$. For $n \geq 3$, they can be visualized, respectively, as the n rotations of the regular n-gon, and the $2n$ symmetries (rotations and reflections) of the regular n-gon. See Figure 1.4.

The 3-dimensional point groups are well-studied (see Section 1.10 below). In one sentence, they can be characterized as the symmetry groups of the five Platonic solids and of the regular n-side prisms, and their subgroups. This gives a frame for classifying these groups, but it does not give the full information. It remains to work out what

[4] In the list of orientation-reversing polyhedral groups that are Coxeter groups [24, Figure 17], the 6th and 8th entries, which are the Coxeter-Dynkin diagrams for the orientation-reversing extensions of $T \times_{C_3} T$ and $J \times_J^* J^1$, must be exchanged.

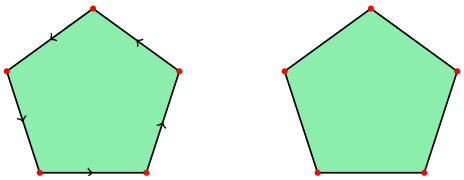

Figure 1.4.: The group C_5 consisting of the rotational symmetries of the regular pentagon, and the group D_{10} of all symmetries of the regular pentagon.

the subgroups are, and moreover, there are duplications, for example: certain Platonic solids are polar to each other; the vertices of the cube are contained in the vertices of an icosahedron; and in turn, they contain the vertices of a tetrahedron; a cube is a special quadrilateral prism.

1.5. The 4-dimensional orthogonal transformations

1.5.1. Orientation-preserving transformations

We call a 4-dimensional orientation-preserving transformation a *rotation*. In some appropriate basis with coordinates x_1, x_2, x_3, x_4, every rotation has the form

$$R_{\alpha_1,\alpha_2} = \begin{pmatrix} \cos\alpha_1 & -\sin\alpha_1 & 0 & 0 \\ \sin\alpha_1 & \cos\alpha_1 & 0 & 0 \\ 0 & 0 & \cos\alpha_2 & -\sin\alpha_2 \\ 0 & 0 & \sin\alpha_2 & \cos\alpha_2 \end{pmatrix} = \begin{pmatrix} R_{\alpha_1} & 0 \\ 0 & R_{\alpha_2} \end{pmatrix} = \operatorname{diag}(R_{\alpha_1}, R_{\alpha_2}) \tag{1.1}$$

in block form, using the rotation matrices $R_\alpha = \left(\begin{smallmatrix} \cos\alpha & -\sin\alpha \\ \sin\alpha & \cos\alpha \end{smallmatrix}\right)$ as building blocks [16, §12.1]. If $\alpha_2 = 0$, we have a *simple rotation*: a rotation in the x_1x_2-plane by the angle α_1, leaving the complementary x_3x_4-plane fixed. Thus, the general rotation is the product of two simple rotations in two orthogonal planes, and we call it more specifically a *double rotation*. If $\alpha_2 \neq \pm\alpha_1$ then the two planes are uniquely determined. Each plane is an *invariant plane*: as a set, it is fixed by the operation.

If $\alpha_1 = \alpha_2 = \pi$, the matrix is the negative identity matrix, and we have the *central inversion* or *antipodal map*, which we denote by $-\mathrm{id}$. In $\mathbb{R}^4$, this is an orientation-preserving transformation.

1.5.2. Absolutely orthogonal planes and circles

When we speak of orthogonal planes in 4-space, we always mean "absolutely" orthogonal, in the sense that every vector in one plane is orthogonal to every vector in the other plane.

We will mostly study the situation on the sphere. Here, an invariant plane becomes an *invariant great circle*, and there are *absolutely orthogonal great circles*.

1.5.3. Left and right rotations

The rotations with $\alpha_2 = \pm\alpha_1$ play a special role: Every point is moved by the same angle $|\alpha_1|$, and there is no unique pair of invariant planes. The rotations with $\alpha_2 = \alpha_1$ are *left rotations*, and the rotations with $\alpha_2 = -\alpha_1$ are *right rotations*. It is easy to see that every rotation R_{α_1,α_2} is the product of a left and a right rotation (with angles $(\alpha_1 \pm \alpha_2)/2$). This representation is unique, up to a multiplication of both factors with $-\mathrm{id}$. Left rotations commute with right rotations. These facts are not straightforward,

but they follow easily from the quaternion representation that is discussed below. The product of a left rotation by β_L and a right rotation by β_R is a rotation $R_{\beta_L+\beta_R,\beta_L-\beta_R}$.

1.5.4. Orientation-reversing transformations

An orientation-reversing transformation has the following form, in some appropriate basis with coordinates x_1, x_2, x_3, x_4:

$$\bar{R}_\alpha = \begin{pmatrix} \cos\alpha & -\sin\alpha & 0 & 0 \\ \sin\alpha & \cos\alpha & 0 & 0 \\ 0 & 0 & -1 & 0 \\ 0 & 0 & 0 & 1 \end{pmatrix} = \operatorname{diag}(R_\alpha, -1, 1) \tag{1.2}$$

It operates in some three-dimensional subspace x_1, x_2, x_3 and leaves one axis x_4 fixed. The x_3-axis is inverted. For $\alpha = 0$, we have a mirror reflection in a hyperplane, $\bar{R}_0 = \operatorname{diag}(1, 1, -1, 1)$. For $\alpha = \pi$, we have $\bar{R}_\pi = \operatorname{diag}(-1, -1, -1, 1)$, which could be interpreted as a reflection in the x_4-axis. In general, we have a rotary-reflection, which has two unique invariant planes: In one plane, it acts as a rotation by α; in the other plane, it has two opposite fixpoints in S^3, and two other opposite points that are swapped. The square of an orientation-reversing transformation $\bar{R}_\alpha$ is always a simple rotation.

1.5.5. Quaternion representation

The quaternions $x_1 + x_2 i + x_3 j + x_4 k$ are naturally identified with the vectors $x = (x_1, x_2, x_3, x_4) \in \mathbb{R}^4$. We identify the set of unit quaternions with S^3, the 3-sphere, and the set of pure unit quaternions $v_1 i + v_2 j + v_3 k$ with the points (v_1, v_2, v_3) on S^2, the 2-sphere.

Every 4-dimensional rotation can be represented by a pair $[l, r]$ of unit quaternions $l, r \in S^3$. See [14, §4.1]. The pair $[l, r]$ operates on the vectors $x \in \mathbb{R}^4$, treated as quaternions, by the rule

$$[l, r] \colon x \mapsto \bar{l} x r.$$

The representation of rotations by quaternion pairs is unique except that $[l, r] = [-l, -r]$. The rotations $[l, 1]$ are the *left rotations*, and the rotations $[1, r]$ are the *right rotations*: They correspond to quaternion multiplication from the left and from the right. A left or right rotation moves every point by the same angular distance α. In fact, as we shall see (Proportion 2.2.7(ii)), a left or right rotation by an angle α other than 0 or π defines a *Hopf bundle*, a decomposition of the 3-sphere S^3 into circles, each of which is rotated in itself by α. As transformations on S^3, they operate as left screws and right screws, respectively. See Section 2.2.1.

We compose transformations by writing them from left to right, i.e. $[l_1, r_1][l_2, r_2]$ denotes the effect of first applying $[l_1, r_1]$ and then $[l_2, r_2]$.[5] Accordingly, composition can be carried out as componentwise quaternion multiplication: $[l_1, r_1][l_2, r_2] = [l_1 l_2, r_1 r_2]$.

Every orientation-reversing transformation can be represented as

$$*[l, r] \colon x \mapsto \bar{l} \bar{x} r.$$

See [14, §4.1]. The stand-alone symbol $*$ is alternate notation for quaternion conjugation $*[1, 1] \colon x \mapsto \bar{x}$. Then $*[a, b]$ can be interpreted as a composition of the operations $*$ and $[a, b]$. Geometrically, the transformation $*$ maps (x_1, x_2, x_3, x_4) to $(x_1, -x_2, -x_3, -x_4)$, and it is a reflection in the x_1-axis. The transformation $-*$ maps (x_1, x_2, x_3, x_4) to $(-x_1, x_2, x_3, x_4)$, and it is a reflection in the hyperplane $x_1 = 0$.

[5] Du Val [23] used the opposite convention, and accordingly his notation $[l, r]$ denotes the map $x \mapsto l x \bar{r}$.

The inverse transformations are given by these formulas:

$$[l,r]^{-1} = [\bar{l},\bar{r}]$$
$$(*[l,r])^{-1} = *[\bar{r},\bar{l}] = [\bar{l},\bar{r}]* \tag{1.3}$$

The last equation in (1.3) is also interesting: We may put the $*$ operation on the other side of a transformation $[l,r]$ after swapping the components l and r.

For $l = r$, it is easy to see that $[l,l]$ maps the point 1 to itself, and thus operates only on the pure quaternion part. Thus, the pairs $[l,l]$ act as 3-dimensional rotations. For $l = \cos\alpha + \sin\alpha(ui + vj + wk)$, $[l,l]$ performs a rotation by 2α around the axis with unit vector $(u,v,w) \in \mathbb{R}^3$. We will denote $[l,l]$ by $[l]\colon x \mapsto \bar{l}xl$. When viewed as an operation on the unit sphere S^2, $[l]$ is a *clockwise* rotation by 2α around the point (u,v,w).[6] Note that, when the quaternion l is used as a left rotation $[l,1]$ or a right rotation $[1,l]$ in 4-space, every point is rotated only by α, not by 2α.

1.6. The classic approach to the classification

For a finite subgroup $G \leqslant \mathrm{SO}(4)$, we can consider the group

$$A = \{\, (l,r) \in S^3 \times S^3 \mid [l,r] \in G \,\},$$

which is a two-fold cover of G, as each rotation $[l,r] \in G$ is represented by two quaternion pairs (l,r) and $(-l,-r)$ in A. The elements l and r of these pairs form the *left and the right group* of G:

$$L := \{\, l \mid (l,r) \in A \,\}, \quad R := \{\, r \mid (l,r) \in A \,\}$$

These are finite groups of quaternions.

Proposition 1.6.1. *There is a one-to-one correspondence between*

1. *The finite subgroups G of* $\mathrm{SO}(4)$
2. *The subgroups A of $L \times R$ that contain the element $(-1,-1)$, where L and R are finite groups of unit quaternions.*

Since there are only five possibilities for finite groups of unit quaternions (including two infinite families, see Section 1.11), this makes it easy, in principle, to determine the finite subgroups of SO(4).

One task of this program, the enumeration of the subgroups A of a direct product $L \times R$ is guided by Goursat's Lemma, which was established by Goursat [30] in this very context: The groups

$$L_0 := \{\, l \mid (l,1) \in A \,\}, \quad R_0 := \{\, r \mid (1,r) \in A \,\}$$

form normal subgroups of L and R, which we call the *left and right kernel* of G. The group A, and hence G, is determined by L, R, L_0, R_0 and an isomorphism $\Phi : L/L_0 \to R/R_0$ between the factor groups:

$$G = \{\, [l,r] \in \mathrm{SO}(4) \mid l \in L,\ r \in R,\ \Phi(lL_0) = rR_0 \,\}$$

[6] Measuring the rotation angle clockwise is opposite to the usual convention of regarding the counterclockwise direction as the mathematically positive direction. This is a consequence of writing the operation $[l]$ as $x \mapsto \bar{l}xl$ (as opposed to the alternative $x \mapsto lx\bar{l}$, which was chosen, for example, by Du Val [23]) and regarding the quaternion axes i, j, k as a right-handed coordinate frame of 3-space, see [18, Exercise 6.4 on p. 67, answer on pp. 189–190].

The task reduces to the enumeration of all possibilities for the components L, R, L_0, R_0, Φ, and to the less trivial task of determining which parameters lead to geometrically equal groups.

This approach underlies all classifications so far, and we call it the *classic* classification.

1.7. Previous classifications

- Goursat [30], in 1889, classified the finite groups of motions of *elliptic 3-space*. Elliptic 3-space can be interpreted as the 3-sphere S^3 in which antipodal points are identified. Hence, these groups can be equivalently described as those groups in O(4) that contain the central inversion $-\mathrm{id}$ (the so-called diploid groups, see Section 1.12).

- Threlfall and Seifert [67, 68], in a series of two papers in 1931 and 1933, extended this to the groups of Euclidean space, but they only concentrated on the chiral groups, i.e., the groups of SO(4). Their goal was to study the quotient spaces of the 3-sphere under fixpoint-free group actions, because these lead to *space forms*, spaces of constant curvature without singularities.[7]

- Hurley [37], in 1951, independently of Threlfall and Seifert, built on Goursat's classification and extended it to O(4). However, he considered only the crystallographic groups, see Appendix D.

- Du Val [23], independently of Hurley, in a small monograph from 1964, took up Goursat's classification and extended it to all groups. From a geometric viewpoint, he extensively discussed the symmetries of the 4-dimensional regular polytopes.

- Conway and Smith [14] in a monograph from 2003, took up the classification task again, correcting some omissions and duplications of the previous classifications. They gave geometric descriptions for the polyhedral and axial groups in terms of Coxeter's notation.

1.7.1. Related work

- De Medeiros and Figueroa-O'Farrill [22], in 2012, classified the groups of order pairs $(l, r) \in S^3 \times S^3$ of unit quaternions under componentwise multiplication (using Goursat's Lemma again). These form the 4-dimensional spin group Spin(4). Since this is a double cover of SO(4), the results should confirm the classification of the chiral point groups. Indeed, Tables 16–18 in [22, Appendix B] give references to SO(4) and the classification of [14].[8]

[7] The term "Diskontuinuitätsbereich" in the title of [67, 68] is used like a well-established concept that does not require a definition. In the contemporary literature, it means what we today call a fundamental domain. Seifert and Threlfall were in particular interested in its topological properties, referring by "Diskontuinuitätsbereich" to the quotient space under a group action, with a specification how the boundary faces of the fundamental domain are to be pairwise identified. Du Val [23, § 30] also takes this interpretation and calls it a *group-set space*, where *group-set* is his term for orbit.

In modern usage, "region of discontinuity" has other meanings, closer to the literal meaning of the words, where discontinuity plays a role.

[8] However, besides noticing a few typographical errors, we found some discrepancies in these tables: (i) The 6th entry in Table 18 lists a group $\pm[C_{2k+1} \times \bar{D}_{4m}]$. We cannot match this with anything in the Conway–Smith classification, even allowing for one typo. (ii) The last entry in Table 4.2 of [14] is $+\frac{1}{f}[C_{mf} \times C_{nf}]$. This group does not appear in the tables of [22]. We don't know whether these discrepancies arose in the translation from the classification in [22] to the notions of SO(4) or they indicate problems in the classification itself.

- Marina Maerchik, in 1976 [47], investigated the groups that are generated by reflections and simple rotations (also in higher dimensions), as reported in Lange and Mikhaîlova [42], (The term "pseudoreflections" in the title of [47] refers to simple rotations.)
- We mention that the approach of understanding the 4-dimensional groups through their orbits was pioneered by Robinson [60], who, in 1931, studied the orbits of the polyhedral groups. He focused on the orbits themselves and their convex hulls (and not on the polar orbit polytopes as we do).

1.8. Conjugacy, geometrically equal groups

Conjugation with a rotation $[a, b]$ transforms a group into a different group, which is geometrically the same, but expressed in a different coordinate system. Conjugation transforms an orientation-preserving transformation $[l, r]$ as follows:

$$[a, b]^{-1}[l, r][a, b] = [a^{-1}la, b^{-1}rb]$$

Its effect is thus a conjugation of the left group by a and an independent conjugation of the right group by b. As a conclusion, we can represent the left group L and the right group R in any convenient coordinate system of our choice, and it is no loss of generality to choose a particular representative for each finite group of quaternions. (Section 1.11 specifies the representatives that we use.)

1.9. Obtaining the achiral groups

The classic approach by Goursat's Lemma leads only to the chiral groups. Since the chiral part of an achiral group is an index-2 subgroup, every achiral group G is obtained by extending a chiral group H with some orientation-reversing element

$$e = *[a, b].$$

We will now derive some conditions on e, and possibly by modifying the group G into a geometrically conjugate group, constrain e to a finite number of possibilities.

Let H be a chiral group with left group L and right group R. For each $[l, r] \in H$, we must have $e^{-1}[l, r]e \in H$, i.e., H is normalized by e:

$$e^{-1}[l, r]e = *[\bar{b}, \bar{a}][l, r]*[a, b] = [\bar{a}ra, \bar{b}lb] \in H$$

This means that $\bar{a}ra \in L$ and $\bar{b}lb \in R$ for every $[l, r] \in H$, which implies $\bar{a}Ra = L$ and $\bar{b}Lb = R$, i.e., L and R are conjugate.

We conjugate G with $[1, a]$, transforming G to some geometrically equivalent group G' with left group L' and right group R'. Let us see what happens to an arbitrary element $[l, r]$:

$$[1, \bar{a}][l, r][1, a] = [l, \bar{a}ra] \tag{1.4}$$

The set of values $\bar{a}ra$ forms the new right group $R' = \bar{a}Ra = L$, while the left group remains unchanged: $L' = L$. Thus, we have achieved $L' = R'$, i.e., the left and right groups are not just conjugate, but equal.

The extending element $e = *[a, b]$ is transformed as follows:

$$e' := [1, \bar{a}]*[a, b][1, a] = *[1, ba] = *[1, c] \tag{1.5}$$

Thus we have simultaneously achieved $e' = *[1, c]$. Moreover,

$$e'e' = *[1, c]*[1, c] = [c, c] \in H,$$

and thus, c must be an element of $L = R$.

Proposition 1.9.1. *W.l.o.g., we can assume $L = R$, and the extending element is of the form $e = *[1, c]$, with $c \in L$.*

This reduces the extending element to a finite number of possibilities. Conway and Smith [14, p. 51] have sketched some additional considerations, which allow to further restrict the extending element, sometimes at the cost of giving up the condition $L = R$, see Figure G.4 on p. 166.

Conjugation by $[a, a]$ changes the transformations as follows:

$$[a, a]^{-1}[l, r][a, a] = [a^{-1}la, a^{-1}ra]$$
$$[a, a]^{-1}*[l, r][a, a] = *[a^{-1}la, a^{-1}ra]$$

Its effect is thus a conjugation of the left and right group $L = R$ by a. As for the chiral groups, we can therefore choose any convenient representation of the left and right group L in Proposition 1.9.1.

1.10. Point groups in 3-space and their quaternion representation

Table 1.1 lists the three-dimensional point groups that we will use. We will refer to them by the notation of Conway and Smith [14], given in the first column. As alternate notations, we give the orbifold notation, the Hermann-Mauguin notation or international symbol [35], and the Coxeter notation, which we will revisit in Chapter 5.

the chiral groups					
CS	orbifold	I.T.	Coxeter name	order	orientation-preserving symmetries of ...
$+C_n$	**nn**	n	$[n]^+$	n	the n-sided pyramid $n \geq 1$)
$+D_{2n}$	**22n**	$n2$	$[2, n]^+$	$2n$	the n-sided prism ($n \geq 1$)
$+T$	**332**	23	$[3, 3]^+$	12	the tetrahedron
$+O$	**432**	432	$[3, 4]^+$	24	the octahedron / the cube
$+I$	**532**	532	$[3, 5]^+$	60	the icosahedron / the dodecahedron
achiral polyhedral groups					
CS	orbifold	I.T.	Coxeter name	order	description of the group
TO	$*$**332**	$\bar{4}3m$	$[3, 3]$	24	all symmetries of the tetrahedron
$\pm T$	**3**$*$**2**	$m\bar{3}$	$[3^+, 4]$ or $[^+3, 4]$	24	the pyritohedral group
$\pm O$	$*$**432**	$m\bar{3}m$	$[3, 4]$	48	all symmetries of the octahedron
$\pm I$	$*$**532**	$53m$	$[3, 5]$	120	all symmetries of the icosahedron

Table 1.1.: Some point groups in 3 dimensions

The table contains all polyhedral groups (3 chiral and 4 achiral ones): groups consisting of symmetries of regular polytopes. The groups that are not polyhedral (subgroups of the symmetry groups of regular prisms, related to the frieze groups) include, besides $+C_n$ and $+D_{2n}$, five additional classes of *achiral* groups, which are not listed here. In total, there are 14 types of three-dimensional point groups. Note that the subscript $2n$ in D_{2n} is always even; we follow the convention of using the *order* of the group, not the number of sides of the polygon or prism of which it is the symmetry group.

The notations $+I, \pm I$, etc. for the polyhedral groups are easy to remember. The one that requires some attention is the full symmetry group of the tetrahedron, which is

denoted by TO, as opposed to the pyritohedral group $\pm T$, which is obtained by extending $+T$ by the central reflection, and which we have discussed extensively in Section 1.1.

1.11. Finite groups of quaternions

The finite groups of quaternions are [14, Theorem 12]:

$$\begin{aligned} 2I &= \langle i_I, \omega \rangle & 2D_{2n} &= \langle e_n, j \rangle \\ 2O &= \langle i_O, \omega \rangle & 2C_n &= \langle e_n \rangle \\ 2T &= \langle i, \omega \rangle & 1C_n &= \langle e_{n/2} \rangle \quad (n \text{ odd}) \end{aligned}$$

The generators are defined in terms of the following quaternions, which we will use throughout:

$$\begin{aligned} \omega &= \tfrac{1}{2}(-1+i+j+k) && \text{(order 3)} \\ i_O &= \tfrac{1}{\sqrt{2}}(j+k) && \text{(order 4)} \\ i_I &= \tfrac{1}{2}(i+\tfrac{\sqrt{5}-1}{2}j+\tfrac{\sqrt{5}+1}{2}k) && \text{(order 4)} \\ e_n &= \cos\tfrac{\pi}{n} + i\sin\tfrac{\pi}{n} && \text{(order } 2n\text{)} \end{aligned} \tag{1.6}$$

We follow Conway and Smith's notation for these groups. For each group $+G < \mathrm{SO}(3)$ (see the upper part of Table 1.1), there is quaternion group $2G$ of twice the size, containing the quaternions $\pm l$ for which $[l]$ represents a rotation in $+G$. All these groups contain the quaternion -1. In addition, there are the odd cyclic groups $1C_n$, of order n. They cannot arise as left or right groups, because $(-1,-1)$ is always contained in A and hence the left and right groups contain the quaternion -1.

1.12. Notations for the 4-dimensional point groups, diploid and haploid groups

We use the notation by Conway and Smith [14] for 4-dimensional point groups G, except for the toroidal groups, where we will replace it with our own notation. If L and R are 3-dimensional orientation-preserving point groups, $\pm[L \times R]$ denotes full product group $\{\,[l,r] \mid (l,r) \in 2L \times 2R\,\}$, of order $2|L|\cdot|R|$. Note that the groups $2L$ and $2R$ that appear in the definition are quaternion groups, while the notation shows only the corresponding rotation groups $L, R \in \mathrm{SO}(3)$.

A group that contains the negation $-\mathrm{id} = [1,-1]$ is called a *diploid* group. A diploid index-f subgroup of $\pm[L \times R]$ is denoted by $\pm\frac{1}{f}[L \times R]$. It is defined by two normal subgroups of $2L$ and of $2R$ of index f. Different possibilities for the normal subgroups and for the isomorphism Φ are distinguished by various ornamentations of the notation, see Appendix G for some of these cases.

A *haploid* group, which does not contain the negation $-\mathrm{id}$, is denoted by $+\frac{1}{f}[L \times R]$, and it is an index-2 subgroup of the corresponding diploid group $\pm\frac{1}{f}[L \times R]$. Achiral groups are index-2 extensions of chiral groups, and they are also denoted by various decorations.

Du Val [23] writes the groups as $(\mathbf{L}/\mathbf{L_0};\mathbf{R}/\mathbf{R_0})$, where the boldface letters distinguish quaternion groups from the corresponding 3-dimensional rotation groups. Again, various ornamentations denote different cases of normal subgroups and the isomorphism Φ. Achiral extensions are denoted by a star. We will not work with this notation except for reference in our tables, and then we will omit the boldface font. In some cases, we had to adapt Du Val's names, see Table 6.3 and footnote 19 on p. 77.

2 Hopf fibrations

We give a self-contained presentation of Hopf fibrations. In many places in the literature, one particular Hopf map is introduced as "the Hopf map", either in terms of four real coordinates or two complex coordinates, leading to "the Hopf fibration". In some sense, this is justified, as all Hopf bundles are (mirror-)congruent. However, for our characterization, we need the full generality of Hopf bundles.

Our treatment was inspired by Lyons [46], but we did not see it anywhere in this generality. As a tool, we introduce a parameterization of the great circles in S^3, which might be useful elsewhere. We also define *oriented* Hopf bundles: families of consistently oriented great circles.

We summarize the main statements:

- The great circles in S^3 can be parameterized by pairs p, q of pure unit quaternions, or equivalently, by pairs of points $p, q \in S^2$ (Section 2.1). The choice of parameters is unique except that $K_p^q = K_{-p}^{-q}$. The twofold ambiguity of the parameters can be used to specify an orientation of the circles (Section 2.1.2).

- The great circles K_p^q with fixed q form a partition of S^3, which we call the *left Hopf bundle* $\mathcal{H}^q$. It naturally comes with a *left Hopf map* $h^q \colon S^3 \to S^2$, which maps all points of K_p^q to the point $p \in S^2$.

  This map provides a bijection between the circles of the left Hopf bundle $\mathcal{H}^q$ and the points on S^2.

  Similarly, the great circles K_p^q with fixed p form a *right Hopf bundle* $\mathcal{H}_p$, with a *right Hopf map* h_p, etc. In the following, we will mention only the left Hopf bundles, but all statements hold also with left and right reversed.

- Every great circle of S^3 belongs to a unique left Hopf bundle. In other words, the left Hopf bundles form a partition of the set of great circles of S^3.

- For every left Hopf bundle $\mathcal{H}^q$, there is a one-parameter family of right rotations that maps every circle in $\mathcal{H}^q$ to itself, rotating each circle by the same angle α.

  Conversely, a right rotation by an angle $\alpha \notin \{0, \pi\}$ rotates every point of S^3 by the same angle α, and the set of circles along which these rotations happen form a left Hopf bundle (Proposition 2.2.7).

- The following statements discuss the behavior of Hopf bundles under orthogonal transformations (Proposition 2.2.5):
  - Any left rotation leaves the left Hopf bundle $\mathcal{H}^q$ fixed, as a partition. It permutes the great circles of the bundle.
  - Any rotation maps the left Hopf bundle $\mathcal{H}^q$ to another left Hopf bundle. Any two left Hopf bundles are congruent (by some right rotation).
  - Left Hopf bundles and right Hopf bundles are mirrors of each other.

- The intersection of a left Hopf bundle and a right Hopf bundle consists of two absolutely orthogonal circles (Corollary 2.2.3).

- Any two great circles in the same Hopf bundle are Clifford-parallel (Proposition 2.2.8). This means that a point moving on one circle maintains a constant distance to the other circle.

2.1. Parameterizing the great circles in S^3

Definition 2.1.1. For any two pure unit quaternions $p, q \in S^2$, we define the following subset of unit quaternions:

$$K_p^q := \{\, x \in S^3 \mid [x]p = q \,\} \tag{2.1}$$

This can be interpreted as the set of rotations on S^2 that map p to q.

Proposition 2.1.2. *K_p^q has an alternative representation*

$$K_p^q = \{\, x \in S^3 \mid [p, q]x = x \,\}, \tag{2.2}$$

and it forms a great circle in S^3. Moreover, every great circle in S^3 can be represented in this way, and the choice of parameters $p, q \in S^2$ is unique except that $K_p^q = K_{-p}^{-q}$.

This gives a convenient parameterization of the great circles in S^3 (or equivalently, the planes in $\mathbb{R}^4$) by pairs of points on S^2, which might be useful in other contexts. For example, they might be used to define a notion of distance between great circles (or planes in $\mathbb{R}^4$). (Other distance measures are discussed in [41, 40] and [13]. The connection to these different distance notions remains to be explored.)

Before giving the proof, let us make a general remark about quaternions. Multiple meanings can be associated to a unit quaternion x: Besides treating it (i) as a point on S^3, we can regard it (ii) as a rotation $[x]$ of S^2, or (iii) as a left rotation $[x, 1]$ of S^3, or (iv) as a right rotation $[1, x]$ of S^3. Rather than fixing an opinion on what a quaternion really *is* (cf. [2, p. 298]), we capitalize on this ambiguity and freely switch between the definitions (2.1) and (2.2).

Proof of Proposition 2.1.2. The two expressions (2.1) and (2.2) are equivalent by a simple rearrangement of terms:

$$[x]p = q \iff \bar{x}px = q \iff px = xq \iff x = \bar{p}xq \iff x = [p, q]x$$

The expression (2.2) shows that K_p^q is the set of fixpoints of the rotation $[p, q]$. Since p and q are unit quaternions, the rotation $[p, q]$ is a simple rotation by 180° (a half-turn). Its set of fixpoints is a two-dimensional plane, or when restricted to unit quaternions, a great circle.

Conversely, if a great circle K is given and we want to determine p and q, we know that we are looking for a simple rotation by 180° whose set of fixpoints is K. This rotation is uniquely determined, and its quaternion representation $[p, q]$ is unique up to flipping both signs simultaneously. □

The effect of orthogonal transformations on great circles is expressed easily in our parameterization:

Proposition 2.1.3. *Let $p, q \in S^2$. Then for any $l, r \in S^3$,*

(i) $[l, r]K_p^q = K_{[l]p}^{[r]q}$.

(ii) $(*[l, r])K_p^q = K_{[l]q}^{[r]p}$, *and in particular,* $*K_p^q = K_q^p$.

Proof. The following calculation proves part (i).

$$\begin{aligned}[l,r]K_p^q &= \{\, \bar{l}xr \mid \bar{x}px = q \,\} \\ &= \{\, y \mid r\bar{y}\bar{l}ply\bar{r} = q \,\} = \{\, y \mid \bar{y}\bar{l}ply = \bar{r}qr \,\} = \{\, y \mid [y][l]p = [r]q \,\} = K_{[l]p}^{[r]q},\end{aligned}$$

where we have substituted x by $y := \bar{l}xr$. Part (ii) follows from part (i) and $*K_p^q = K_q^p$. This last statement expresses the fact that the inverse rotations $[\bar{x}]$ of the rotations $[x]$ that map p to q are the rotations mapping q to p. More formally,

$$*K_p^q = \{\, \bar{x} \mid \bar{x}px = q \,\} = \{\, y \mid yp\bar{y} = q \,\} = \{\, y \mid p = \bar{y}qy \,\} = K_q^p,$$

with $y := \bar{x}$. □

The elements of K_p^p form a subgroup of the quaternions [24]: According to (2.1), K_p^p is the stabilizer of p. Its cosets can be characterized by Proposition 2.1.3(i):

Corollary 2.1.4. *The left cosets of K_p^p are the circles $K_{p'}^p$, and the right cosets of K_p^p are the circles $K_p^{p'}$, for arbitrary $p' \in S^2$.* □

We emphasize that the two parameters p and q in K_p^q "live on different spheres S^2": Any relation between them has no intrinsic geometric meaning, and will be changed by coordinate transformations according to Proposition 2.1.3. This is despite the fact that $p = q$ has an algebraic significance, since the circle K_p^p goes through the special quaternion 1, which is one of the coordinate axes, and hence K_p^p forms a subgroup of quaternions.

2.1.1. Keeping a circle invariant

The following proposition characterizes the transformations that map a given great circle to itself. Moreover, it describes the action of these transformations when restricted to that circle. For a pure unit quaternion $p \in S^2$ and an angle $\theta \in \mathbb{R}$ we use the notation

$$\exp p\theta := \cos\theta + p\sin\theta,$$

so that $[\exp p\theta]$ is a clockwise rotation around p by 2θ on S^2.

Proposition 2.1.5. *Consider the circle K_p^q, for $p, q \in S^2$. The rotations $[l,r]$ that leave K_p^q invariant fall into two categories, each of which is a two-parameter family.*

(a) *The orientation-preserving case: $[l]p = p$ and $[r]q = q$.*

Every transformation in this family can be written as $[\exp p\varphi, \exp q\theta]$ for $\varphi, \theta \in \mathbb{R}$. This transformation acts on the circle K_p^q as rotation by $|\theta - \varphi|$.

(b) *The orientation-reversing case: $[l]p = -p$ and $[r]q = -q$.*

After choosing two fixed quaternions $p', q' \in S^2$ orthogonal to p and q, respectively, they can be written as the transformations $[p' \exp p\varphi, q' \exp q\theta]$ for $\varphi, \theta \in \mathbb{R}$, and they act on K_p^q as reflections.

Note that the transformations that we consider are always orientation-preserving when considered in 4-space; they can be orientation-reversing when considered as (2-dimensional) operations on the circle K_p^q.

Proof. Let $[l,r] \in \mathrm{SO}(4)$ be a rotation. Then we have the following equivalences.

$$[l,r]K_p^q = K_p^q \iff K_{[l]p}^{[r]q} = K_p^q \iff ([l]p = p \wedge [r]q = q) \vee ([l]p = -p \wedge [r]q = -q)$$

For the first case, the transformations $[l]$ on S^2 that leave the point p fixed are the rotations around p, and they are given by the quaternions $l = \exp p\varphi$, and similarly for r. For the second case, the transformations $[l]$ on S^2 that map p to $-p$ can be written as a composition of $[p']$, which maps p to $-p$, and an arbitrary rotation around the axis through p and $-p$, which is expressed as $[\exp p\varphi]$. This establishes that $[l, r]$ can be written in the claimed form.

We now investigate the action of these rotations on K_p^q.

(a) Let $x \in K_p^q$. Since $xq = px$, we have $x \exp q\theta = (\exp p\varphi)x$. In particular,

$$[\exp p\varphi, \exp q\theta]x = \exp(-p\varphi)x \exp q\theta = \exp(-p\varphi)(\exp p\theta)x = (\exp p(-\varphi + \theta))x.$$

Thus, $[\exp p\varphi, \exp q\theta]$ acts on K_p^q like the left multiplication with $\exp p(\theta - \varphi)$, which (being a left rotation) moves every point by the angle $|\theta - \varphi|$.

(b) It is enough to show that $[p', q']$ acts as a reflection on K_p^q. We will show that $K_p^q \cap K_{p'}^{q'} \neq \emptyset$ and $K_p^q \cap K_{p'}^{-q'} \neq \emptyset$. Thus, there is a point $x \in K_p^q$ with $[p', q']x = x$ and another point $y \in K_p^q$ with $[p', q']y = -y$, and this means that $[p', q']$ fixes some, but not all, points on K_p^q, and thus its action cannot be a rotation.

Let $[x_0]$ be a rotation that maps p to q. Then it maps p' to some point p'' that is orthogonal to q. Let $[y_0]$ be the rotation that fixes q and maps p'' to q'. The rotation $[x_0 y_0]$ maps p to q and p' to q'. Thus, $x_0 y_0 \in K_p^q \cap K_{p'}^{q'}$. Similarly, if $[z_0]$ is the rotation that fixes q and maps p'' to $-q'$, then $x_0 z_0 \in K_p^q \cap K_{p'}^{-q'}$. □

Proposition 2.1.6. *The great circles K_p^q and $K_p^{-q} = K_{-p}^q$ are absolutely orthogonal.*

Proof. The simple rotation $[p, -q] = [-p, q]$ maps $x \in K_p^q$ to $-x \in K_p^q$. That is, $[p, -q]$ preserves (not pointwise) K_p^q. Since K_p^{-q} is the fixed circle of $[p, -q]$ and the invariant circles of a simple rotation are absolutely orthogonal, we are done. □

2.1.2. Oriented great circles

By Proportion 2.1.5, the left rotation $[\exp(-p\theta), 1]$ has the same effect on the circle K_p^q as the right rotation $[1, \exp q\theta]$. This allows us to specify an orientation for K_p^q. For some starting point $x \in K_p^q$, we write

$$K_p^q = \{\, (\exp p\theta)x \mid \theta \in \mathbb{R} \,\} = \{\, x \exp q\theta \mid \theta \in \mathbb{R} \,\}, \tag{2.3}$$

and both parameterizations traverse the circle in the same sense, for increasing θ. We may thus introduce the notation $\vec{K}_p^q$ to denote an *oriented great circle* on S^3. If we use $\vec{K}_{-p}^{-q}$ in (2.3), the same circle will be traversed in the *opposite sense*. Thus, we obtain a notation for oriented great circles on S^3, and for this notation, the choice of parameters $p, q \in S^2$ is unique. Only for an oriented circle, the phrase "rotation by $\pi/4$" or "rotation by $-\pi/3$" has a well-defined meaning, and we can give a more specific version of Proposition 2.1.5a: The operation $[\exp p\varphi, \exp q\theta]$ rotates $\vec{K}_p^q$ by $\theta - \varphi$.

In Appendix E, we give a direct geometric view of this orientation, based on the original interpretation of K_p^q as the set of rotations on S^2 that map p to q (Definition 2.1.1).

Proposition 2.1.3 extends to oriented circles as follows:

Proposition 2.1.7. $[l, r]\vec{K}_p^q = \vec{K}_{[l]p}^{[r]q}$ *and* $*\vec{K}_p^q = \vec{K}_{-q}^{-p}$.

Proof. For $x \in K_p^q$,

$$[l, r](x \exp q\theta) = \bar{l}x(\exp q\theta)r = \bar{l}xr\bar{r}(\exp q\theta)r = (\bar{l}xr)\exp(\bar{r}qr\theta) = y \exp(([r]q)\theta)$$

with $y = \bar{l}xr \in [l,r]K_p^q = K_{[l]p}^{[r]q}$. Thus, the orientation that we get on $[l,r]\vec{K}_p^q$ coincides with the orientation prescribed in (2.3) for $\vec{K}_{[l]p}^{[r]q}$. Similarly,

$$*(x \exp q\theta) = (\exp \bar{q}\theta)\bar{x} = \exp(-q\theta)\, y$$

with $y = \bar{x} \in *K_p^q = K_q^p = K_{-q}^{-p}$, and this is the correct orientation for $\vec{K}_{-q}^{-p}$ in accordance with (2.3). □

2.2. Hopf bundles

Hopf bundles are families of circles K_p^q with fixed p or with fixed q:

Definition 2.2.1. Let $q_0 \in S^2$ be a pure unit quaternion. The *left Hopf bundle* $\mathcal{H}^{q_0}$ is

$$\mathcal{H}^{q_0} := \{\, K_q^{q_0} \mid q \in S^2 \,\},$$

and the *right Hopf bundle* $\mathcal{H}_{q_0}$ is

$$\mathcal{H}_{q_0} := \{\, K_{q_0}^{q} \mid q \in S^2 \,\}.$$

The *oriented* left and right Hopf bundles are defined analogously:

$$\vec{\mathcal{H}}^{q_0} := \{\, \vec{K}_q^{q_0} \mid q \in S^2 \,\}$$
$$\vec{\mathcal{H}}_{q_0} := \{\, \vec{K}_{q_0}^{q} \mid q \in S^2 \,\}$$

The convention for left and right was adopted from Dunbar [24]: According to Corollary 2.1.4, the circles $K_q^{q_0}$ of the left Hopf bundle $\mathcal{H}^{q_0}$ are the *left* cosets of the circle $K_{q_0}^{q_0}$.

We can naturally assign a Hopf map to each bundle, such that the circles of a bundle become the fibers of the associated Hopf map:

Definition 2.2.2. Let $q_0 \in S^2$ be a pure unit quaternion. The *left Hopf map* associated with q_0 is

$$\begin{aligned} h^{q_0} \colon S^3 &\to S^2 \\ x &\mapsto [\bar{x}]q_0 = xq_0\bar{x}, \end{aligned}$$

and the *right Hopf map* associated with q_0 is

$$\begin{aligned} h_{q_0} \colon S^3 &\to S^2 \\ x &\mapsto [x]q_0 = \bar{x}q_0x. \end{aligned}$$

Corollary 2.2.3. *The following statements are direct consequences of the definitions:*

- *The choice of the parameter q_0 in the left Hopf bundle $\mathcal{H}^{q_0}$ is unique except that $\mathcal{H}^{q_0} = \mathcal{H}^{-q_0}$. As oriented Hopf bundles, $\vec{\mathcal{H}}^{q_0}$ and $\vec{\mathcal{H}}^{-q_0}$ contain the same circles in opposite orientation.*

  The same statement holds for right Hopf bundles.

- *No two different left Hopf bundles share a circle. That is,*

  $$\mathcal{H}^{p_0} \cap \mathcal{H}^{p_1} = \emptyset \text{ if } p_0 \neq \pm p_1.$$

  A similar statement holds for right Hopf bundles.

- *A left Hopf bundle intersects a right Hopf bundle in exactly two circles, which are absolutely orthogonal:*

$$\mathcal{H}_{q_0} \cap \mathcal{H}^{p_0} = \{K^{p_0}_{q_0}, K^{-p_0}_{q_0} = K^{p_0}_{-q_0}\}.$$

- *Every great circle $K^{p_0}_{q_0}$ in S^3 belongs to a unique left Hopf bundle $\mathcal{H}^{p_0}$ and to a unique right Hopf bundle $\mathcal{H}_{q_0}$.*

From Proposition 2.1.7, we can directly work out the effect of a transformation on an (oriented) Hopf bundle:

Proposition 2.2.4. *(a) $[l,r]\vec{\mathcal{H}}^q = \vec{\mathcal{H}}^{[r]q}$ and $[l,r]\vec{\mathcal{H}}_p = \vec{\mathcal{H}}_{[l]p}$; (b) $*\vec{\mathcal{H}}^q = \vec{\mathcal{H}}_{-q}$ and $*\vec{\mathcal{H}}_p = \vec{\mathcal{H}}^{-p}$.*

We get consequences about the operations that leave a Hopf bundle invariant and about mappings between Hopf bundles.

Proposition 2.2.5. *The following statements about the operations that leave a left Hopf bundle invariant hold, and similar statements hold for right Hopf bundles.*

(i) *Any left rotation leaves an oriented left Hopf bundle $\vec{\mathcal{H}}^q$ invariant. It permutes the great circles of the bundle.*

(ii) *A right rotation $[1,r]$ leaves the oriented left Hopf bundle $\vec{\mathcal{H}}^q$ invariant iff $[r]q = q$.*

(iii) *A right rotation $[1,r]$ maps the oriented left Hopf bundle $\vec{\mathcal{H}}^q$ to the opposite bundle $\vec{\mathcal{H}}^{-q}$ iff $[r]q = -q$.*

(iv) *Any two oriented left Hopf bundles are congruent, and can be mapped to each other by a right rotation.*

(v) *Any oriented right Hopf bundle and any oriented left Hopf bundle are mirrors of each other.* □

We can summarize properties (i)–(iii) in the following statement, which characterizes the transformations that leave a given left Hopf bundle invariant, in analogy to Proposition 2.1.5.

Proposition 2.2.6.

(i) *A rotation $[l,r]$ preserves $\mathcal{H}^{q_0}$ if and only if $[r]q_0 = \pm q_0$.*

(ii) *More precisely, these rotations come in two families.*

  (a) *The rotations with $[r]q_0 = q_0$ can be written as $[l, \exp q_0\theta]$ for $\theta \in \mathbb{R}$, and they map $\vec{\mathcal{H}}^{q_0}$ to $\vec{\mathcal{H}}^{q_0}$, preserving the orientation of the circles.*

  (b) *The rotations with $[r]q_0 = -q_0$ can be written as $[l, q' \exp q_0\theta]$ for $\theta \in \mathbb{R}$, where $q' \in S^2$ is some fixed quaternion orthogonal to q_0. They map $\vec{\mathcal{H}}^{q_0}$ to $\vec{\mathcal{H}}^{-q_0}$, reversing the orientation of the circles.*

Note that an orientation-reversing transformation sends a left Hopf bundle to a right one, and those two share exactly two circles. Thus, no orientation-reversing transformation can preserve a Hopf bundle.

2.2.1. Left and right screws

A generic rotation has two circles that it leaves invariant. The left and right rotations are special: they have infinitely many invariant circles, and as we will see, these circles form a Hopf bundle. In contrast to Proposition 2.2.6, we now discuss rotations that leave every *individual* circle of a Hopf bundle invariant:

Proposition 2.2.7.

(i) *For the oriented left Hopf bundle $\vec{\mathcal{H}}^{q_0}$, the one-parameter subgroup of right rotations $[1, \exp q_0\varphi]$ rotates every circle of $\vec{\mathcal{H}}^{q_0}$ in itself by the same angle φ.*

(ii) *Conversely, for a right rotation $[1, r]$ with $r \neq 1, -1$, the set of circles that it leaves invariant forms a left Hopf bundle $\mathcal{H}^{q_0}$, and $[1, r]$ rotates every circle of $\vec{H}^{q_0}$ in itself by the same angle φ.*

Proof. Part (i) is a direct consequence of the definition (2.3) of oriented circles.

According to Proposition 2.1.5, the right rotation $[1, r]$ leaves a circle K_p^q invariant iff $[r]q = q$. (Case (b) of Proposition 2.1.5, where $[l]p = -p$, does not apply since $l = 1$.) After writing $r = \exp q_0\varphi$ with $\varphi \neq 0, \pi$, the condition $[r]q = q$ translates to $q = \pm q_0$, and the circles $\{ K_p^{\pm q_0} \mid p \in S^2 \}$ form the Hopf bundle $\mathcal{H}^{q_0}$. The last part of the statement repeats (i). □

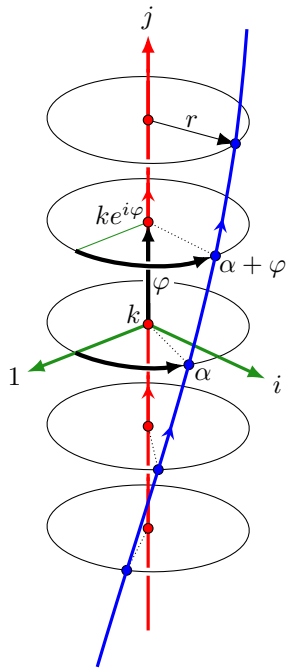

Figure 2.1.: A right screw

Geometrically, these rotations are *screw motions*. If we look at one circle $K_p^{q_0}$ from the bundle, the adjacent circles form helices that wind around this circle, see Figure 2.1. The right multiplication by $\exp q_0\varphi$ effects a forward motion of φ *along* every circle, and a simultaneous clockwise rotation by the same angle φ *around* the circle, when seen in the direction of the forward movement, and is thus a *right screw*.[9] In contrast to the

[9] While not everything that is associated to right rotations is "right", it is a lucky coincidence that at least right rotations effect right screws, and left rotations effect left screws. This view depends on the convention that we have chosen in Section 1.3 for viewing parts of the 3-sphere as three-dimensional space.

Here is a check of this fact at an example: Figure 2.1 shows the situation around the point

situation in Euclidean 3-space, these screws have no distinguished axis. The blue circle seems to wind around the red circle, but this is an artifact of the projection of this picture. All circles are in fact equivalent, and the situation looks the same for every circle of the bundle.

2.2.2. Clifford-parallel circles

We measure the *distance* between two points $p, q \in S^3$ as the geodesic distance on the sphere, which equals the angular distance along the great circle through p and q: $\operatorname{dist}(p,q) := \arccos\langle p,q\rangle$, where $\langle p,q\rangle$ denotes the scalar product. The distance between two sets $K, K' \subseteq S^3$ is $\operatorname{dist}(K,K') = \inf\{\operatorname{dist}(p,q) \mid p \in K, q \in K'\}$.

Two great circles K and K' in S^3 are called *Clifford-parallel* if $\operatorname{dist}(x,K')$ does not depend on $x \in K$. See for example [7, Section 18.8] for more information on Clifford parallelism.

Proposition 2.2.8 ([7, Exercise 18.11.18])**.** *Great circles in the same Hopf bundle $\mathcal{H}^q$ are Clifford-parallel, and* $\operatorname{dist}(K_p^q, K_r^q) = \operatorname{dist}(p,r)/2$.

Proof. By Proposition 2.1.5a, the right rotations $[1, \exp q\theta]$ rotate $x \in K_p^q$ along the circle K_p^q while keeping K_r^q invariant as a set. Thus, $\operatorname{dist}(x, K_r^q)$ is constant as x moves on K_p^q, showing that K_p^q and K_r^q are Clifford-parallel.

Since K_r^q is a left coset of K_q^q, by applying some left rotation to K_p^q and K_r^q, we may assume that $r = q$. That is, it is enough to show that $\operatorname{dist}(K_p^q, K_q^q) = \operatorname{dist}(p,q)/2$. Since $1 \in K_q^q$ and the circles K_p^q and K_p^p are Clifford parallel, it is enough to show that $\operatorname{dist}(K_p^q, 1) = \operatorname{dist}(p,q)/2$.

The points $x = \cos\alpha + v\sin\alpha \in K_p^q$ represent the rotations $[x]$ on S^2 that map p to q, and $\operatorname{dist}(x,1) = \arccos\cos\alpha = \alpha$, assuming $0 \le \alpha \le \pi$. Thus, we are trying to minimize α, which is half the rotation angle of $[x]$. The rotation that minimizes the rotation angle is the one that moves p to q along the great circle through p and q, and its rotation angle 2α is $\operatorname{dist}(p,q)$. □

We mention that Clifford parallelism arises in two kinds: left and right, accordingly as the circles belong to a common left or right Hopf bundle. Each kind of Clifford parallelism is transitive, but Clifford parallelism in itself is not.

$(x_1,x_2,x_3,x_4) = (0,0,0,1) \equiv k \in K_{-i}^i$. According to our conventions from Section 1.3, we draw this in 3-space by projecting to the tangent space $x_4 = 1$, i.e., omitting the x_4-coordinate, and drawing $(x_1,x_2,x_3) \equiv (1,i,j)$ as a right-handed coordinate system. The great circle K_{-i}^i is invariant under the family of right rotations $[1, \exp i\varphi]$, which move the point k along the circle:

$$\vec{K}_{-i}^i = \{\, k\exp i\varphi \,\} = \{\, k(\cos\varphi + i\sin\varphi) \,\} = \{\, k\cos\varphi + j\sin\varphi \,\}$$

The tangent vector at $\varphi = 0$ points in the direction $j \equiv (0,0,1,0)$.

Let us look at a small circle of radius r around K_{-i}^i, centered at k: It lies in a plane parallel to the $1,i$-plane and can be written as

$$\tfrac{1}{\sqrt{1+r^2}}(k + r(\cos\alpha + i\sin\alpha)) = \tfrac{1}{\sqrt{1+r^2}}(k + r\exp i\alpha).$$

The right rotation $[1, \exp i\varphi]$ maps this to

$$\tfrac{1}{\sqrt{1+r^2}}(k + r\exp i\alpha)\exp i\varphi = \tfrac{1}{\sqrt{1+r^2}}(k\exp i\varphi + r\exp i(\alpha+\varphi))$$

i.e., it increases α together with φ. As can be seen in Figure 2.1, this is a right screw.

Du Val [23, § 14, p. 36], for example, considers right quaternion multiplications as left screws, without giving reasons for this choice, and he draws his illustrations accordingly. On the other hand, Coxeter [18, Chapter 6, p. 70] considers right quaternion multiplications as right screws.

2.3. Classification of the point groups

We make a coarse classification of the groups by their invariant Hopf bundles. The following observation of Dunbar [24, p. 124] characterizes this in terms of the left and right groups.

Proposition 2.3.1. *A 4-dimensional point group leaves some left Hopf bundle invariant if and only if its right group is cyclic or dihedral. A similar statement holds for right Hopf bundles and the left group.*

Proof. By Proposition 2.2.6(i), a transformation $[l, r] \in \mathrm{SO}(4)$ preserves $\mathcal{H}^{q_0}$ if and only if $[r]$ keeps the line through q_0 invariant. The set of such r's form an infinite group that is isomorphic to $\mathrm{O}(2)$. Its finite subgroups are either cyclic or dihedral. □

As we have seen, the left and right groups L and R are one of the five classes $2I, 2O, 2T, 2D_{2n}$, and $2C_n$. Besides the infinite families of cyclic groups $2C_n$ and dihedral groups $2D_{2n}$, there are the three polyhedral groups $2I, 2O, 2T$. Accordingly, we get a rough classification into three classes of groups.

1. The left subgroup is cyclic or dihedral, and the right subgroup is polyhedral, or vice versa.

   These groups leave some left or right Hopf bundle invariant, and they are the *tubical groups*, to be discussed in Chapter 3.

2. Both the left and right subgroup are cyclic or dihedral.

   These groups leave some both some left and some right Hopf bundle invariant. They form a large family, the *toroidal groups*, to be discussed in Chapter 4.

3. Both the left and right subgroup are polyhedral.

   These groups leave no Hopf bundle invariant. There are finitely many groups of this class: the polyhedral groups and the axial groups.

For all classes except the tubical groups, there is the possibility that $L = R$, and hence we also consider the achiral extensions of these groups.

2.4. The Clifford torus

The toroidal groups are characterized as leaving both some left Hopf bundle $\mathcal{H}_p$ and some right Hopf bundle $\mathcal{H}^q$ invariant. By Corollary 2.2.3, these two bundles intersect in two orthogonal circles $K^q_p \cup K^{-q}_p$, and hence these two circles must also be invariant. We conclude that the set $\mathbb{T}^q_p$ of points that are equidistant from these two circles is also invariant. We will see that this set is a *Clifford torus*. It has several alternative representations.

$$\begin{aligned}
\mathbb{T}^q_p &= \{\, x \in S^3 \mid \mathrm{dist}(x, K^q_p) = \mathrm{dist}(x, K^{-q}_p) \,\} \\
&= \{\, x \in S^3 \mid \mathrm{dist}(x, K^q_p) = \tfrac{\pi}{4} \,\} \\
&= \{\, x \in S^3 \mid \mathrm{dist}(x, K^{-q}_p) = \tfrac{\pi}{4} \,\} \\
&= \{\, x \in S^3 \mid \mathrm{dist}(x, K^q_p) = \mathrm{dist}(x, K^q_{-p}) \,\}
\end{aligned} \tag{2.4}$$

Proposition 2.1.3 tells us how an orthogonal transformation acts on the circle K^q_p that defines the torus $\mathbb{T}^q_p$. As an immediate corollary, we obtain:

Proposition 2.4.1. *Let $p, q \in S^2$. Then for any $l, r \in S^3$,*

(i) $[l,r]\mathbb{T}^q_p = \mathbb{T}^{[r]q}_{[l]p}$.

(ii) $(*[l,r])\mathbb{T}^q_p = \mathbb{T}^{[r]p}_{[l]q}$, *and as a special case,* $*\mathbb{T}^q_p = \mathbb{T}^p_q$.

From $\mathbb{T}^q_p$, we can recover the two defining circles $K^q_p \cup K^{-q}_p$ as those points whose distance from $\mathbb{T}^q_p$ takes the extreme values $\pi/4$:

$$K^q_p \cup K^{-q}_p = \{x \in S^3 \mid \operatorname{dist}(x, \mathbb{T}^q_p) = \tfrac{\pi}{4}\}$$

Since the choice of parameters p, q for circles K^q_p is unique up to simultaneous sign changes, the choice of parameters $p, q \in S^2$ for the torus $\mathbb{T}^q_p$ is unique up to independent sign changes: $\mathbb{T}^q_p = \mathbb{T}^{-q}_{-p} = \mathbb{T}^q_{-p} = \mathbb{T}^{-q}_p$.

By Proposition 2.4.1, any two Clifford tori are related by an appropriate orientation-preserving transformation. There are no "left" or "right" Clifford tori. Thus, it is sufficient to study one special torus. In particular, $\mathbb{T}^i_i$ is the "standard" Clifford torus:

$$\mathbb{T}^i_i = \{\, \tfrac{1}{\sqrt{2}}(\cos\theta, \sin\theta, \cos\varphi, \sin\varphi) \mid 0 \le \theta, \varphi < 2\pi \,\} = \{\, x \in \mathbb{R}^4 \mid x_1^2 + y_1^2 = x_2^2 + y_2^2 = \tfrac{1}{2} \,\} \tag{2.5}$$

It is a square flat torus, and we name the coordinates (x_1, y_1, x_2, y_2) to emphasize that it is the Cartesian product of a circle of radius $\sqrt{1/2}$ in the x_1, y_1-plane and a circle of radius $\sqrt{1/2}$ in the x_2, y_2-plane. For this torus, the two circles of extreme distance are K^i_i and K^{-i}_i, the great circles in the x_1, y_1-plane and in the x_2, y_2-plane.

In Section 4.11.2, we will see another torus, $\mathbb{T}^i_k$, with a different, but equally natural equation (4.10).

3 The tubical groups

In this chapter we consider the point groups that preserve a left or a right Hopf bundle, but *not both*. By Proposition 2.3.1, these groups are characterized as the groups for which the left or the right group, but not both, is cyclic or dihedral. These groups will be called *tubical groups*. We have chosen this name because, as we will see (see for instance Figure 3.1), for large enough order, the polar orbit polytope consists of intertwined congruent tube-like structures.[10]

Since any two left (resp. right) Hopf bundles are congruent, it is enough to consider the tubical groups that preserve a specific left (resp. right) Hopf bundle. We will call these the *left tubical groups* and the *right tubical groups*. Since left and right Hopf bundles are mirror-congruent, we can restrict our attention to the left tubical groups.

The classic classification leads to 11 classes of left tubical groups. Table 3.1 lists them with the notation from Conway and Smith [14, Table 4.1] in the first column, together with their generators. In Appendix F, we depict subgroup relations between these groups.

$G \leqslant \mathrm{SO}(4)$	parameter n	generators	order	$G^h \leqslant \mathrm{O}(3)$
cyclic type				
$\pm[I \times C_n]$	$n \geq 1$	$[i_I, 1], [\omega, 1]; [1, e_n]$	$120n$	$+I$
$\pm[O \times C_n]$	$n \geq 1$	$[i_O, 1], [\omega, 1]; [1, e_n]$	$48n$	$+O$
$\pm\frac{1}{2}[O \times C_{2n}]$	$n \geq 1$	$[i, 1], [\omega, 1]; [1, e_n]; [i_O, e_{2n}]$	$48n$	$+O$
$\pm[T \times C_n]$	$n \geq 1$	$[i, 1], [\omega, 1]; [1, e_n]$	$24n$	$+T$
$\pm\frac{1}{3}[T \times C_{3n}]$	$n \geq 1$	$[i, 1]; [1, e_n]; [\omega, e_{3n}]$	$24n$	$+T$
dihedral type				
$\pm[I \times D_{2n}]$	$n \geq 2$	$[i_I, 1], [\omega, 1]; [1, e_n], [1, j]$	$240n$	$\pm I$
$\pm[O \times D_{2n}]$	$n \geq 2$	$[i_O, 1], [\omega, 1]; [1, e_n], [1, j]$	$96n$	$\pm O$
$\pm\frac{1}{2}[O \times \overline{D}_{4n}]$	$n \geq 2$	$[i, 1], [\omega, 1]; [1, e_n], [1, j]; [i_O, e_{2n}]$	$96n$	$\pm O$
$\pm\frac{1}{2}[O \times D_{2n}]$	$n \geq 2$	$[i, 1], [\omega, 1]; [1, e_n]; [i_O, j]$	$48n$	TO
$\pm\frac{1}{6}[O \times D_{6n}]$	$n \geq 1$	$[i, 1]; [1, e_n]; [i_O, j], [\omega, e_{3n}]$	$48n$	TO
$\pm[T \times D_{2n}]$	$n \geq 2$	$[i, 1], [\omega, 1]; [1, e_n], [1, j]$	$48n$	$\pm T$

Table 3.1.: Left tubical groups [14, Table 4.1]. See (1.6) on p. 16 for definitions of the quaternions i_I, i_O, ω, e_n.

According to the right group, there are 5 tubical group classes of *cyclic type* and 6 tubical group classes of *dihedral type*. The left Hopf bundle that they leave invariant is $\mathcal{H}^i$. This follows from Proposition 2.2.6(ii) and our choice for the generators of $2C_n$ and $2D_{2n}$. The cyclic-type groups are those tubical groups that moreover preserve the consistent orientation of the circles in $\mathcal{H}^i$. That is, they preserve $\vec{\mathcal{H}}^i$. Each of these classes is parameterized by a positive integer n, which is the largest integer n such that $[1, e_n]$ is in the group.

In some cases the parameter n starts from 2 in order to exclude the groups D_2, which is geometrically the same as C_2. We also exclude $\pm\frac{1}{2}[O \times \overline{D}_4]$ because the notation $\overline{D}_{4n}$ indicates that the normal subgroup D_{2n} of D_{4n} is used, and not C_{2n}. For $n = 1$, this

[10] There is a notion of *tubular groups*, which is something completely different, see for example [11].

distinction disappears, and hence $\pm\frac{1}{2}[O\times\overline{D}_4]$ is geometrically the same as $\pm\frac{1}{2}[O\times D_4]$ (see also Appendix G.1). In this case and in all other cases where C_2 and D_2 are exchanged, the respective groups are conjugate under $[1, \frac{1}{\sqrt{2}}(i+j)]$, which exchanges $[1,i]$ with $[1,j]$.

Convention. For ease of use, we drop the word "left" from "left tubical group" and call it simply "tubical group" in this chapter. We will denote $\mathcal{H}^i$ by $\mathcal{H}$ and call it *the* Hopf bundle. We will also denote $h^i(x) = xi\bar{x}$ by $h(x)$ and call it *the* Hopf map.

3.1. Orbit circles

An element of a tubical group has one of the following two forms, and Proposition 2.1.5 describes its action on the circles of $\mathcal{H}$:

- $[l, e_m^s]$, which maps $\vec{K}_p$ to $\vec{K}_{[l]p}$, and
- $[l, je_m^s]$, which maps K_p to $K_{-[l]p}$ with a reversal of orientation. More precisely, this rotation maps $\vec{K}_p = \vec{K}_p^i$ to $\vec{K}_{[l]p}^{-i}$, which is the reverse of $\vec{K}_{-[l]p}^{i} = \vec{K}_{-[l]p}$. These elements occur only in the groups of dihedral type.

Thus, the rotations permute the Hopf circles of $\mathcal{H}$. Via the one-to-one correspondence of the Hopf map, they induce mappings on the Hopf sphere S^2:

Proposition 3.1.1. *A tubical group G induces a 3-dimensional point group G^h via the Hopf map h. This group G^h is isomorphic to $G/\langle[1,e_n]\rangle$, where n is the largest integer such that $[1,e_n] \in G$.*

Proof. The above considerations show that $[l, e_m^s]$ induces the orientation-preserving transformation $[l]$ on S^2, and $[l, je_m^s]$ induces the orientation-reversing transformation $-[l]$ on S^2. We are done since the image of G in the homomorphism

$$\begin{aligned} G &\to \mathrm{O}(3) \\ [l, e_m^s] &\mapsto [l] \\ [l, je_m^s] &\mapsto -[l] \end{aligned}$$

is G^h, and the kernel is $\langle[1,e_n]\rangle$. □

The column "$G^h \leqslant \mathrm{O}(3)$" in Table 3.1 lists the induced group for each tubical group G. Tubical groups of cyclic type induce chiral groups G^h, and tubical groups of dihedral type induce achiral groups G^h.

As a consequence, the orbit of some starting point $v \in S^3$ can be determined as follows:

1. The starting point lies on the circle $K_{h(v)}$. The subgroup $\langle[1,e_n]\rangle$ generates a regular $2n$-gon in this circle.
2. For each $t \in G^h$, there is a coset of elements that map $K_{h(v)}$ to the circle $K_{t(h(v))}$, and these elements generate a regular $2n$-gon in this circle.

Proposition 3.1.2. *Let G be a tubical group. The orbit of a point $v \in S^3$ is the union of regular $2n$-gons on the circles $K_{t(h(v))}$ for $t \in G^h$.* □

We call these circles the *orbit circles* of G.

If the G^h-orbit of $h(v)$ is not free, several of these $2n$-gons will share the same circle, and they may overlap. The $2n$-gons may coincide, or they may form polygons with more vertices. It turns out that they can intersperse to form a regular $2fn$-gon or, in the case of dihedral-type groups, the union of two regular $2fn$-gons, for some $1 \leq f \leq 5$.

The G^h-orbit of $h(v)$ is always free when the starting point does not lie on a rotation center or a mirror of G^h. The following corollary follows directly from the previous proposition.

Corollary 3.1.3. *Let G be a tubical group and let $v \in S^3$ be a point. If the G^h-orbit of $h(v)$ is free, then the G-orbit of v is also free.* □

For tubical groups of cyclic type, the orbit has the following nice property.

Proposition 3.1.4. *Let G be a cyclic-type tubical group. The G-orbit of a point $v \in S^3$, up to congruence, depends only on the circle of $\mathcal{H}$ on which v lies.*

Proof. Rotation of v along $K_{h(v)}$ can be performed by a right rotation of the form $[1, \exp\theta i]$. Since the right group of G is cyclic, elements of G have the form $[l, e_m^s]$. These elements commute with right rotations of the form $[1, \exp\theta i]$. In particular,

$$\text{orbit}([1, \exp\theta i]v, G) = [1, \exp\theta i]\text{orbit}(v, G). \qquad \square$$

3.2. Tubes

If n is large, the orbit fills the orbit circles densely. Figure 3.1a shows the cells (i.e. facets) of the polar orbit polytope that correspond to orbit points on three orbit circles. Here orbit points form a regular 80-gon on each orbit circle. We clearly see twisted and intertwined tubes, which are characteristic for these groups, and which we have used to assign their names. Figures 3.1c and 3.1e show a single cell. It has two large flat faces, where successive cells are stacked on top of each other with a slight twist. On the boundary of the tubes in Figure 3.1a we can distinguish two different sets of "parallel" curves. One set of curves comes from the boundaries between successive *slices* (cells) of the tubes, and the other set of curves is a trace of the slices of the adjacent tubes. At first sight, it is hard to know which of the two line patterns is which. In Figure 3.1b, we have cut the tubes open to show where the boundaries between the slices are, revealing also the three orbit circles.

If we let n grow to infinity, the tubes become smooth, see Figure 3.1d. We explore the limiting shape of these tubes in Section 3.3. We will see that the tubes are either 3-sided, 4-sided, or 5-sided, and their shape as well as their structure, how they share common boundaries and how they meet around edges, can be understood in terms of the spherical Voronoi diagram on the Hopf sphere S^2. Figure 3.1f shows this Voronoi diagram for our example.

We will show some more examples of cells below (Figures 3.7 and 3.8) and in Appendix B. In general, the cell of a polar orbit polytope of a tubical group for large enough n will always exhibit the following characteristic features.

- It is a thin slice with a roughly polygonal shape.
- The top and bottom faces are parallel.
- Moreover, the top and bottom faces are congruent and slightly twisted with a right screw. (There are, however exceptions for tubical groups of dihedral type: With some choices of starting points, there is an alternative way of stacking the slices: every other slice is upside down, as in Figure 3.4.)
- The top and bottom faces approach the shape of a triangle, quadrilateral or pentagon with curved sides.
- The sides are decorated with slanted patterns, which come from the boundaries of the adjacent tubes.

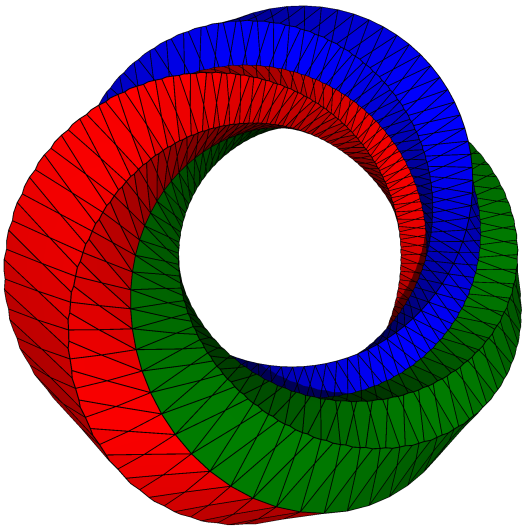

(a) Three tubes

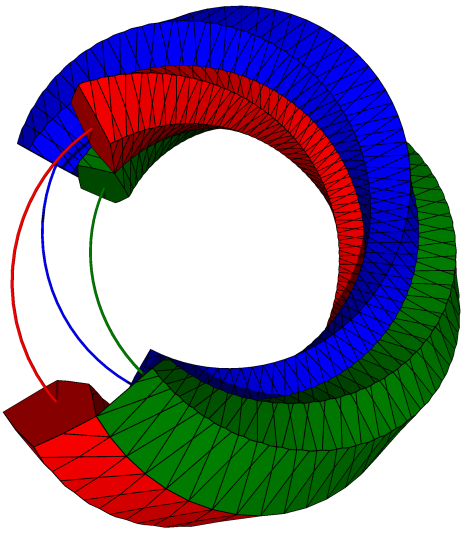

(b) Three partial tubes

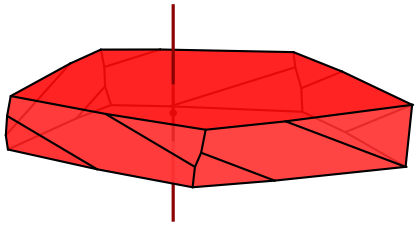

(c) A single cell

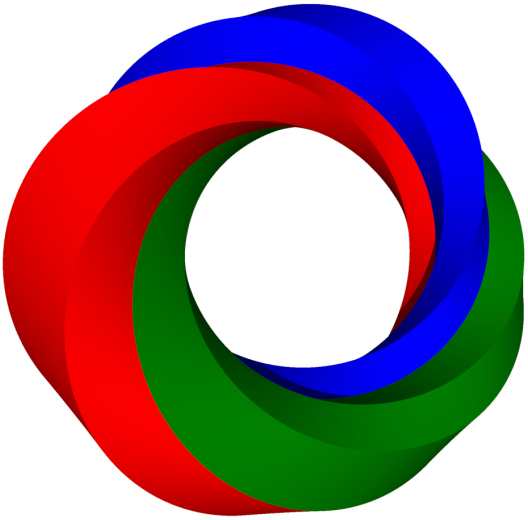

(d) Three smooth tubes

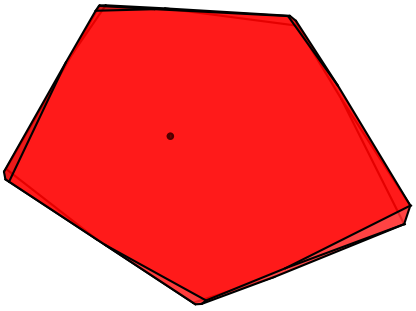

(e) Top view of a cell in orthogonal projection

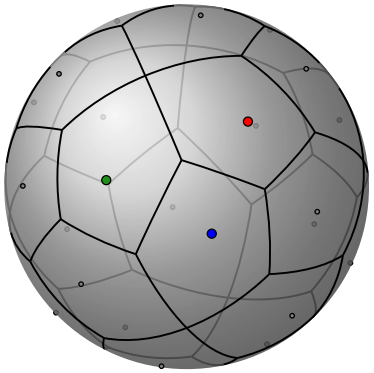

(f) Voronoi diagram on the Hopf sphere

Figure 3.1.: (a) Three tubes (out of twenty-four) of the polar $\pm[O \times C_n]$-orbit polytope for a generic starting point v and $n = 40$. Each tube consists of 80 cells (slices). The tubes are shown in a central projection. (b) Some of the cells are removed to make the slices visible. We also show the corresponding orbit circles. (c) A single cell (with its cell axis) from those tubes, in a perspective view from the side, and (e) a top view in orthogonal projection. (f) The spherical Voronoi diagram of the $+O$-orbit of $h(v)$. The colored points correspond to the tubes of the same color. (d) The tubes as n goes to infinity.

- The tube twists around the orbit circle by one full 360° turn as it closes up on itself.

If n is small, these properties break down: The circles are not filled densely enough to ensure that the cells are thin slices. Sometimes they are regular or Archimedean polytopes, and the orbit polytopes coincide with those of polyhedral groups, and the "tubes" may even be disconnected, see for example Figures B.1 or B.9 in Appendix B. See Section 3.12 for more examples.

Figure 3.1 shows a case where the $2n$-gons lie on different circles. Then the orbit is free: for any two cells, there is a unique transformation in the group that moves one cell to the other. If the starting point is generic enough, the cells have no symmetries. (See Proposition 3.4.1 below for a precise statement.) Then the given group is the symmetry group of its orbit polytope: There is a unique transformation mapping one cell to the other even among *all* orthogonal transformations, not just the group elements.

3.2.1. Mapping between adjacent cells

Definition 3.2.1. The *cell axis* of a cell of the polar orbit polytope is the orthogonal projection of the orbit circle into the 3-dimensional hyperplane of the cell.

The cell axis thus gives the direction in which consecutive cells are stacked upon each other along the orbit circle. It is a line going through the orbit point. Figure 3.1c shows a cell together with its axis. The cell axis is not necessarily a symmetry axis. The cell axis intersects the boundary of the cell in two *poles*.

This is where consecutive cells are attached to each other (unless n is too small and the tubes are disconnected.) More precisely: For the orbit polytope of a generic starting point, the next cell is attached as follows. We translate the cell C from the bottom pole to the top pole. Call the new cell C'. We rotate C' slightly until its bottom face matches the top face of C, and we attach it there (with a bend into the fourth dimension, as for every polytope).

3.3. The geometry of the tubes

We investigate the structure of the tubes in the limiting case as $n \to \infty$, where they become smooth objects. As n gets larger, the orbit circle is filled more and more densely, and the slices get thinner. In the limit, every slice becomes a flat plane convex region, which we call a *tangential slice*. The tangential slices around an orbit circle sweep out the *tangential tube* as v moves around the circle. The limit of the polar orbit polytope consists of tangential tubes, and this is what is shown in Figure 3.1d. The central projections of these tubes and slices to the sphere are the *spherical tubes* and the *spherical slices* of these tubes. The spherical tubes are the Voronoi diagram on S^3 of the orbit circles.

This gives us a way to generalize these notations to any finite set of circles from a common Hopf bundle. For that we first need the definition of the spherical Voronoi diagram. Let $\mathcal{X}$ be a finite collection of nonempty subsets of S^d, and let $X \in \mathcal{X}$ be one of these subsets. The *spherical Voronoi cell* of X with respect to $\mathcal{X}$ is

$$\mathrm{Vor}_{\mathcal{X}}(X) := \{x \in S^d \mid \mathrm{dist}(x, X) \leq \mathrm{dist}(x, Y) \text{ for all } Y \in \mathcal{X}\}.$$

The spherical Voronoi cells of the subsets in $\mathcal{X}$ give a decomposition of S^d, denoted by $\mathrm{Vor}_{\mathcal{X}}$ and called the *spherical Voronoi diagram*. If the subsets in $\mathcal{X}$ are singletons, we get the usual spherical Voronoi diagram.

Let $\mathcal{C}$ be a finite set of at least two circles from a common Hopf bundle, and let $K \in \mathcal{C}$ be one of them. We can assume that the common Hopf bundle is $\mathcal{H}$. The Voronoi cell of K with respect to $\mathcal{C}$ is called a *spherical tube*. The intersection of $\mathrm{Vor}_{\mathcal{C}}(K)$ with the

hyperplane perpendicular to K at a point $v \in K$ gives two (2-dimensional) patches. One contains v and one contains $-v$. These are *spherical slices*. The *tangential slices* and *tangential tubes* are defined as above in the special case of orbit circles.

We will show that the spherical tubes are bounded by patches of Clifford tori (Theorem 3.3.2), and the tangential slices are polygons of circular arcs (Theorem 3.3.3).

3.3.1. The spherical tubes

Given that the circles belong to a common Hopf bundle and the Hopf map transforms distances appropriately (Proposition 2.2.8), it is no surprise that the Voronoi diagram of the set of *circles* on S^3 is closely related to the Voronoi diagram of the corresponding *points* on S^2 (see Figure 3.1f.)

Proposition 3.3.1. *Let $\mathcal{C} \subset \mathcal{H}$ be a finite set of circles from $\mathcal{H}$, and let $K \in \mathcal{C}$ be one of them. The spherical tube $\mathrm{Vor}_{\mathcal{C}}(K)$ is the union of circles from $\mathcal{H}$ that are the preimages under h of the points in $\mathrm{Vor}_{h(\mathcal{C})}(h(K))$, where $h(\mathcal{C}) := \{\, h(C) \mid C \in \mathcal{C} \,\}$.*

Proof. First we will show that for any point $x' \in \mathrm{Vor}_{\mathcal{C}}(K)$, the great circle K' from $\mathcal{H}$ on which x' lies is also in $\mathrm{Vor}_{\mathcal{C}}(K)$. Since all the circles in $\mathcal{H}$ are Clifford-parallel (Proposition 2.2.8), $\mathrm{dist}(K', C) = \mathrm{dist}(x', C)$ for all $C \in \mathcal{C}$. Thus, we get the following equivalence.

$$\mathrm{dist}(x', K) \leq \mathrm{dist}(x', C) \iff \mathrm{dist}(K', K) \leq \mathrm{dist}(K', C),$$

for all $C \in \mathcal{C}$. That is, $K' \subset \mathrm{Vor}_{\mathcal{C}}(K)$. By Proposition 2.2.8 we know that

$$\mathrm{dist}(K', K) \leq \mathrm{dist}(K', C) \iff \mathrm{dist}(h(K'), h(K)) \leq \mathrm{dist}(h(K'), h(C)),$$

for all $C \in \mathcal{C}$. That is, $K' \in \mathrm{Vor}_{\mathcal{C}}(K)$ if and only if $h(K') \in \mathrm{Vor}_{h(\mathcal{C})}(h(K))$. □

3.3.2. The spherical tube boundaries

Theorem 3.3.2. *Let $\mathcal{C} \subset \mathcal{H}$ be a finite set of circles from $\mathcal{H}$. The boundaries of the corresponding spherical tubes consist of patches of Clifford tori. The edges of these tubes are great circles from $\mathcal{H}$.*

Proof. As in Proposition 3.3.1, the boundary between two tubes is the preimage, under the Hopf map h, of the boundary between the two corresponding Voronoi regions in $\mathrm{Vor}_{h(\mathcal{C})}$. Such a boundary edge on the Hopf sphere S^2 is contained in a great circle. A great circle can be described as the points that are equidistant from two antipodal points $\pm p$ on S^2, and under the inverse Hopf map, these become the points on S^3 that are equidistant from two absolutely orthogonal circles K_p and K_{-p}, and this is, by definition, a Clifford torus.

The tube edges, where three or more tubes meet, are the preimages of the Voronoi vertices of $\mathrm{Vor}_{h(\mathcal{C})}$. Thus, they are circles from $\mathcal{H}$. □

3.3.3. The tangential slices

Theorem 3.3.3. *Let $\mathcal{C} \subset \mathcal{H}$ be a finite set of circles from $\mathcal{H}$. The corresponding tangential slices are (flat) convex regions bounded by circular arcs.*

Proof. Let $K \in \mathcal{C}$ be one of the circles. We want to consider the tangential slice of K at a point $v \in K$. Without loss of generality, we may assume that $v = i$, because the left rotation $[-vi, 1]$ preserves $\mathcal{H}$ (see Proposition 2.2.5(i)) and maps v to i. Then K is actually K_i, the great circle through the points 1 and i.

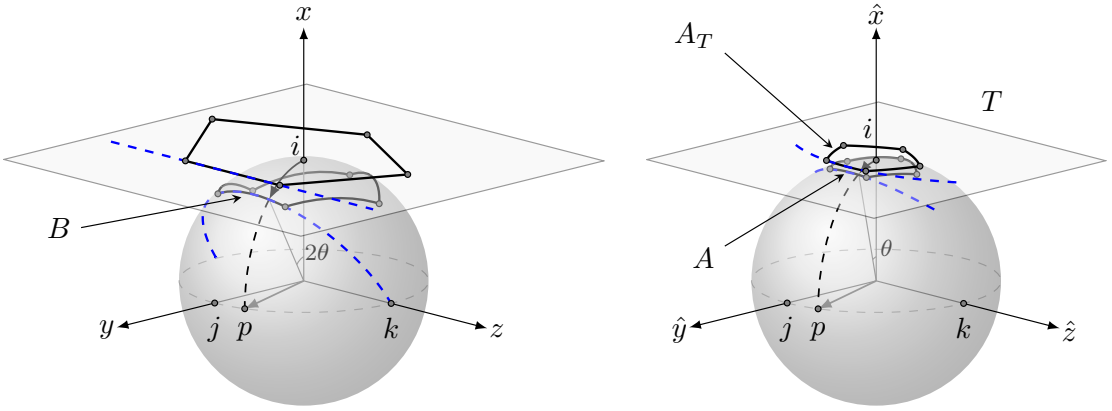

(a) S^2 (b) $S_0 \subset Q$

Figure 3.2.: The procedure to get the tangential slice A_T. (a) The spherical pentagon B is the Voronoi cell of the point $i = h(K_i)$ with respect to $h(\mathcal{C})$. The pentagon in the plane passing through i is the central projection of B onto that plane. (b) The spherical pentagon A is the spherical slice at i, which we get from a radial contraction of B. The circular-arc pentagon A_T in the tangent plane T passing through i is the corresponding tangential slice, which we get from a central projection of A to T. This example is constructed from the orbit circles of Figure 3.1.

The tangent direction of K at v is the quaternion 1. The hyperplane Q perpendicular to K at v is spanned by i, j and k, which we represent in a 3-dimensional coordinate system $\hat{x}, \hat{y}, \hat{z}$, see Figure 3.2b. Q intersects S^3 in a great 2-sphere S_0. The spherical tube $\mathrm{Vor}_{\mathcal{C}}(K)$ cuts out two opposite patches from S_0: the spherical slices. Denote by A the slice that contains v. The slice A intersects each circle of $\mathrm{Vor}_{\mathcal{C}}(K)$. Thus, by Proposition 3.3.1, $h(A)$ equals $\mathrm{Vor}_{h(\mathcal{C})}(h(v))$, which we will denote by B.

Using spherical coordinates, a point in S_0 has the form $i\cos\theta + p\sin\theta$, where the direction vector p is a unit vector in the $\hat{y}, \hat{z}$-plane that plays the role of the longitude, and $\theta \in \mathbb{R}$ is the angular distance on S_0 between that point and i. See Figure 3.2. Since p and i are pure unit quaternions, they anticommute, and in particular, $pip = -ipp = i$. We will now apply the Hopf map h to a point in S_0:

$$\begin{aligned} h(i\cos\theta + p\sin\theta) &= (i\cos\theta + p\sin\theta)\, i\, (-i\cos\theta - p\sin\theta) \\ &= i\cos^2\theta - pip\sin^2\theta + p\cos\theta\sin\theta + p\cos\theta\sin\theta \\ &= i(\cos^2\theta - \sin^2\theta) + 2p\cos\theta\sin\theta \\ &= i\cos 2\theta + p\sin 2\theta. \end{aligned}$$

That is, h maps a point whose angular distance from i is θ to the point in the same direction but with angular distance 2θ. Thus, if we identify S_0 with S^2 using the natural identification (on S^2, we denote the i, j and k directions by x, y and z, respectively), we see that A is obtained from B by a *radial contraction*. That is, we look from i in all directions and multiply the angular distance between i and each point in B by $1/2$.

The intersection of Q with the (3-dimensional) tangent space of S^3 at v is the 2-dimensional tangent plane T of S_0 at v. For our choice $v = i$, T is the plane in Q defined by $\hat{x} = 1$. The tangential slice lies in this plane.

So to get the tangential slice A_T at v, we radially contract B to get A, and then centrally project A to T. We will describe this procedure algebraically. The radial contraction towards i is the map

$$i\cos\theta + p\sin\theta \mapsto i\cos\tfrac{\theta}{2} + p\sin\tfrac{\theta}{2}.$$

This map is not uniquely determined at the South Pole ($\theta = \pi$), and we will tacitly exclude this point from further consideration. Writing p as $j\cos\varphi + k\sin\varphi$, the map can be described as follows:

$$\begin{pmatrix} x \\ y \\ z \end{pmatrix} = \begin{pmatrix} \cos\theta \\ \cos\varphi\sin\theta \\ \sin\varphi\sin\theta \end{pmatrix} \mapsto \begin{pmatrix} \hat{x} \\ \hat{y} \\ \hat{z} \end{pmatrix} = \begin{pmatrix} \cos\frac{\theta}{2} \\ \cos\varphi\sin\frac{\theta}{2} \\ \sin\varphi\sin\frac{\theta}{2} \end{pmatrix}$$

Using the identities $\cos\frac{\theta}{2} = \frac{\sqrt{1+\cos\theta}}{\sqrt{2}}$ and $\sin\theta = 2\sin\frac{\theta}{2}\cos\frac{\theta}{2}$, the map is written as follows.

$$(x, y, z) \mapsto (\hat{x}, \hat{y}, \hat{z}) = \frac{1}{\sqrt{2}}\Big(\sqrt{1+x}, \frac{y}{\sqrt{1+x}}, \frac{z}{\sqrt{1+x}}\Big)$$

Combining this with the central projection from the origin onto T gives the following map f.

$$f\colon (x, y, z) \mapsto (\hat{x}, \hat{y}, \hat{z}) = \Big(1, \frac{y}{1+x}, \frac{z}{1+x}\Big) = \Big(1, \frac{y/x}{1+1/x}, \frac{z/x}{1+1/x}\Big)$$

If we apply f to a boundary edge of B, it will turn out the resulting curve is part of a circle. The boundary edges of B are arcs of great circles on S^2. We obtain such an arc by centrally projecting to S^2 a straight segment in the tangent plane of S^2 at $h(v) = i$. Without loss of generality suppose that one of these segments lies on the line $(x, y, z) = (1, c_0, t)$, $t \in \mathbb{R}$, for some constant $c_0 \neq 0$, see the blue line in Figure 3.2a. The central projection of this line to S^2 lies on the great circle

$$\Big\{ \frac{\pm 1}{\sqrt{c_0^2 + t^2 + 1}}(1, c_0, t) \;\Big|\; t \in \mathbb{R} \Big\}.$$

See the blue curve in Figure 3.2a. The map f transforms this great circle into the set

$$\Big\{ \Big(1, \frac{c_0}{1 \pm \sqrt{c_0^2 + t^2 + 1}}, \frac{t}{1 \pm \sqrt{c_0^2 + t^2 + 1}}\Big) \;\Big|\; t \in \mathbb{R} \Big\}. \tag{3.1}$$

See the blue curve in the tangent plane in Figure 3.2b. Straightforward manipulations show that this set is a circle:

$$\hat{y} = \frac{c_0}{1 \pm \sqrt{c_0^2 + t^2 + 1}} \iff \pm\hat{y}\sqrt{c_0^2 + t^2 + 1} = c_0 - \hat{y}$$
$$\iff \hat{y}^2 c_0^2 + \hat{y}^2 t^2 + \hat{y}^2 = \hat{y}^2 - 2c_0\hat{y} + \hat{y}_0^2 \iff \hat{y}^2 c_0^2 + \hat{y}^2 t^2 + 2c_0\hat{y} = c_0^2$$

Dividing both sides by c_0^2 and then substituting the relation $\frac{\hat{z}}{\hat{y}} = \frac{t}{c_0}$, which follows from (3.1), gives

$$\hat{y}^2 + \hat{z}^2 + \frac{2}{c_0}\hat{y} = 1 \iff \Big(\hat{y} + \frac{1}{c_0}\Big)^2 + \hat{z}^2 = \frac{c_0^2 + 1}{c_0^2}, \tag{3.2}$$

which is the equation of a circle. □

The circle defined in (3.2) belongs to the pencil of circles through the points $(\hat{x}, \hat{y}, \hat{z}) = (1, 0, \pm 1)$, because these points fulfill the equations (3.2). The center $(\hat{x}, \hat{y}, \hat{z}) = (1, -\frac{1}{c_0}, 0)$ lies on the axis $(\hat{x}, \hat{y}, \hat{z}) = \lambda(c_0, -1, 0)$ perpendicular to the plane $c_0 x = y$ containing the great circle and the line that started the construction.

If the set of great circles $\mathcal{C}$ in the previous theorem are the orbit circles of a tubical group G, then the spherical Voronoi cell B on S^2 can have 3, 4 or 5 sides, because the

cells form a tiling of the sphere with equal cells. Thus, the spherical slice is also 3, 4 or 5 sided. In particular, we get the following corollary.

Corollary 3.3.4. *The tangential slice of an orbit of a tubical group is a convex plane region whose boundary consists of 3, 4, or 5 circular arcs.*

3.3.4. The tangential tube boundaries

The boundary surfaces of the tangential tubes (shown in Figure 3.1d) carry some interesting structures, but we don't know what these surfaces are.

The points on such a surface are equidistant from two circles K and K', and we denote the surface by $B(K, K')$. We know from Theorem 3.3.2 that its central projection to the sphere is a Clifford torus $\mathbb{T}$, whose image $h(\mathbb{T})$ is the bisector between $h(K)$ and $h(K')$ on S^2. According to the relation between Voronoi diagrams and polar orbit polytopes (as briefly discussed in Section 1.1.2), a circle $K \in \mathcal{H}$ that belongs to $\mathbb{T}$ is expanded by some factor, depending on the distance to K and K', to become a circle on $B(K, K')$. Thus, the surface $B(K, K')$ is fibered by circles (of different radii) around the origin.

Another fibration by circles, this time of equal radii, can be obtained by taking the circular arc that forms the boundary of the tangential slice towards K', and sweeping it along the circle K. In Figure 3.2b, the circle K proceeds from the point i into the fourth dimension, and the circular boundary arc must simultaneously wind around K as it moves along K. A third fibration, by circles of the same radius, is obtained in an analogous way from K'. Each of these fibrations leads to a straightforward parametric description of $B(K, K')$.

Alternatively, an implicit description $B(K, K')$ by two equations can be obtained as the intersection of two "tangential hypercylinders" in which the two tangential tubes of K and K' lie. (If the circle K is described by the system $x_1^2 + x_2^2 = 1$, $x_3 = x_4 = 0$ in an appropriate coordinate system, its tangential hypercylinder is obtained by omitting the equations $x_3 = x_4 = 0$.)

3.4. Generic starting points

We return to the analysis of the polar orbit polytope, and start with the easy generic case.

Proposition 3.4.1. *Let G be a tubical group whose right group is C_n or D_n for $n \geq 6$. Let $v \in S^3$ be a point. If the G^h-orbit of $h(v)$ has no symmetries other than G^h, then the same holds for the G-orbit of v: the symmetry group of this orbit is G.*

Proof. Since no C_n or D_n for $n \geq 6$ is contained in a polyhedral group, the only groups containing G are tubical. In particular, the symmetry group H of the G-orbit of v is tubical. Since the symmetry group of the G^h-orbit of $h(v)$ is G^h by assumption, the point $h(v)$ does not lie on any rotation center or a mirror of a supergroup of G^h. In particular, the H^h-orbit of $h(v)$ is free. Thus, by Corollary 3.1.3, the H-orbit of v is free. So G and H have the same order. Since $G \leqslant H$, we get $G = H$. □

According to our goal of obtaining a geometric understanding through the orbit polytope, as described in Figure 1.2 in Chapter 1, we are done, in principle. Since the cell has no nontrivial symmetries, *all* symmetries of a cell are in G. We are in the branch of Figure 1.2 that requires no further action. Every cell can be mapped to every other cell in a unique way.

In particular, for two consecutive cells on a tube it is obvious what the transformation between them is: a small translation along the orbit circle combined with a slight twist

around the orbit circle, or in other words, a right screw, effected by the right rotation $[1, e_n]$.

Between cells on different tubes, the transformation is not so obvious. For example, in Figure 3.1c, we see a vertical zigzag of three short edges between the front corner of the upper (roughly pentagonal) face and the corresponding corner of the lower face. These edges are part of a longer sequence of edges, where 3 tubes meet, and which closes in a circular way. How are the cells arranged around this "axis", and how does the group map between them? To investigate this question, it is helpful to move the starting point closer to the axis to look what happens there. In particular, this will help us to distinguish different classes of groups G with the same group G^h. We will see an example in Section 3.14. Eventually, we will also consider starting points *on* the axis.

3.5. Starting point close to a mirror

Let G be a dihedral-type tubical group, and $p \in S^2$ be a point close to the mirror of a reflection of G^h. Moreover, assume that p does not lie on any rotation center of G^h. The point p has a *neighboring partner* p', which is obtained from p by reflecting it across that mirror. We call the corresponding circles K_p and $K_{p'}$ *neighboring circles*. The red point and the blue point in Figure 3.3a form a neighboring pair for the group $\pm T$.

We will now discuss the G-orbit under different choices for the starting point v on K_p.

Case 1. Choose $v \in K_p$ such that for each orbit point, the closest point on the neighboring circle is also in the orbit. See Figure 3.3c. Thus, in the polar G-orbit polytope, each cell has a "big" face that directly faces the closest point on the neighboring circle.

Case 2. If we move v in one direction, the orbit points on the neighboring circle move in the opposite direction. We choose v such that the orbit points on neighboring circles are in "alternating positions". That is, the distance between orbit points on neighboring circles is maximized. See Figure 3.3d. Thus, in every cell of the polar G-orbit polytope, the side that is close to the neighboring circle is divided into two faces, on each a cell of the neighboring tube is stacked.

Case 3. Figure 3.3e shows an intermediate situation.

3.6. Starting point on a mirror

It is also interesting to see what happens if we move p to lie on that mirror of G^h. We still assume that p does not lie on any rotation center of G^h. In this case, the neighboring pairs on S^2 coincide, and thus the corresponding neighboring circles also coincide. We describe next what happens in each of the previous cases.

Case 1. The orbit points coincide in pairs, and thus they form a regular $2n$-gon on K_p. Each orbit point can be mapped to any other orbit point by two different elements of G, one of which rotates K_p and one of which reverses the orientation of K_p. Thus, in the polar orbit polytope, each cell has a half-turn symmetry that flips the direction of the cell axis, and exchanges the top and bottom faces. We call it a *flip symmetry*. (For small n, top and bottom faces might not be defined.)

It is interesting to notice that for this choice of the starting point, the G-orbit of v coincides with the orbit of v under the cyclic-type index-2 subgroup G_C of G. Since the G_C-orbit is the same up to congruence for any starting point on

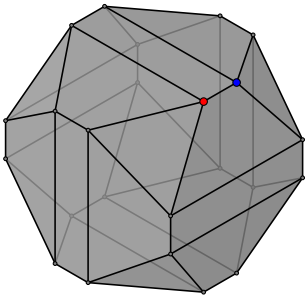

(a) The $\pm T$-orbit polytope of p.

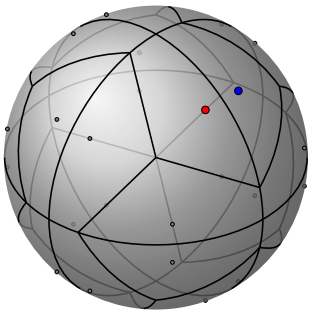

(b) The spherical Voronoi diagram of the orbit.

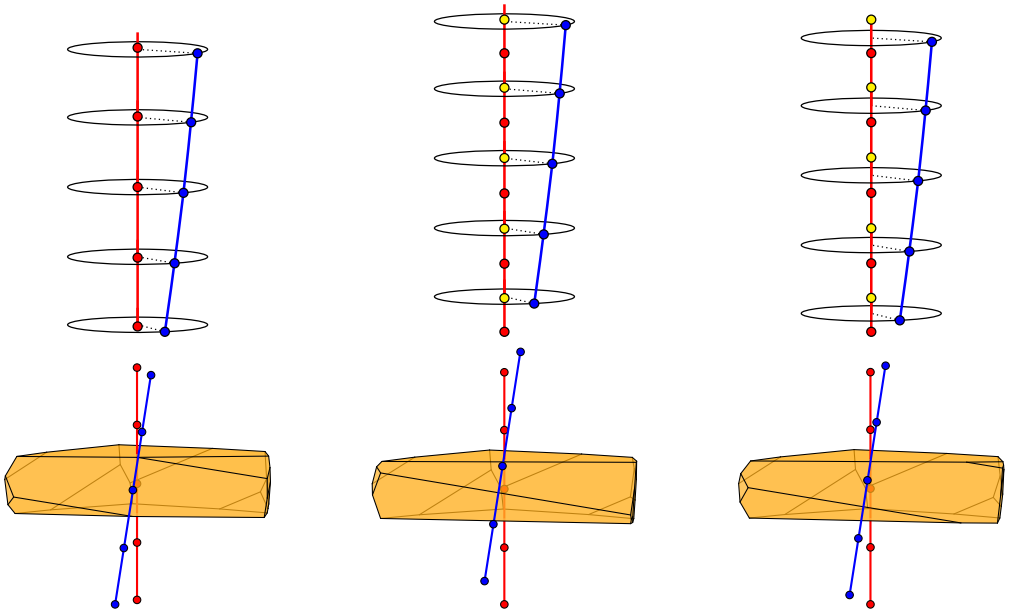

(c) (d) (e)

Figure 3.3.: Orbits of the group $G = \pm[T \times D_{20}]$ for a starting point v whose image $p := h(v)$ lies near a mirror of $G^h = \pm T$. The top row shows the three-dimensional $\pm T$-orbit polytope of p and the corresponding spherical Voronoi diagram. The red and the blue points form a neighboring pair. The next row shows different possible configurations for orbit points on the corresponding neighboring circles. Red points and blue points are orbit points on the two neighboring circles. Yellow points are midpoints of orbit points on the red circle. They are not orbit points. The third row shows a cell of the corresponding polar orbit polytope.

K_p (Proposition 3.1.4), the G_C-orbit of *any* starting point on K_p has the extra symmetries coming from a dihedral-type group that is geometrically equal to G. (This geometrically equal group has the generators of G with j replaced by a different unit quaternion q' orthogonal to i, which is the quaternion q' from Proposition 2.1.5(b).) We put this in a proposition since we will need it later.

Proposition 3.6.1. *Let G_C be a cyclic-type tubical group, and let G_D be a dihedral-type tubical group containing G_C as an index-2 subgroup. If p lies on a mirror of G_D^h, then the G_C-orbit of any point on K_p has the symmetries from (a geometrically equal copy of) G_D.*

Case 2. Orbit points on K_p form a regular $4n$-gon. Each orbit point can be mapped to any other orbit point by a unique element of G. However, this orbit has extra symmetries, which come from the supergroup of G that we obtain by extending G by the new symmetry $[1, e_{2n}]$. This orbit of the supergroup follows

the behavior described in Case 1. Accordingly, each cell of the polar G-orbit polytope has a flip symmetry.

In almost all choices for G, the supergroup has the same class as G but with twice the parameter n. The only exceptional case is $G = \pm\frac{1}{2}[O \times \overline{D}_{4n}]$. In this case, the supergroup is $\pm[O \times D_{4n}]$.

Case 3. Orbit points on K_p form two regular $2n$-gons whose union is a $4n$-gon with equal angles, and side lengths alternating between two values. The orbit points come in close pairs. Accordingly, the cells of the polar orbit polytope come in a sequence of alternating "up-and-down pancakes" stacked upon each other. See the two cells in Figure 3.4.

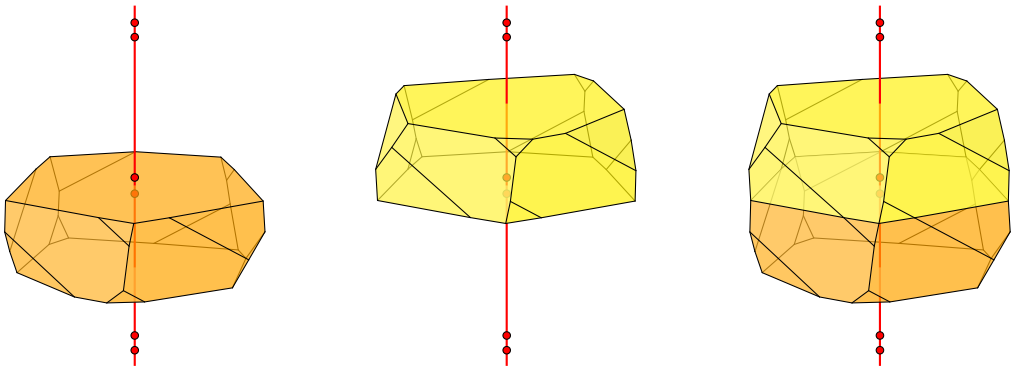

Figure 3.4.: Two cells stacked upon each other with a 180° rotation. The two left figures show each cell individually.

3.7. Starting point close to a rotation center

Let G be a cyclic-type tubical group, and let p be an f-fold rotation center[11] of G^h. Let $[g] \in G^h$ be the clockwise rotation of G^h around p by $\frac{2\pi}{f}$. That is, $g = \cos\frac{\pi}{f} + p\sin\frac{\pi}{f}$.

Choose a point $p_1 \in S^2$ close to p. Since p_1 avoids rotation centers of G^h, its images under $[g]$ are all distinct:

$$p_1,\ p_2 := [g]p_1,\ \ldots,\ p_f := [g]^{f-1}p_1$$

Figure 3.5a and Figure 3.6a show these points around a 4-fold rotation center and a 5-fold rotation center, respectively.

We want to describe the G-orbit for a starting point on K_{p_1}. By Proposition 3.1.4, any point on K_{p_1} will give the same G-orbit, up to congruence. Thus, let $v \in K_{p_1}$ be any point on K_{p_1} and consider its G-orbit.

We will now discuss the G-orbit of v under different assumptions on the subgroup H of elements of G that preserve K_p.

Case 1. H contains a simple rotation fixing K_p of order f: Orbit points around K_p can be grouped into regular f-gons (if $f \geq 3$) or pairs (if $f = 2$). See Figure 3.5c and Figure 3.6c.

Case 2. H contains no simple rotation fixing K_p: Orbit points around K_p form different types of staircases. See Figures 3.5d and 3.5f, and Figures 3.6d–3.6g.

[11] We call p an *f-fold* rotation center of some 3-dimensional point group if f is the largest order of a rotation around p in that group. Hence, a 4-fold rotation center of a group is *not* a 2-fold rotation center of that group.

Case 3. H contains a simple rotation fixing K_p of order not equal to f: This case can only occur when $f = 4$ and the order of that simple rotation is 2. Orbit points around K_p can be grouped into pairs. See Figure 3.5e.

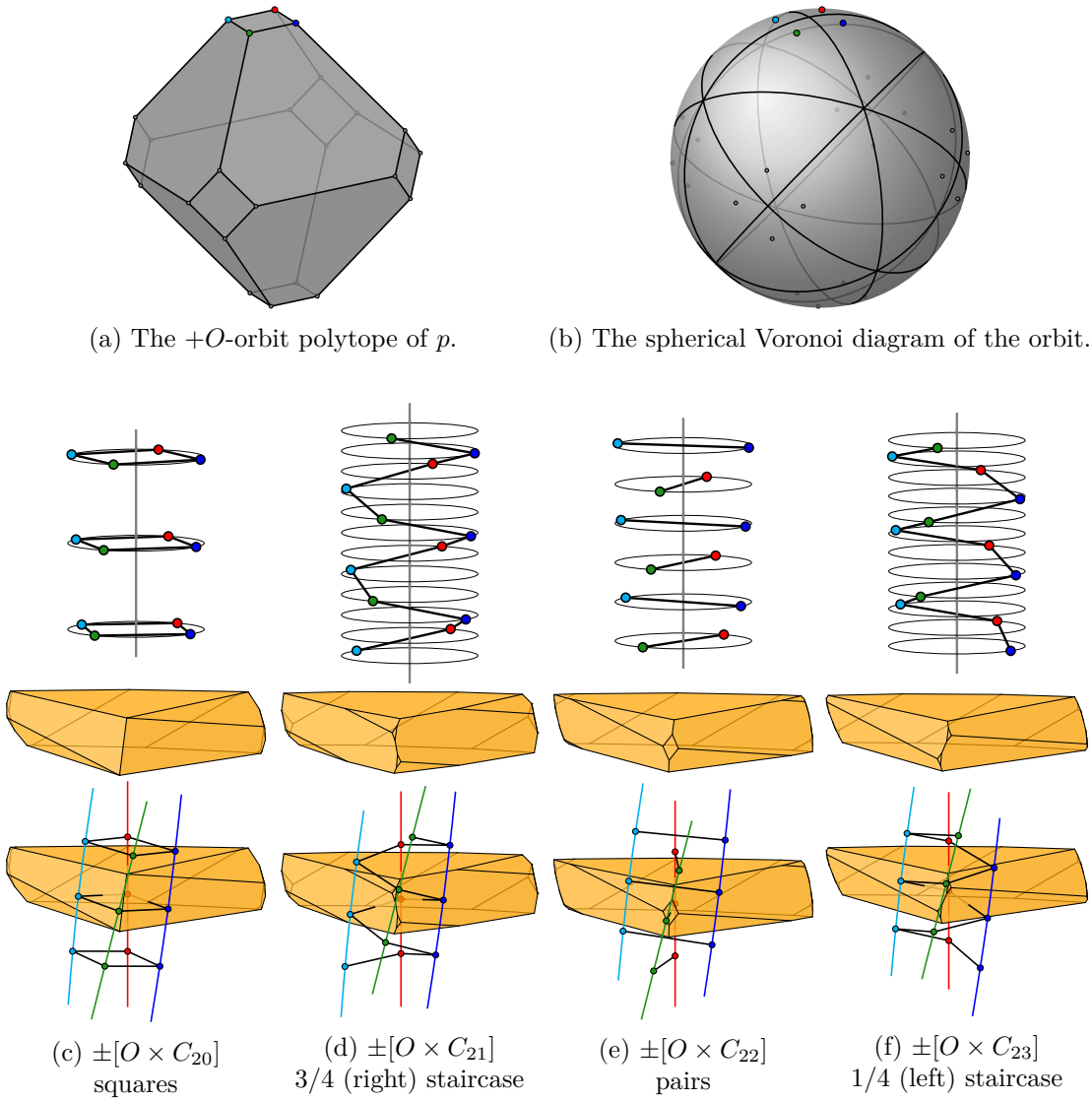

(a) The $+O$-orbit polytope of p.

(b) The spherical Voronoi diagram of the orbit.

(c) $\pm[O \times C_{20}]$ squares

(d) $\pm[O \times C_{21}]$ 3/4 (right) staircase

(e) $\pm[O \times C_{22}]$ pairs

(f) $\pm[O \times C_{23}]$ 1/4 (left) staircase

Figure 3.5.: Orbits of the groups $G = \pm[O \times C_n]$ for a starting point v whose image $p := h(v)$ lies near a 4-fold rotation center of $G^h = +O$. The top row shows the three-dimensional $+O$-orbit polytope of p and the corresponding spherical Voronoi diagram. The four images of p under the 4-fold rotation are colored. The next row shows all possible configurations for orbit points on the corresponding colored circles. The vertical line in each figure is the great circle of $\mathcal{H}$ that correspond to the rotation center. The third row shows a cell of the corresponding polar orbit polytope, and the bottom row combines the previous two rows.

3.8. Starting point on a rotation center

It is also interesting to see what happens if we move p_1 to p. In this case, the points $p_1, \ldots, p_f$ coincide with p, and thus the corresponding circles $K_{p_1}, \ldots, K_{p_f}$ coincide with K_p. We describe next what happens in each of the previous cases.

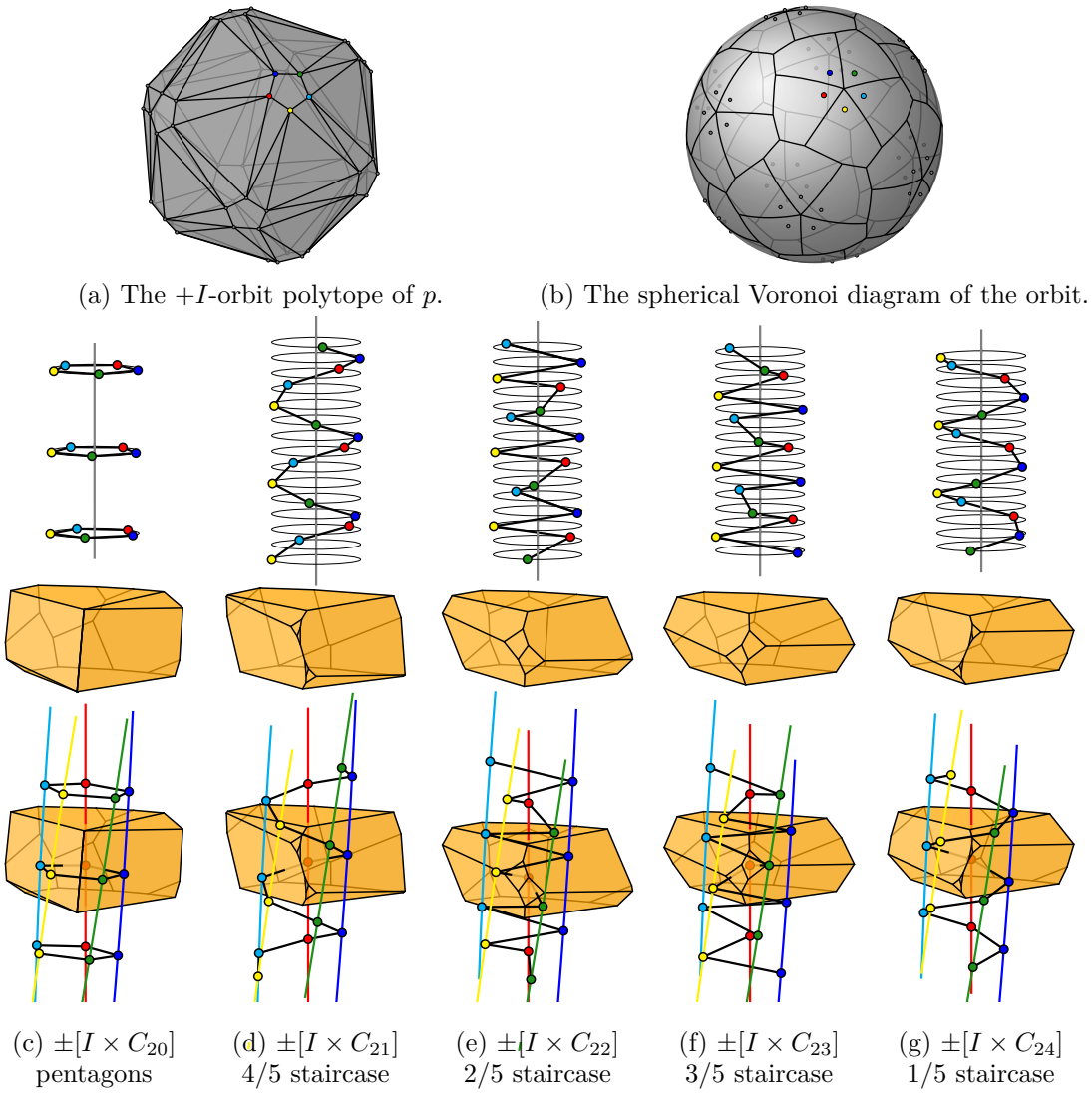

(a) The $+I$-orbit polytope of p.

(b) The spherical Voronoi diagram of the orbit.

(c) $\pm[I \times C_{20}]$ pentagons

(d) $\pm[I \times C_{21}]$ 4/5 staircase

(e) $\pm[I \times C_{22}]$ 2/5 staircase

(f) $\pm[I \times C_{23}]$ 3/5 staircase

(g) $\pm[I \times C_{24}]$ 1/5 staircase

Figure 3.6.: Orbits of the groups $G = \pm[I \times C_n]$ for a starting point v whose image $p := h(v)$ lies near a 5-fold rotation center of $G^h = +I$. The top row shows the three-dimensional $+I$-orbit polytope of p and the corresponding spherical Voronoi diagram. The five images of p under the 5-fold rotation are colored. The next row shows all possible configurations for orbit points on the corresponding colored circles. The vertical line in each figure is the great circle of $\mathcal{H}$ that correspond to the rotation center. The third row shows a cell of the corresponding polar orbit polytope, and the bottom row combines the previous two rows.

Case 1. The orbit points coincide in groups of size f, and thus they form a regular $2n$-gon on K_p. Each orbit point can be mapped to itself by f different elements of G. Thus, in the polar orbit polytope, each cell has an f-fold rotational symmetry whose axis is the cell axis.

Case 2. Orbit points on K_p form a regular $2fn$-gon. Each orbit point can be mapped to itself by a unique element of G. However, the orbit has extra symmetries, which come from the supergroup of G that we obtain by extending G by the new symmetry $[1, e_{fn}]$. Thus, in total, each orbit point can be mapped to itself by f symmetries. Accordingly, in the polar orbit polytope, each cell has an f-fold rotational symmetry whose axis is the cell axis.

Case 3. Orbit points on K_p form a regular $4n$-gon. Each orbit point can be mapped to

itself by 2 different elements of G. However, the orbit has extra symmetries, which come from the supergroup of G that we obtain by extending G by the new symmetry $[1, e_{2n}]$. Thus, each orbit point can be mapped to itself by *extra* 2 symmetries. Accordingly, in the polar orbit polytope, each cell has a 4-fold rotational symmetry whose axis is the cell axis.

See Section 3.9 for particular examples and Appendix B for a coverage of all groups.

3.8.1. Supergroups of cyclic type

The cyclic-type supergroups described in Case 2 and Case 3 are listed in Table 3.2 for each group class and each type of rotation center. For large enough n, this supergroup is the largest cyclic-type symmetry group of the orbit. In most cases, this is the same class of group with a larger parameter n. The only exception are the groups $G = \pm[T \times C_n]$ when p is a 2-fold rotation center of $G^h = +T$. As can be seen in Table 3.2, the symmetry groups of cyclic type of the orbit are then of the form $\pm[O \times C_{n'}]$ or $\pm\frac{1}{2}[O \times C_{n'}]$.

The reason for this exceptional behavior can already be seen at the level of the groups G^h in three dimensions: On S^2, the group $+T$ is an index-2 subgroup of $+O$. The 2-fold rotation centers p of $+T$ coincide with the 4-fold rotation centers of $+O$, and the orbit has size 6 in both cases.

The group $G_1 := \pm[T \times C_n]$ is an index-2 subgroup of $G_2 := \pm[O \times C_n]$. One can show that when $n \equiv 0 \bmod 4$, the orbits of both groups have a simple rotation fixing K_p of order 2 (for G_1) and of order 4 (for G_2). In particular, both orbits follow Case 1 above and they form a regular $2n$-gon on each orbit circle. Since they also have the same orbit circles, these two orbits coincide. The other cases ($n \equiv 2 \bmod 4$, and n odd) are similar.

Accordingly, all cells of the groups $\pm[T \times C_n]$ when p is a 2-fold rotation center (Section B.4.2), appear also as cells of the groups $\pm\frac{1}{2}[O \times C_{n'}]$ when p is a 4-fold rotation center (Figure 3.8), and those when n is a multiple of 4 also appear for the groups $\pm[O \times C_{n'}]$ (Section B.2.1).

It is perhaps instructive to look at a particular example and compare the groups $\pm[T \times C_{24}]$ (Figure B.9) and $\pm\frac{1}{2}[O \times C_{24}]$ (Figure 3.8 for $n = 12$), which have equal, 4-sided cells. The allowed rotations between consecutive cells, apart from the necessary adjustment of $\pi/24$, are $0°$ and $180°$ in the first case and $\pm 90°$ in the second case. The common supergroup that has all four rotations is $\pm[O \times C_{24}]$ (Figure B.3).

3.8.2. Supergroups of dihedral type, and flip symmetries

For each cyclic-type tubical group and for each rotation center p of its induced group on S^2, there is a dihedral-type tubical group whose induced group on S^2 has a mirror through p, and the cyclic-type group is an index-2 subgroup of the dihedral-type group. Thus, by Proposition 3.6.1, the orbit of the cyclic-type group for a starting point on K_p has extra symmetries coming from (a geometrically equal copy of) that dihedral-type tubical group. In particular, each cell of the polar orbit polytope will have a flip symmetry. See the figures in Section 3.9 and Appendix B. The dihedral-type supergroups are listed in Table 3.2.

3.9. Two examples of special starting points

In this section we will discuss two cases of non-generic starting points. In particular, we want to consider orbits of cyclic-type tubical groups where the image of the starting point under h is a rotation center of the induced group. In Table 3.2 and Appendix B, we summarize the results for the remaining groups and rotation centers.

center type	#tubes	n	orbit size	cyclic-type supergroup	dihedral-type supergroup	figure
$\pm[I \times C_n]$						
5-fold	12	0 mod 5 else	$24n$ $120n$	– $\pm[I \times C_{5n}]$	$\pm[I \times D_{2n}]$ $\pm[I \times D_{10n}]$	3.7
3-fold	20	0 mod 3 else	$40n$ $120n$	– $\pm[I \times C_{3n}]$	$\pm[I \times D_{2n}]$ $\pm[I \times D_{6n}]$	B.1
2-fold	30	0 mod 2 else	$60n$ $120n$	– $\pm[I \times C_{2n}]$	$\pm[I \times D_{2n}]$ $\pm[I \times D_{4n}]$	B.2
$\pm[O \times C_n]$						
4-fold	6	0 mod 4 2 mod 4 else	$12n$ $24n$ $48n$	– $\pm[O \times C_{2n}]$ $\pm[O \times C_{4n}]$	$\pm[O \times D_{2n}]$ $\pm[O \times D_{4n}]$ $\pm[O \times D_{8n}]$	B.3
3-fold	8	0 mod 3 else	$16n$ $48n$	– $\pm[O \times C_{3n}]$	$\pm[O \times D_{2n}]$ $\pm[O \times D_{6n}]$	B.4
2-fold	12	0 mod 2 else	$24n$ $48n$	– $\pm[O \times C_{2n}]$	$\pm[O \times D_{2n}]$ $\pm[O \times D_{4n}]$	B.5
$\pm\frac{1}{2}[O \times C_{2n}]$						
4-fold	6	2 mod 4 0 mod 4 else	$12n$ $24n$ $48n$	– $\pm[O \times C_{2n}]$ $\pm[O \times C_{4n}]$	$\pm\frac{1}{2}[O \times \overline{D}_{4n}]$ $\pm[O \times D_{4n}]$ $\pm[O \times D_{8n}]$	3.8
3-fold	8	0 mod 3 else	$16n$ $48n$	– $\pm\frac{1}{2}[O \times C_{6n}]$	$\pm\frac{1}{2}[O \times \overline{D}_{4n}]$ $\pm\frac{1}{2}[O \times \overline{D}_{12n}]$	B.6
2-fold	12	0 mod 2 else	$24n$ $48n$	– $\pm\frac{1}{2}[O \times C_{4n}]$	$\pm\frac{1}{2}[O \times \overline{D}_{4n}]$ $\pm\frac{1}{2}[O \times \overline{D}_{8n}]$	B.7
$\pm[T \times C_n]$						
3-fold	4	0 mod 3 else	$8n$ $24n$	– $\pm[T \times C_{3n}]$	$\pm\frac{1}{2}[O \times D_{2n}]$ $\pm\frac{1}{2}[O \times D_{6n}]$	B.8
2-fold	6	0 mod 4 2 mod 4 else	$12n$ $12n$ $24n$	$\pm[O \times C_n]$ $\pm\frac{1}{2}[O \times C_{2n}]$ $\pm\frac{1}{2}[O \times C_{4n}]$	$\pm[O \times D_{2n}]$ $\pm\frac{1}{2}[O \times \overline{D}_{4n}]$ $\pm\frac{1}{2}[O \times \overline{D}_{8n}]$	B.9
$\pm\frac{1}{3}[T \times C_{3n}]$						
3-fold I	4	1 mod 3 else	$8n$ $24n$	– $\pm[T \times C_{3n}]$	$\pm\frac{1}{6}[O \times D_{6n}]$ $\pm\frac{1}{2}[O \times D_{6n}]$	B.11
3-fold II	4	2 mod 3 else	$8n$ $24n$	– $\pm[T \times C_{3n}]$	$\pm\frac{1}{6}[O \times D_{6n}]$ $\pm\frac{1}{2}[O \times D_{6n}]$	B.10
2-fold	6	0 mod 2 else	$12n$ $24n$	– $\pm\frac{1}{3}[T \times C_{6n}]$	$\pm\frac{1}{6}[O \times D_{6n}]$ $\pm\frac{1}{6}[O \times D_{12n}]$	B.12

Table 3.2.: The columns "cyclic-type supergroup" and "dihedral-type supergroup" indicate the largest symmetry group of the orbit that is tubical of that type. In Section 3.9, we extensively discuss two cases from the table. For the other cases, we summarize the results in Appendix B. The last column refers to the figure that shows cells of the corresponding polar orbit polytope with different values for n. The two types of 3-fold rotation centers for $\pm\frac{1}{3}[T \times C_{3n}]$ (3-fold I and 3-fold II) are defined in Section 3.14.

3.9.1. $\pm[I \times C_n]$, 5-fold rotation center

Let $G = \pm[I \times C_n]$. We want to consider the G-orbit of a point whose image under h is a 5-fold rotation center p of $+I$. By Proposition 3.1.4, any starting point on K_p will give the same orbit, up to congruence. Notice also that the other orbit circles correspond to the other 5-fold rotation centers of $+I$. Thus, choosing p to be an arbitrary 5-fold rotation center will yield the same orbit, up to congruence.

So let p be the 5-fold rotation center $p = \frac{1}{\sqrt{\varphi^2+1}}(0, 1, \varphi)$, where $\varphi = \frac{1+\sqrt{5}}{2}$. Then $g = -\omega i_I = \cos\frac{\pi}{5} + p\sin\frac{\pi}{5} \in 2I$ defines the 72° clockwise rotation $[g] \in +I$ around p. By Proposition 2.1.5, we know the elements of G that preserve K_p. These elements form a subgroup $H = \langle [g, 1], [1, e_n] \rangle$ of order $10n$. Proposition 2.1.5 also tells us the H acts on K_p as a 2-dimensional cyclic group.

The rotation $[g, 1]$ rotates $\vec{K}_p$ by $-\frac{\pi}{5}$, while $[1, e_n]$ rotates it by $\frac{\pi}{n}$. Thus, the G-orbit of a point on K_p forms a regular $\mathrm{lcm}(2n, 10)$-gon on K_p. We will discuss the orbit of a point $v \in K_p$ depending on the value of n. Figure 3.7 shows cells of the polar orbit polytopes for different values of n.

- If n is a multiple of 5, then the orbit points form a regular $2n$-gon on each orbit circle. So, every orbit point can be mapped to itself by 5 different elements of G. This is reflected on the cells of the polar orbit polytope where each cell has a 5-fold rotational symmetry whose axis is the cell axis.

  This case corresponds to Case 1 in Section 3.8, where H contains a simple rotation of order 5 fixing K_p.

  The element $[1, e_n]$ of G maps an orbit point to an adjacent one on the same circle. Correspondingly, on each tube, the cells of the polar orbit polytope are stacked upon each other with a right screw by $\frac{\pi}{n}$.

- If n is not a multiple of 5, then the orbit points form a regular $10n$-gon on each orbit circle. That is, the orbit is free. So, every orbit point can be mapped to itself by a unique element of G. However, this orbit has extra symmetries. In particular, the rotation $[1, e_{5n}]$ maps each orbit point to an adjacent one on the same circle. Adjoining $[1, e_{5n}]$ to G gives the supergroup $\pm[I \times C_{5n}]$, whose orbit of n follows the first case. Accordingly, each cell of the polar orbit polytope has a 5-fold symmetry whose axis is the cell axis.

  This case corresponds to Case 2 in Section 3.8, where H does not contain any simple rotation fixing K_p.

  The symmetry $[1, e_{5n}]$ (which is not in G) maps an orbit point to an adjacent one on the same circle. Correspondingly, on each tube, the cells of the polar orbit polytope are stacked upon each other with a right screw by $\frac{\pi}{5n}$.

In accordance with Section 3.8.2, every cell has a flip symmetry, which is not included in G. It comes from (a group geometrically equal to) the group $\pm[I \times D_{2n}]$, which contains G as an index-2 subgroup.

The top and bottom faces in each cell are congruent. They resemble the shape of a pentagon. This corresponds to the fact that the spherical Voronoi cell of the $+I$-orbit of p on the 2-sphere is a spherical regular pentagon, as shown in the top right picture of Figure 3.7. (Refer to the discussion in Section 3.3.)

Since the $+I$-orbit of p has size 12, the G-orbit of v lies on 12 orbit circles. Accordingly, the cells of the polar orbit polytope can be decomposed into 12 tubes, each with $\mathrm{lcm}(2n, 10)$ cells. In the PDF-file of this article, the interested reader can click on the pictures in Figure 3.7 for an interactive visualization of these tubes. We refer to Section 3.13 for more details.

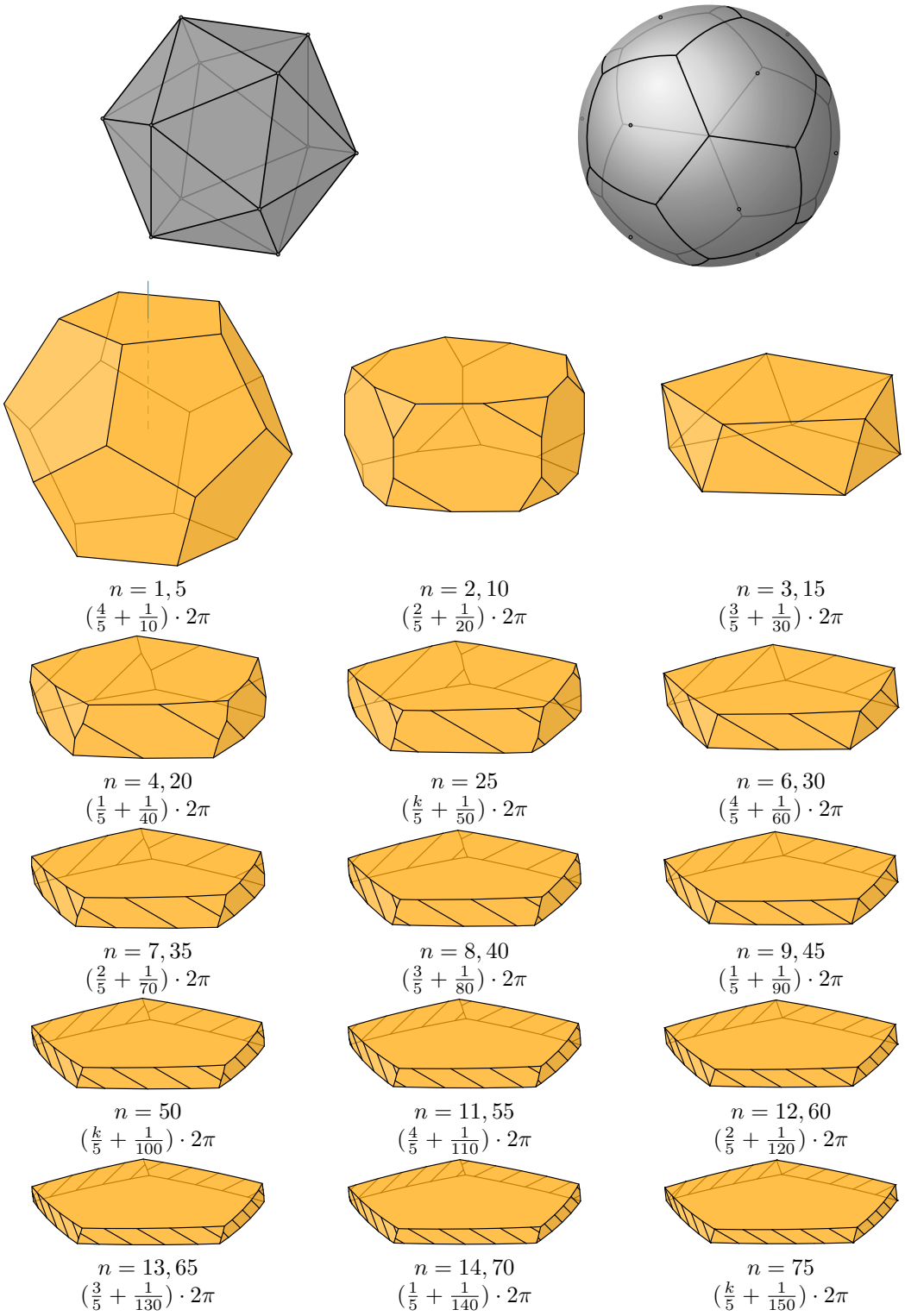

Figure 3.7.: The $+I$-orbit polytope of the 5-fold rotation center $p = (1/\sqrt{\varphi^2 + 1})(0, 1, \varphi)$ of $+I$, where $\varphi = (1 + \sqrt{5})/2$ (top left), and the spherical Voronoi diagram of that orbit (top right). The remaining pictures show cells of polar $\pm[I \times C_n]$-orbit polytopes for a starting point on K_p for different values of n. In addition we indicate the counterclockwise angle (as seen from the top) by which the group rotates as it proceeds from a cell to the consecutive cell above. When the same orbit arises for several values of n, then the indicated angle is the unique valid angle only for the smallest value n_0 that is specified. For a larger value $n = 5n_0$, this can be combined with arbitrary multiples of a 5-fold rotation. The polar orbit polytope can be decomposed into 12 tubes, each with $\mathrm{lcm}(2n, 10)$ cells. The blue vertical line indicates the cell axis, the direction towards the next cell along K_p. For an appropriate choice of starting point on K_p, the group $\pm[I \times D_{2n}]$ produces the same orbit.

In accordance with the program set out in Figure 1.2 in Chapter 1 to understand the group by its action on the orbit polytope, we will now work out how each cell is mapped to the adjacent cell in the same tube. This requires a small number-theoretic calculation. The mapping between adjacent cells is obtained in cooperation between the right group and the left group. In particular, to get a rotation by $\frac{2\pi}{\mathrm{lcm}(2n,10)}$ along the orbit circle $\vec{K}_p$, we have to combine a left rotation by $-a\cdot\frac{\pi}{5}$ with a right rotation by $b\cdot\frac{\pi}{n}$, resulting in the angle

$$\frac{b\pi}{n}-\frac{a\pi}{5}=\frac{2\pi}{\mathrm{lcm}(2n,10)}. \tag{3.3}$$

For example, for $n=12$ we can solve this by $a=2, b=5$. The right screw angle between consecutive slices (or orbit points) is then $\frac{b\pi}{n}+\frac{a\pi}{5}$. Using (3.3), this can be rewritten as

$$\frac{a\pi}{5}+\frac{b\pi}{n}=\frac{2a\pi}{5}+\frac{2\pi}{\mathrm{lcm}(2n,10)}=\left(\frac{a}{5}+\frac{1}{\mathrm{lcm}(2n,10)}\right)\cdot 2\pi, \tag{3.4}$$

which is $(\frac{2}{5}+\frac{\pi}{120})\cdot 2\pi$ in our example. This angle is always of the form $(\frac{a}{5}+\frac{1}{\mathrm{lcm}(2n,10)})\cdot 2\pi$ for some integer a, in accordance with the requirement to match the pentagonal shape. The value a can never be 0. The rotation angles for different values of n are listed in Figure 3.7.

When n is not a multiple of 5, there is one element of the group that maps a cell to the upper adjacent one. Thus, a has a unique value. When n is a multiple of 5, each cell has a 5-fold symmetry included in the group. Thus, all values of a are permissible.

3.9.2. $\pm\frac{1}{2}[O\times C_{2n}]$, 4-fold rotation center

Let $G=\pm\frac{1}{2}[O\times C_{2n}]$. We want to consider the G-orbit of a point whose image under h is a 4-fold rotation center p of $+O$. The discussion will closely parallel that of the group from the previous section, but in connection with the 4-fold rotation, we will also meet Case 3. Any of the 4-fold rotation centers p gives the same orbit. So let p be the 4-fold rotation center $p=(0,1,0)$. Then $g=-\omega i_O=\cos\frac{\pi}{4}+p\sin\frac{\pi}{4}\in 2O$ defines the 90° clockwise rotation $[g]\in+O$ around p. By Proposition 2.1.5, we determine the elements of G that preserve K_p as the subgroup $H=\langle[g,e_{2n}],[1,e_n]\rangle$ of order $8n$, which acts on K_p as a 2-dimensional cyclic group. The rotation $[g,e_{2n}]$ rotates $\vec{K}_p$ by $-\frac{\pi}{4}+\frac{\pi}{2n}=-\frac{(n-2)\pi}{4n}$. Its order is

$$\frac{2\pi}{\gcd(\frac{(n-2)\pi}{4n},2\pi)}=\frac{2\pi}{\frac{\pi}{4n}\gcd(n-2,8n)}=\frac{8n}{\gcd(n-2,8n-8(n-2))}=\frac{8n}{\gcd(n-2,16)}.$$

The other operation, $[1,e_n]$ rotates it by $\frac{\pi}{n}$. Thus, the G-orbit of a point on K_p forms a regular polygon with $\mathrm{lcm}(2n,\frac{8n}{\gcd(n-2,16)})$ sides on K_p. The denominator $\gcd(n-2,16)$ can take the values $1,2,4,8,16$, but in the overall expression, the values $4,8,16$ make no distinction, and thus we can simplify the expression for the number of sides to $\frac{8n}{\gcd(n-2,4)}$.

The structure of the orbit of a point $v\in K_p$ depends on n. Cells of the polar orbit polytopes for different values of n are shown in Figure 3.8.

- If $n-2$ is a multiple of 4, then $\gcd(n-2,4)=4$ and $\frac{8n}{\gcd(n-2,4)}=2n$. The orbit points form a regular $2n$-gon on each orbit circle, and every point can be mapped to itself by 4 different elements of G. This is reflected on the polar orbit polytope where each cell has a 4-fold symmetry whose axis is the cell axis.

  This corresponds to Case 1 in Section 3.8, where H contains a simple rotation of order 4 fixing K_p.

  The element $[1,e_n]$ of G maps an orbit point to an adjacent one on the same circle. Correspondingly, on each tube, the cells of the polar orbit polytope are stacked

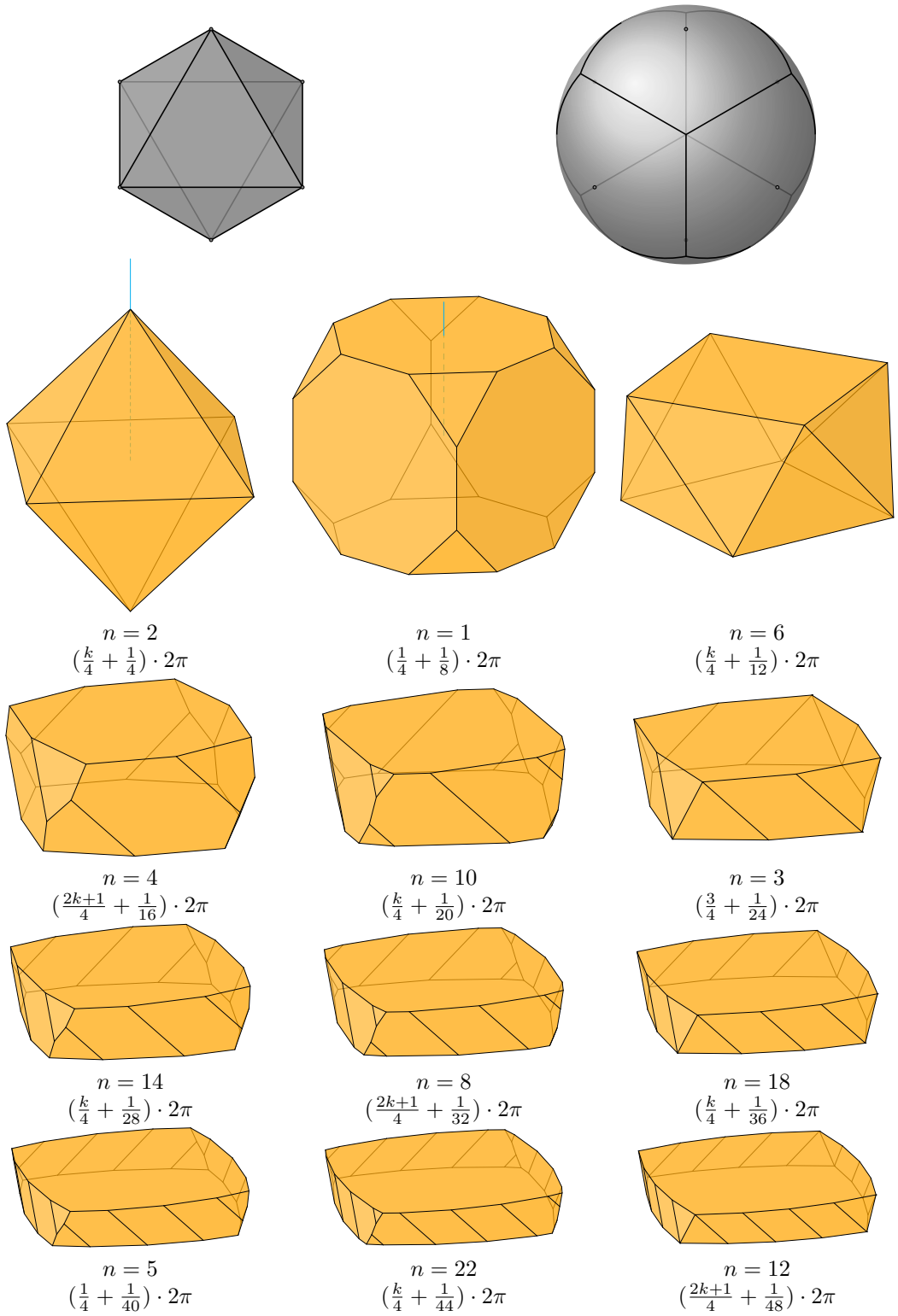

Figure 3.8.: The $+O$-orbit polytope of the 4-fold rotation center $p = (0, 1, 0)$ of $+O$ (top left), and the spherical Voronoi diagram of that orbit (top right). The remaining pictures show cells of polar $\pm\frac{1}{2}[O \times C_{2n}]$-orbit polytopes for a starting point on K_p for different values of n. In addition we indicate the counterclockwise angle (as seen from the top) by which the group rotates as it proceeds from a cell to the consecutive cell above. The polar orbit polytope can be decomposed into 6 tubes, each with $\frac{8n}{\gcd(n-2,4)}$ cells. The blue vertical line indicates the cell axis, the direction towards the next cell along K_p. For an appropriate choice of starting point on K_p, the group $\pm\frac{1}{2}[O \times \overline{D}_{4n}]$ produces the same orbit. When $n = 2$, the cells that should form a tube touch each other only in a vertex.

upon each other with a right screw by $\frac{\pi}{2n}$.

- If $n-2 \equiv 2 \bmod 4$, then $\gcd(n-2,4) = 2$ and $\frac{8n}{\gcd(n-2,4)} = 4n$. The orbit points form a regular $4n$-gon on each orbit circle, and every point can be mapped to itself by 2 different elements of G. However, this orbit has extra symmetries. In particular, the rotation $[1, e_{2n}]$ maps each orbit point to an adjacent one on the same circle. Adjoining $[1, e_{2n}]$ to G gives the supergroup $\pm[O \times C_{2n}]$, which contains G as an index-2 subgroup. Thus, each orbit point can be mapped to itself by 2 extra symmetries that are not in G. Accordingly, as in the first case, every cell of the polar orbit polytope has a 4-fold symmetry whose axis is the cell axis.

  This corresponds to Case 3 in Section 3.8, where H contains a simple rotation of order 2 fixing K_p.

  The symmetry $[1, e_{2n}]$ (which is not in G) maps an orbit point to adjacent one on the same circle. Correspondingly, on each tube, the cells of the polar orbit polytope are stacked upon each other with a right screw by $\frac{\pi}{2n}$.

- If $n-2$ is odd, then $\gcd(n-2,4) = 1$ and $\frac{8n}{\gcd(n-2,4)} = 8n$. The orbit is free. The orbit forms a regular $8n$-gon on each orbit circle. Every point can be mapped to any other point by a unique element of G. Again, the orbit has extra symmetries. In particular, the rotation $[1, e_{4n}]$ maps each orbit point to an adjacent one on the same circle. Adjoining $[1, e_{4n}]$ to G gives the supergroup $\pm[O \times C_{4n}]$, which contains G as an index-4 subgroup. Thus, each orbit point can be mapped to itself by 4 symmetries. Accordingly, as in the other cases, every cell of the polar orbit polytope has a 4-fold symmetry whose axis is the cell axis.

  This corresponds to Case 2 in Section 3.8, where H does not contain a simple rotation fixing K_p.

  The symmetry $[1, e_{4n}]$ (which is not in G) maps an orbit point to the next one on the same circle. Correspondingly, on each tube, the cells of the polar orbit polytope are stacked upon each other with a right screw by $\frac{\pi}{4n}$.

In accordance with Section 3.8.2, every cell has a flip symmetry, which is not included in G. It comes from (a group geometrically equal to) the group $\pm\frac{1}{2}[O \times \overline{D}_{4n}]$, which contains G as an index-2 subgroup.

The top and bottom faces in each cell are congruent. They resemble the shape of a rounded square, in agreement with the quadrilateral Voronoi cell on the 2-sphere, as shown in the top right figure in Figure 3.8.

Since the $+O$-orbit of p has size 6, the G-orbit of v lies on 6 orbit circles. Accordingly, the cells of the polar orbit polytope can be decomposed into 6 tubes, each with $\frac{8n}{\gcd(n-2,4)}$ cells.

Similar to the previous section, one can work out the right screw angle (in G) between consecutive slices. To summarize: When $n-2$ is odd, there is a unique angle of the form: $(\frac{k_0}{4} + \frac{1}{8n}) \cdot 2\pi$ (with specific $k_0 = 1$, 2, or 3). When $n-2 \equiv 2 \bmod 4$, there are two angles: $(\frac{2k+1}{4} + \frac{1}{4n}) \cdot 2\pi$ (with arbitrary k). When $n-2$ is a multiple of 4, there are four angles: $(\frac{k}{4} + \frac{1}{2n}) \cdot 2\pi$ (with arbitrary k).

3.10. Consequences for starting points near rotation centers

In Sections 3.7 and 3.8 we have discussed the different cases that can arise for an orbit *near* a rotation axis and *on* a rotation axis. Indeed, we can confirm this relation by comparing Figure 3.6 and Figure 3.7. By the analysis that lead to Figure 3.6, an orbit

of $\pm[I \times C_n]$ near a 5-fold rotation axis forms a 4/5, 2/5, 3/5, or 1/5 staircase if $n \equiv 1, 2, 3, 4 \bmod 5$, respectively, and it forms pentagons if n is a multiple of 5. We can check in Figure 3.7 that these values are precisely the specified rotations (up to the twist by $\frac{\pi}{5n}$), except when n is a multiple of 5, and in that case all five rotations are allowed. Similarly, Figure 3.5 corresponds with Figure B.3.

Conversely, we can consult the appropriate entries in Appendix B for orbits *on* a rotation axis to conclude what type of pentagons, quadrilaterals, triangles, pairs, or staircases to expect for an orbit *near* this rotation axis.

3.11. Mappings between different tubes

Continuing the discussion of the tubes for the groups $G = \pm\frac{1}{2}[O \times C_{2n}]$, from Section 3.9.2, we will now continue with the program set out in Figure 1.2 in Chapter 1, by asking, for this example, how cells in different tubes are mapped to each other. The cells in Figure 3.8 have a roughly four-sided shape. At *corners* of these quadrilaterals, three tubes meet.

To understand what is happening there, we imagine putting a starting point v' near a corner. Then $h(v')$ is near a three-fold rotation center of $+O$. Near such a rotation center, the orbit forms either a set of triangles, or a left or right staircase. As just discussed, we can check this by consulting the pictures for the orbit *on* a three-fold rotation axis: Figure B.6.

We see that those cells of Figure 3.8 that have a straight line segment A between the top and the bottom face at the corners ($n = 6, 3, 18, 12$) correspond to cases where the orbit of v' consists of triangles. Indeed, one can imagine three cells arranges around a common edge A. (The cells don't lie perpendicular to the axis A, but they are twisted.)

For the remaining cases ($n = 1, 4, 10, 14, 8, 5, 22$) the edge is broken into three parts between the top and the bottom face, and this is where the cells are arranged in a staircase-like fashion.

3.12. Small values of n

For small values of n, some of the cyclic-type tubical groups recover well-known decompositions of regular/uniform polytopes into tubes (or more commonly knows as rings). These appear in various places in the literature. We list some of the references. Next to each group, we state the rotation center of the induced group that is the image of the starting point.

- $\pm[I \times C_1]$ and 5-fold rotation center (Figure 3.7): We get the decomposition of the 120-cell into 12 tubes, each with 10 regular dodecahedra.[12]. Figure 5.2 shows a picture of three dodecahedra from one tube, see also [23, Figure 21], [15, p. 75] and Coxeter [18, p. 53].
- $\pm[O \times C_1]$ and 4-fold rotation center (Figure B.3): We get the decomposition of the bitruncated 24-cell (the 48-cell) into 6 tubes, each with 8 truncated cubes, stacked upon the octagonal faces.
- $\pm[O \times C_1]$ and 3-fold rotation center (Figure B.4): We get the decomposition of the bitruncated 24-cell (the 48-cell) into 8 tubes, each with 6 truncated cubes, stacked upon the triangular faces. [15, p. 75-76].

[12] A remarkable paper model of a Schlegel diagram with two rings was produced by Robert Webb, https://youtu.be/2nTLI89vdzg. An interesting burr puzzle was made in [64] using pieces of these rings.

- $\pm[T \times C_1]$ and 3-fold rotation center (Figure B.8): We get the decomposition of the 24-cell into 4 tubes, each with 6 octahedra [15, p. 74], [3].
- $\pm[T \times C_1]$ and 2-fold rotation center (Figure B.9): We get the decomposition of the 24-cell into 6 tubes, each with 4 octahedra, touching each other via vertices.
- $\pm\frac{1}{3}[T \times C_3]$ and 3-fold (type I) rotation center (Figure B.10): This is a degenerate case. We get the decomposition of the hypercube into 4 "tubes", but each "tube" is just a pair of opposite cube faces.

We remark that the orbit of $G = \pm[L \times C_1]$, is the same, up to congruence, for any starting point. This follows since the G-orbit of a point $v \in \mathbb{R}^4$ can be obtained from the G-orbit of the quaternion 1 by applying the rotation $[1, v]$:

$$\text{orbit}(v, G) = \{\, \bar{l}v \mid l \in L\} = [1, v]\{\, \bar{l} \mid l \in L\} = [1, v]\text{orbit}(1, G).$$

3.13. Online gallery of polar orbit polytopes

The interested reader can explore polar orbit polytopes for the cyclic-type tubical groups with all special choices of starting points in an online gallery that provides interactive three-dimensional views.[13]

The polytopes are shown in a central projection to the three-dimensional tangent space at the starting point v of the orbit. The projection center lies outside the polytope, close to the cell F_0 opposite to v. In the projection, F_0 becomes the outer cell that (almost) encloses all remaining projected cells. The orientation of the outer cell is reversed with respect to the other cells. We are mostly interested not in F_0 but in the cells near v, which are distorted the least in the projection, and as a consequence, we go with the majority and ensure that *these* cells are oriented according to our convention (Section 1.3). For large values on n, we have refrained from constructing true Schlegel diagrams, because this would have resulted in tiny inner cells. As a result, cells near the boundary of the projection wrap around and overlap.

The goal of the gallery is to show the decomposition of the polytopes into tubes, and how these tubes are structured and interact with each other. It is possible to remove cells one by one to see more structure. The order of the cells is based on the distances of their orbit points to the starting point v.

3.14. $\pm[T \times C_n]$ versus $\pm\frac{1}{3}[T \times C_{3n}]$

Looking at the tubical groups in Table 3.1, we see that there are groups G with the same induced symmetry group G^h on S^2. Thus, for the same starting point, these groups have the same orbit circles. However, they differ in the way how the points on different circles are arranged relative to each other.

In this section we will consider the case where the induced group is $+T$. For the same n, we will compare the actions of $\pm[T \times C_n]$ and $\pm\frac{1}{3}[T \times C_{3n}]$ on and around the circles of $\mathcal{H}$ that correspond to rotation centers of $+T$. We will see that these two groups have different sets of fixed circles of $\mathcal{H}$, which correspond to 3-fold rotation centers of $+T$. On such a fixed circle, the size of the orbit is reduced by a factor of 3 (from $24n$ to $8n$, see Table 3.2). In Figures 3.10 and 3.11, we visualize the effect of that difference on the orbit points and the cells of the polar orbit polytope around these circles. We will see that triangles and both types of staircases appear in $\pm[T \times C_n]$ and $\pm\frac{1}{3}[T \times C_{3n}]$, depending on n. In this sense, there is no sharp geometric distinction between the two families.

[13] https://www.inf.fu-berlin.de/inst/ag-ti/software/DiscreteHopfFibration/. In the PDF-file of this article, the pictures of the cells in the figures in Section 3.9 and Appendix B are linked to the corresponding entries in the gallery.

2-fold rotation center. Let $p \in S^2$ be a 2-fold rotation center of $+T$ and let $[g] \in +T$ be the 180° rotation around p. If n is even, then $[g, e_2]$ is in both groups, and it is a simple rotation that fixes K_p. If n is odd, then K_p is not fixed. Thus, for the same n, $\pm[T \times C_n]$ and $\pm\frac{1}{3}[T \times C_{3n}]$ have the same set of fixed circles that correspond to 2-fold rotation centers of $+T$.

3-fold rotation center. The eight 3-fold rotation centers of $+T$ belong to two conjugacy classes, depending on which $+T$-orbit they are in. The rotation centers of *type I*, are the ones in the orbit of $p_0 = (-1, -1, -1)$, and the rotation centers of *type II*, are the ones in the orbit of $-p_0 = (1, 1, 1)$. We will see that the group $\pm[T \times C_n]$ does not distinguish between the circles K_{p_0} and K_{-p_0}. In particular, the orbit of a starting point on p_0 is congruent to the one of a starting point on $-p_0$. However, this is not the case for $\pm\frac{1}{3}[T \times C_{3n}]$.

The quaternion $-\omega \in 2T$ defines the 120° clockwise rotation $[-\omega]$ around p_0. That is $-\omega = \cos\frac{\pi}{3} + p_0 \sin\frac{\pi}{3}$. The quaternion $-\omega^2 \in 2T$ defines the 120° clockwise rotation $[-\omega^2]$ around $-p_0$. That is $-\omega^2 = \cos\frac{\pi}{3} - p_0 \sin\frac{\pi}{3}$.

By Proposition 2.1.5, the set of rotations that preserve K_{p_0} is the same as the set of rotations that preserve K_{-p_0}. Let's look at these rotations inside each of the two groups.

- The elements of $\pm[T \times C_n]$ that preserve K_{p_0} (and K_{-p_0}) form the subgroup

$$\langle [-\omega, 1], [1, e_n] \rangle = \langle [-\omega^2, 1], [1, e_n] \rangle$$

of order $6n$. The rotation $[-\omega, 1]$ rotates K_{p_0} by $\frac{\pi}{3}$ in one direction, while $[1, e_n]$ rotates it by $\frac{\pi}{n}$ in the other direction. Thus, the $\pm[T \times C_n]$-orbit of a starting point on K_{p_0} forms a regular $\mathrm{lcm}(2n, 3)$-gon on K_{p_0}. Similarly, the $\pm[T \times C_n]$-orbit of a starting point on K_{-p_0} forms a regular $\mathrm{lcm}(2n, 3)$-gon on K_{-p_0}. In particular, if n is a multiple of 3, $\pm[T \times C_n]$ has a simple rotation $([-\omega, e_3])$ fixing K_p and a simple rotation $([-\omega^2, e_3])$ fixing K_{-p_0}. If n is not a multiple of 3, $\pm[T \times C_n]$ has no simple rotation fixing K_{p_0} or K_{-p_0}, and the orbit points on the three circles form a left or right staircase.

- The elements of $\frac{1}{3}[T \times C_{3n}]$ that preserve K_{p_0} (and K_{-p_0}) form the subgroup

$$\langle [-\omega, e_{3n}], [1, e_n] \rangle = \langle [-\omega^2, e_{3n}^2], [1, e_n] \rangle$$

of order $6n$. We will now consider the action of this subgroup on the circles K_{p_0} and K_{-p_0}. On K_{p_0}, the rotation $[-\omega, e_{3n}]$ rotates K_{p_0} by $\frac{\pi}{3} - \frac{\pi}{3n} = \frac{(n-1)\pi}{3n}$. Its order is

$$\frac{2\pi}{\gcd(\frac{(n-1)\pi}{3n}, 2\pi)} = \frac{2\pi}{\gcd(\frac{\pi}{3n}(n-1), 6n\frac{\pi}{3n})} = \frac{2\pi}{\frac{\pi}{3n}\gcd(n-1, 6n)} = \frac{6n}{\gcd(n-1, 6)}.$$

Thus, the $\pm\frac{1}{3}[T \times C_{3n}]$-orbit of a starting point on K_{p_0} forms a regular polygon with $\mathrm{lcm}(2n, \frac{6n}{\gcd(n-1,6)}) = \frac{6n}{\gcd(n-1,3)}$ sides. In particular, if $n-1$ is a multiple of 3, $\pm\frac{1}{3}[T \times C_{3n}]$ has a simple rotation fixing K_{p_0}. Otherwise, G has no simple rotation fixing K_{p_0}. On K_{-p_0}, the rotation $[-\omega^2, e_{3n}^2]$ rotates K_{-p_0} by $\frac{\pi}{3} - \frac{2\pi}{3n} = \frac{(n-2)\pi}{3n}$. Its order is

$$\frac{2\pi}{\gcd(\frac{(n-2)\pi}{3n}, 2\pi)} = \frac{2\pi}{\gcd(\frac{\pi}{3n}(n-2), 6n\frac{\pi}{3n})} = \frac{2\pi}{\frac{\pi}{3n}\gcd(n-2, 6n)} = \frac{6n}{\gcd(n-2, 12)}.$$

Thus, the $\pm\frac{1}{3}[T \times C_{3n}]$-orbit of a starting point on K_{-p_0} forms a regular polygon with $\mathrm{lcm}(2n, \frac{6n}{\gcd(n-2,12)}) = \frac{6n}{\gcd(n-2,3)}$ sides. In particular, if $n-2$ is a multiple of

3, $\pm\frac{1}{3}[T \times C_{3n}]$ has a simple rotation fixing K_{-p_0}. Otherwise, G has no simple rotation fixing K_{-p_0}.

To summarize, $\pm[T \times C_n]$ fixes K_{p_0} and K_{-p_0} if and only if $n \equiv 0 \bmod 3$. While, $\pm\frac{1}{3}[T \times C_{3n}]$ fixes K_{p_0} if and only if $n \equiv 1 \bmod 3$, and it fixes K_{-p_0} if and only if $n \equiv 2 \bmod 3$.

Here, we have discussed the situation in terms of orbits near the axis. As discussed in Section 3.10, the results can be checked against Figures B.8, B.11, and B.10.

Figure 3.9.: The $+T$-orbit polytope of a starting point near a 3-fold rotation center of $+T$ (left), and the spherical Voronoi diagram of this orbit (right). The picture looks the same for a Type I or a Type II center.

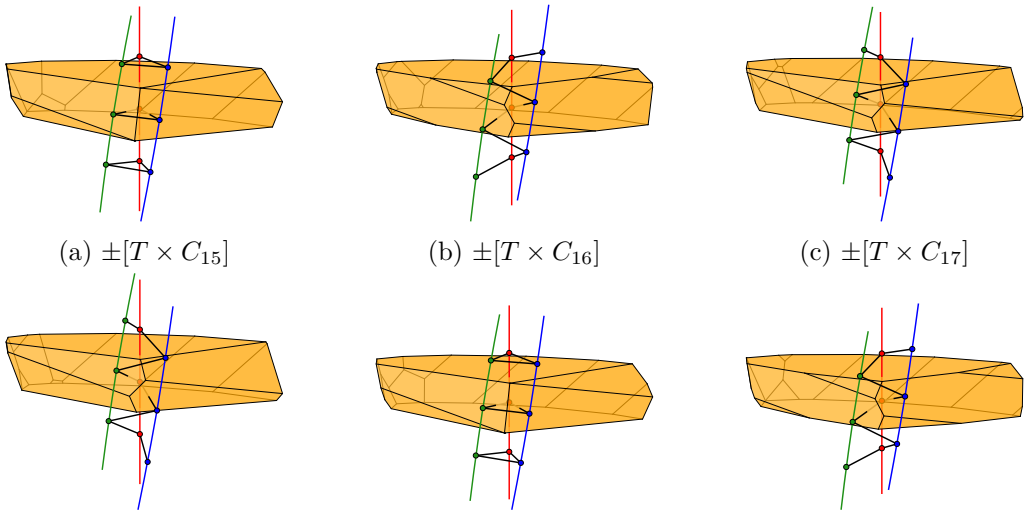

(a) $\pm[T \times C_{15}]$ (b) $\pm[T \times C_{16}]$ (c) $\pm[T \times C_{17}]$

(d) $\pm\frac{1}{3}[T \times C_{45}]$ (e) $\pm\frac{1}{3}[T \times C_{48}]$ (f) $\pm\frac{1}{3}[T \times C_{51}]$

Figure 3.10.: Cells of polar orbit polytopes of the corresponding groups, where the image of the starting point lies near a 3-fold rotation center of type I. The colors are in correspondence with Figure 3.9.

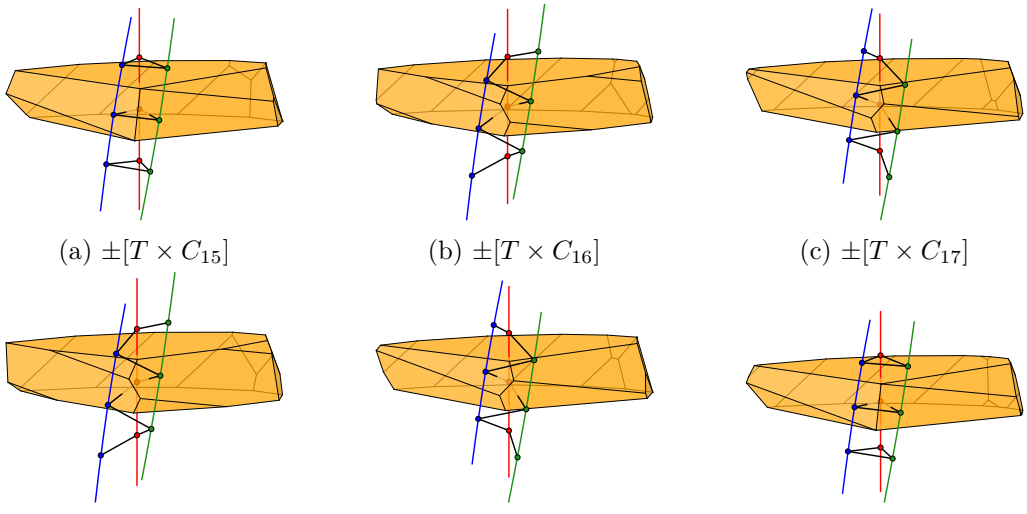

(a) $\pm[T \times C_{15}]$ (b) $\pm[T \times C_{16}]$ (c) $\pm[T \times C_{17}]$

(d) $\pm\frac{1}{3}[T \times C_{45}]$ (e) $\pm\frac{1}{3}[T \times C_{48}]$ (f) $\pm\frac{1}{3}[T \times C_{51}]$

Figure 3.11.: Cells of polar orbit polytopes of the corresponding groups, where the image of the starting point lies near a 3-fold rotation center of type II. The colors are in correspondence with Figure 3.9.

4 The toroidal groups

4.1. The invariant Clifford torus

We will now study the large class of groups of type $[D \times D]$ or $[C \times C]$ or $[C \times D]$, where both the left and the right group are cyclic or dihedral. At the beginning of Section 2.4, we have seen that these groups have an invariant Clifford torus $\mathbb{T}^q_p$. All tori $\mathbb{T}^q_p$ are the same up to orthogonal transformations. We can thus, without loss of generality, restrict our attention to the standard torus $\mathbb{T}^i_i$. Indeed this is the torus that is left invariant by the left and right multiplication with the groups $\pm[D_{2m} \times D_{2n}]$ and their subgroups, as follows from Proposition 2.2.6. When we speak of *the torus* in this chapter, we mean the torus $\mathbb{T}^i_i$ and we denote it by $\mathbb{T}$.

Since we also have cases where the left and right subgroup are equal, we also have to deal with their achiral extensions. According to Proposition 1.9.1, the extending element can be taken as $e = *[1, c]$, which is a composition of $*\colon (x_1, y_1, x_2, y_2) \mapsto (x_1, -y_1, -x_2, -y_2)$, which leaves the torus fixed, with $[1, c]$, for an element c of the right group, which also leaves the torus fixed. This means that the achiral extensions can also be found among the groups that leave the torus fixed.

We call these groups, namely the subgroups $\pm[D_{2m} \times D_{2n}]$ and their achiral extensions, the *toroidal groups*.

We will study and classify these groups by focusing on their action on $\mathbb{T}$. In particular, it will be of secondary interest whether the groups are chiral or achiral, or which Hopf bundles they preserve. These properties were important to derive the existence of the invariant torus, but we will not use them for the classification.

Since $\mathbb{T}$ is a two-dimensional flat surface, the symmetry groups acting on $\mathbb{T}$ bear much resemblance to the discrete symmetry groups of the plane, i.e., the wallpaper groups. These groups are well-studied and intuitive. All wallpaper groups except those that contain 3-fold rotations will make their appearance (12 out of the 17 wallpaper groups). The reason for excluding 3-fold rotations is that a Clifford torus has two distinguished directions, which are perpendicular to each other, and these directions must be preserved. We don't assume familiarity with the classification of the wallpaper groups. We will develop the classification as we go and adapt it to our needs.

4.2. Torus coordinates and the torus foliation

The Clifford torus belongs to a foliation of S^3 by a family of tori, which, in terms of Cartesian coordinates (x_1, y_1, x_2, y_2), have the equations

$$x_1^2 + y_1^2 = r_1^2,\ x_1^2 + y_2^2 = r_2^2 \tag{4.1}$$

for fixed radii r_1, r_2 with $0 < r_1, r_2 < 1$ and $r_1^2 + r_2^2 = 1$. The standard Clifford torus has the parameters $r_1 = r_2 = \sqrt{1/2}$. As limiting cases, $r_1 = 1$ gives the great circle in the x_1, y_1-plane, and $r_1 = 0$ gives the great circle in the x_2, y_2-plane. Every torus in this family is the Cartesian product of two circles, and thus is a flat torus, with a locally Euclidean metric, forming a $2\pi r_1 \times 2\pi r_2$ rectangle with opposite sides identified.

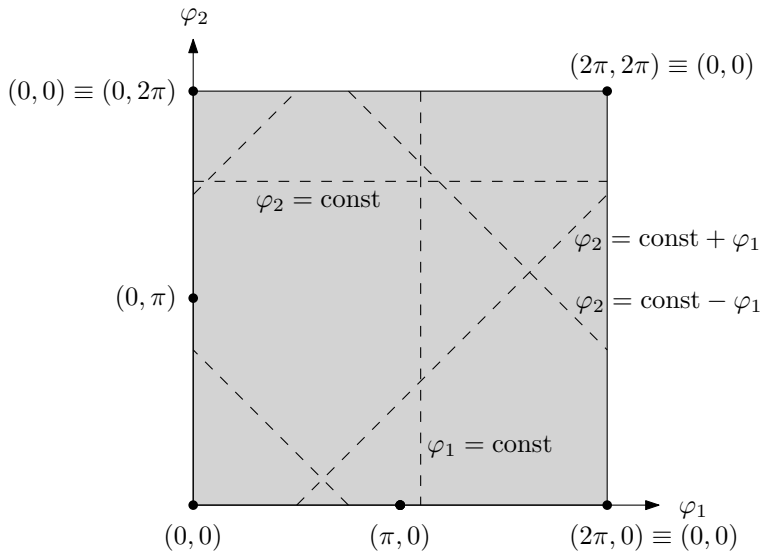

Figure 4.1.: Torus coordinates for the Clifford torus

The best way to see the mapping to the rectangle is to use double polar coordinates:

$$\begin{pmatrix} x_1 \\ y_1 \\ x_2 \\ y_2 \end{pmatrix} = \begin{pmatrix} r_1 \cos \varphi_1 \\ r_1 \sin \varphi_1 \\ r_2 \cos \varphi_2 \\ r_2 \sin \varphi_2 \end{pmatrix} \tag{4.2}$$

Then φ_1 and φ_2 (appropriately scaled) can be used as rectangular two-dimensional coordinates, see Figure 4.1.

The lines with $\varphi_1 = \text{const}$ and $\varphi_2 = \text{const}$ are what we would normally call meridian circles and parallel circles of the torus, except that there is no natural way to distinguish the two classes. These circles have radius $\sqrt{1/2}$. The 45° lines with $\varphi_2 = \text{const} + \varphi_1$ and $\varphi_2 = \text{const} - \varphi_1$ are great circles. They are the circles from the Hopf bundles $\mathcal{H}_i$ and $\mathcal{H}^i$.

Figure 4.2 gives a picture of corresponding patches around the origin $\varphi_1 = \varphi_2 = 0$ for three tori. The middle one is the Clifford torus with $r_1 = r_2 = \sqrt{1/2} \approx 0.7$, the top one has $r_1 = 0.55 < r_2 \approx 0.835$, and the bottom one has the reversed values r_1 and r_2.

Each torus is intrinsically flat, i.e., isometric to the Euclidean plane in every small patch, but, as the figure suggests, it is embedded as a "curved" surface inside S^3. The only "lines" in the torus that are geodesics of S^3 are those that are parallel to the diagonal lines $\varphi_2 = \pm\varphi_1$. The dotted "vertical" lines connect points with the same φ_1, φ_2-coordinates on different tori. They are great circles, and they intersect every torus of the family orthogonally.

In Section 4.11.2, we will see the easy equation $x_1 x_3 = x_2 x_4$ (4.9) for the same torus in a different coordinate system.

4.3. Symmetries of the torus

Since the torus is locally like the Euclidean plane, and the plane is the universal covering space of the torus, we can investigate the isometric symmetries of the torus by studying the isometries of the plane. However, not every isometry of the plane can be used as a symmetry of the torus; it must be "compatible" with the torus structure. The following theorem makes this precise:

Theorem 4.3.1. *There is a one-to-one correspondence between*

- *groups G of isometries of the torus $[0, 2\pi) \times [0, 2\pi)$,*

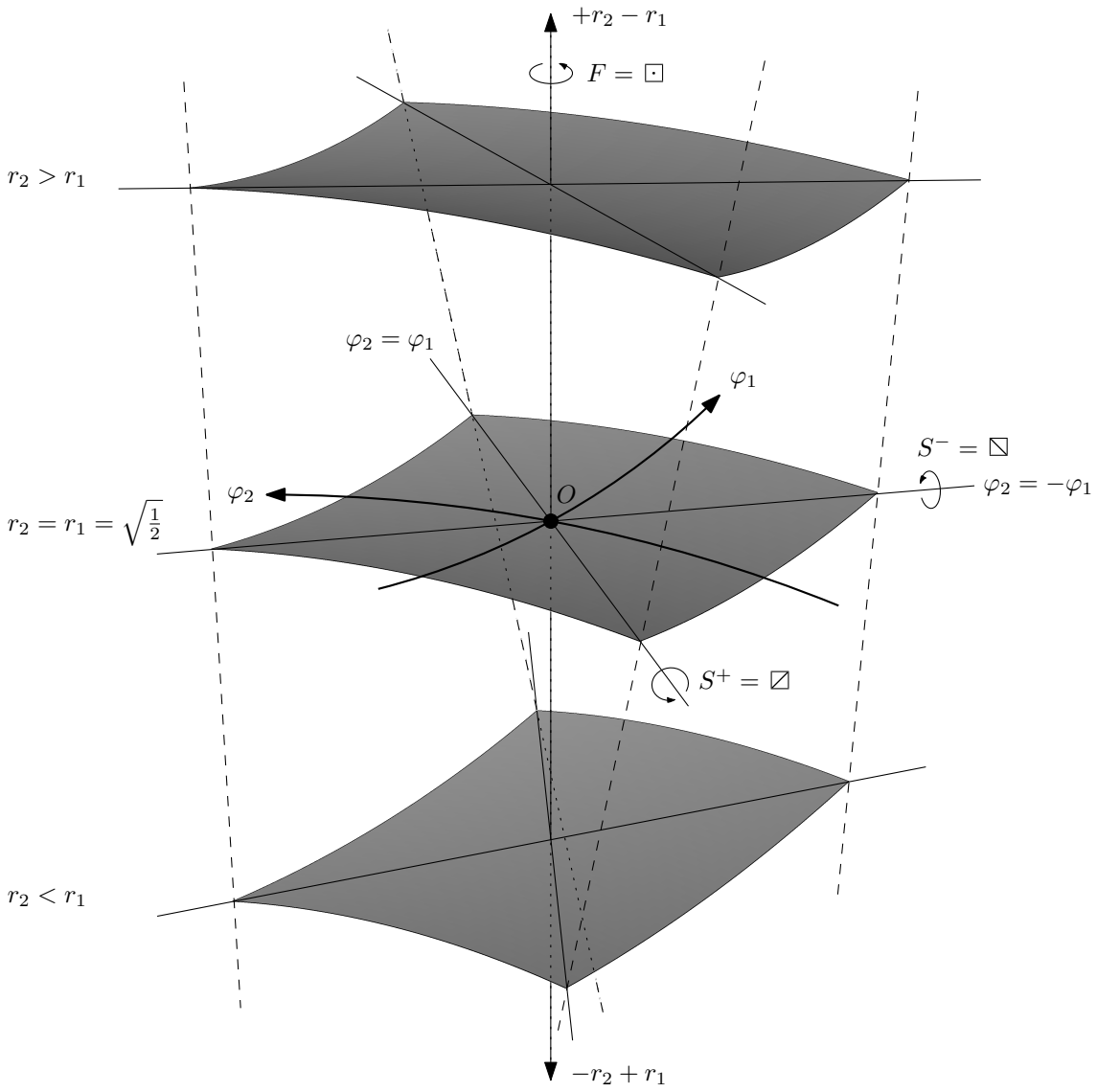

Figure 4.2.: Patches of flat tori in the 3-sphere. This illustration is a central projection from the 3-sphere to the 3-dimensional tangent hyperplane at the point $O = (\sqrt{1/2}, 0, \sqrt{1/2}, 0)$, which is the marked point in the center. Great circles, i.e. geodesics on the 3-sphere, appear as straight lines. The axes of the *flip* half-turns F and the *swap* half-turns S^+ and S^- are indicated.
The tangent in direction φ_1 points in the direction $(0, 1, 0, 0)$ and the tangent vector in direction φ_2 points in the direction $(0, 0, 0, 1)$. The "perpendicular direction", which is the vertical axis $+r_2 - r_1$ in the figure, is the direction $(-\sqrt{1/2}, 0, \sqrt{1/2}, 0)$.

- *groups $\hat{G}$ of isometries $x \mapsto Ax + t$ of the (φ_1, φ_2)-plane with the following properties:*
  - (i) *The directional part A of every isometry in $\hat{G}$ keeps the integer grid $\mathbb{Z}^2$ invariant.*
  - (ii) *The group contains the two translations $\varphi_1 \mapsto \varphi_1 + 2\pi$ and $\varphi_2 \mapsto \varphi_2 + 2\pi$.*

The proof uses the following lemma, which shows how to lift torus isometries to plane isometries:

Lemma 4.3.2. *Let Λ denote the scaled integer grid $\{ (k_1 2\pi, k_2 2\pi) \mid k_1, k_2 \in \mathbb{Z} \}$, and let $p\colon \mathbb{R}^2 \to \mathbb{R}^2|_\Lambda$ be the quotient map from the plane to the torus $[0, 2\pi) \times [0, 2\pi)$:*

$$p(\varphi_1, \varphi_2) = (\varphi_1 \bmod 2\pi, \varphi_2 \bmod 2\pi)$$

For every isometry T of the torus $[0, 2\pi) \times [0, 2\pi)$, there is an isometry $\hat{T}$ of the plane with the following properties.

(a) *$T(p(x)) = p(\hat{T}(x))$ for all $x \in \mathbb{R}^2$.*

(b) *$\hat{T}$ maps the grid Λ to a translate of Λ.*

The isometry $\hat{T}$ is unique up to translation by a grid vector $t \in \Lambda$.

Proof. Pick some point y_0 of the torus and let $T(y_0) = y_0'$. Find points $x_0, x_0' \in \mathbb{R}^2$ with $y_0 = p(x_0)$ and $y_0' = p(x_0')$. Since p is locally injective, the mapping T can be lifted to a mapping $\hat{T}(x) = p^{-1}(T(p(x)))$ in some neighborhood $N(x_0)$ of $x_0 \in \mathbb{R}^2$:

$$\begin{array}{lcc} \mathbb{R}^2\colon & x_0 & \xrightarrow{\hat{T}} & x_0' \\ & {\scriptstyle p}\downarrow & & \downarrow{\scriptstyle p} \\ \mathbb{T}\colon & y_0 & \xrightarrow[T]{} & y_0' \end{array} \tag{4.3}$$

In other words, $\hat{T}(x_0) = x_0'$, and for all $x \in N(x_0)$:

$$p(\hat{T}(x)) = T(p(x)) \tag{4.4}$$

Moreover, since both p and T are locally isometries, $\hat{T}$ is an isometry in $N(x_0)$. This isometry can be extended to a unique isometry $\hat{T}$ of the plane.

To extend the validity of (4.4) from $N(x_0)$ to the whole plane, we look at a path $x_0 + \lambda t$ from x_0 to an arbitrary point $x_0 + t$ of the plane, where $(0 \le \lambda \le 1)$. On the torus, it corresponds to a path $p(x_0 + \lambda t)$, which is mapped to an image path $T(p(x_0 + \lambda t))$, which in turn can be lifted to a path on $\mathbb{R}^2$. Since p is locally invertible and an isometry, (4.4) must hold along the whole path, and therefore for an arbitrary point $x_0 + t$ of the plane. This is claim (a).

To show claim (b), consider any $t \in \Lambda$. By (4.4),

$$p(\hat{T}(t)) = T(p(t)) = T(p(0))$$

that is, all values $\hat{T}(t)$ for $t \in \Lambda$ project to the same point $T(p(0))$ on the torus. It follows that the image of Λ under $\hat{T}$ is contained in a translate of Λ. But then it must be *equal* to this translate of Λ.

Once x_0 and x_0' have been chosen, the construction gives a unique transformation $\hat{T}$. The result can be varied by adding an arbitrary translation $t \in \Lambda$ to x_0 (before applying $\hat{T}$) or $t' \in \Lambda$ to x_0' (after applying $\hat{T}$). By property (b), it makes no difference whether we are allowed to translate by an element of Λ before applying $\hat{T}$ or after (or both). This proves the uniqueness claim of the lemma. □

As a consequence, we can write a torus isometry like a plane isometry in the form $x \mapsto Ax + t$ with an orthogonal matrix A and a translation vector t, bearing in mind that t is unique only up to grid translations.

Proof of Theorem 4.3.1. Given a group G, we can construct the lifted group $\hat{G}$ as the set of lifted isometries $\hat{T}$ of the transformations $T \in G$ according to the lemma. The group property of $\hat{G}$ can be easily shown by extending the diagram (4.3):

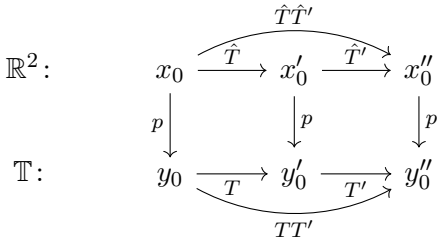

The translations $\varphi_1 \mapsto \varphi_1 + 2\pi$ and $\varphi_2 \mapsto \varphi_2 + 2\pi$ arise as lifts of the identity $\mathrm{id} \in G$. It is clear that a matrix A keeps the scaled integer grid $\Lambda := \{\, (k_1 2\pi, k_2 2\pi) \mid k_1, k_2 \in \mathbb{Z} \,\}$ invariant (Property (b)) if and only if it keeps the standard integer grid $\mathbb{Z}^2$ invariant (Property (i)).

Conversely, given a transformation $\hat{T}$ in the group $\hat{G}$, we can define T as follows: For a point y_0 of the torus, pick a point x_0 with $p(x_0) = y_0$, and define $T(y_0)$ through the relation (4.3): $T(y_0) := p(\hat{T}(x_0))$. The choice of x_0 is ambiguous. It is determined only up a translation by $t \in \Lambda$, but we see that this has no effect on $T(y_0)$:

$$p(\hat{T}(x_0 + t)) = p(\hat{T}(x_0) + t') = p(\hat{T}(x_0))$$

By property (i), or property (b), $t' \in \Lambda$, and therefore the ambiguity evaporates through the projection p. □

4.3.1. Torus translations

The simplest operations are the ones that appear as translations on the torus, modulo 2π. We denote them by

$$R_{\alpha_1,\alpha_2} \colon (\varphi_1, \varphi_2) \mapsto (\varphi_1 + \alpha_1, \varphi_2 + \alpha_2)$$

in accordance with (1.1). In this notation, a left rotation $[\exp \alpha i, 1]$ turns out to be a negative translation along the 45° direction: $T_{-\alpha,-\alpha}$. A right rotation $[1, \exp \alpha i]$ is a translation in the $-45°$ direction: $R_{\alpha,-\alpha}$. Arbitrary torus translations can be composed from left and right rotations, and the general translation is written in quaternion notation as

$$R_{\alpha_1,\alpha_2} = \left[\exp(\tfrac{-\alpha_1-\alpha_2}{2} i),\ \exp(\tfrac{\alpha_1-\alpha_2}{2} i)\right].$$

The torus translations $R_{\alpha,0}$ and $R_{0,\alpha}$ along the φ_1 and φ_2-axis are simple rotations, leaving the x_2, y_2-plane or the x_1, y_1-plane fixed, respectively.

One should bear in mind that all "translations", as they appear on the torus, are actually rotations of S^3. (Only the left and right rotations among them may be called *translations of* S^3 with some justification, because they correspond to the translations in elliptic 3-space.)

4.3.2. The directional group: symmetries with a fixed point

We pick the point $O = (\sqrt{1/2}, 0, \sqrt{1/2}, 0)$ with torus coordinates $\varphi_1 = \varphi_2 = 0$ as a reference point or origin on $\mathbb{T}$. Every isometry of $\mathbb{T}$ can be decomposed in a unique way

into a symmetry that leaves O fixed (the *directional part*), plus a torus translation (the *translational part*).

Let us therefore study the symmetries that leave O fixed. In the plane, these would be all rotations and reflections. However, according to Theorem 4.3.1 we can only use symmetries that leave the standard square grid $\mathbb{Z}^2$ invariant, apart from a translation. This allows rotations by multiples of 90°, as well as reflections in the coordinate axes and in the 45°-lines.

In the plane, these seven operations together with the identity form the dihedral group D_8, the symmetries of the square. We denote the group by $D_8^{\mathbb{T}}$, to indicate that we think of the transformations of S^3 that leave the torus $\mathbb{T}$ invariant. Table 4.1 summarizes these operations and their properties. For each operation, we have chosen a symbol indicating the axis direction in case of a reflection, or otherwise some suggestive sign, and a name. We also give the quaternion representation, the effect in terms of the φ_1, φ_2-coordinates, and the order of the group element.

Some transformations may *swap* the two sides of $\mathbb{T}$, exchanging the tori with parameters r_1, r_2 and r_2, r_1. This is indicated by a "$-$" in the column "side", and the names of these operations include the term "swap". The nonswapping operations leave every torus of the foliation (4.1) invariant, not just the "central" Clifford torus.

The column "det" indicates whether the operation is orientation-preserving ($+$) or orientation-reversing ($-$). One must keep in mind that the operation on the torus $\mathbb{T}$ induces a transformation of the whole S^3, and what appears as a reflection in the planar φ_1, φ_2-picture of $\mathbb{T}$ may or may not be an orientation-reversing transformation of S^3. Thus, it may at first sight come as a surprise that the *torus swap* ◪ is orientation-preserving. The reason is that it goes together with a swap of the sides. As shown in Figure 4.2, it is actually a half-turn around the axis S^+. (The product of the signs in the "side" and "det" columns tells whether the operation is orientation-preserving when considered purely in the plane.)

Figure 4.2 makes it clear why there is no "pure swap", no "inversion" at the central torus that would keep the torus pointwise fixed and swap the two sides of the torus: such a mapping would flip the dashed perpendicular lines and thus map the long side of the rectangular patch on the top to the short side of the rectangular patch at the bottom. We see that a swap is only possible if it goes hand in hand with an exchange of the φ_1 and φ_2 axes. In particular, such an exchange comes with the rotations by $\pm 90°$, the right and left *swapturn* operations, which are accordingly orientation-reversing.

The column "conj." indicates operations that are conjugate to each other, i.e., geometrically equivalent. Thus, for example, the operation ◫ may, in a different coordinate system, appear as the operation ⊟. By contrast, ◪ and ◩ are distinguished: the axis of ◪ belongs to the invariant left Hopf bundle $\mathcal{H}^i$, and the axis of ◩ belongs to the invariant right Hopf bundle $\mathcal{H}_i$. The operations ◪ and ◩ are mirrors of each other, i.e., conjugate under an orientation-reversing transformation. This is indicated in the last column.

When viewed in isolation, the half-turns $S^+ =$ ◪, $S^- =$ ◩, and $F =$ ⊡ are conjugate to each other. However, they are distinct when considering only transformations that leave the torus invariant.

4.3.3. Choice of coordinate system

The conjugacies discussed above introduces ambiguities in the representation of torus translations, which depend on the choice of the coordinate system for a given invariant torus. R_{α_1,α_2} may, in a different coordinate system, appear as $R_{-\alpha_1,-\alpha_2}$ (conjugacy by ⊡), or as R_{α_2,α_1} (conjugacy by ◪), or as $R_{-\alpha_2,-\alpha_1}$ (conjugacy by ◩). (The operation $R_{\alpha_1,-\alpha_2}$ or $R_{-\alpha_1,\alpha_2}$ is its mirror operation.) The choice of origin in the φ_1, φ_2-plane, on the other hand, has no influence on the torus translations. It only affects the other operations.

symbol	name	$[l,r]$	$(\varphi_1,\varphi_2)\to$	order	side	det	conj.	mirror
□	identity	$[1,1]$	(φ_1,φ_2)	1	+	+	–	□
◫	horizontal reflection	$*[i,i]$	$(-\varphi_1,\varphi_2)$	2	+	−	⊟	–
⊟	vertical reflection	$*[k,k]$	$(\varphi_1,-\varphi_2)$	2	+	−	◫	–
⊡	torus flip $F=\boxminus\cdot\boxplus$	$[j,j]$	$(-\varphi_1,-\varphi_2)$	2	+	+	–	⊡
◪	torus swap S^+	$[i,k]$	(φ_2,φ_1)	2	−	+	–	◩
◩	alternate torus swap S^-	$[-k,i]$	$(-\varphi_2,-\varphi_1)$	2	−	+	–	◪
⟲	left swapturn ◪ · ◫	$*[-j,1]$	$(\varphi_2,-\varphi_1)$	4	−	−	⟲	–
⟲	right swapturn $⟲^{-1}$	$*[1,j]$	$(-\varphi_2,\varphi_1)$	4	−	−	⟲	–

Table 4.1.: The directional parts of the torus symmetries, the elements of the group $D_8^{\mathbb{T}}$. Some come in conjugate pairs, as indicated in the column "conj.", meaning that they are geometrically equivalent. The conjugacy is established by any of the operations ◪ or ◩ in these cases. The torus flip ⊡ commutes with all other operations. The last column shows the mirror transformation for each transformation of determinant +1 (the orientation-preserving transformations).

group	name	chirality	swapping	conjugate	mirror
□ = {□}	translation	chiral	no	–	□
◫ = {□, ◫}	reflection	achiral	no	⊟, by ◪	–
⊟ = {□, ⊟}	reflection	achiral	no	◫, by ◪	–
⊡ = {□, ⊡}	flip	chiral	no	–	⊡
⊞ = {□, ◫, ⊟, ⊡}	full reflection	achiral	no	–	–
◪ = {□, ◪}	swap	chiral	yes	–	◩
◩ = {□, ◩}	swap	chiral	yes	–	◪
⊠ = {□, ◪, ◩, ⊡}	full swap	chiral	yes	–	⊠
⟲ = {□, ⟲, ⊡, ⟲} ≅ C_4	swapturn	achiral	yes	–	–
✳ = {□, ⟲, ⊡, ⟲, ◫, ⊟, ◪, ◩}	full torus	achiral	yes	–	–

Table 4.2.: The 10 subgroups of $D_8^{\mathbb{T}}$. A group is achiral if it contains an orientation-reversing transformation. A group is swapping if it contains a transformation that swaps the two sides of the torus. The fifth column shows to which other groups the group is conjugate by an orientation-preserving transformation. The last column shows the mirror group of each chiral group, i.e., the conjugate group by an orientation-reversing transformation. (Each achiral group in this list is its own mirror image.)

4.3.4. The directional group and the translational subgroup

We have mentioned that every symmetry of the torus can be decomposed in a unique way (after fixing an origin) into a directional part and a translational part.

For a group G, the torus translations contained in it form a normal subgroup, the *translational subgroup*, which we denote by $G_\square$. The directional parts of the group operations form the *directional group* of G. It is a subgroup of $D_8^{\mathbb{T}}$, and we will use it as a coarse classification of the toroidal groups. (The directional group is isomorphic to the factor group $G/G_\square$.)

The ten subgroups of $D_8^{\mathbb{T}}$ are listed in Table 4.2, together with a characteristic symbol and a name. Figure 4.3 shows their pictorial representation.

The following lemma is useful in order to restrict the translational subgroup for a given directional group.

Lemma 4.3.3. *For a group G of torus symmetries, the translational subgroup $G_\square$ is closed under every symmetry in the directional group of G.*

Proof. Assume that $t\in G_\square$, and we have an operation in $G/G_\square$ that is represented by an orthogonal 2×2 matrix A. This means that G contains some transformation $x\mapsto Ax+b$. If we conjugate the translation $x\mapsto x+t$ with this transformation, we get $x\mapsto A(A^{-1}(x-b)+t)+b=x+At$, i.e., a translation by At. □

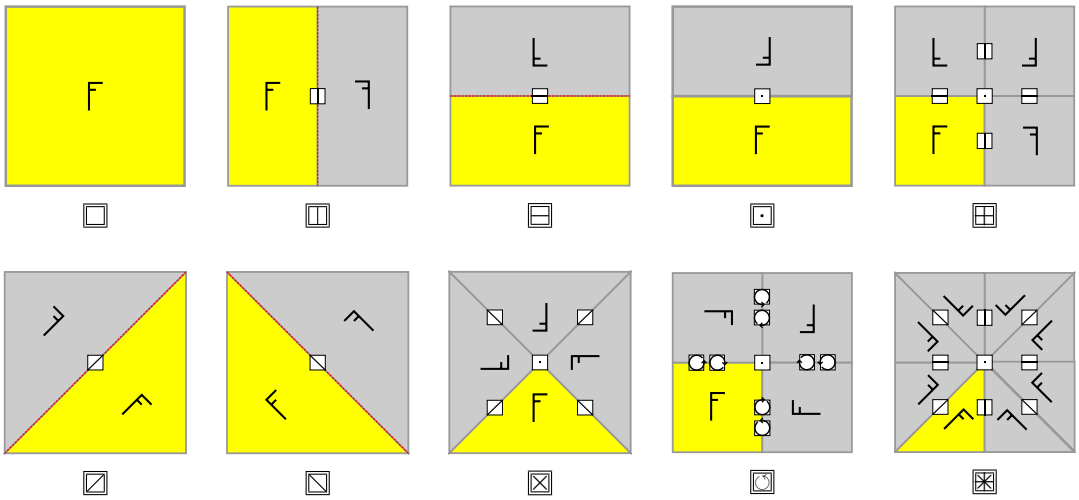

Figure 4.3.: The 10 subgroups of $D_8^{\mathbb{T}}$. See Table 4.2.

4.4. Overview of the toroidal groups

After fixing the directional group, we have to look at the translational subgroup, and the interaction between the two. The result is summarized as follows.

Proposition 4.4.1. *The 4-dimensional point groups that have an invariant torus can be classified into 25 infinite families of toroidal groups, among them*

- *2 three-parameter families*
- *19 two-parameter families*
- *4 one-parameter families*

as shown in Table 4.3.

The last column of Table 4.3 shows the names of these groups in the classification of Conway and Smith.[14] We make a comparison in Section 4.12.

There is one difficulty that we have not addressed: We look at the groups that leave one particular Clifford torus invariant. However, there are some groups, in particular small groups, that have several invariant Clifford tori. This leads to ambiguities. For example, a torus translation by 180° on one torus may appear as a swapturn ⊘ on a different torus. We investigate these cases in detail in Section 4.11.

The natural constraint on the parameters m and n is $m, n \geq 1$ in all cases of Table 4.3, in the sense that all these choices (in a few cases under the additional constraint that $m \equiv n \pmod 2$) lead to valid groups. (But note that some extra evenness constraints are already built into the notation, for example, when we write $\boxslash^{\mathbf{pm}}_{2m,2n}$ instead of $\boxslash^{\mathbf{pm}}_{m,n}$.) For the swapturn groups $\boxcircle_{a,b}$, the natural choices are $a, b \geq 0$ except for $(a, b) = (0, 0)$. The stricter conditions on m and n in Table 4.3 are imposed in order to exclude duplications.

We will now go through the categories one by one. This closely parallels the classification of the wallpaper groups. When appropriate, we use the established notations for wallpaper groups to distinguish the torus groups. We have to choose suitable parameters for the different dimensions of each wallpaper group, and in some cases, we have to refine the classification of wallpaper groups because different axis directions are distinguished.

[14] To get a closer correspondence with our parameterization for the groups of type □ and ⊡ in the first two rows, we swap the role of the left and right factors in the generators given in Conway and Smith. Effectively, we consider the mirror groups. Accordingly, we have adapted the Conway–Smith convention of writing $\frac{1}{f}[C_m \times C_n^{(s)}]$, by decorating the *left* factor with the parameter s. More details are given in Appendix G.

group	order	parameters	names in Conway–Smith [14, Tables 4.1–4.3]	
torus translation groups (chiral, wallpaper group **p1**)				
$\square^{(s)}_{m,n}$	mn	$m,n\geq 1$, $-\frac{m}{2}\leq s\leq\frac{n-m}{2}$	$m\equiv 0 \pmod 2$: $\pm\frac{1}{f}[C^{(s')}_{mf/2}\times C_n]$ $m\equiv 1 \pmod 2$: $+\frac{1}{f}[C^{(s')}_{mf}\times C_n]$	
torus flip groups (chiral, wallpaper group **p2**)				
$\boxdot^{(s)}_{m,n}$	$2mn$	$m,n\geq 1$, $-\frac{m}{2}\leq s\leq\frac{n-m}{2}$ $(m,n)\neq(1,1),(2,1)$	$m\equiv 0 \pmod 2$: $\pm\frac{1}{2f}[D^{(f-s')}_{mf}\times D_{2n}]$ $m\equiv 1 \pmod 2$: $+\frac{1}{2f}[D^{(2f-s')}_{2mf}\times D_{2n}]$	
torus swap groups (chiral)			n even	n odd
$\boxslash^{\mathbf{pm}}_{2m,2n}$	$4mn$	$m,n\geq 2$	$\pm[D_{2m}\times C_n]$	$\pm\frac{1}{2}[D_{2m}\times C_{2n}]$
$\boxslash^{\mathbf{pg}}_{2m,2n}$	$4mn$	$m\geq 2, n\geq 1$	$\pm\frac{1}{2}[D_{2m}\times C_{2n}]$	$\pm[D_{2m}\times C_n]$
$\boxslash^{\mathbf{cm}}_{m,n}$	$2mn$	$m\geq 3, n\geq 2$, $m-n$ even	$\pm\frac{1}{2}[\overline{D}_{2m}\times C_n]$	$+\frac{1}{2}[D_{2m}\times C_{2n}]$
$\boxbslash^{\mathbf{pm}}_{2m,2n}$	$4mn$	$m,n\geq 2$	mirrors of the groups $\boxslash^{\mathbf{pm}}_{2n,2m}$	
$\boxbslash^{\mathbf{pg}}_{2m,2n}$	$4mn$	$m\geq 1, n\geq 2$	mirrors of the groups $\boxslash^{\mathbf{pg}}_{2n,2m}$	
$\boxbslash^{\mathbf{cm}}_{m,n}$	$2mn$	$m\geq 2, n\geq 3$, $m-n$ even	mirrors of the groups $\boxslash^{\mathbf{cm}}_{n,m}$	
full torus swap groups (chiral)			m	n even / n odd
$\boxtimes^{\mathbf{p2mm}}_{2m,2n}$	$8mn$	$m,n\geq 2$	m even	$\pm[D_{2m}\times D_{2n}]$ / $\pm\frac{1}{2}[D_{2m}\times\overline{D}_{4n}]$
			m odd	$\pm\frac{1}{2}[\overline{D}_{4m}\times D_{2n}]$ / $\pm\frac{1}{4}[D_{4m}\times\overline{D}_{4n}]$
$\boxtimes^{\mathbf{p2mg}}_{2m,2n}$	$8mn$	$m,n\geq 2$	m even	$\pm\frac{1}{2}[D_{2m}\times\overline{D}_{4n}]$ / $\pm[D_{2m}\times D_{2n}]$
			m odd	$\pm\frac{1}{4}[D_{4m}\times\overline{D}_{4n}]$ / $\pm\frac{1}{2}[\overline{D}_{4m}\times D_{2n}]$
$\boxtimes^{\mathbf{p2gm}}_{2m,2n}$	$8mn$	$m,n\geq 2$	m even	$\pm\frac{1}{2}[\overline{D}_{4m}\times D_{2n}]$ / $\pm\frac{1}{4}[D_{4m}\times\overline{D}_{4n}]$
			m odd	$\pm[D_{2m}\times D_{2n}]$ / $\pm\frac{1}{2}[D_{2m}\times\overline{D}_{4n}]$
$\boxtimes^{\mathbf{p2gg}}_{2m,2n}$	$8mn$	$m,n\geq 2$	m even	$\pm\frac{1}{4}[D_{4m}\times\overline{D}_{4n}]$ / $\pm\frac{1}{2}[\overline{D}_{4m}\times D_{2n}]$
			m odd	$\pm\frac{1}{2}[D_{2m}\times\overline{D}_{4n}]$ / $\pm[D_{2m}\times D_{2n}]$
$\boxtimes^{\mathbf{c2mm}}_{m,n}$	$4mn$	$m,n\geq 3$, $m-n$ even	$m\equiv n$	$\pm\frac{1}{2}[\overline{D}_{2m}\times\overline{D}_{2n}]$ / $+\frac{1}{4}[D_{4m}\times\overline{D}_{4n}]$
torus reflection groups (achiral)				
$\square^{\mathbf{pm}}_{m,n}$	$2mn$	$m,n\geq 1$	$+$ or $\pm\frac{1}{f}[C_{n'f}\times C^{(s)}_{n'f}]\cdot 2^{(0)}$ or $+\frac{1}{f}[C_{n'f}\times C^{(s)}_{n'f}]\cdot 2^{(2)}$	
$\square^{\mathbf{pg}}_{m,n}$	$2mn$	$m,n\geq 1$	$+$ or $\pm\frac{1}{f}[C_{n'f}\times C^{(s)}_{n'f}]\cdot 2^{(1)}$ or $+\frac{1}{f}[C_{n'f}\times C^{(s)}_{n'f}]\cdot 2^{(0)}$	
$\square^{\mathbf{cm}}_{m,n}$	$4mn$	$m,n\geq 1$	$\pm\frac{1}{f}[C_{n'f}\times C^{(s)}_{n'f}]\cdot 2^{(0)}$ or $+\frac{1}{f}[C_{n'f}\times C^{(s)}_{n'f}]\cdot 2^{(0)}$	
full torus reflection groups (achiral)				
$\boxplus^{\mathbf{p2mm}}_{m,n}$	$4mn$	$m\geq n\geq 1$, $(m,n)\neq(1,1)$	$\pm\frac{1}{2f}[D_{2n'f}\times D^{(s)}_{2n'f}]\cdot 2^{(\alpha,\beta)}$ or $+\frac{1}{2f}[D_{2n'f}\times D^{(s)}_{2n'f}]\cdot 2^{(\alpha,\beta)}$	
$\boxplus^{\mathbf{p2mg}}_{m,n}$	$4mn$	$m,n\geq 1$, $(m,n)\neq(1,1)$		
$\boxplus^{\mathbf{p2gg}}_{m,n}$	$4mn$	$m\geq n\geq 1$, $(m,n)\neq(1,1)$		
$\boxplus^{\mathbf{c2mm}}_{m,n}$	$8mn$	$m\geq n\geq 1$, $(m,n)\neq(1,1)$	$\pm$ or $+\frac{1}{2f}[D_{2n'f}\times D^{(s)}_{2n'f}]\cdot 2^{(0,0)}$	
torus swapturn groups (achiral, wallpaper group **p4**)				
$\circlearrowleft_{a,b}$	$4(a^2{+}b^2)$	$a\geq b\geq 0$	$a\equiv b \pmod 2$: $\pm\frac{1}{2f}[D_{2nf}\times D^{(s)}_{2nf}]\cdot\overline{2}$	
		$a\geq 2$, $(a,b)\neq(2,0)$	$a\not\equiv b \pmod 2$: $+\frac{1}{2f}[D_{2nf}\times D^{(s)}_{2nf}]\cdot\overline{2}$	
full torus groups (achiral)			n even	n odd
$\boxtimes^{\mathbf{p4mmU}}_{n}$	$8n^2$	$n\geq 3$	$\pm\frac{1}{2}[\overline{D}_{2n}\times\overline{D}_{2n}]\cdot 2$	$+\frac{1}{4}[D_{4n}\times\overline{D}_{4n}]\cdot 2_1$
$\boxtimes^{\mathbf{p4gmU}}_{n}$	$8n^2$	$n\geq 3$	$\pm\frac{1}{2}[\overline{D}_{2n}\times\overline{D}_{2n}]\cdot\overline{2}$	$+\frac{1}{4}[D_{4n}\times\overline{D}_{4n}]\cdot 2_3$
$\boxtimes^{\mathbf{p4mmS}}_{n}$	$16n^2$	$n\geq 2$	$\pm[D_{2n}\times D_{2n}]\cdot 2$	$\pm\frac{1}{4}[D_{4n}\times\overline{D}_{4n}]\cdot 2$
$\boxtimes^{\mathbf{p4gmS}}_{n}$	$16n^2$	$n\geq 2$	$\pm\frac{1}{4}[D_{4n}\times\overline{D}_{4n}]\cdot 2$	$\pm[D_{2n}\times D_{2n}]\cdot 2$

Table 4.3.: Overview of the toroidal groups. In the Conway–Smith names, we write n' and s' when these parameters don't directly correspond to our parameters n, s.

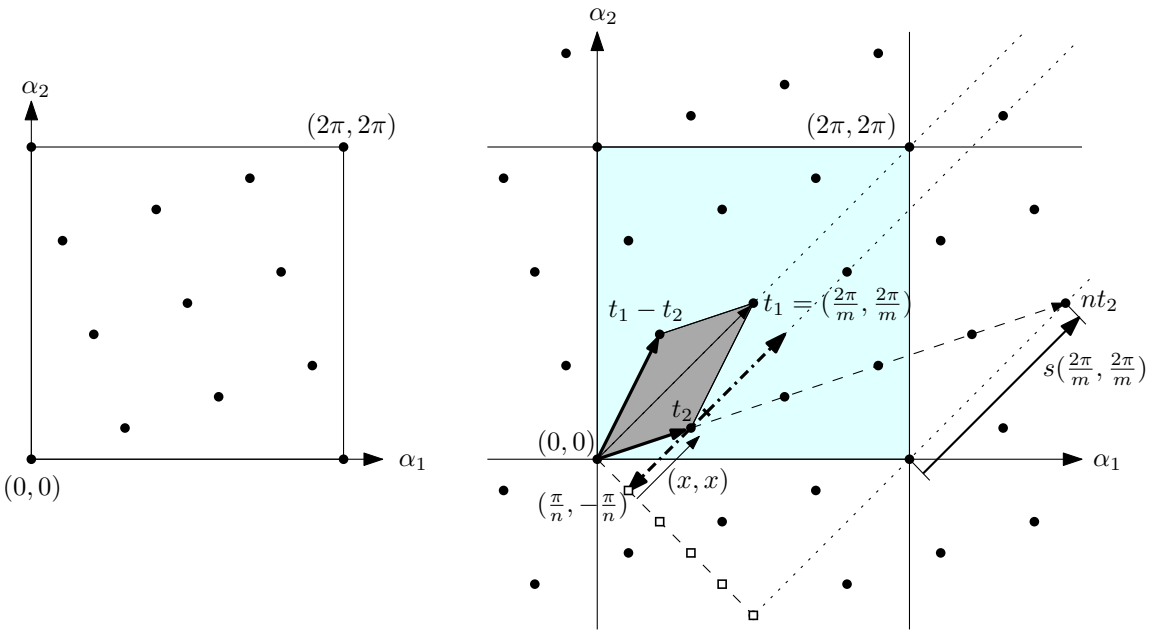

Figure 4.4.: A lattice of torus translations. In the right part, we see that it is given by the parameters $m = 2$, $n = 5$, and $s = 1$. The vectors $t_1 = (\pi, \pi)$ and $t_2 = (\frac{\pi}{5}, -\frac{\pi}{5}) + (\frac{2\pi}{5}, \frac{2\pi}{5}) = (\frac{3\pi}{5}, \frac{\pi}{5})$ generate the group $\square^{(1)}_{2,5}$. This lattice happens to be a square lattice, but this plays no role.

4.5. The torus translation groups, type □

These are the groups that contain only torus translations. The pure translation groups are the simplest class, but they are also the richest type of groups, requiring three parameters for their description. The translations (α_1, α_2) with $R_{\alpha_1,\alpha_2} \in G$ form an additive group modulo $(2\pi, 2\pi)$, and hence a lattice modulo $(2\pi, 2\pi)$. In accordance with Theorem 4.3.1 we can also view it as a lattice in the plane that contains all points whose coordinates are multiples of 2π, see Figure 4.4.

We parameterize these lattices with three parameters m, n, s: The lattice subdivides the principal diagonal from $(0, 0)$ to $(2\pi, 2\pi)$ into some number $m \geq 1$ of segments. Then we choose $t_1 = (\frac{2\pi}{m}, \frac{2\pi}{m})$ as the first generator of the lattice. The second parameter $n \geq 1$ is the number of lattice lines parallel to the principal diagonal that run between $(0, 0)$ and $(2\pi, 0)$, including the last one through $(2\pi, 0)$. In the figure, we have $m = 2$ and $n = 5$. On each such line, the points are equidistant with distance $\frac{2\pi}{m} \cdot \sqrt{2}$. The first parallel lattice line thus contains a unique point $t_2 = (\frac{\pi}{n}, -\frac{\pi}{n}) + (x, x)$ with $0 \leq x < \frac{2\pi}{m}$, and we choose x as the third parameter. The range from which t_2 can be chosen is indicated by a double arrow in the figure.

We still have to take into account the ambiguity from the choice of the coordinate system (Section 4.3.3). The choice of origin is no problem, since a translation does not depend on the origin. Also, the "flip" ambiguity from ⊡ is no problem at all: Rotating the coordinate system by 180° maps the lattice to itself. The "swap" ambiguity from ◪, however, is more serious, as it exchanges the coordinate axes: $\alpha_1 \leftrightarrow \alpha_2$. (From ⧅, we get no extra ambiguity, since ⧅ = ⊡ · ◪.)

To eliminate this ambiguity, we look at the vectors $t_1 - t_2$ and t_2. They form also a lattice basis, and they span a parallelogram whose diagonal t_1 lies on the $\alpha_1 = \alpha_2$ axis. The alternate choice of the basis will reflect the parallelogram at this diagonal. Thus, the choices x and $\frac{2\pi}{m} - x$ will lead to the same group. We can achieve a unique representative by stipulating that t_2 is not longer than $t_1 - t_2$. This means that we restrict t_2 to the lower

half of the range, including the midpoint, which is marked in the figure: $0 \le x \le \frac{\pi}{m}$.[15]

Finally, we look at the point nt_2, which lies on the 45° line through $(2\pi, 0)$. We have to ensure that it is one of the existing lattice points on this line because additional points would contradict the choice of m. Thus

$$nt_2 = (\pi, -\pi) + (nx, nx) = (2\pi, 0) + s(\tfrac{2\pi}{m}, \tfrac{2\pi}{m})$$

for some integer s, or in other words

$$x = \frac{\pi}{n} + s \cdot \frac{2\pi}{mn}$$

Combining this with the constraint $0 \le x \le \frac{\pi}{m}$, we get

$$-\frac{m}{2} \le s \le -\frac{m}{2} + \frac{n}{2} \tag{4.5}$$

This range contains $\lceil \frac{n}{2} \rceil$ integers if m is odd and $\lceil \frac{n+1}{2} \rceil$ integers if m is even. In particular, there is always at least one possible value s.

Proposition 4.5.1. *The point groups that contain only torus translations can be classified as follows:*

For any integers $m, n \ge 1$ and any integer s in the range (4.5), there is one such group, the torus translation group $\boxplus^{(s)}_{m,n}$, of order mn. It is generated by $R_{\frac{2\pi}{m}, \frac{2\pi}{m}}$ and $R_{\frac{2\pi}{n} + \frac{2s\pi}{mn}, \frac{2s\pi}{mn}}$.

In terms of quaternions, these generators are $[\exp(-\frac{2\pi}{m}i), 1]$ and $[\exp(-\frac{(m+2s)\pi}{mn}i), \exp\frac{\pi i}{n}]$. We emphasize that the two parameters m and n play different roles in this parameterization, and there is no straightforward way to read off the parameters of the mirror group from the original parameters m, n, s. (See for example the entries 11/01 and 11/02 in Table D.1.)

We have observed above that x and $x' = \frac{2\pi}{m} - x$ lead to the same group, and the same is true for $x' = \frac{2\pi}{m} + x$. In terms of s this means that the parameters $s' = -m - s$ and $s' = s + n$ lead to the same group as s. In Section 4.11, when we discuss duplications, it will be convenient to allow values s outside the range (4.5). In particular, it is good to remember that $s = 0$ corresponds to a generating point on the α_1-axis.

4.5.1. Dependence on the starting point

Proposition 4.5.2. *Any two full-dimensional orbits of a toroidal translation group are linearly equivalent.*

Proof. Let G be a toroidal translation group. We will show that any full-dimensional G-orbit can be obtained from the G-orbit of the point $(\frac{1}{\sqrt{2}}, 0, \frac{1}{\sqrt{2}}, 0)$ by applying an invertible linear transformation.

Let $v \in \mathbb{R}^4$ be a point whose G-orbit is full-dimensional. This is equivalent to requiring that the projections of v to the x_1, y_1-plane and to the x_2, y_2-plane are not zero. We can map v to a point v' of the form $(r_1, 0, r_2, 0)$, with $r_1 \ne 0$ and $r_2 \ne 0$, by applying a

[15] This easy way of dealing with the duplications caused by ▨ is the reason for preferring the oblique axes of Figure 4.4 for measuring the parameters m and n over the more natural α_1, α_2-axes. This oblique system is also aligned with the specification of the group by its left and right group (of left translations and right translations) that underlies the classic classification, see Appendix G. Curiously, these duplications caused by ▨ were overlooked by Conway and Smith [14], although they had escaped none of the previous classifications [30, p. 62, groupe I], [67, p. 20, item §1, formula (2)], [23, p. 55, first paragraph].

rotation of the form

$$R_{\alpha_1,\alpha_2} = \begin{pmatrix} R_{\alpha_1} & 0 \\ 0 & R_{\alpha_2} \end{pmatrix}. \tag{4.6}$$

The new point v' can be mapped to the point $(\frac{1}{\sqrt{2}}, 0, \frac{1}{\sqrt{2}}, 0)$ by applying a matrix of the form

$$\operatorname{diag}(\lambda_1, \lambda_1, \lambda_2, \lambda_2) = \begin{pmatrix} \lambda_1 & 0 & 0 & 0 \\ 0 & \lambda_1 & 0 & 0 \\ 0 & 0 & \lambda_2 & 0 \\ 0 & 0 & 0 & \lambda_2 \end{pmatrix}. \tag{4.7}$$

Since torus translations commute with the linear transformations (4.6) and (4.7), we are done. □

Frieder and Ladisch [26, Proposition 6.3 and Corollary 8.4] proved that the same conclusion holds for any abelian group: All full-dimensional orbits are linearly equivalent to each other in this case.

4.6. The torus flip groups, type ⊡

These groups are generated by torus translations together with a single torus flip. Adding the flip operation is completely harmless. Conjugation with a flip changes R_{α_1,α_2} to $R_{-\alpha_1,-\alpha_2}$, and therefore does not change the translation lattice at all. The order of the group doubles.

If we choose the origin at the center of a 2-fold rotation induced by a torus flip, then ⊡$^{(s)}_{m,n}$ is generated by

$$[\exp(-\tfrac{2\pi i}{m}), 1], [\exp(-\tfrac{(m+2s)\pi i}{mn}), \exp\tfrac{\pi i}{n}], [j, j].$$

4.7. Groups that contain only one type of reflection

These are the torus reflection groups ◫ and ⊟, as well as the torus swap groups ⧄ and ⧅. The groups of type ◫ and ⊟ are geometrically the same, because ⧄ (or ⧅) exchanges vertical mirrors with horizontal mirrors. Thus, Table 4.3 contains no entries for ⊟. The groups ⧄ and ⧅ are mirrors, and their treatment is similar.

If the directional part of a transformation is a reflection (in the plane), the transformation itself can be either a reflection or a glide reflection. In both cases there is an invariant line. We will classify the groups by placing a letter F on the invariant line and looking at its orbit.

We need a small lemma that is familiar from the classification of the wallpaper groups:

Lemma 4.7.1. *If a two-dimensional lattice has an axis of symmetry, then the lattice is either*

(1) a rectangular lattice that is aligned with the axis, or

(2) a rhombic lattice, which contains in addition the midpoints of the rectangles.

In case (1), the symmetry axis goes through a lattice line or half-way between two lattice lines. In case (2), the symmetry axis goes through a lattice line.

For an example, see the upper half of Figure 4.6, where the mirror lines are drawn as solid lines.

Proof. Assume without loss of generality that the symmetry axis is the y-axis. (We may have to translate the lattice so that it no longer contains the origin.) With every lattice point (x, y), the lattice contains also the mirror point $(-x, y)$, and thus $(2x, 0)$ is a horizontal lattice vector. It follows that there must be a lattice point (x_0, y_0) with smallest positive x-coordinate, since otherwise there would be arbitrarily short lattice vectors.

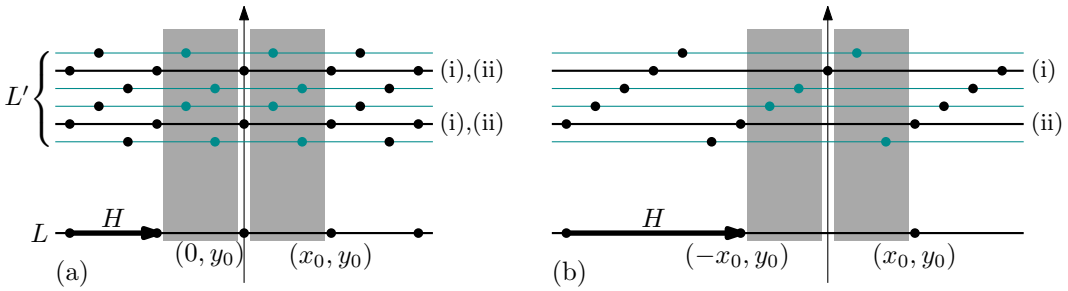

Figure 4.5.: Different possibilities for the lattice line L'. The gray area is forbidden.

Consider the horizontal lattice line L through (x_0, y_0). There are two cases, see Figure 4.5. (a) $(0, y_0)$ is also a lattice point, and $(H, 0) = (x_0, 0)$ is a lattice basis vector. (b) $(0, y_0)$ is not a lattice point, and $(H, 0) = (2x_0, 0)$ is a lattice basis vector. Now look at the next-higher horizontal lattice line L' above L, and choose a lattice point (x', y') on L'. L' contains the points $(x' + kH, y')$ for $k \in \mathbb{Z}$, and therefore a point (x, y') in the interval $-H/2 \le x \le H/2$. The value of x cannot be in the range $-x_0 < x < 0$ or $0 < x < x_0$ because this would contradict the choice of (x_0, y_0). Thus, either (i) $x = 0$ or (ii) both points $(\pm x_0, y')$ are in the lattice. In case (a), both possibilities (i) and (ii) hold simultaneously, and this leads to a rectangular lattice with the axis through lattice points. If (b) and (ii) holds, we have a rectangular lattice with the axis between lattice lines. If (b) and (i) holds, we have a rhombic lattice. □

4.7.1. The torus reflection groups, type ◫

We distinguish two major cases.

M) The group contains a mirror reflection.

G) The group contains only glide reflections.

In both cases, every orientation-reversing transformation has a vertical invariant line. (Actually, since the translation $\varphi_1 \mapsto \varphi_1 + 2\pi$ is always an element of the group, by Theorem 4.3.1, the invariant lines come in pairs $\varphi_1 = \beta$ and $\varphi_1 = \beta + \pi$.)

As announced, we observe the orbit of the letter F. We put the bottom endpoint of the F on an invariant line ℓ. First we look at the orbit under those transformations that leave ℓ invariant, see the left side of Figure 4.6. In case G, the images with and without reflection alternate along ℓ. In case M, they are mirror images of each other.

In case M, we have a mirror symmetry, and by Lemma 4.3.3, the translational subgroup must be closed under the mirror symmetry. Lemma 4.7.1 gives the two possibilities of a rectangular or a rhombic translational subgroup. Combining these translations with the mirror operations leads to the two cases in the top row of Figure 4.6.

In case G, we cannot apply Lemma 4.7.1 right away. Let H be the vertical distance between consecutive points on the axis. If we combine each glide reflection with a vertical translation by $-H$, we get mirror reflections, as in case M. To this modified group, we can apply Lemma 4.7.1, and we conclude that the translational group must either form a rectangular or a rhombic pattern. Adding back the translation by H to the orientation-reversing transformations leads to the results in the lower row of Figure 4.6. In the rhombic case in the lower right picture we see that, when we try to combine glide reflections with a rhombic translational subgroup, we generate mirror symmetries, and

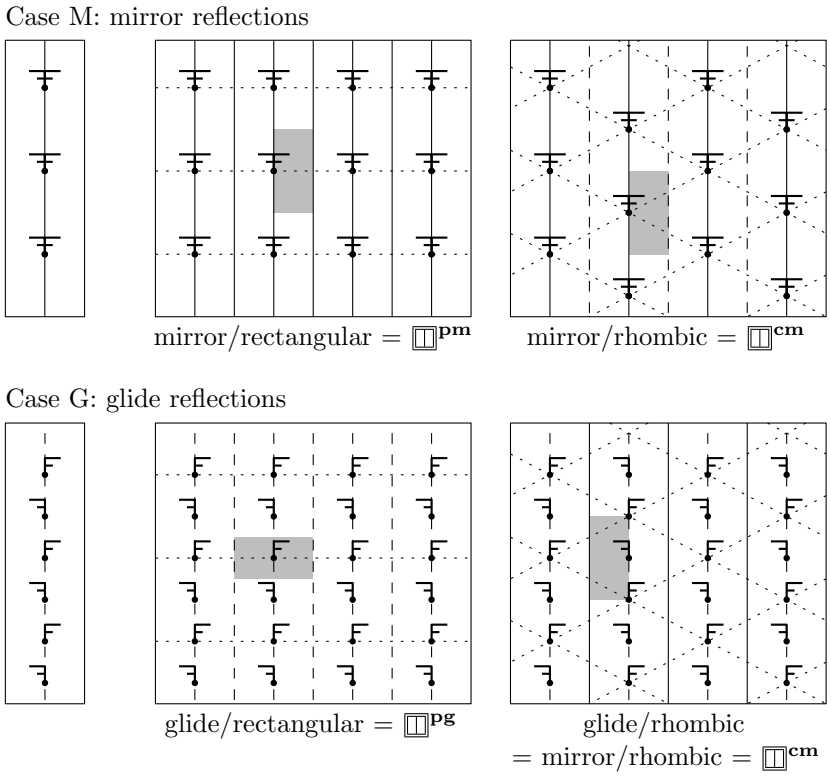

Figure 4.6.: Torus reflection groups, type ◫. Combinations of a vertical mirror/glide reflection axis with either a rectangular or a rhombic grid. Invariant lines are shown as solid lines if they act as mirrors, otherwise dashed. The dotted lines indicate the lattice of translations, and the shaded area is a fundamental domain.

thus, this case really belongs to case M. The picture looks different from the corresponding picture in the upper row because there are two alternating types of invariant lines: mirror lines, and lines with a glide reflection. Depending on where we put the F, we get different pictures.

We are thus left with three cases, which we denote by superscripts that are chosen in accordance with the International Notation for these wallpaper groups:

- mirror/rectangular: ◫$^{\mathbf{pm}}$,
- mirror/rhombic: ◫$^{\mathbf{cm}}$, and
- glide/rectangular: ◫$^{\mathbf{pg}}$.

The groups are parameterized by two parameters $m \geq 1$ and $n \geq 1$, the dimensions of the rectangular grid of translations in the φ_1 and φ_2 directions, see the left part of Figure 4.7.

Since the invariant lines give a distinguished direction, we need not worry about duplications when exchanging m and n. The order of each group G is twice the order of the translational subgroup $G_\square$.

4.7.2. The torus swap groups

For the groups of type ⧄, we have to turn the picture by 45°. We have the same three cases, ⧄$^{\mathbf{pm}}$, ⧄$^{\mathbf{cm}}$, and ⧄$^{\mathbf{pg}}$, but we must adapt the definition of m and n, see the right part of Figure 4.7. We divide the principal diagonal from $(0,0)$ to $(2\pi, 2\pi)$ into m parts and the secondary diagonal from $(0,0)$ to $(2\pi, -2\pi)$ into n parts. We cannot choose m and n freely because the midpoint $(2\pi, 0)$ of the square spanned by these two diagonal directions, which represents the identity mapping, is always part of the lattice. Therefore, for the rectangular lattice cases ⧄$^{\mathbf{pm}}$ and ⧄$^{\mathbf{pg}}$, m and n must be even, and the number

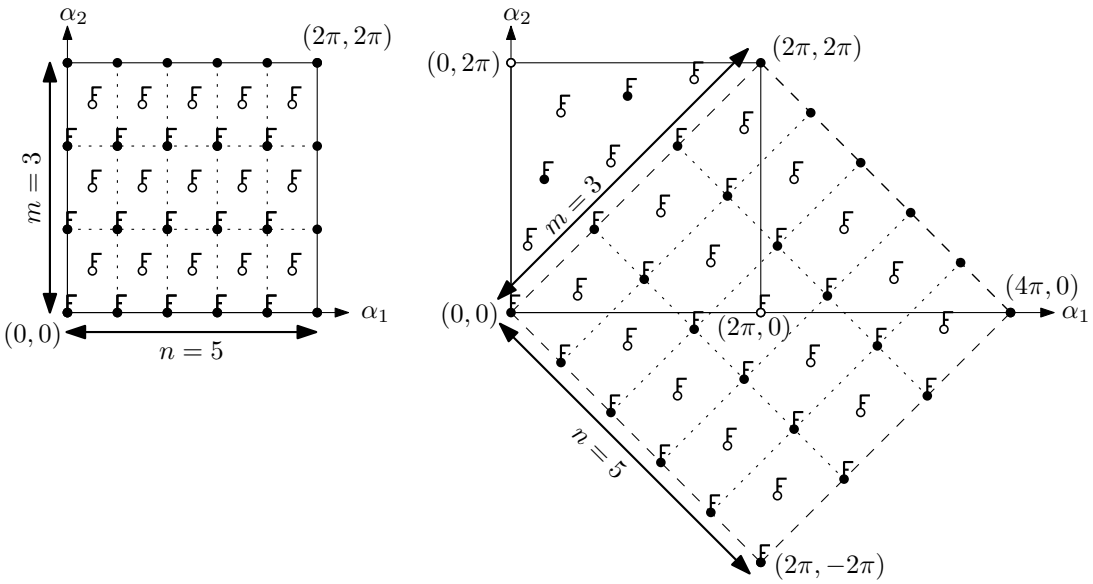

Figure 4.7.: Left: Parameters for the translational subgroup of the groups with vertical invariant lines, type ◫. We divide the vertical axis into m equal parts and the horizontal axis into n equal parts. In the rectangular case, the grid consists only of the mn black points. In the rhombic case, the white points are also present, for $2mn$ translations in total.
Right: For the groups of type ◪, the axes are tilted clockwise by 45° and longer by the factor $\sqrt{2}$.

of lattice points on the torus is $mn/2$. (We loose a factor of 2 compared to ◫, because the tilted square in the figure covers the torus twice.) For the rhombic lattice case $◪^{\mathbf{cm}}$, m and n must have the same parity, and the number of lattice points on the torus is mn.

We mention that the parameter m in this case coincides with the parameter m for the translations-only case □ of Figure 4.4. The parameter n coincides in the rhombic case; in the rectangular case, it is twice as big.

As mentioned, the groups of type ◩ are mirrors of the groups of type ◪, and we need not discuss them separately.

Generators for ◫, ◪ and ◩. Whenever a mirror line exists (**cm** and **pm**), we choose the origin of the coordinate system on such a line; otherwise (**pg**), we place it on an axis of glide reflection. With these conventions, the groups can be generated by the generators listed in Table 4.4.

group	generators
$◫^{\mathbf{pm}}_{m,n}$	$[e^{\frac{\pi i}{m}}, e^{\frac{\pi i}{m}}], [e^{\frac{\pi i}{n}}, e^{-\frac{\pi i}{n}}], *[i, i]$
$◫^{\mathbf{pg}}_{m,n}$	$[e^{\frac{\pi i}{m}}, e^{\frac{\pi i}{m}}], [e^{\frac{\pi i}{n}}, e^{-\frac{\pi i}{n}}], *[i, i][e^{\frac{\pi i}{2m}}, e^{\frac{\pi i}{2m}}]$
$◫^{\mathbf{cm}}_{m,n}$	$[e^{\frac{\pi i}{m}}, e^{\frac{\pi i}{m}}], [e^{\frac{\pi i}{n}}, e^{-\frac{\pi i}{n}}], [e^{\frac{\pi i}{2m}+\frac{\pi i}{2n}}, e^{\frac{\pi i}{2m}-\frac{\pi i}{2n}}], *[i, i]$
$◩^{\mathbf{pm}}_{2m,2n}$	$[e^{\frac{\pi i}{m}}, 1], [1, e^{\frac{\pi i}{n}}], [-k, i]$
$◩^{\mathbf{pg}}_{2m,2n}$	$[e^{\frac{\pi i}{m}}, 1], [1, e^{\frac{\pi i}{n}}], [1, e^{\frac{\pi i}{2n}}][-k, i]$
$◩^{\mathbf{cm}}_{m,n}$	$[e^{\frac{i2\pi}{m}}, 1], [1, e^{\frac{i2\pi}{n}}], [e^{\frac{\pi i}{n}}, e^{\frac{\pi i}{m}}], [-k, i]$
$◪^{\mathbf{pm}}_{2m,2n}$	$[e^{\frac{\pi i}{m}}, 1], [1, e^{\frac{\pi i}{n}}], [i, k]$
$◪^{\mathbf{pg}}_{2m,2n}$	$[e^{\frac{\pi i}{m}}, 1], [1, e^{\frac{\pi i}{n}}], [e^{\frac{\pi i}{2m}}, 1][i, k]$
$◪^{\mathbf{cm}}_{m,n}$	$[e^{\frac{i2\pi}{m}}, 1], [1, e^{\frac{i2\pi}{n}}], [e^{\frac{\pi i}{n}}, e^{\frac{\pi i}{m}}], [i, k]$

Table 4.4.: Generators for torus reflection groups and torus swap groups

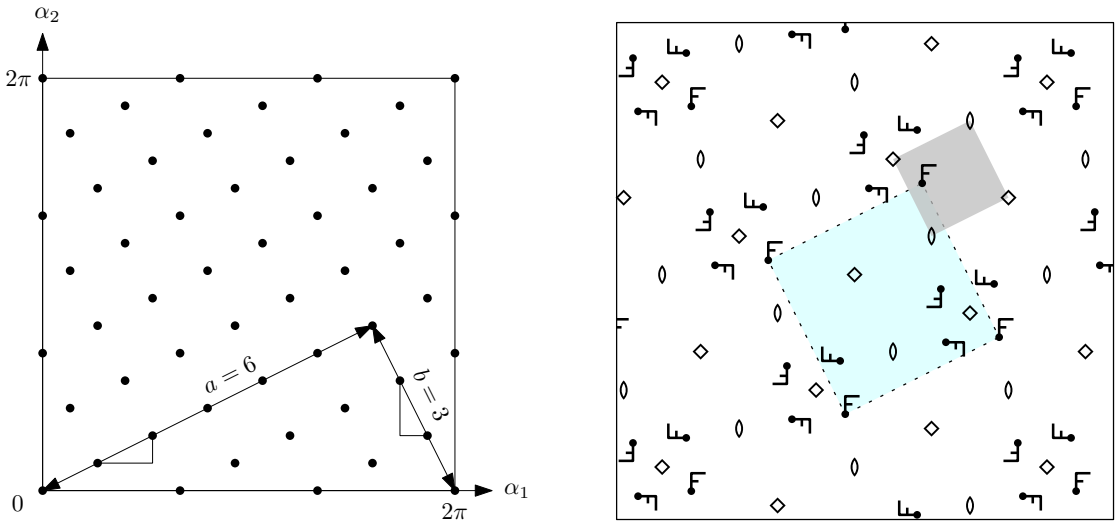

Figure 4.8.: Left: Parameterizing a square grid. Right: The wallpaper group **p4** corresponding to the groups ⊡. The centers of 4-fold rotations are marked by diamonds, the centers of 2-fold rotations are marked by "digons" in the form of a lense. The dotted light-blue square indicates the square lattice of the subgroup of translations, arbitrarily anchored at an upright F.

4.8. The torus swapturn groups, type ⊡

By Lemma 4.3.3, the lattice of translations must be a square grid. The left part of Figure 4.8 shows how we parameterize a square grid on the torus. We take the sides $a \geq 0$ and $b \geq 0$ of the grid rectangle spanned by the two points $(0, 0)$ and $(2\pi, 0)$, measured in grid units. Since $(0, b)$ leads to the same grid rectangle as $(b, 0)$, we require $a \geq 1$.

Conjugation by ◹ reflects the grid at the principal diagonal. Since the grid is symmetric under 90° rotations, this has the same effect as reflection at a vertical axis, and it is easy to see that such a reflection swaps the parameters a and b. Thus, (a, b) and (b, a) describe the same group, and we can assume $a \geq b$ without loss of generality.

The number of grid points, i.e., the size of the translational subgroup, is $a^2 + b^2$, and the order is $4(a^2 + b^2)$. The right part of Figure 4.8 shows the various centers of 2-fold and 4-fold rotations, and a typical orbit. This corresponds to the wallpaper group **p4**.

The grid is generated by the two orthogonal vectors $(\alpha_1, \alpha_2) = 2\pi(\frac{a}{a^2+b^2}, \frac{b}{a^2+b^2})$ and $(\alpha_1, \alpha_2) = 2\pi(\frac{b}{a^2+b^2}, -\frac{-a}{a^2+b^2})$, with $c = \sqrt{a^2 + b^2}$. If we choose the origin at the center of a 4-fold rotation induced by a swapturn, then $⊡_{a,b}$ can be generated by

$$[\exp \tfrac{(-a-b)\pi i}{a^2+b^2}, \exp \tfrac{(a-b)\pi i}{a^2+b^2}], [\exp \tfrac{(a-b)\pi}{a^2+b^2}, \exp \tfrac{(a+b)\pi i}{a^2+b^2}], *[-j, 1].$$

4.9. Groups that contain two orthogonal reflections, type ⊞ and ⊠

As in the case of ◫, we distinguish, for each axis separately, whether there are mirror reflections or only glide reflections. We know that the glide reflection case is inconsistent with the rhombic lattice (cf. Section 4.7.1). Hence, we have the following cases, see Figure 4.9.

- The grid of translations is a rhombic grid. In this case, both axes directions must be mirrors: **c2mm**.

- The grid of translations is a rectangular grid. In this case each axis direction can be a mirror direction or a glide reflection
  - **p2mm**. Two mirror directions
  - **p2mg**. One mirror direction and one glide direction
  - **p2gg**. Two glide directions

In **p2mg**, the two families of invariant lines are distinguishable: one family of parallel lines consists of mirror lines, whereas the perpendicular family has only glide reflections. Thus, there are two different types, where the two directions change roles.

However, for ⊞, we need not distinguish two versions of ⊞$^{\mathbf{p2mg}}$, because conjugation with ⊘ maps one to the other. For ⊠, on the other hand, the two versions are distinct. They are mirror images. We distinguish ⊠$^{\mathbf{p2mg}}$, where the mirror lines are parallel to the principal diagonal $\varphi_2 = +\varphi_1$, and ⊠$^{\mathbf{p2gm}}$, where the mirror lines are parallel to the secondary diagonal direction $\varphi_2 = -\varphi_1$.[16] The parameters m and n have the same meaning as in the corresponding groups ⊟ and ⊘.

These groups contain torus flips, as the product of two perpendicular reflections. We choose the origin on the center of a 2-fold rotation induced by a torus flip. For the groups **c2mm**, we place origin at the intersection of two mirror lines. Then the groups can be generated by the generators given in Table 4.5.

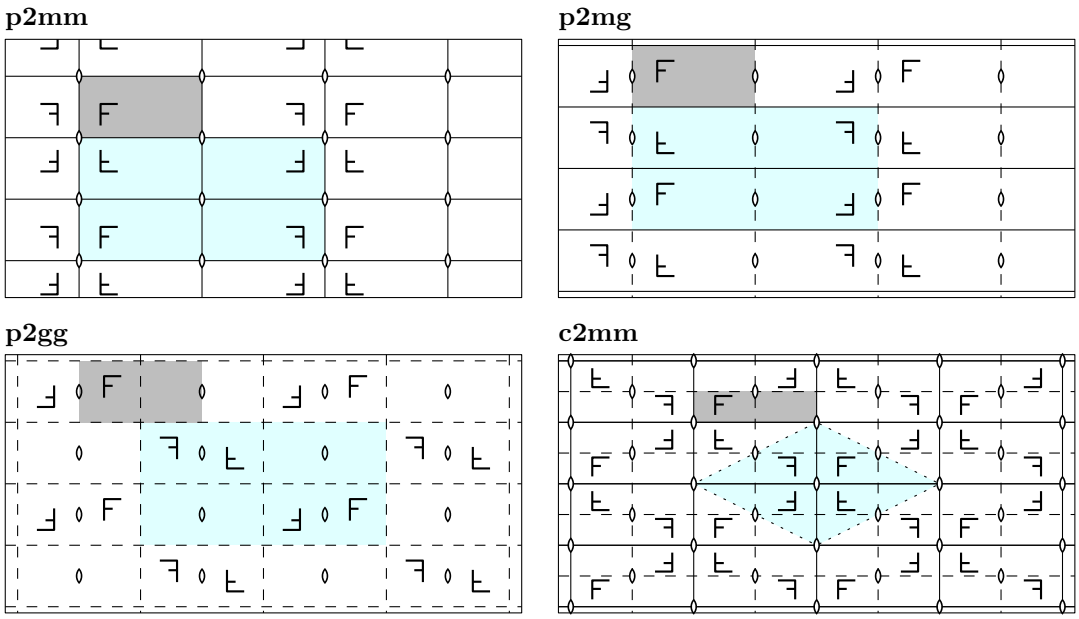

Figure 4.9.: The four types of groups with two orthogonal families invariant lines. The light-blue region indicates the lattice of translations. For better visibility, the letter F is moved away from the mirror lines. Axes of mirror reflection are shown as solid lines, and axes of glide reflection are dashed. As in Figure 4.8, lenses mark centers of 2-fold rotations.

4.10. The full torus groups, type ⊠

Finally, we have the groups where all directional transformations are combined. The conditions of ⊞ and ⊠ force the lattice to be a rectangular lattice both in the φ_1, φ_2

[16] This is in accordance with previous editions of the International Tables of X-Ray Crystallography, which explicitly provided variations of the symbols for different "settings" [35, Table 6.1.1, p. 542 in the 1952/1969 edition]: short symbol **pmg**, full symbol **p2mg**, or **p2gm** for other setting.

group	generators
$\boxplus^{\mathbf{p2mm}}_{m,n}$	$[e^{\frac{\pi i}{m}}, e^{\frac{\pi i}{m}}], [e^{\frac{\pi i}{n}}, e^{-\frac{\pi i}{n}}], *[i,i], *[k,k]$
$\boxplus^{\mathbf{p2mg}}_{m,n}$	$[e^{\frac{\pi i}{m}}, e^{\frac{\pi i}{m}}], [e^{\frac{\pi i}{n}}, e^{-\frac{\pi i}{n}}], *[i,i][e^{\frac{\pi i}{2n}}, e^{-\frac{\pi i}{2n}}], *[k,k][e^{\frac{\pi i}{2n}}, e^{-\frac{\pi i}{2n}}]$
$\boxplus^{\mathbf{p2gg}}_{m,n}$	$[e^{\frac{\pi i}{m}}, e^{\frac{\pi i}{m}}], [e^{\frac{\pi i}{n}}, e^{-\frac{\pi i}{n}}], *[i,i][e^{\frac{\pi i}{2m}+\frac{\pi i}{2n}}, e^{\frac{\pi i}{2m}-\frac{\pi i}{2n}}], *[k,k][e^{\frac{\pi i}{2m}+\frac{\pi i}{2n}}, e^{\frac{\pi i}{2m}-\frac{\pi i}{2n}}]$
$\boxplus^{\mathbf{c2mm}}_{m,n}$	$[e^{\frac{\pi i}{m}}, e^{\frac{\pi i}{m}}], [e^{\frac{\pi i}{n}}, e^{-\frac{\pi i}{n}}], [e^{\frac{\pi i}{2m}+\frac{\pi i}{2n}}, e^{\frac{\pi i}{2m}-\frac{\pi i}{2n}}], *[i,i], *[k,k]$
$\boxtimes^{\mathbf{p2mm}}_{2m,2n}$	$[e^{\frac{\pi i}{m}}, 1], [1, e^{\frac{\pi i}{n}}], [i,k], [-k,i]$
$\boxtimes^{\mathbf{p2mg}}_{2m,2n}$	$[e^{\frac{\pi i}{m}}, 1], [1, e^{\frac{\pi i}{n}}], [1, e^{\frac{\pi i}{2n}}][i,k], [1, e^{\frac{\pi i}{2n}}][-k,i]$
$\boxtimes^{\mathbf{p2gm}}_{2m,2n}$	$[e^{\frac{\pi i}{m}}, 1], [1, e^{\frac{\pi i}{n}}], [e^{\frac{\pi i}{2m}}, 1][i,k], [e^{\frac{\pi i}{2m}}, 1][-k,i]$
$\boxtimes^{\mathbf{p2gg}}_{2m,2n}$	$[e^{\frac{\pi i}{m}}, 1], [1, e^{\frac{\pi i}{n}}], [e^{\frac{\pi i}{2m}}, e^{\frac{\pi i}{2n}}][i,k], [e^{\frac{\pi i}{2m}}, e^{\frac{\pi i}{2n}}][-k,i]$
$\boxtimes^{\mathbf{c2mm}}_{m,n}$	$[e^{\frac{i2\pi}{m}}, 1], [1, e^{\frac{i2\pi}{n}}], [e^{\frac{\pi i}{m}}, e^{\frac{\pi i}{n}}], [i,k], [-k,i]$
$\boxtimes^{\mathbf{p4mmU}}_{n}$	$[e^{\frac{\pi i}{n}}, e^{\frac{\pi i}{n}}], [e^{\frac{\pi i}{n}}, e^{-\frac{\pi i}{n}}], [i,k], *[i,i]$
$\boxtimes^{\mathbf{p4gmU}}_{n}$	$[e^{\frac{\pi i}{n}}, e^{\frac{\pi i}{n}}], [e^{\frac{\pi i}{n}}, e^{-\frac{\pi i}{n}}], [i,k][e^{\frac{\pi i}{n}}, 1], *[i,i][e^{\frac{\pi i}{n}}, 1]$
$\boxtimes^{\mathbf{p4mmS}}_{n}$	$[e^{\frac{\pi i}{n}}, 1], [1, e^{\frac{\pi i}{n}}], [i,k], *[i,i]$
$\boxtimes^{\mathbf{p4gmS}}_{n}$	$[e^{\frac{\pi i}{n}}, 1], [1, e^{\frac{\pi i}{n}}], [i,k][e^{\frac{\pi i}{2n}}, e^{\frac{\pi i}{2n}}], *[i,i][e^{\frac{\pi i}{2n}}, e^{\frac{\pi i}{2n}}]$

Table 4.5.: Generators for full torus reflection groups, full torus swap groups, and full torus groups

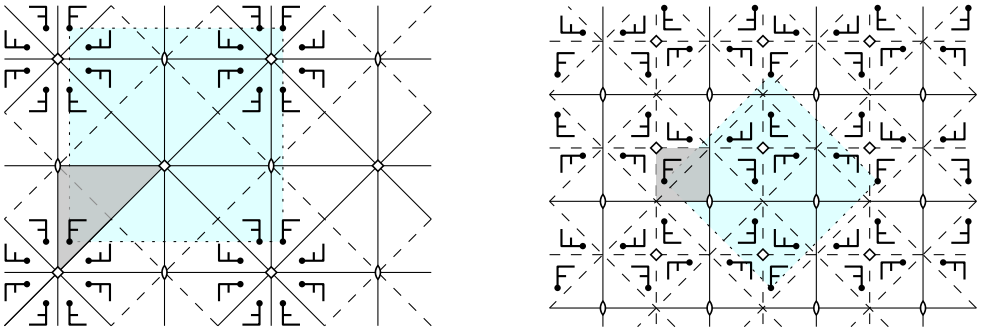

(a) mirror reflections, upright grid (**p4mm**U) (b) glide reflections, slanted grid (**p4gm**S)

Figure 4.10.: Two of the four types of groups $\boxtimes$. Small squares denote centers of 4-fold rotations. For each figure, there exists a rotated version by 45°, where $\boxtimes^{\mathbf{p4mmU}}$ becomes $\boxtimes^{\mathbf{p4mmS}}$, and $\boxtimes^{\mathbf{p4gmS}}$ becomes $\boxtimes^{\mathbf{p4gmU}}$.

axis direction and in the ±45° direction, possibly with added midpoints (rhombic case). This means that the lattice is a *square* lattice. It appears as a *rectangular* lattice in one pair of perpendicular directions and as a *rhombic* lattice in the other directions.

Thus, there are only two cases for the translation lattice: The square $n \times n$ lattice with n^2 translations (the upright grid "U", Figure 4.10a), and its rhombic extension with $2n^2$ translations (the slanted grid "S", Figure 4.10b).

Let us first consider the slanted case, see Figure 4.10b. The lattice appears as a rhombic lattice for the $\boxplus$ directions. From the point of view of the subgroups of type $\boxplus$, we know that this means that the "glide reflection" case is excluded (cf. the discussion in Section 4.7.1). There must be mirror reflections in the horizontal and vertical axes.

For the $\boxtimes$ directions, the lattice appears as a rectangular lattice. According to Section 4.9 we can have the cases mirror/mirror, mirror/glide, glide/glide. But since 90° rotations are included, the mixed mirror/glide case is impossible. Two cases remain, which we call $\boxtimes^{\mathbf{p4mmS}}$ and $\boxtimes^{\mathbf{p4gmS}}$. The latter is shown in Figure 4.10b. When the lattice appears as a square lattice for the $\boxplus$ directions, the two pairs of directions $\boxplus$ and $\boxtimes$ change roles, and we have two more groups, $\boxtimes^{\mathbf{p4mmU}}$ and $\boxtimes^{\mathbf{p4gmU}}$. The first one is shown in Figure 4.10a. The groups $\boxtimes^{\mathbf{p4mm}}$ have mirrors in all four directions, whereas the groups $\boxtimes^{\mathbf{p4gm}}$ have mirrors in two directions only.

To list the generators for the full torus groups, we choose the origin of the coordinate

system on the center of a 4-fold rotation induced by a swapturn, see Table 4.5.

This concludes the discussion of the toroidal groups. The reader who wishes to practice the understanding of these classes might try to count, as an exercise, all groups of order 100, see Appendix C.

4.11. Duplications

As we have seen, every subgroup of a group $\pm[D_{2m} \times D_{2n}]$ has an invariant torus. So far, we have analyzed the groups that leave a *fixed* torus invariant. We have already mentioned that some subgroups have more than one invariant Clifford torus, and this leads to duplications. Unfortunately, when it comes to weeding out duplications, all classifications (including the classic classification) become messy.[17]

We analyze the situation as follows. Every orientation-preserving transformation is of the form R_{α_1,α_2}, with $-\pi \leq \alpha_1, \alpha_2 \leq \pi$. If $\alpha_1 \neq \pm\alpha_2$, there is a unique pair of absolutely orthogonal invariant planes, and hence, there is a unique invariant Clifford torus *on which the transformation appears as a torus translation.* We call this torus the *primary* invariant torus.

Our strategy is to analyze the situation backwards. We look at all orientation-preserving transformations that are not torus translations, we write them in the form R_{α_1,α_2} and determine the translation vector (α_1, α_2) by which they would appear on their primary invariant torus. The result is summarized in the following proposition. The torus translations that lead to ambiguity are shown in Figure 4.11:

Proposition 4.11.1. *The orientation-preserving transformations that have more than one invariant torus are the following:*

(a) *Simple half-turns of the form* $\mathrm{diag}(-1,-1,1,1)$.

On their primary torus, they appear as torus translation by $(\pi, 0)$ *or* $(0, \pi)$. *There is an infinite family of alternate tori for which they are interpreted as torus flips or torus swaps.*

(b) *Double rotations* $R_{\alpha,\pi\pm\alpha}$.

On an alternate torus, they appear as reflections or glide reflections associated to torus swaps ⊿ *or* ⊾.

(c) *Left and right rotations* $R_{\alpha,\pm\alpha}$, *including* id *and* $-$id. *(For* $\alpha = \pm\pi/2$, *these fall also under case (b).)*

A left rotation $R_{\alpha,\alpha}$ *with* $\alpha \neq \pm\pi/2$ *appears as a torus translation by* (α, α) *or by* $(-\alpha, -\alpha)$ *on every invariant torus.*

Similarly, a right rotation $R_{\alpha,-\alpha}$ *with* $\alpha \neq \pm\pi/2$ *appears as a torus translation by* $(\alpha, -\alpha)$ *or by* $(-\alpha, \alpha)$ *on every invariant torus.*

Proof. The orientation-preserving transformations that are not torus translations are ⊡ (torus flips) and ⊿ and ⊾ (reflections and glide reflections associated to torus swaps).

Every torus flip is a half-turn, and these are covered in case (a).

Let us look at reflections and glide reflections associated to the torus swaps ⊿. The torus swap ⊿ at the principal diagonal is the transformation $[i, k]$. Both i and k are pure quaternions, in accordance with the fact that ⊿ is a half-turn. The general torus swap of type ⊿ is obtained by combining $[i, k]$ with an arbitrary torus translation $[\exp \beta_l i, \exp \beta_r i]$:

$$[i \exp \beta_l i, k \exp \beta_r i] = [\exp(\tfrac{\pi}{2} i) \exp \beta_l i, k(\cos \beta_r + i \sin \beta_r)] = [\exp((\tfrac{\pi}{2} + \beta_l)i), k \cos \beta_r + j \sin \beta_r]$$

[17] The difficulty caused by these ambiguous transformations, in particular in connection with achiral groups, was already acknowledged by Hurley [37, p. 656–7].

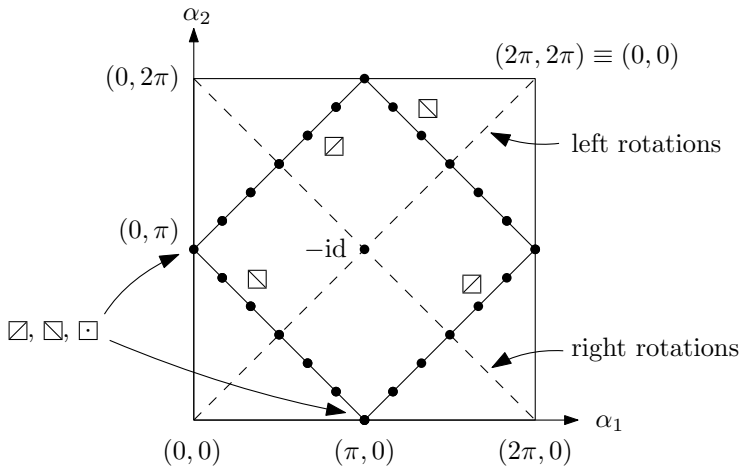

Figure 4.11.: The torus translations on the tilted square are ambiguous: they can appear as rotations of different types, as indicated. Left and right rotations (on the diagonal) also have no unique invariant torus, but they appear as left and right rotations on any invariant torus.

The right component $k \cos \beta_r + j \sin \beta_r$ is still a unit quaternion (rotation angle $\pi/2$), and hence the right rotation $[1, \exp \beta_r i]$ has no effect on the type of the transformation. This is in accordance with the fact that, on the φ_1, φ_2-torus, a right rotation is a translation perpendicular to the reflection axis of ◿, whose effect is just to move the reflection axis. The left rotation, however, changes the rotation angle from $\pi/2$ to $\pi/2 + \beta_l$. The result is a rotation of type $R_{\pi+\beta_l,\beta_l}$. As a torus translation R_{α_1,α_2}, it lies on the line $\alpha_1 = \alpha_2 + \pi$ (and $\alpha_1 = \alpha_2 - \pi$, considering that angles are taken modulo 2π), see Figure 4.11.

The operations of type ◺ are the mirrors of ◿, and hence they appear on the reflected lines $\alpha_1 = -(\alpha_2 \pm \pi)$.

Left and right rotations have infinitely many invariant tori, but cause no confusion for our classification, because a left rotation will appear as the same left rotation on *any* invariant torus (possibly with an inverted angle), except when it falls under case (b). □

We note the curious fact that the operations that don't have a unique invariant torus coincide with the operations whose squares are left or right rotations.

Corollary 4.11.2. *A group may have more than one invariant torus only if the translational subgroup contains only elements on the diagonals and on the tilted square in Figure 4.11.*

This excludes from the search for duplications those groups for which the translational subgroup is sufficiently rich, i.e., when both parameters m and n are large. Still it leaves a large number of cases where one of the parameters is small. We present the list of duplications below.

4.11.1. List of Duplications

As mentioned, we have imposed the stricter conditions on m and n (and a and b) in Table 4.3 in order to exclude all duplications. As a rule, among equal groups, we have chosen the group with the larger subgroup of torus translations (with the chosen invariant torus) to stay in the table.

Table 4.6 lists every group G_1 that is excluded from Table 4.3, together with a group G_2 to which it is conjugate, and a conjugation that converts the second group to the first one. The conjugations depend on the specific parameterizations that we have chosen and

that were given with each class of groups discussed above, in particular in Tables 4.4 and 4.5.

In this chapter, we use the notation $G_1 \doteq G_2$ for groups that are geometrically the same, i.e., conjugate under an orientation-preserving transformation, and we reserve the sign "=" for groups that are equal in our chosen coordinate system.

In some classes, the choice of the two parameters m and n is symmetric (e.g., $\boxplus^{\mathbf{p2mm}}_{m,n} \doteq \boxplus^{\mathbf{p2mm}}_{n,m}$). In those cases, we have achieved uniqueness by requiring $m \geq n$ in Table 4.3. Such symmetries between the parameters, and other general relations are listed first for each type of group in Table 4.6. This is followed by a list of groups with small parameters that are explicitly excluded in Table 4.3.

We have made some simplifications to keep the table compact. As mentioned previously, we sometimes refer to groups $\square^{(s)}_{m,n}$ or $\boxdot^{(s)}_{m,n}$ where the parameter s lies outside the "legal" range (4.5), in order to avoid case distinctions. The parameter s can be brought into that range by using the equalities $\square^{(s)}_{m,n} = \square^{(s\pm m)}_{m,n} \doteq \square^{(-n-s)}_{m,n}$, and similarly for $\boxdot$. If the permissible range of parameters s contains only one integer, we omit the parameter and denote the group simply by $\square_{m,n}$ or $\boxdot_{m,n}$. In such a case, any choice of s will lead to the same group.

We have a few cases with more than two equal groups:

$$\boxslash^{\mathbf{cm}}_{1,1} \doteq \boxbslash^{\mathbf{cm}}_{1,1} \doteq \boxdot^{(0)}_{1,1} \doteq \square^{(0)}_{1,2} = \langle \mathrm{diag}(1,1,-1,-1)\rangle \text{ (order 2)}$$

$$\boxslash^{\mathbf{pm}}_{2,2} \doteq \boxbslash^{\mathbf{pm}}_{2,2} \doteq \boxdot^{(-1)}_{2,1} \doteq \square^{(0)}_{2,2} = \langle \mathrm{diag}(1,1,-1,-1), \mathrm{diag}(-1,-1,1,1)\rangle \cong D_4 \text{ (order 4)}$$

$$\boxtimes^{\mathbf{p2gg}}_{2,2} \doteq \boxslash^{\mathbf{pm}}_{4,2} \doteq \boxbslash^{\mathbf{pm}}_{2,4} \doteq \square^{(-2)}_{4,2} = \langle \mathrm{diag}(R_{\pi/2}, R_{\pi/2}), \mathrm{diag}(R_{\pi/2}, R_{-\pi/2})\rangle \text{ (order 8)}$$

$$\boxtimes^{\mathbf{p2gm}}_{2,2} \doteq \boxslash^{\mathbf{cm}}_{2,2} \doteq \boxslash^{\mathbf{pm}}_{2,4} \doteq \boxdot^{(-1)}_{2,2} \doteq \langle -\mathrm{id}, \mathrm{diag}(1,-1,1,-1), \mathrm{diag}(R_{\pi/2}, R_{-\pi/2})\rangle \text{ (order 8)}$$

$$\boxtimes^{\mathbf{p2mg}}_{2,2} \doteq \boxbslash^{\mathbf{cm}}_{2,2} \doteq \boxbslash^{\mathbf{pm}}_{4,2} \doteq \boxdot^{(-2)}_{4,1} \doteq \langle -\mathrm{id}, \mathrm{diag}(1,-1,1,-1), \mathrm{diag}(R_{\pi/2}, R_{\pi/2})\rangle \text{ (order 8)}$$

$$\boxtimes^{\mathbf{p4gmU}}_{1} \doteq \boxplus^{\mathbf{p2gg}}_{2,1} \doteq \boxplus^{\mathbf{p2gg}}_{1,2} \doteq \langle \mathrm{diag}(-1,-1,1,1), \mathrm{diag}(1,1,-1,1), \mathrm{diag}(1,1,1,-1)\rangle \text{ (order 8)}$$

$$\boxtimes^{\mathbf{c2mm}}_{2,2} \doteq \boxtimes^{\mathbf{p2mm}}_{4,2} \doteq \boxtimes^{\mathbf{p2mm}}_{2,4} \doteq \boxdot^{(-2)}_{4,2} \text{ (order 16)}$$

To reduce case distinctions, some of these groups G_1 point to groups G_2 that are themselves excluded in Table 4.3, and which must be looked up again in Table 4.6.

The conjugations in Table 4.6 were found by computer search for particular values of m. In many cases, the conjugate group or the conjugacy mapping depends on the parity of some parameter. We tried to simplify the entries of the table by manually adjusting them. All conjugations were checked by computer for $m \leq 100$.

When the groups are translated to the Conway-Smith classification using Table 4.3, the duplications have easy algebraic justifications: For example, C_2 and D_2 are obviously the same group. Also, $\bar{D}_4$ can be replaced by D_4, see Appendix G.1 for more information.

4.11.2. A duplication example

By way of example, we treat one duplication in detail:

$$\boxtimes^{\mathbf{c2mm}}_{1,n} \doteq \boxdot^{(\frac{n-1}{2})}_{1,2n}, \text{ for odd } n. \tag{4.8}$$

Figure 4.12 shows the action of these groups on the torus for $n = 5$. We can confirm that, in accordance with Corollary 4.11.2, the 10 torus translations of $\boxdot^{(2)}_{1,10}$ lie only on a diagonal and on the line $\alpha_1 + \alpha_2 = \pm\pi$. The latter 5 translations become reflections and glide reflections in $\boxtimes^{\mathbf{c2mm}}_{1,5}$. More precisely, in accordance with Figure 4.11, they are the reflections at the $\boxbslash$ diagonal (4 glide reflections and one reflection). The picture shows actually more glide reflection and reflection axes than the order of the group would allow. The reason is that every glide reflection in this group can also be interpreted as a reflection, at a different axis.

G_1	G_2	$[\hat{l},\hat{r}]$	G_1	G_2	$[\hat{l},\hat{r}]$
chiral groups					
$\square^{(s)}_{m,n}$	$\square^{(s+n)}_{m,n}$	$[1,1]$ (equal)	$\boxdot^{(s)}_{m,n}$	$\boxdot^{(s+n)}_{m,n}$	$[1,1]$ (equal)
$\square^{(s)}_{m,n}$	$\square^{(-m-s)}_{m,n}$	$[i,k]=\boxslash$	$\boxdot^{(s)}_{m,n}$	$\boxdot^{(-m-s)}_{m,n}$	$[i,k]=\boxslash$
			$\boxdot_{1,1}$	$\square_{1,2}$	$[i+j,1+k]$
			$\boxdot_{2,1}$	$\square^{(0)}_{2,2}$	$[i+j,i+j]$
$\boxbslash^{\mathbf{pm}}_{4m-2,2}$	$\boxdot_{4m-2,1}$	$[j+k,i+j]$	$\boxslash^{\mathbf{pm}}_{2,4m-2}$	$\boxdot^{(-1)}_{2,2m-1}$	$[i+j,j+k]$
$\boxbslash^{\mathbf{pm}}_{4m,2}$	$\boxdot_{4m,1}$	$[1,i+j]$	$\boxslash^{\mathbf{pm}}_{2,4m}$	$\boxdot^{(-1)}_{2,2m}$	$[i+j,1]$
$\boxbslash^{\mathbf{pm}}_{2,4m-2}$	$\square^{(2m-2)}_{2,4m-2}$	$[i+k,1]$	$\boxslash^{\mathbf{pm}}_{2m,2}$	$\square^{(0)}_{2m,2}$	$[1,i+k]$
$\boxbslash^{\mathbf{pm}}_{2,4m}$	$\square^{(-2)}_{4,2m}$	$[i+k,1]$			
$\boxbslash^{\mathbf{pg}}_{2,4m-2}$	$\square^{(-2)}_{4,2m-1}$	$[i+k,1]$	$\boxslash^{\mathbf{pg}}_{2m,2}$	$\square^{(1)}_{2m,2}$	$[1,i+k]$
$\boxbslash^{\mathbf{pg}}_{2,4m}$	$\square^{(2m-1)}_{2,4m}$	$[i+k,1]$			
$\boxbslash^{\mathbf{cm}}_{2m+1,1}$	$\boxdot_{2m+1,1}$	$[j+k,1-k]$	$\boxslash^{\mathbf{cm}}_{1,2m+1}$	$\boxdot^{(m)}_{1,2m+1}$	$[i+j,j+k]$
$\boxbslash^{\mathbf{cm}}_{1,4m-3}$	$\square^{(2m-2)}_{1,8m-6}$	$[i+k,1]$	$\boxslash^{\mathbf{cm}}_{4m-3,1}$	$\square_{4m-3,2}$	$[1,1-j]$
$\boxbslash^{\mathbf{cm}}_{1,4m-1}$	$\square^{(2m-1)}_{1,8m-2}$	$[1-j,1]$	$\boxslash^{\mathbf{cm}}_{4m-1,1}$	$\square_{4m-1,2}$	$[1,i+k]$
$\boxbslash^{\mathbf{cm}}_{2,4m-2}$	$\boxbslash^{\mathbf{pm}}_{4,4m-2}$	$[i+j,1]$	$\boxslash^{\mathbf{cm}}_{4m-2,2}$	$\boxslash^{\mathbf{pm}}_{4m-2,4}$	$[1,i+j]$
$\boxbslash^{\mathbf{cm}}_{2,4m}$	$\boxbslash^{\mathbf{pg}}_{4,4m}$	$[i+k,1]$	$\boxslash^{\mathbf{cm}}_{4m,2}$	$\boxslash^{\mathbf{pg}}_{4m,4}$	$[1,i+k]$
$\boxtimes^{\mathbf{p2mm}}_{2m,2}$	$\boxdot^{(0)}_{2m,2}$	$[1,i+k]$	$\boxtimes^{\mathbf{p2mm}}_{2,4m-2}$	$\boxdot^{(2m-2)}_{2,4m-2}$	$[i+k,1]$
			$\boxtimes^{\mathbf{p2mm}}_{2,4m}$	$\boxdot^{(-2)}_{4,2m}$	$[i+k,1]$
$\boxtimes^{\mathbf{p2gm}}_{2m,2}$	$\boxdot^{(1)}_{2m,2}$	$[1,i+k]$	$\boxtimes^{\mathbf{p2mg}}_{2,4m-2}$	$\boxdot^{(-2)}_{4,2m-1}$	$[i+k,1]$
			$\boxtimes^{\mathbf{p2mg}}_{2,4m}$	$\boxdot^{(2m-1)}_{2,4m}$	$[i+k,1]$
$\boxtimes^{\mathbf{p2gm}}_{2,4m-2}$	$\boxslash^{\mathbf{cm}}_{2,4m-2}$	$[i+j,j+k]$	$\boxtimes^{\mathbf{p2mg}}_{4m-2,2}$	$\boxbslash^{\mathbf{cm}}_{4m-2,2}$	$[j+k,i+j]$
$\boxtimes^{\mathbf{p2gm}}_{2,4m}$	$\boxslash^{\mathbf{pm}}_{4,4m}$	$[i+j,1]$	$\boxtimes^{\mathbf{p2mg}}_{4m,2}$	$\boxbslash^{\mathbf{pm}}_{4m,4}$	$[1,i+j]$
$\boxtimes^{\mathbf{p2gg}}_{4m-2,2}$	$\boxbslash^{\mathbf{pm}}_{4m-2,4}$	$[j+k,i+j]$	$\boxtimes^{\mathbf{p2gg}}_{4m,2}$	$\boxbslash^{\mathbf{cm}}_{4m,2}$	$[1,i+j]$
$\boxtimes^{\mathbf{p2gg}}_{2,4m-2}$	$\boxslash^{\mathbf{pm}}_{4,4m-2}$	$[i+j,j+k]$	$\boxtimes^{\mathbf{p2gg}}_{2,4m}$	$\boxslash^{\mathbf{cm}}_{2,4m}$	$[i+j,1]$
$\boxtimes^{\mathbf{c2mm}}_{4m-3,1}$	$\boxdot_{4m-3,2}$	$[1,1-j]$	$\boxtimes^{\mathbf{c2mm}}_{4m-2,2}$	$\boxtimes^{\mathbf{p2mm}}_{4m-2,4}$	$[j+k,i+j]$
$\boxtimes^{\mathbf{c2mm}}_{4m-1,1}$	$\boxdot_{4m-1,2}$	$[1,1+j]$	$\boxtimes^{\mathbf{c2mm}}_{4m,2}$	$\boxtimes^{\mathbf{p2gm}}_{4m,4}$	$[1,i+k]$
$\boxtimes^{\mathbf{c2mm}}_{1,4m-3}$	$\boxdot^{(2m-2)}_{1,8m-6}$	$[1+j,1]$	$\boxtimes^{\mathbf{c2mm}}_{2,4m-2}$	$\boxtimes^{\mathbf{p2mm}}_{4,4m-2}$	$[i+j,j+k]$
$\boxtimes^{\mathbf{c2mm}}_{1,4m-1}$	$\boxdot^{(2m-1)}_{1,8m-2}$	$[1-j,1]$	$\boxtimes^{\mathbf{c2mm}}_{2,4m}$	$\boxtimes^{\mathbf{p2mg}}_{4,4m}$	$[i+k,1]$
achiral groups					
$\boxplus^{\mathbf{p2mm}}_{m,n}$	$\boxplus^{\mathbf{p2mm}}_{n,m}$	$[i,k]=\boxslash$	$\boxcirc_{a,b}$	$\boxcirc_{b,a}$	$[i,k]=\boxslash$
$\boxplus^{\mathbf{p2gg}}_{m,n}$	$\boxplus^{\mathbf{p2gg}}_{n,m}$	$[i,k]=\boxslash$	$\boxcirc_{1,0}$	$\boxminus^{\mathbf{pg}}_{2,1}$	$[1+k,1-i+j+k]$
$\boxplus^{\mathbf{c2mm}}_{m,n}$	$\boxplus^{\mathbf{c2mm}}_{n,m}$	$[i,k]=\boxslash$	$\boxcirc_{1,1}$	$\boxminus^{\mathbf{pg}}_{2,2}$	$[1+k,1+i-j+k]$
$\boxplus^{\mathbf{p2mm}}_{1,1}$	$\boxminus^{\mathbf{pm}}_{1,2}$	$[1+k,1-k]$	$\boxcirc_{2,0}$	$\boxplus^{\mathbf{p2gg}}_{2,2}$	$[1+k,1+k]$
$\boxplus^{\mathbf{p2mg}}_{1,1}$	$\boxminus^{\mathbf{pm}}_{2,1}$	$[1+k,i-j]$			
$\boxplus^{\mathbf{p2gg}}_{1,1}$	$\boxminus^{\mathbf{pg}}_{1,2}$	$[1+k,1-k]$			
$\boxplus^{\mathbf{c2mm}}_{1,1}$	$\boxminus^{\mathbf{pm}}_{2,2}$	$[1+k,1-k]$			
$\circledast^{\mathbf{p4mmU}}_{1}$	$\boxplus^{\mathbf{p2mg}}_{1,2}$	$[1+k,1-i-j-k]$	$\circledast^{\mathbf{p4gmU}}_{1}$	$\boxplus^{\mathbf{p2gg}}_{2,1}$	$[1+k,1+i-j+k]$
$\circledast^{\mathbf{p4mmU}}_{2}$	$\boxplus^{\mathbf{c2mm}}_{2,2}$	$[1+k,1+k]$	$\circledast^{\mathbf{p4gmU}}_{2}$	$\boxcirc_{2,2}$	$[1+j,1+j]$
$\circledast^{\mathbf{p4mmS}}_{1}$	$\boxplus^{\mathbf{p2mg}}_{2,2}$	$[1+k,1+i+j-k]$	$\circledast^{\mathbf{p4gmS}}_{1}$	$\boxminus^{\mathbf{cm}}_{2,2}$	$[1+k,1+k]$

Table 4.6.: Duplications. The range of the parameter m is $m \geq 1$ in all cases. The group G_1 is obtained from G_2 by conjugation with $h := [\frac{\hat{l}}{\|\hat{l}\|}, \frac{\hat{r}}{\|\hat{r}\|}]$. That is, $G_1 = h^{-1}G_2h$.

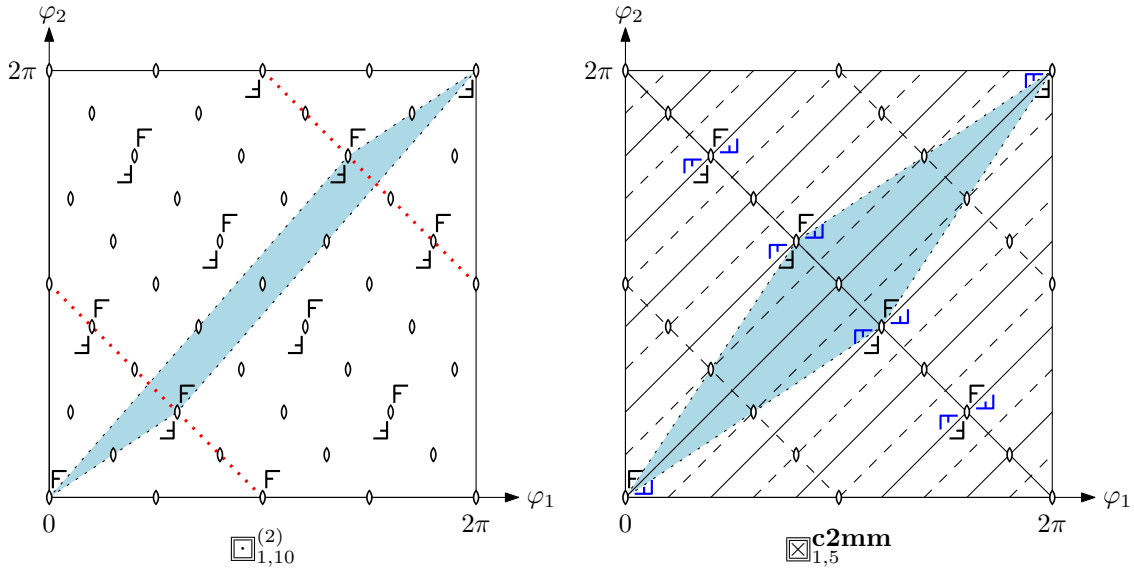

Figure 4.12.: Duplication example, $\boxdot^{(2)}_{1,10} \doteq \boxtimes^{\mathbf{c2mm}}_{1,5}$

We now prove the conjugacy formally. Since these groups have the same order $4n$, it is enough to show that $G_2 = \boxdot^{(\frac{n-1}{2})}_{1,2n}$ is contained in $G_1 = \boxtimes^{\mathbf{c2mm}}_{1,n}$. We do this by checking that the generators of G_2, under conjugation by the element h from Table 4.6, are elements of G_1. Here are the generators we gave for these groups:

$$G_1 = \boxtimes^{\mathbf{c2mm}}_{1,n} = \langle [1,1], [1, e^{\frac{i2\pi}{n}}], [-1, e^{\frac{\pi i}{n}}], [i,k], [-k,i] \rangle \quad \text{(see Table 4.5)}$$
$$G_2 = \boxdot^{(\frac{n-1}{2})}_{1,2n} = \langle [e^{-2\pi i}, 1], [-i, e^{\frac{\pi i}{2n}}], [j,j] \rangle = \langle [-i, e^{\frac{\pi i}{2n}}], [j,j] \rangle \quad \text{(see Section 4.6)}$$

We have to choose different conjugations depending on the value of n modulo 4.

- For $\boxtimes^{\mathbf{c2mm}}_{1,4m-1} \doteq \boxdot^{(2m-1)}_{1,8m-2}$, we do conjugation by $h_1 = [1-j, 1]$:

$$[\tfrac{1+j}{2}, 1][-i, e^{\frac{\pi i}{8m-2}}][1-j,1] = [k, e^{\frac{\pi i}{8m-2}}] = [k, e^{\frac{i(14m-3)\pi}{8m-2}}] = [k,-i][1, e^{\frac{i2\pi}{4m-1}}]^m \in G_1$$
$$[\tfrac{1+j}{2}, 1][j,j][1-j,1] = [j,j] = [i,k][-k,i] \in G_1$$

- For $\boxtimes^{\mathbf{c2mm}}_{1,4m-3} \doteq \boxdot^{(2m-2)}_{1,8m-6}$, we do conjugation by $h_2 = [1+j, 1]$:

$$[\tfrac{1-j}{2}, 1][-i, e^{\frac{\pi i}{8m-6}}][1+j,1] = [-k, e^{\frac{\pi i}{8m-6}}] = [j,j][1, e^{\frac{i2\pi}{4m-3}}]^{m-1}[i,k] \in G_1$$
$$[\tfrac{1-j}{2}, 1][j,j][1+j,1] = [j,j] = [i,k][-k,i] \in G_1$$

We can also study this transformation geometrically: What happens to the torus under this coordinate transformation? On which other torus do the glide reflections of $\boxtimes^{\mathbf{c2mm}}_{1,n}$ appear as torus translations? Indeed, there is another simple equation for a Clifford torus that is commonly used. We can transform our equation for the torus $\mathbb{T}$ as follows:

$$\begin{aligned} x_1^2 + x_2^2 &= x_3^2 + x_4^2 \\ x_2^2 - x_4^2 &= x_3^2 - x_1^2 \\ (x_2 - x_4)(x_2 + x_4) &= (x_3 + x_1)(x_3 - x_1) \qquad (4.9) \\ \tilde{x}_2 \tilde{x}_4 &= \tilde{x}_1 \tilde{x}_3, \qquad (4.10) \end{aligned}$$

with transformed coordinates $(\tilde{x}_1, \tilde{x}_2, \tilde{x}_3, \tilde{x}_4)$. This is, for example, how the torus is introduced in Coxeter [18, Eq. (4.41)], who has a separate section on "the spherical torus" [18,

§4.4, p. 35–37].

Now, the coordinate change from (4.9) to (4.10) is precisely what the transformation $h_1 = [1-j, 1]$ in our example achieves: $[1-j, 1]$ maps the quaternion units $(1, i, j, k) \equiv (x_1, x_2, x_3, x_4)$ to $(1+j, i-k, -1+j, i+k) \equiv (x_1+x_3, x_2-x_4, -x_1+x_3, x_2+x_4) = (\tilde{x}_1, \tilde{x}_2, \tilde{x}_3, \tilde{x}_4)$. Many conjugations in Table 4.6 are of this form.

The reason why we have chosen the example (4.8) for manual confirmation is that it corresponds to one of two duplications in the Conway-Smith classification that are not literally mentioned there:

$$+\tfrac{1}{4}[D_4 \times \bar{D}_{4n}] \doteq +\tfrac{1}{4}[D_4 \times D^{(1)}_{4n}] \text{ for odd } n.$$
$$\pm\tfrac{1}{4}[D_4 \times \bar{D}_{4n}] \doteq \pm\tfrac{1}{4}[D_4 \times D^{(1)}_{4n}]$$

The second equality appears in Table 4.6 as $\boxtimes^{\mathbf{p2mm}}_{2,2m}$ for odd m and $\boxtimes^{\mathbf{p2gm}}_{2,2m}$ for even m. The reason behind these duplications is discussed in Section G.1.

4.12. Comparison with the classification of Conway and Smith

Looking at the right column of Table 4.3, we see that our classification and the classification of Conway and Smith [14] have some similarity in the rough categorization. For example the "mixed" groups of type $[C \times D]$ are the torus swap groups (type ⧄). In the finer details, however, the two classifications are often quite at odds with each other. Groups that come from one geometric family correspond to different classes in the CS classification from the algebraic viewpoint, depending on parity conditions. On the other hand, some groups that belong together algebraically appear in different categories of our classification.

While we acquired some understanding of the classic classification of the toroidal groups according to Conway and Smith [14], in particular, of the simplest case of the torus translation groups (type ⧈, corresponding to $[C \times C]$, see Appendix G), most entries in the right column of Table 4.3 were filled with the help of a computer, by generating the groups from the specified generators and comparing them by the fingerprints described in Section 7.2, and recognizing patterns.

One reason for the difficulty is the distinction between haploid and diploid groups, a term borrowed from biology by Conway and Smith [14]. A group is *diploid* if it contains the central reflection $-\mathrm{id}$; otherwise, it is *haploid*.[18] In the classic classification, the diploid groups arise easily, but the haploid groups must be specially constructed as index-2 subgroups of diploid groups. Thus, the presence or absence of $-\mathrm{id}$ appears at the very beginning of the classic classification by quaternions. In the notation of [14], diploid and haploid groups are distinguished by the prefix $\pm$ and $+$.

For our geometric construction of the toroidal groups, this distinction is ephemeral. The central reflection $-\mathrm{id}$ is the torus translation $R_{\pi,\pi}$ in the center of the parameter square. It depends on some parity conditions of the translation parameters whether this element belongs to $G_\square$. (For example, one can easily work out from Figure 4.7 that the groups $\square^{\mathbf{pm}}$ and $\square^{\mathbf{pg}}$ are diploid if m and n are even. The groups $\square^{\mathbf{cm}}$ are diploid if m and n have the same parity.)

In elliptic geometry, where opposite points of S^3 are identified, the distinction between haploid and the corresponding diploid groups disappears, or in other words, only diploid groups play a role in elliptic space.

[18] Threlfall and Seifert [67, § 5] used the terms *zweistufig* and *einstufig* for these groups.

5 The polyhedral groups

We will now explain the polyhedral groups, which are related to the regular 4-dimensional polytopes. The regular 4-dimensional polytopes have a rich and beautiful structure. They and their symmetry groups have been amply discussed in the literature, see for example [16, Chapters VIII and XIII], [23, §26, §27], and therefore we will be brief, except that we study in some more detail the groups that come in enantiomorphic pairs. Table 5.1 gives an overview,[19] and Table A.1 in Appendix A lists these groups with generators and cross references to other classifications.

We mention that pictures of the cube, the 120-cell, the 24-cell, and the bitruncated 24-cell (also known as the 48-cell, defined in Section 5.6.1) arise among the illustrations for the tubical groups, see Section 3.12.

5.1. The Coxeter notation for groups

For the geometric description of the groups, we will use the notations of Coxeter, with adaptations by Conway and Smith [14, §4.4].

In the basic Coxeter group notation, a sequence of $n-1$ numbers $[p, q, \ldots, r, s]$ stands for the symmetry group of a certain n-dimensional regular polytope (if it exists), which is denoted by $\{p, q, \ldots, r, s\}$. (See the headings of Table 5.1 for the 4-dimensional regular polytopes.) This group is generated by n reflections $R_1, \ldots, R_n$. Each reflection is its own mirror: $(R_i)^2 = 1$, and any two adjacent reflections generate a rotation whose order is specified in the sequence: $(R_1R_2)^p = (R_2R_3)^q = \cdots = (R_{n-1}R_n)^s = 1$. Nonadjacent mirrors are perpendicular: $R_iR_j = R_jR_i$ for $|i-j| \geq 2$.

G^+ denotes the chiral part of the group G, which contains products of an even number of reflections. When just one of the numbers $p, q, \ldots, r, s$ is even, say that between R_k and R_{k+1}, there are three further subgroups. The two subgroups $[{}^+p, q, \ldots, r, s]$ and $[p, q, \ldots, r, s^+]$ consist of words that use respectively $R_1, \ldots, R_k$ and $R_{k+1}, \ldots, R_n$ an even number of times. Their intersection is the index-4 subgroup $[{}^+p, q, \ldots, r, s^+]$. Coxeter's original notation for $[{}^+p, q, \ldots]$ is $[p^+, q, \ldots]$.

A second pair of brackets, like in $[[3, 3, 3]]$, indicates a swap between a polytope and its polar, following [17]. Some further extensions of the notation will be needed for the axial groups in Chapter 6, see Table 6.3. In some cases, we have extended the Coxeter notations in an ad-hoc manner, allowing us to avoid other ad-hoc extensions of [14].

5.2. Strongly inscribed polytopes

We say that a polytope P is *strongly inscribed* in a polytope Q if every vertex of P is a vertex of Q, and every facet of Q contains a facet of P. Figure 5.1 shows two three-dimensional examples. This relation between P and Q is reversed under polarity: With

[19] In Du Val's enumeration of the achiral groups [23, p. 61], the descriptions of the orientation-reversing elements of the groups #41 $(T/V; T/V)^*$ and #42 $(T/V; T/V)^*_-$ are swapped by mistake. We follow Goursat and Hurley and go with the convention that the group with the more natural choice of elements should be associated to the name without a distinguishing subscript. Du Val himself, in the detailed discussion of these groups [23, p. 73], follows the same (correct) interpretation.

CS name	Du Val # and name	Coxeter name	order	method
symmetries of the 120-cell $Q_{120} = \{5,3,3\}$ / the 600-cell $P_{600} = \{3,3,5\}$				
$\pm[I \times I] \cdot 2$	50. $(I/I; I/I)^*$	$[3,3,5]$	14400	
$\pm[I \times I]$	30. $(I/I; I/I)$	$[3,3,5]^+$	7200	chiral part
$\pm[I \times O]$	29. $(I/I; O/O)$	$[[3,3,5]^+_{\frac{1}{5}L}]$	2880	inscribed polar & swap
$\pm[O \times I]$	29. $(O/O; I/I)$	$[[3,3,5]^+_{\frac{1}{5}R}]$	2880	inscribed polar & swap
$\pm[I \times T]$	24. $(I/I; T/T)$	$[3,3,5]^+_{\frac{1}{5}L}$	1440	inscribed polar
$\pm[T \times I]$	24. $(T/T; I/I)$	$[3,3,5]^+_{\frac{1}{5}R}$	1440	inscribed polar
symmetries of the 24-cell $P_T = \{3,4,3\}$ and its polar 24-cell P_{T_1}				
$\pm[O \times O] \cdot 2$	48. $(O/O; O/O)^*$	$[[3,4,3]]$	2304	
$\pm[O \times O]$	25. $(O/O; O/O)$	$[[3,4,3]]^+$	1152	chiral part
$\pm\frac{1}{2}[O \times O] \cdot 2$	45. $(O/T; O/T)^*$	$[3,4,3]$	1152	nonswapping
$\pm\frac{1}{2}[O \times O] \cdot \bar{2}$	46. $(O/T; O/T)^*_-$	$[[3,4,3]^+]$	1152	swap with mirror
$\pm\frac{1}{2}[O \times O]$	28. $(O/T; O/T)$	$[3,4,3]^+$	576	chiral & nonswapping
$\pm[T \times T] \cdot 2$	43. $(T/T; T/T)^*$	$[3,4,3^+]$	576	edge orientation
$\pm[O \times T]$	23. $(O/O; T/T)$	$[[^+3,4,3^+]]_L$	576	diagonal marking
$\pm[T \times O]$	23. $(T/T; O/O)$	$[[^+3,4,3^+]]_R$	576	diagonal marking
$\pm[T \times T]$	20. $(T/T; T/T)$	$[^+3,4,3^+]$	288	2 dual edge orientations
symmetries of the hypercube $\{4,3,3\}$ / the cross-polytope $\{3,3,4\}$				
$\pm\frac{1}{6}[O \times O] \cdot 2$	47. $(O/V; O/V)^*$	$[3,3,4]$	384	
$\pm\frac{1}{6}[O \times O]$	27. $(O/V; O/V)$	$[3,3,4]^+$	192	chiral part
$\pm\frac{1}{3}[T \times T] \cdot 2$	41. $(T/V; T/V)^*$	$[^+3,3,4]$	192	even permutations
$\pm\frac{1}{3}[T \times \overline{T}] \cdot 2$	42. $(T/V; T/V)^*_-$	$[3,3,4^+]$	192	2-coloring
$\pm\frac{1}{3}[T \times T]$	22. $(T/V; T/V)$	$[^+3,3,4^+]$	96	2-coloring & chiral
symmetries of the simplex $\{3,3,3\}$ and its polar				
$\pm\frac{1}{60}[I \times \overline{I}] \cdot 2$	51. $(I^\dagger/C_2; I/C_2)^{\dagger *}$	$[[3,3,3]]$	240	
$\pm\frac{1}{60}[I \times \overline{I}]$	32. $(I^\dagger/C_2; I/C_2)^\dagger$	$[[3,3,3]]^+$	120	chiral part
$+\frac{1}{60}[I \times \overline{I}] \cdot 2_1$	51′. $(I^\dagger/C_1; I/C_1)^{\dagger *}$	$[3,3,3]$	120	nonswapping
$+\frac{1}{60}[I \times \overline{I}] \cdot 2_3$	51′. $(I^\dagger/C_1; I/C_1)^{\dagger *}_-$	$[[3,3,3]^+]$	120	swap with mirror
$+\frac{1}{60}[I \times \overline{I}]$	32′. $(I^\dagger/C_1; I/C_1)^\dagger$	$[3,3,3]^+$	60	chiral & nonswapping

Table 5.1.: The polyhedral groups

respect to an origin that lies inside P, the polar polytope Q^Δ will be strongly inscribed in P^Δ.

In four dimensions, we will show two instances of this phenomenon where a rotated copy of the polar polytope P^Δ of a polytope P can be strongly inscribed into P. Among the *regular* polytopes in three dimensions, there are just some degenerate cases, where every facet of Q contains only an *edge* of P: In a cube Q, a regular tetrahedron P can be inscribed, with the six edges of P on the six square sides of Q. In a dodecahedron Q, a cube P can be inscribed, with its twelve edges on the twelve pentagons of Q. The tetrahedron inscribed in a dodecahedron does not fall in this category, since its edges go through the interior of the dodecahedron.

5.3. Symmetries of the simplex

The full symmetry group of the 4-simplex is $[3,3,3]$. The group $[[3,3,3]]$ additionally swaps (by negation) the simplex with its polar. The chiral versions are $[3,3,3]^+$ and $[[3,3,3]]^+$. The group $[[3,3,3]^+]$ allows the flip to the polar only in connection with a

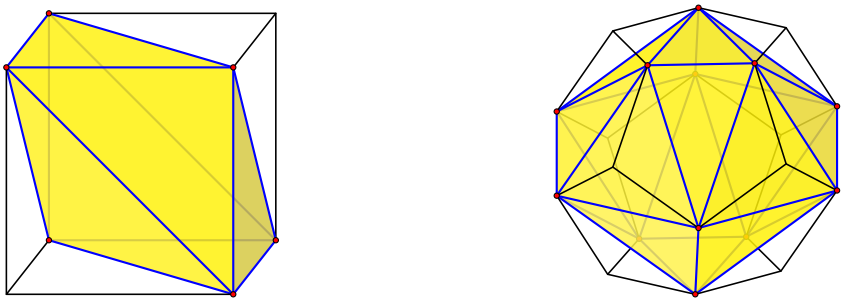

Figure 5.1.: A cube with a strongly inscribed (non-regular) octahedron (left). A dodecahedron with a strongly inscribed (non-regular) icosahedron (right).

reversal of orientation.

5.4. Symmetries of the hypercube (and its polar, the cross-polytope)

The full symmetry group of the hypercube is $[3,3,4]$. It is isomorphic to the semidirect product of coordinate permutations with sign flips $\{(\pm1,\pm1,\pm1,\pm1)\} \rtimes S_4$. This group has four subgroups.

The cube has a natural 2-coloring of the vertices that gives alternating colors to adjacent vertices. One can check that the vertices of each color form a cross-polytope. This cross-polytope is strongly inscribed in the cube: Each facet of the hypercube contains exactly one (tetrahedral) facet of that cross-polytope. The subgroup $[3,3,4^+]$ contains those elements that preserve the 2-coloring. Equivalently, these are the elements that have an even number of sign changes.

The subgroup $[^+3,3,4]$ contains those elements that have an even permutation of coordinates. It is isomorphic to $\{(\pm1,\pm1,\pm1,\pm1)\} \rtimes A_4$. The subgroup $[^+3,3,4^+]$ is their intersection. The subgroup $[3,3,4]^+$ contains the orientation-preserving transformations. These are the transformations where the parity of the sign changes matches the parity of the permutation.

It is interesting to note that the 3-dimensional group $[3,4]$ closely mirrors the picture for $[3,3,4]$, see Table 5.2. Both in three and four dimensions, the "half-cube" is itself a regular polytope: in 3 dimensions, it is the regular tetrahedron, while in 4 dimensions, it is the cross-polytope. The subgroup $[3,4^+] = TO$ preserves the 2-coloring of the vertices, i.e. it contains all symmetries of the tetrahedron. Its subgroup $[^+3,4^+] = +T$ contains the orientation-preserving symmetries of the tetrahedron. The group $[^+3,4] = \pm T$ contains the orientation-preserving symmetries of the tetrahedron together with its central reflection. It is also characterized as those symmetries that subject the three space axes to an even permutation. The group $[3,4]^+$ contains all orientation-preserving transformations in $[3,4]$. For the groups $+T$ and TO we have used alternate Coxeter names, which are equivalent to the standard ones, in order to highlight the analogy with 4 dimensions, cf. [12, p. 390].

4 dimensions	order	3 dimensions	order	description
$[3,3,4]$	384	$[3,4] = \pm O$	48	the full symmetry group
$[3,3,4]^+$	192	$[3,4]^+ = +O$	24	chiral part (preserves orientation)
$[^+3,3,4]$	192	$[^+3,4] = \pm T$	24	even permutation of coordinates
$[3,3,4^+]$	192	$[3,4^+] = [3,3] = TO$	24	preserves the 2-coloring
$[^+3,3,4^+]$	96	$[^+3,4^+] = [3,3]^+ = +T$	12	all three constraints above

Table 5.2.: Analogy between symmetries of the 4-dimensional and 3-dimensional cube

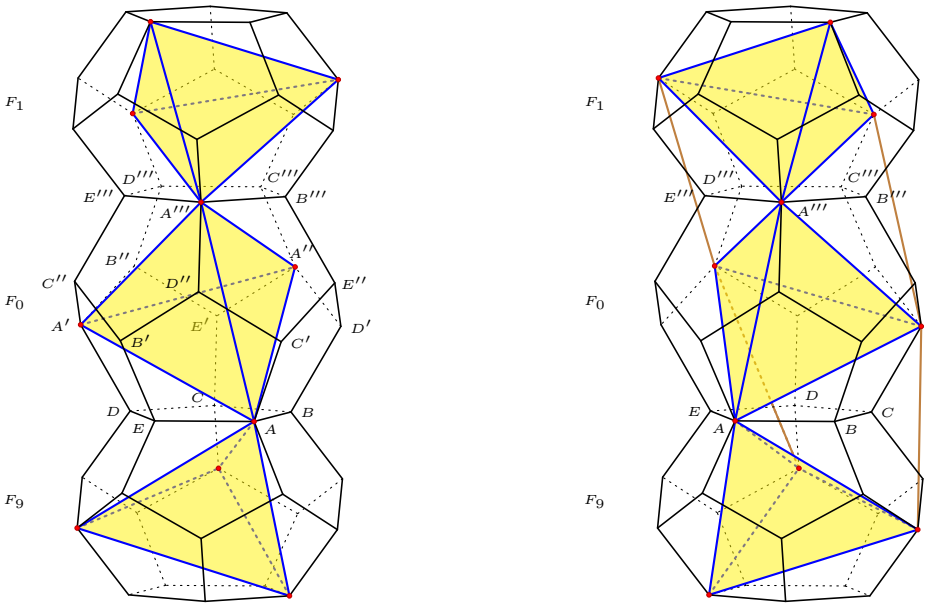

(a) left tetrahedra (b) right tetrahedra

Figure 5.2.: A sequence of inscribed tetrahedra in three successive dodecahedra of the 120-cell Q_{120}. The red vertices form a 600-cell P'_{600}. This is an orthogonal projection to the tangent space in the center of the middle cell, and this is why the adjacent cells are foreshortened.

5.5. Symmetries of the 600-cell (and its polar, the 120-cell)

The 120 quaternions $2I$ form the vertices of a 600-cell $P_{600} = \{3, 3, 5\}$. These quaternions are the centers of the 120 dodecahedra of the polar 120-cell $Q_{120} = \{5, 3, 3\}$, which has 600 vertices. The full symmetry group of P_{600} (or Q_{120}) is $[3, 3, 5]$. Its chiral version is $[3, 3, 5]^+$.

The group has four interesting subgroups, which come in enantiomorphic versions. Under the left rotations by elements of $2I$, or in other words, under the group $\pm[I \times C_1]$, the 600 vertices of Q_{120} decompose into five orbits, as shown by the five labels A, B, C, D, E for the cell F_0 in Figure 5.2a, cf. [23, Figure 22, p. 84]. We can regard this as a 5-coloring of the vertices. (The points of each color are labeled X, X', X'', X''' according to the horizontal levels in this picture, but this grouping has otherwise no significance.) One can indeed check that the mapping from a pentagonal face to the opposite face with a left screw by $\pi/5$, as effected by the elements of $\pm[I \times C_1]$, preserves the coloring.

The vertices of one color form a regular tetrahedron inscribed in a regular dodecahedron, and there are thus five ways inscribe such a "left" tetrahedron in a regular dodecahedron. There is an analogous "right" 5-coloring by the orbits under $\pm[C_1 \times I]$, and correspondingly, there are five ways of inscribing a "right" tetrahedron in a regular dodecahedron. One such tetrahedron is shown in Figure 5.2b.[20] The left and right tetrahedra are mirrors of each other, and they can be distinguished by looking at the paths of length 3 on the dodecahedron between vertices of a tetrahedron: These paths are either S-shaped zigzag paths (for left tetrahedra) or they have the shape of an inverted S (for right tetrahedra).

Every color class consists of the points $2I \cdot p_0$ for some starting point p_0, and hence

[20] The unions of these five or ten tetrahedra inside a dodecahedron form nice nonconvex star-like polyhedral compounds, see [23, Figures 14 and 15a–b]. See also https://blogs.ams.org/visualinsight/2015/05/15/dodecahedron-with-5-tetrahedra/ from the AMS blog "Visual Insight".

it forms a rotated copy P'_{600} of the 600-cell P_{600}. This polytope is strongly inscribed in Q_{120}: For each dodecahedron of Q_{120}, there is a unique left rotation in $\pm[I \times C_1]$ mapping F_0 to this dodecahedron, and in this way we get 120 images of the starting tetrahedron. Figure 5.2a shows these tetrahedra in three adjacent dodecahedra. (As a sanity check, one can perform a small calculation: A vertex is shared by four tetrahedra—one tetrahedron in each of the four dodecahedra meeting in the vertex—, and this gives a consistent vertex count, since every tetrahedron has four vertices and $120 \cdot 4/4 = 120$.)

The red points in Figure 5.2b form part of an analogous 600-cell P'^R_{600} spanned by right inscribed tetrahedra. Some additional edges of this P'^R_{600}, which don't lie in the three dodecahedra that are shown, are drawn in brown.

The group $\pm[I \times T]$ consists of those symmetries of that simultaneously preserve the 120-cell Q_{120} and its strongly inscribed "left" 600-cell P'_{600}. To see this, consider the dodecahedral cell F_0 that is centered at the quaternion 1. As mentioned, each left multiplication by an element $2I$ maps F_0, together with its inscribed tetrahedron $AA'A''A'''$ to a unique dodecahedral cell of Q_{120} with the corresponding tetrahedron. To understand the full group, we have to consider those group elements that keep F_0 fixed. $\pm[I \times T]$ consists of the elements $[l, r]$ with $(l, r) \in 2I \times 2T$. The transformation $[l, r]$ keeps F_0 fixed iff it maps 1 to 1, and this is the case iff $l = r$. These elements are the elements $[r, r] = [r]$ with $r \in 2T$, in other words, they form the tetrahedral group $\pm T$. And indeed, the symmetries of F_0 that keep the tetrahedron $AA'A''A'''$ invariant form a tetrahedral group.

We chose $[3, 3, 5]^+_{\frac{1}{5}L}$ as an ad-hoc extension of Coxeter's notation for the group $\pm[I \times T]$, to indicate a $1/5$ fraction of the group $[3, 3, 5]^+$.

Now, there is also the original 600-cell P_{600}, the polar of the Q_{120}, having one vertex in the center of each dodecahedron. This gives rise to a larger group $[[3, 3, 5]^+_{\frac{1}{5}L}] = \pm[I \times O]$ where the two 600-cells P_{600} and P'_{600} (properly scaled) are swapped. This group is not a subgroup of any other 4-dimensional point group.

When the starting point s is chosen in the center of the dodecahedral cell of Q_{120}, the polar orbit polytope of this group has 240 cells. Figure 5.3 shows such a cell C. The points of the orbit closest to s are four vertices of the dodecahedron (say, those of color A, the red points in Figure 5.2a). They form a tetrahedral cell of P'_{600}, and they are responsible for the rough tetrahedral shape of C. The centers of the twelve neighboring dodecahedra in Q_{120} give rise to the twelve small triangular faces, which are the remainders of the twelve pentagons of the original dodecahedral cell, when the polar is not present. In addition, there are four neighboring cells that are adjacent through hexagonal faces, opposite the large 12-gons. They are centered at vertices of P'_{600}. Two of these are shown as red points in Figure 5.2a, the point adjacent to C in the lower cell F_9, and the point adjacent to D''' in the upper cell F_1. The cell has chiral tetrahedral symmetry $+T$. In particular, it is not mirror-symmetric. In [24, Figure 9], this cell is shown together with a fundamental domain inside it. Incidentally, this cell (and the orbit polytope) coincides with that of the tubical group $\pm[I \times C_4]$ when the starting point is chosen on a two-fold rotation center (Figure B.2).

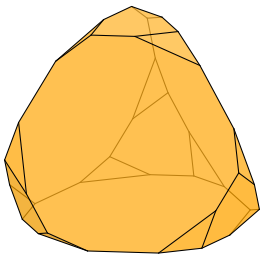

Figure 5.3.: A cell C of the polar orbit polytope of the group $\pm[I \times O]$

If we use the "right" 5-coloring we get the corresponding groups $[3,3,5]^+_{\frac{1}{5}R} = \pm[T \times I]$ and $[[3,3,5]^+_{\frac{1}{5}R}] = \pm[O \times I]$. See Figure 5.2b. These four groups come in two enantiomorphic pairs. The two corresponding groups are mirrors of each other. (They are therefore *metachiral groups* in the terminology of Conway and Smith [14, §4.6].)

5.6. Symmetries of the 24-cell

The set of 24 quaternions of $2T$ form the vertices of a regular 24-cell P_T. The complete symmetry group of P_T is $[3,4,3]$, and its chiral version is $[3,4,3]^+$.

The points of P_T can be 3-colored: There are 8 vertices of P_T whose coordinates are the permutations of $(\pm1,0,0,0)$. They form a cross-polytope. The 16 remaining vertices are of the form $(\pm1/2,\pm1/2,\pm1/2,\pm1/2)$. They are the vertices of a 4-cube, and they can be naturally divided into two color groups of 8, as mentioned in Section 5.4. In total, we have three groups of 8 vertices, which we interpret as a *3-coloring* of the vertices by the colors a,b,c, see Figure 5.4a. Every triangular face contains vertices from all three colors. Thus, every symmetry of P_T induces a permutation of the colors.

We can look at those symmetries for which the permutations of the colors is even. In other words, besides the identity, we allow only cyclic shifts. These form the subgroup $[3,4,3^+]$. Another way to express this is to establish an *orientation of the edges* according to some cyclic ordering of the colors $a \to b \to c \to a$ (a *coherent orientation* [16, §8.3]). The subgroup $[3,4,3^+]$ consists of those elements that preserve this edge orientation. (This is analogous to the pyritohedral group $\pm T$ in three dimensions, which can also be described as preserving the orientation of the edges of the octahedron shown in Figure 5.4a.)

The 24-cell is a self-dual polytope. In fact, the vertices of the polar polytope P_{T_1} (properly scaled) are the quaternions in the coset of $2T$ in $2O$. If we add to $[3,4,3]$ the symmetries that swap P_T and P_{T_1}, we get the group $[[3,4,3]]$, the symmetry group of the joint configuration $P_O = P_T \cup P_{T_1}$. Its chiral version is $[[3,4,3]]^+$. The subgroup $[[3,4,3]^+]$ contains the symmetries that exchange P_T and P_{T_1} only in combination with a reversal of orientation. This group is interesting, because it is achiral, but it contains no reflections.

The polar polytope also has a three-coloring of its vertices. (One can give the partition explicitly in terms of the coordinates, as for P_T: The vertices of P_{T_1} are the centers of the facets of P_T, properly scaled, and their coordinates (x_1,x_2,x_3,x_4) are all permutations of the coordinates $(\pm1,\pm1,0,0)/\sqrt{2}$. The three color classes are characterized by the condition $|x_1| = |x_2|$, $|x_1| = |x_3|$, and $|x_1| = |x_4|$, respectively.) We can interpret this 3-coloring as a 3-coloring of the *cells* of P_T, which we denote by A,B,C. The group $[^+3,4,3]$ contains those symmetries of P_T for which the permutation of the colors of the *cells* is even. This group is of course geometrically the same as $[3,4,3^+]$, but we can also have both conditions: $[^+3,4,3^+]$.

5.6.1. A pair of enantiomorphic groups

Finally, we have two more groups, which are mirrors of each other. To understand these groups, let us look at the polar orbit polytope of $P_O = P_T \cup P_{T_1}$: The octahedral cells of the 24-cell shrink to truncated cubes with 6 regular octagons and 8 triangles as faces, see Figure 5.4b. This polytope is sometimes called the bitruncated 24-cell, or truncated-cubical tetracontaoctachoron. We will simply refer to it as the *48-cell*. The small triangles are remainders from the triangular faces of the original octahedral cells of the 24-cell, which are centered at the points P_T.

Figure 5.4b shows a cell of color A. The triangles lead to adjacent cells, colored B or C, and we have labeled the triangles accordingly. The octagons lead to cells centered at

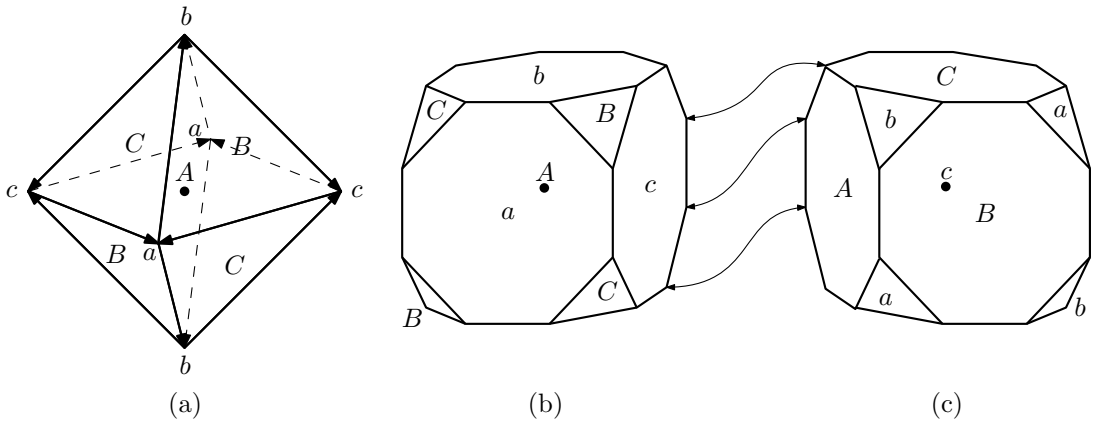

Figure 5.4.: (a) An octahedral cell of the 24-cell with a consistent edge orientation. (b) The 48-cell consists of 48 truncated cubes.

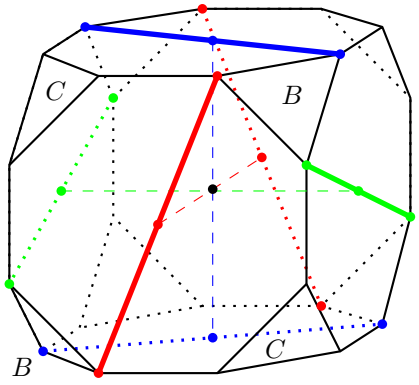

Figure 5.5.: Decoration of the truncated cube by diagonals.

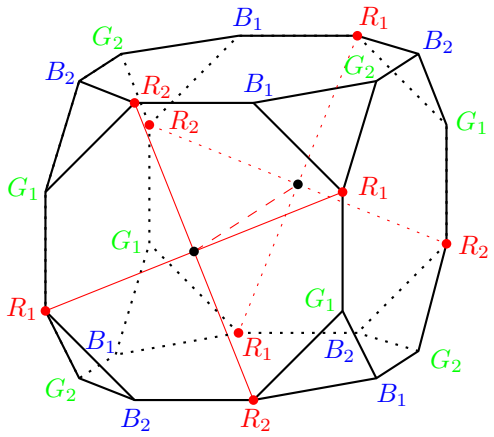

Figure 5.6.: The 6 orbits of the vertices under $\pm[O \times C_1]$ (left multiplication with $2O$)

points of P_T, and we have labeled them with the corresponding color a, b, or c.

Figure 5.4c shows an adjacent "dual" cell of the 48-cell, centered at a point of color c. Note that these two cells are not attached in a straight way, but by a screw of 45°. We can enforce the screw to be a left screw by decorating each of the six octagonal faces with a diagonal, as shown in Figure 5.5. The group $\pm[O \times C_1]$ will map one selected cell to each cell by a unique left multiplication with an element of $2O$ and hence will carry the diagonal pattern to every truncated cube of the 48-cell. The diagonals on adjacent cells match: A left rotation that maps a cell to the adjacent cell performs a left screw by 45°, and one can check in Figure 5.5 that the screw that maps an octagon to the opposite octagon while maintaining the diagonal is a left screw.

The group $\pm[O \times T]$ is the group that preserves the set of diagonals (ignoring the colors). This can be confirmed as in the case $\pm[I \times T]$ in Section 5.5: The group that fixes a cell should be the tetrahedral group $+T$, and indeed, the diagonal pattern of Figure 5.5 has tetrahedral symmetry: The diagonals connect only the B-triangles, and the B-triangles form a tetrahedral pattern. We have chosen the ad-hoc extension of Coxeter's notation $[[^+3,4,3^+]]_L$ for the group $\pm[O \times T]$ to indicate that it extends the operations $[^+3,4,3^+]$ by a swap between P_T and the polar polytope P_{T_1}, and this swap is effected by *left* rotations.

Of course, there is a mirror pattern of Figure 5.5, which leads to the mirror group $\pm[T \times O] = [[^+3,4,3^+]]_R$, and these two groups are enantiomorphic.

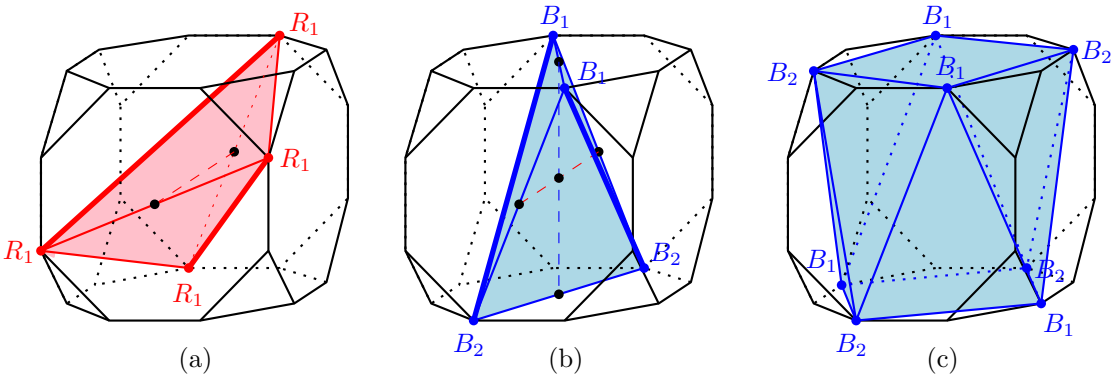

Figure 5.7.: Facets inscribed in the truncated cube

Analogies with three dimensions. As pointed out by Du Val [23, p. 71], there is a strong analogy between the symmetries of the different self-dual polytopes in three and in four dimensions, as shown in Table 5.3. The simplex is a self-dual regular polytope, both in 4 dimensions (Section 5.3) and in 3 dimensions. In 3 dimensions, moreover, the simplex and its polar form the cube, and thus we have used alternate Coxeter notations to highlight the analogy (opposite ones from Table 5.2, where the analogy with the cube is emphasized). Only five of the symmetries of the 24-cell and its polar are used.

From the viewpoint of the cross-polytope, one could also match the group $\pm[T\times T]\cdot 2 = [3,4,3^+] = [^+3,4,3]$ of order 576 with the pyritohedral group $\pm T = [^+3,4]$ of order 24, because they are both based on consistent edge orientations.

4-simplex	order	24-cell	order	3-simplex	order	description
$[[3,3,3]]$	240	$[[3,4,3]]$	2304	$[[3,3]] = [3,4] = \pm O$	48	all symmetries
$[[3,3,3]]^+$	120	$[[3,4,3]]^+$	1152	$[[3,3]]^+ = [3,4]^+ = +O$	24	chiral part
$[3,3,3]$	120	$[3,4,3]$	1152	$[3,3] = TO$	24	nonswapping
$[[3,3,3]^+]$	120	$[[3,4,3]^+]$	1152	$[[3,3]^+] = [^+3,4] = \pm T$	24	swap with mirror
$[3,3,3]^+$	60	$[3,4,3]^+$	576	$[3,3]^+ = +T$	12	chiral & nonswapping

Table 5.3.: Analogies between symmetries of self-dual polytopes

A strongly inscribed polar polytope. The convex hull of the points $P_O = P_T \cup P_{T_1}$ is a polytope with 288 equal tetrahedral facets, which we call the *288-cell*. It is polar to the 48-cell. We perform the same procedure as in Section 5.5 and split the vertices of the 48-cell into orbits under the action of $\pm[O \times C_1]$. We will see that this leads to another instance of a polytope with a strongly inscribed copy of its polar. However, we won't get any new groups.

The 48-cell has 288 vertices, and they are partitioned into 6 orbits of size 48, as shown in Figure 5.6, cf. Du Val [23, Figure 24, p. 85]: There is a natural partition of the colors into three pairs R_1, R_2; G_1, G_2; and B_1, B_2, according to the opposite octagons to which the colors belong. (The partition of each pair into R_1 and R_2, etc., is arbitrary.) Indeed, one can check that the transition from an octagon to the opposite octagon with a left screw of 45° preserves the six colors (indicated for the red colors by two corresponding crosses.) Likewise, the transition from a triangle to the opposite triangle with a left screw of 60° preserves the colors.

Now, as in Section 5.5, the points of one color form a right coset of $2O$, and hence they form a rotated and scaled copy P'_O of the 288-cell P_O. This polytope is strongly inscribed in the 48-cell: Each truncated cube of the 48-cell contains one tetrahedron of P'_O. Figure 5.7a shows one such tetrahedron, spanned by the vertices of color R_1.

The geometry of this tetrahedron becomes clearer after rotating it by 45° around the

midpoints of the front and back octagons, as in Figure 5.7b. We see that the tetrahedron has four equal sides, whose length is the diagonal of the octagons, and two opposite sides of larger length, equal to the diagonal of a circumscribed square. The 2-faces are therefore congruent isosceles triangles. Such a tetrahedron is called a *tetragonal disphenoid*.[21]

The symmetry group of the 48-cell together with its strongly inscribed 288-cell P'_O is the tubical group $\pm[O \times D_4]$, because the symmetry group of the disphenoid inside the truncated cube is only the vierergruppe D_4, consisting of half-turns through edge midpoints.

We can try to start with the rotated tetrahedra of Figure 5.7b, spanned by two opposite diagonals used for the decoration in Figure 5.6, hoping to recover the group $\pm[O \times T]$. However, this tetrahedron contains vertices of *two* colors B_1 and B_2, and its orbit will thus contain the union of the orbits B_1 and B_2. Inside each truncated cube, the convex hull forms a quadratic antiprism, as shown Figure 5.7c. (The convex hull contains 48 such antiprisms plus 192 tetrahedral cells, for a total of 240 facets.)

[21] The side length of the "untruncated" cube is $\sqrt{8} - 2 \approx 0.8$, which equals the edge length of a circumscribed 8-gon around a unit circle. Hence the two long edges of the tetrahedra, highlighted in bold, have length $\sqrt{2}(\sqrt{8}-2) = 4-\sqrt{8} \approx 1.17$. The four short edges have length $\sqrt{8(10-\sqrt{98})} \approx 0.9$, and the edge length of the 48-cell is $6 - \sqrt{32} \approx 0.34$.

6 The axial groups

These are the finite subgroups of the direct product $\mathrm{O}(3) \times \mathrm{O}(1)$. The subgroup $\mathrm{O}(1)$ operates on the 4-th coordinate x_4, and we denote its elements by $\mathrm{O}(1) = \{+x_4, -x_4\}$. Here $+x_4$ is the identity, and $-x_4$ denotes the reflection of the 4-th coordinate.

Let G be such an axial group. Let $G_3 \in \mathrm{O}(3)$ be the "projection" of G on $\mathrm{O}(3)$. That is,

$$G_3 := \{\, g \in \mathrm{O}(3) \mid (g, +x_4) \in G \text{ or } (g, -x_4) \in G \,\}.$$

If G_3 itself is a 3-dimensional axial group, i.e. $G \leqslant \mathrm{O}(2) \times \mathrm{O}(1)$, then we may call G a *doubly axial group*. In this case, we prefer to regard G as a toroidal group in $\mathrm{O}(2) \times \mathrm{O}(1) \times \mathrm{O}(1) \leqslant \mathrm{O}(2) \times \mathrm{O}(2)$ and classify it as such. (These groups are the subgroups of $\boxplus^{\mathbf{p2mm}}_{m,2}$.) Hence from now on, we assume that G_3 is not an axial 3-dimensional group, i.e., we assume that $G_3 \leqslant O(3)$ is one of the seven *polyhedral* 3-dimensional groups. These are well-understood, and thus the axial groups are quite easy to classify. There are 21 axial groups (excluding the doubly axial groups), and their full list is given below in Table 6.3, with references to other classifications from the literature. Together with the polyhedral groups in Table 5.1, these groups exhaust all entries in [14, Tables 4.2 and 4.3] except the toroidal groups. Table A.1 in Appendix A lists them with generators and cross references to other classifications.

Note that the product $\mathrm{O}(3) \times \mathrm{O}(1)$ used here is different from the product $\pm[L \times R]$ on which the classic classification is based. Both are direct products in the group-theoretic sense, but $\mathrm{O}(3) \times \mathrm{O}(1)$ is a direct sum, a "Cartesian" product in a straightforward geometric sense, consisting of pairs of independent transformations in orthogonal subspaces, whereas the product $\pm[L \times R]$, which is specific to $\mathrm{SO}(4)$, refers to the representation $[l, r]$ by pairs of quaternions, which have by themselves a significance as operations $[l]$ and $[r]$ in $\mathrm{SO}(3)$.

We will now derive the axial groups systematically. Let $G_3^{+x_4} \leqslant \mathrm{O}(3)$ be the subgroup of G_3 of those elements that don't negate the 4-th coordinate. That is,

$$G_3^{+x_4} := \{\, g \in \mathrm{O}(3) \mid (g, +x_4) \in G \,\}.$$

The subgroup $G_3^{+x_4}$ is either equal to G_3, or it is an index-2 subgroup of G_3.

If $G_3^{+x_4} = G_3$, there are two cases, which are both easy: we can form the "pyramidal" group $G_3 \times \{+x_4\}$, which does not move the 4-th dimension at all, or the full "prismatic" group $G_3 \times \{+x_4, -x_4\}$. This gives two axial groups for each three-dimensional polyhedral group $G_3 \leqslant \mathrm{SO}(3)$, and they are listed in Table 6.1, together with their "CS names" following Conway and Smith [14], and their "Coxeter names", which are explained in Table 6.3.

The prismatic groups are never chiral. The pyramidal group $G_3 \times \{+x_4\}$ is chiral iff G_3 is: These are the groups $+I$, $+O$, and $+T$.

We are left with the case that $G_3^{+x_4}$ is an index-2 subgroup H of G_3. In this case, the group G is uniquely determined by H and G_3: It consists of the elements $(g, +x_4)$ for $g \in H$ and $(g, -x_4)$ for $g \in G_3 - H$. We denote this group as "H in G_3". As an abstract group, it is isomorphic to G_3. There are seven index-2 containments among the three-dimensional polyhedral groups. (See [14, Figures 3.9 and 3.10] for an overview about

G_3			pyramidal groups $G_3 \times \{+x_4\}$			prismatic groups $G_3 \times \{+x_4, -x_4\}$		
name	orbitope	I.T.	CS name	Cox.	order	CS name	Cox. name	order
$\pm I$	$*\mathbf{532}$	$53m$	$+\frac{1}{60}[I \times I] \cdot 2_3$	$[3,5]$	120	$\pm\frac{1}{60}[I \times I] \cdot 2$	$2.[3,5]$	240
$+I$	$\mathbf{532}$	532	$+\frac{1}{60}[I \times I]$	$[3,5]^+$	60	$+\frac{1}{60}[I \times I] \cdot 2_1$	$[3,5]^\circ$	120
$\pm O$	$*\mathbf{432}$	$m3m$	$+\frac{1}{24}[O \times O] \cdot 2_3$	$[3,4]$	48	$\pm\frac{1}{24}[O \times O] \cdot 2$	$2.[3,4]$	96
$+O$	$\mathbf{432}$	432	$+\frac{1}{24}[O \times O]$	$[3,4]^+$	24	$+\frac{1}{24}[O \times O] \cdot 2_1$	$[3,4]^\circ$	48
TO	$*\mathbf{332}$	$\bar{4}3m$	$+\frac{1}{12}[T \times \overline{T}] \cdot 2_1$	$[3,3]$	24	$+\frac{1}{24}[O \times \overline{O}] \cdot 2_1$	$[2,3,3]$	48
$\pm T$	$\mathbf{3}*\mathbf{2}$	$m3$	$+\frac{1}{12}[T \times T] \cdot 2_3$	$[^+3,4]$	24	$\pm\frac{1}{12}[T \times T] \cdot 2$	$2.[^+3,4]$	48
$+T$	$\mathbf{332}$	23	$+\frac{1}{12}[T \times T]$	$[3,3]^+$	12	$+\frac{1}{12}[T \times T] \cdot 2_1$	$[^+3,4]^\circ$	24

Table 6.1.: Pyramidal and prismatic axial groups (except doubly axial groups)

hybrid axial groups				
$G_3^{+x_4}$ in G_3	CS name	Coxeter name	order	methods
$+I$ in $\pm I$	$\pm\frac{1}{60}[I \times I]$	$2.[3,5]^+$	120	center, chirality
$\pm T$ in $\pm O$	$+\frac{1}{24}[O \times \overline{O}] \cdot 2_3$	$[2,3,3]^\circ$	48	edge orientation
$+O$ in $\pm O$	$\pm\frac{1}{24}[O \times O]$	$2.[3,4]^+$	48	center, chirality
TO in $\pm O$	$\pm\frac{1}{12}[T \times \overline{T}] \cdot 2$	$2.[3,3]$	48	center, alternation
$+T$ in $\pm T$	$\pm\frac{1}{12}[T \times T]$	$2.[3,3]^+$	24	center, chirality
$+T$ in $+O$	$+\frac{1}{12}[T \times \overline{T}] \cdot 2_3$	$[3,3]^\circ$	24	alternation
$+T$ in TO	$+\frac{1}{24}[O \times \overline{O}]$	$[2,3,3]^+$	24	chirality

Table 6.2.: Hybrid axial groups (except doubly axial groups)

all index-2 containments in O(3).) They lead to seven "hybrid axial groups", which are listed in Table 6.2.

There are several methods by which such an index-2 containment can be constructed, and we indicate in the table which methods are applicable:

1. Chirality: $G_3^{+x_4}$ is the chiral part of an achiral group G_3. In this case, the resulting group will be chiral, because the orientation-reversing elements of G_3 are composed with the reflection of the axis. In other words, G is the chiral part $(G_3 \times \{x_4, -x_4\})^+$ of the prismatic group $G_3 \times \{x_4, -x_4\}$.

2. Center: $G_3^{+x_4}$ does not contain the central reflection. In this case, an index-2 extension G_3 of $G_3^{+x_4}$ can always be obtained by adjoining the central reflection (in $\mathbb{R}^3$). The resulting group "$G_3^{+x_4}$ in G_3" is equivalently thought of as simply adjoining the central reflection (in $\mathbb{R}^4$) to $G_3^{+x_4}$. These groups can be recognized as having their Coxeter names prefixed with "2.". G is achiral iff $G_3^{+x_4}$ is achiral, and in this case, the construction is simultaneously a case of the chirality method.

3. Alternation: This applies to the octahedral groups, which are symmetries of the cube. The vertices of the cube can be two-colored. The subgroup consists of those transformations that preserve the coloring.

4. Edge orientation: There is only one case where this applies, namely the pyritohedral group $\pm T$ as a subgroup of the full octahedral group $\pm O$. The edges of the octahedron can be *coherently* oriented in such a way that the boundary of every face is a directed cycle. The subgroup consists of those transformations that preserve this orientation (cf. the use of the edge orientation for the 24-cell and its polar, Section 5.6).

Often, the same result can be obtained by two methods. For example, TO in $\pm O$ results both from alternation and from center.

The 21 axial groups					
pyramidal groups $G_3 \times \{+x_4\}$					
G_3	CS name	Du Val # and name	Cox.	BBNZW	order
$\pm I$	$+\frac{1}{60}[I \times I] \cdot 2_3$	$49'$. $(I/C_1; I/C_1)^*$	$[3,5]$	n.cryst.	120
$+I$	$+\frac{1}{60}[I \times I]$	$31'$. $(I/C_1; I/C_1)$	$[3,5]^+$	n.cryst.	60
$\pm O$	$+\frac{1}{24}[O \times O] \cdot 2_3$	$44'$. $(O/C_1; O/C_1)^{*\prime}$	$[3,4]$	25/10	48
$+O$	$+\frac{1}{24}[O \times O]$	$26'$. $(O/C_1; O/C_1)'$	$[3,4]^+$	25/03	24
TO	$+\frac{1}{12}[T \times \overline{T}] \cdot 2_1$	$40'$. $(T/C_1; T/C_1)^*$	$[3,3]$	24/04	24
$\pm T$	$+\frac{1}{12}[T \times T] \cdot 2_3$	$39'$. $(T/C_1; T/C_1)^*_c$	$[^+3,4]$	25/02	24
$+T$	$+\frac{1}{12}[T \times T]$	$21'$. $(T/C_1; T/C_1)$	$[3,3]^+$	24/01	12
prismatic groups $G_3 \times \{+x_4, -x_4\}$					
G_3	CS name	Du Val # and name	Cox.	BBNZW	order
$\pm I$	$\pm\frac{1}{60}[I \times I] \cdot 2$	49. $(I/C_2; I/C_2)^*$	$2.[3,5]$	n.cryst.	240
$+I$	$+\frac{1}{60}[I \times I] \cdot 2_1$	$49'$. $(I/C_1; I/C_1)^*_-$	$[3,5]^\circ$	n.cryst.	120
$\pm O$	$\pm\frac{1}{24}[O \times O] \cdot 2$	44. $(O/C_2; O/C_2)^*$	$2.[3,4]$	25/11	96
$+O$	$+\frac{1}{24}[O \times O] \cdot 2_1$	$44'$. $(O/C_1; O/C_1)^{*\prime}_-$	$[3,4]^\circ$	25/07	48
TO	$+\frac{1}{24}[O \times \overline{O}] \cdot 2_1$	$44''$. $(O/C_1; O/C_1)^{*\prime\prime}_-$	$[2,3,3]$	25/08	48
$\pm T$	$\pm\frac{1}{12}[T \times T] \cdot 2$	39. $(T/C_2; T/C_2)^*_c$	$2.[^+3,4]$	25/05	48
$+T$	$+\frac{1}{12}[T \times T] \cdot 2_1$	$39'$. $(T/C_1; T/C_1)^*_{c-}$	$[^+3,4]^\circ$	25/01	24
hybrid axial groups $G_3^{+x_4}$ in G_3					
$G_3^{+x_4}$ in G_3	CS name	Du Val # and name	Cox.	BBNZW	order
$+I$ in $\pm I$	$\pm\frac{1}{60}[I \times I]$	31. $(I/C_2; I/C_2)$	$2.[3,5]^+$	n.cryst.	120
$\pm T$ in $\pm O$	$+\frac{1}{24}[O \times \overline{O}] \cdot 2_3$	$44''$. $(O/C_1; O/C_1)^{*\prime\prime}$	$[2,3,3]^\circ$	25/09	48
$+O$ in $\pm O$	$\pm\frac{1}{24}[O \times O]$	26. $(O/C_2; O/C_2)$	$2.[3,4]^+$	25/06	48
TO in $\pm O$	$\pm\frac{1}{12}[T \times \overline{T}] \cdot 2$	40. $(T/C_2; T/C_2)^*$	$2.[3,3]$	24/05	48
$+T$ in $\pm T$	$\pm\frac{1}{12}[T \times T]$	21. $(T/C_2; T/C_2)$	$2.[3,3]^+$	24/02	24
$+T$ in $+O$	$+\frac{1}{12}[T \times \overline{T}] \cdot 2_3$	$40'$. $(T/C_1; T/C_1)^*_-$	$[3,3]^\circ$	24/03	24
$+T$ in TO	$+\frac{1}{24}[O \times \overline{O}]$	$26''$. $(O/C_1; O/C_1)''$	$[2,3,3]^+$	25/04	24

Table 6.3.: Summary of the 21 axial groups (except doubly axial groups). We have included references to the list of crystallographic 4-dimensional groups by Brown, Bülow, Neubüser, Wondratschek, Zassenhaus (BBNWZ) [10], and the names of Du Val [23], together with his numbering which extends the numbering of Goursat.
We use two further adaptations of Coxeter's notation, following [14]: G° is obtained by replacing the orientation-reversing elements g of G by $-g$. An initial "2." indicates doubling the group by adjoining negatives. The 2 in $[2,3,3]$ indicates the presence of an extra "perpendicular" mirror R_1 that commutes with the other reflections.
In Du Val's notation, achiral groups can be recognized by the * superscript. Haploid groups (those whose CS name begins with a $+$) were not considered by Goursat, and Du Val denotes them by adding primes to the numbers of the corresponding diploid groups, such as $44'$ and $44''$. Variations are indicated by various subscript and superscript decorations of the group names. In some cases, a unique notation is only achieved by considering the number and the name together. Thus, we are deviating from Du Val's notation by attaching the primes also to the names. For example, Du Val distinguishes two groups $26'$ and $26''$ with the same name $(O/C_1; O/C_1)$. Accordingly, although this is overlooked in Du Val [23, p. 61], one must also make a distinction between the corresponding achiral groups $44'$ and $44''$. *Each of* these two achiral extensions comes in two variations: $(O/C_1; O/C_1)^*$ and $(O/C_1; O/C_1)^*_-$. This omission in Du Val's list was already noted by Dunbar [24, p. 141, last paragraph].

The group "$G_3^{+x_4}$ in G_3" is chiral if and only if $G_3^{+x_4}$ is chiral and G_3 is achiral, because the elements of $G_3 \setminus G_3^{+x_4}$ are flipped by the x_4-reflection. These are the case of the form "$+G$ in $\pm G$" in the table, plus the group "$+T$ in TO".

The situation is very much analogous to the construction of the achiral groups in O(3) from the chiral groups in SO(3) and their index-2 subgroups in [14, §3.8], except that Conway and Smith prefer to extend by the algebraically simpler central inversion $-\mathrm{id}$ instead of the geometrically more natural reflection of the axial coordinate.

The maximal axial groups are $\pm\frac{1}{60}[I \times I] \cdot 2 = 2.[3,5]$ and $\pm\frac{1}{24}[O \times O] \cdot 2 = 2.[3,4]$. Hence, the axial groups can be characterized as the symmetries of a 4-dimensional prism over an icosahedron or over an octahedron, and the subgroups of these. (This includes, however, the doubly axial groups, which we have classified under the toroidal groups.)

We mention that, among the $3 \times 7 = 21$ axial groups, there are 7 chiral ones and 14 achiral ones. Among the polyhedral groups, there are 14 chiral ones. In addition, there are 14 types of three-dimensional point groups, which split into 7 polyhedral groups and 7 infinite axial families (which correspond to the 7 frieze groups). We have no explanation for the frequent appearance of the magic number 7 and its multiples.

7 Computer calculations

We used the help of computers for investigating the groups and checking the results, as well as for the preparation of the figures and tables. We used SageMath [66] and its interface to the GAP [29] software for group-theoretic calculations. The computer code is available in https://github.com/LaisRast/point-groups.

7.1. Representation of transformations and groups

We represent the orthogonal transformations $[l, r]$ and $*[l, r]$ by the quaternion pair (l, r) and a bit for indicating orientation reversal. In a group, each transformation is represented twice, by the equivalent pairs (l, r) and $(-l, -r)$.

We used two different representations for quaternions: For the elements of $2I$, $2O$, and $2T$, the quaternions $x_1 + x_2 i + x_3 j + x_4$ are represented in the natural way with precise algebraic coefficients, using SageMath's support for algebraic extension fields. For the elements of $2D_{2n}$, we used a tailored representation: These elements are of the form e_n^s or $e_n^s j$, and we represent and manipulate them using the fraction s/n, and a bit that indicates whether the factor j is present. (An exact algebraic representation would have required extension fields of arbitrarily high degree.)

The left group and the right group don't have to use the same representation: For elements of tubical groups, like $[l, r] \in \pm[I \times C_n]$, each of l and r uses its own appropriate representation.

7.2. Fingerprinting

For preparing a catalog of groups, it is useful to have some easily computable invariants. We used the number of elements of each geometric type as a *fingerprint*. This technique was initiated by Hurley [37] in his classification of the 4-dimensional crystallographic groups.

We first discuss the classification of the individual 4-dimensional orthogonal transformations, as introduced in Section 1.5. Every orientation-preserving orthogonal transformation can be written as a block diagonal matrix R_{α_1,α_2} of two rotation matrices (1.1). We must be aware of other angle parameters $R_{\alpha_1',\alpha_2'}$ that describe geometrically the same operation, in other words, that are conjugate by an orientation-preserving transformation (see Section 4.3.3). If we swap the two invariant coordinate planes $(x_1, x_2) \leftrightarrow (x_3, x_4)$, this is an orientation-preserving transformation, and it turns R_{α_1,α_2} into R_{α_2,α_1}. A simultaneous reflection in both coordinate planes ($x_1 \leftrightarrow x_2$ and $x_3 \leftrightarrow x_4$) is also orientation-preserving, and it turns R_{α_1,α_2} into $R_{-\alpha_1,-\alpha_2}$.

Thus, $R_{\alpha_1,\alpha_2} \doteq R_{\alpha_2,\alpha_1} \doteq R_{-\alpha_1,-\alpha_2} \doteq R_{-\alpha_2,-\alpha_1}$. On the other hand, R_{α_1,α_2} and $R_{\alpha_1,-\alpha_2}$ are distinct unless one of the angles is 0 or $\pm\pi$. They are mirrors of each other.

The orientation-reversing transformations $\bar{R}_\alpha$ of (1.2) are characterized by a single angle α. Since the simultaneous negation of x_1 and x_4 turns $\bar{R}_\alpha$ into $\bar{R}_{-\alpha}$, the parameter α can be normalized to the range $0 \le \alpha \le \pi/2$.

Since the angles are rational multiples of π, it is possible to encode the data about the operation into a short code. By collecting the codes of the elements in a group

into a string, we obtained a "fingerprint" of the group, which we used as a key for our catalog.[22] Experimentally, in all cases that we encountered, this method was sufficient to distinguish groups up to conjugacy. (As reported below, we considered, from the infinite families of groups, at least all groups of order up to 100.)

The classification of the elements by Hurley [37] is almost equivalent, except that it disregards the orientation: He classified a transformation by the triplet of coefficients (c_3, c_2, c_0) of its characteristic equation $\lambda^4 - c_3\lambda^3 + c_2\lambda^2 - c_1\lambda + c_0 = 0$: the trace c_3, the second invariant c_2, and the determinant c_0. Since all eigenvalues have absolute value 1, the linear coefficient c_1 is determined by the others through the formula $c_1 = -c_0c_3$. The Hurley triplet determines the eigenvalues and thus the geometric conjugacy type and the rotation angles α_1, α_2, but only up to orientation. R_{α_1,α_2} and $R_{\alpha_1,-\alpha_2}$ have the same spectrum and the same Hurley symbol.

The Hurley symbol. Hurley was interested in the crystallographic groups, and the operations in these groups must have integer coefficients in their characteristic polynomial. This restricts the operations to a finite set. Hurley denoted them by 24 letters (the Hurley symbols).

They were also used in the monumental classification of the four-dimensional crystallographic space groups by Brown, Bülow, Neubüser, Wondratschek, Zassenhaus [10]. Brown et al. refined the classification by splitting the groups into conjugacy classes *under the group operations*, resulting in the *Hurley pattern*. It may happen that several operations are geometrically the same but not conjugate to each other by a transformation of the group that is under consideration.[23]

Brown et al. [10, p. 9] report that their classification, which is more refined than ours but in another respect coarser, since it does not distinguish enantiomorphic groups, was also found to be sufficient to characterize the crystallographic point groups uniquely (up to mirror congruence).

We could use the data in the Tables of [10] to match them with our classification. The results are tabulated in Tables D.1–D.2 in Appendix D.

[22] Here are some details: We actually use the quaternion pair $[l, r]$ for computing the code for a rotation: If $[l, 1]$ and $[1, r]$ are rotations by $a\pi$ and $b\pi$, respectively, we use the pair of rational numbers (a, b) with $0 \le a, b \le 1$. The pair $[-l, -r]$, which represents the same rotation, gives the pair $(1 - a, 1 - b)$, and hence we normalize by requiring that $a < b$ or $a = b \le 1/2$.

For example, the group $\boxplus^{\mathrm{pg}}_{2,4}$ has the fingerprint `0|0:2 0|1:2 1|1/4:4 1|3/4:4 1|1/2:4 *1/2:16`. We tried to make the code concise while keeping it readable. The term `/4` in `1|3/4:4` is a common denominator for both components, and hence `1|3/4` stands for the pair $(a, b) = (\frac{1}{4}, \frac{3}{4})$, denoting a rotation of the form $[\exp\frac{\pi}{4}, \exp\frac{3\pi}{4}] \doteq R_{-\pi/2,\pi}$. The number `:4` after the colon denotes the multiplicity. Since our group representation contains both pairs $[l, r]$ and $[-l, -r]$ for each rotation, the multiplicity is always overcounted by a factor of 2. The group actually contains only two operations $R_{-\pi/2,\pi}$. (The reader may wish to identify them as particular torus translations of this group, see Figure 4.7.) The symbol `0|0` denotes the identity. The orientation-reversing transformations are written with a star. The sign `*`a with a fraction a denotes $\bar{R}_{(1-a)\pi}$. In our example, `*1/2:16` denotes eight operations of the form $\bar{R}_{\pi/2}$. The sum of the written multiplicities is 32, in accordance with the fact that the group has order $32/2 = 16$.

[23] For example, the group 21/03 in [10] of order 12 has the Hurley pattern `1*1I, 1*1E, 2*3E, 1*2S', 1*2B;` in our classification, it corresponds to two enantiomorphic groups, $\boxtimes^{\mathbf{c2mm}}_{1,3}$ and $\boxtimes^{\mathbf{c2mm}}_{3,1}$. The fingerprints of these groups are `0|0:2 0|2/3:4 1|1/2:14 3|5/6:4` and `0|0:2 1|3/6:4 1|3/3:4 1|1/2:14`. Both groups contain 7 half-turns (code `1|1/2`, Hurley symbol `E`). The second group, for example, is actually also a torus flip group: $\boxtimes^{\mathbf{c2mm}}_{3,1} \doteq \boxdot_{3,2}$. In this representation, it has 6 flip operations, which are half-turns. In addition, it contains the torus translation $R_{\pi,0}$, which is another half-turn. This half-turn is not conjugate to the other half-turns by operations of the group. It forms a conjugacy class of its own, as indicated by the code `1*1E` in the Hurley pattern. The 6 flip operations split into two conjugacy classes of size 3, as indicated by the code `2*3E`.

7.3. Computer checks

As mentioned, the classic approach to the classification following Goursat's method yields the chiral groups, and with the exception of the toroidal groups, they are obtained quite painlessly. However, the achiral groups must be found and classified as index-2 extensions of the chiral groups.

This task has been carried out by Du Val [23] and Conway and Smith [14], but they only gave the results. Du Val [23, p. 61] explicitly lists the orientation-reversing elements of each achiral group. Conway and Smith [14, Tables 4.1–4.3] provide generating elements for each group.

A detailed derivation is not presented in the literature. The considerations about the extension from chiral groups to achiral ones are only briefly sketched by Conway and Smith [14, p. 51–52], see Figures G.4–G.5. Since we found this situation unsatisfactory, we ran a brute-force computer check. We generated all subgroups of the groups $\pm[I \times I]$, $\pm[O \times O]$ and $\pm[T \times T]$ and their achiral extensions. No missing groups were discovered. More details are given below.

For the achiral extension of the subgroups of $\pm[C_n \times C_n]$, and $\pm[D_{2n} \times D_{2n}]$, we have supplanted the classic classification by our classification as toroidal groups. Nevertheless, we ran some computer checks also for these groups, see Section 7.5.

7.4. Checking the achiral polyhedral and axial groups

For each group $\pm[I \times I]$, $\pm[O \times O]$ and $\pm[T \times T]$ in turn, we generated all subgroups. We kept only those subgroups for which the left and right subgroup is the full group $2I$, $2O$, or $2T$ respectively. (For an achiral group, we must extend a group whose left group is equal to its right group.)

For each obtained subgroup, we identified the possible extending elements, using the considerations of Section 1.9. Each achiral group was classified by its fingerprint (the conjugacy types of its elements), and for each class, we managed to find geometric conjugations to show that all groups with the same fingerprint are geometrically the same.

We mention some details for the largest group $[I \times I]$. The group $\pm[I \times I]$ was represented by its double-cover $2I \times 2I$, and converted to a permutation group, in order to let GAP generate the subgroups. There are 19,987 subgroups in total, and they were found in about 5 minutes. 14,896 subgroups of them contain the pair $(-1, -1)$, which is necessary to have a double cover of a rotation group in $\pm[I \times I]$, and only 241 of these groups have the left and right subgroups equal to $2I$. These represented the group $\pm[I \times I]$ itself, and 60 different copies of each group $\pm\frac{1}{60}[I \times I]$, $\pm\frac{1}{60}[I \times \bar{I}]$, $+\frac{1}{60}[I \times I]$, $+\frac{1}{60}[I \times \bar{I}]$.

For each of the 241 groups, we tried to extend it by an element $*[1, c]$ in all possible ways, following Proposition 1.9.1. Actually, it is easy to see that elements c and $c' = cx$ that are related by an element x in the kernel lead to the same extension, and thus they need not be tried separately.

This leads to 361 distinct groups. Again there are 60 representatives of each of the six achiral groups with fraction $\frac{1}{60}$, plus one for the group $\pm[I \times I] \cdot 2$ itself.

Since we searched for conjugacies in a systematic but somewhat ad-hoc manner, it took about half a week for the computer to show that all 60 groups in each class are geometrically the same. With hindsight, the multiplicity 60 is not surprising, since there are 60 conjugacies that map the elements of $2I$ to themselves.

7.5. Checking the toroidal groups

The toroidal groups form an infinite family, and hence we can only generate them up to some limit. We set the goal of checking all chiral toroidal groups up to order 200 and all achiral groups up to order 400. For this purpose, we generated all groups $\pm[D_n \times D_n] \cdot 2$ (for even n) and $\pm[C_n \times C_n] \cdot 2$ in the range $100 < n \leq 200$, together with their subgroups.

For generating the subgroups, we took a different approach than for the polyhedral groups: We constructed a permutation group representation of the *achiral* group and computed all its subgroups. We took all subgroups, regardless of whether the left and right group is the full group C_n or D_n. For each chiral group up to order 200 and each achiral group up to order 400 that was generated, we checked that it is conjugate to one on the known groups according to our classification. We also checked whether all known toroidal groups within these size bounds are found. This turned out to be the case with a few exceptions. The exceptions were the chiral groups $\boxslash^{\mathrm{cm}}_{m,n}$, $\boxslash^{\mathrm{cm}}_{n,m}$ $\boxdiagup^{\mathrm{cm}}_{m,n}$, and $\boxdiagup^{\mathrm{cm}}_{n,m}$, for 14 pairs $(m,n) = (3,17), (3,19), (3,23), \ldots, (7,13), (9,11)$ of relatively prime odd numbers m and n, of orders $2mn$ between 100 and 200. The reason that these groups were missed is that they are of the form $+\frac{1}{2}[D_{2m} \times C_{2n}] \leqslant +\frac{1}{2}[D_{2m} \times D_{4n}]$, and the smallest group $\pm[D_{n'} \times D_{n'}] \cdot 2$ that contains them has $n' = 4 \cdot \mathrm{lcm}(m,n)$, which exceeds 200.

This computation requires a workstation with large memory. The group with the largest number of subgroups was $\pm[D_{192} \times D_{192}] \cdot 2$. It has 1,361,642 subgroups. For 1,249,563 of these groups, the order was within the limits. The whole computation took about 10 days on a computer with 256 gigabytes of main memory.

8 Higher dimensions

In the classification of Theorem A, there are categories that we expect in any dimension: the polyhedral groups, which are related to the regular polytopes, the toroidal groups, and the axial groups, which come from direct sums of lower-dimensional groups. On the other hand, the tubical groups are more surprising. They rely on the covering $\mathrm{SO}(3) \times \mathrm{SO}(3) \xrightarrow{2:1} \mathrm{SO}(4)$, which provides a different product structure in terms of lower-dimensional groups than the direct sum.

The scarcity of regular polytopes in high dimensions might be an indication that these groups are not very exciting. On the other hand, the root systems E_6, E_7, and E_8 in 6, 7, and 8 dimensions promise some richer structure in certain dimensions.

In five dimensions, the orientation-preserving case has been settled by Mecchia and Zimmermann [49], see [75, Corollary 2]:

Theorem 8.0.1. *The finite subgroups of the orthogonal group* $\mathrm{SO}(5)$ *are*

(i) *subgroups of* $\mathrm{O}(4) \times \mathrm{O}(1)$ *or* $\mathrm{O}(3) \times \mathrm{O}(2)$ *(the reducible case);*

(ii) *subgroups of the symmetry group* $(\mathbb{Z}_2)^5 \rtimes S_5$ *of the hypercube;*

(iii) *or isomorphic to* A_5*,* S_5*,* A_6 *or* S_6*. (This includes symmetries of the simplex and its polar.)*

The irreducible representations of the groups in (iii) can be looked up in the character tables of the books on Representation Theory. It would be interesting to know what the 5-dimensional representations are in geometric terms (besides the symmetries of the simplex).

This theorem gives only the chiral groups, but in odd dimensions like 5, it is in principle straightforward to derive the achiral groups from the chiral ones: All one needs to know are the chiral groups and their index-2 subgroups. See [14, §3.8] for the three-dimensional case. Briefly, one can say that nothing unexpected happens for the point groups in 5 dimensions.

Six dimensions. The richest part of the 4-dimensional groups were the toroidal groups, which have an invariant Clifford torus. The sphere S^5 contains an analogous three-dimensional torus:

$$x_1^2 + x_2^2 = x_3^2 + x_4^2 = x_5^2 + x_6^2 = 1/3$$

A group that leaves this torus invariant behaves similarly to a three-dimensional space group, involving translations, reflections, and rotations in terms of torus coordinates $\varphi_1, \varphi_2, \varphi_3$. Thus, the three-dimensional space groups will make their appearance in the classification of 6-dimensional point groups.

The situation in 4 dimensions was similar: We have studied the toroidal groups in analogy to the wallpaper groups (the two-dimensional space groups). In contrast to the situation in the plane, a 6-fold rotation in 3-space is not inconsistent with the requirement that the lattice of translations contains a cubical lattice. Thus, we may expect that all of

the 230 three-dimensional space groups show up in the 6-dimensional point groups. (In one dimension lower, we have another instance of this phenomenon: The frieze groups appear as the 3-dimensional axial point groups.)

Thus, a classification of the point groups in 6 dimensions will be much more laborious than in 5 dimensions. It has already been observed by Carl Hermann in 1952 [36, p. 33], in connection with the crystallographic groups, that "going up from an odd dimension to the next higher even one leads by far to more surprises than the opposite case".

Part II.

Realization Spaces of Polytopes

9 On the Dimensions of the Realization Spaces of Polytopes

9.1. History and Results

The study of geometric realizations of convex polytopes goes back to Legendre in 1794, who asked the following question [44, p. 309]: *How many variables are needed to determine a geometric realization of a given (combinatorial type of a) polytope?* In modern terms, Legendre asks for the dimension of the space of geometric realizations of a polytope P, i.e. the space of all choices of coordinates for the vertices of P that lead to a polytope with the same (isomorphic) face lattice.

The case of polygons is straightforward: The number of parameters is two times the number of vertices, which we would now write as $2f_0 = 2f_1$. The first major step is due to Legendre himself [44, Note VIII] and Steinitz [65, Sec. 69], who settled the question in dimension 3, where the number of variables turns out to be the number of edges plus 6. So the Legendre–Steinitz Theorem says that the realization space of any 3-dimensional polytope P is a manifold of dimension $f_1(P) + 6$.

It is natural to ask Legendre's question for d-dimensional polytopes (d-polytopes, for short). An answer was given by Robertson [59, Theorem, p. 18] in 1984: *The realization space of any d-polytope is a smooth submanifold of $\mathbb{R}^{d(f_0+f_{d-1})}$ of dimension $d(f_0 + f_{d-1}) - \mu$*, where $f_0 = f_0(P)$ is the number of vertices and $f_{d-1} = f_{d-1}(P)$ is the number of facets of P, and $\mu = \mu(P) = f_{0,d-1}(P)$ is the number of vertex-facet incidences. We will give explicit examples showing that this answer is incorrect. For the proof of his claim, Robertson represented the realization space as an open subset (defined by strict quadratic inequalities) of the solution set of μ quadratic equations in $\mathbb{R}^{d(f_0+f_{d-1})}$. In such a setting, it is natural to expect that the solution set has the dimension given by the number of variables minus the number of equations, and Robertson's proof is then "built round a simple application of the implicit function theorem" [59, p. 18].

With the Euler–Poincaré equation it is not hard to check that Robertson's claim agrees with what we know in dimensions $d = 1, 2, 3$. For simplicial and for simple polytopes, the realization spaces can be seen as open subspaces of $\mathbb{R}^{df_0}$ resp. $\mathbb{R}^{df_{d-1}}$ (see below). However, Mnëv's Universality Theorem for polytopes from 1986/1988 (Mnëv [50], see also Richter-Gebert [57], as well as the exposition in [58] and Mnëv's web page `http://www.pdmi.ras.ru/~mnev/bhu.html`) implies that the realization space is not in general a manifold: For any semi-algebraic set M defined over the integers one can construct a polytope whose realization space modulo affine transformations is equivalent to M up to certain trivial fibrations. This implies that realization spaces can have very complicated topology (locally, as well as globally), so realization spaces are not manifolds in general, but it does not have immediate implications on the dimension of the realization space.

So it appears that Robertson's claimed theorem is true for the polytopes that we see occurring "in nature", but it is false for very special examples that arise by complicated constructions in the proofs of Mnëv, Richter-Gebert, et al.

We start from Robertson's work. The model for the realization space suggested by him, formalized as the *centered realization space* by Adiprasito & Ziegler [1, 74] (see

Definition 9.2.1) is indeed very natural and convenient, as it is *by definition* a semi-algebraic set (indeed, an open subset of a real-algebraic variety). Therefore, topology and metric are clear and the dimension is well-defined. Moreover, the implicit function theorem is directly applicable in the way that Robertson set it up. From this we get

- a natural and rather general sufficient criterion for the validity of Robertson's claim (see Section 9.3),
- a very simple and natural proof (see [8, Lemma 2.8]) for the Legendre–Steinitz theorem for 3-dimensional polytopes (Corollary 9.4.10), as well as
- a natural tool for the analysis of other classes, with positive as well as negative results.

Our next step is the search for counter-examples (Section 9.5), where we identify the unique three smallest counter-examples to Robertson's claim, for which the realization space is still a smooth manifold, but its dimension is *not* given by the "natural guess" of "number of variables minus number of equations." One of these is particularly simple and easy to describe: It is the bipyramid over a triangular prism (Section 9.5.1).

Finally, we go for an iconic object in polytope theory, the 24-cell. We know from Paffenholz' thesis [52] that the 24-cell is not projectively unique, but its realization space (in our model) has dimension at least 28, which is the dimension of the group of projective transformations on $\mathbb{R}^4$ plus 4. We construct new classes of realizations of the 24-cell, and from these we derive in Section 9.5 that

- the realization space (in our model) has dimension at least 48, which is the dimension of the group of projective transformations on $\mathbb{R}^4$ plus 24, and indeed this is the "natural guess" dimension predicted by Robertson's claim;
- indeed, there are points in the realization space where locally the realization space is a manifold of dimension 48 (Corollary 9.5.9),
- but there are also points in the realization space (such as those given by realizations as a regular polytope) where the realization space is *not* a smooth submanifold of the ambient space $\mathbb{R}^{d(f_0+f_{d-1})} = \mathbb{R}^{192}$ (Theorem 9.5.10).

We doubt that the realization space of the 24-cell is a topological manifold, and indeed we are not sure that it is pure (has the same local dimension everywhere), but this is left open: The 24-cell keeps some of its mystery.

9.2. The centered realization space

For general facts about polytopes, refer to [71]. Let $P \subset \mathbb{R}^d$ be a d-dimensional polytope (or d-polytope, for short). We write $f_i(P)$ (or simply f_i, if the polytope is clear from the context) for the total number of faces of P that have dimension i. In particular, $f_0(P)$ is the number of vertices and $f_{d-1}(P)$ is the number of facets. We write $f_{0,d-1}(P)$ for the number of vertex-facet incidences. We call a polytope $P \subset \mathbb{R}^d$ *centered* if it contains the origin $\mathbf{0}$ in its interior. We can represent every polytope as the convex hull $P = \operatorname{conv}(V)$ of its vertices, where V is a $(d \times f_0)$-matrix and $\operatorname{conv}(V)$ is the convex hull of the columns of V. By rescaling the facet-defining inequalities, we can represent every centered polytope as the intersection of half-spaces

$$P = \{\mathbf{x} \in \mathbb{R}^d \mid A^t\mathbf{x} \leq \mathbf{1}\},$$

where A is a $(d \times f_{d-1})$-matrix. In these two representations, the matrices V and A are unique up to column permutations. Hence, if we label the vertices by subscripts $1, \ldots, f_0$, and label the facets by subscripts $1, \cdots, f_{d-1}$, we make these matrices unique. In this case, we say that P is *labeled*, and we call (V, A) the *combined vertex and facet description* of P.

A labeled d-polytope $Q \subset \mathbb{R}^d$ is said to *realize* P if there exists an isomorphism between the face lattices of P and Q that respects the labeling of their vertices and facets. If Q

was centered, we say that Q is a *centered realization* of P.

We now define the centered realization space model.

Definition 9.2.1 ([1, 74])**.** Let P be a labeled d-polytope with n vertices and m facets. The *centered realization space* of P is the set

$$\mathcal{R}_{\mathbf{0}}(P) := \left\{(V, A) \in \mathbb{R}^{d\times(n+m)} \mid \operatorname{conv}(V) = \{\mathbf{x} \in \mathbb{R}^d \mid A^t\mathbf{x} \leq \mathbf{1}\} \text{ realizes } P\right\}.$$

That is, $\mathcal{R}_{\mathbf{0}}(P)$ is the set of combined vertex and facet descriptions of centered realizations of P.

The next proposition shows that the centered realization space has a nice description as a (basic) semi-algebraic set (over $\mathbb{Z}$), that is, the solution set of a system of polynomial equations and inequalities. In particular, its dimension is well-defined.

Proposition 9.2.2. *Let P be a d-polytope with vertices $\mathbf{v}_1, \ldots, \mathbf{v}_n$ and facets $F_1, \ldots, F_m$. The centered realization space $\mathcal{R}_{\mathbf{0}}(P)$ of P is equal to the set*

$$\left\{(W, B) = (\mathbf{w}_1, \ldots, \mathbf{w}_n, \mathbf{b}_1, \ldots, \mathbf{b}_m) \in \mathbb{R}^{d\times(n+m)} \;\middle|\; \mathbf{w}_i^t\mathbf{b}_j \begin{cases} = 1 & \text{if } \mathbf{v}_i \in F_j \\ < 1 & \text{if } \mathbf{v}_i \notin F_j \end{cases} \right\}.$$

Proof. The equality $\operatorname{conv}(W) = \{\mathbf{x} \in \mathbb{R}^d \mid B^t\mathbf{x} \leq \mathbf{1}\}$ holds since the hyperplanes $\{\mathbf{x} \in \mathbb{R}^d \mid \mathbf{x}^t\mathbf{b}_j = 1\}$ are facet-defining hyperplanes for $\operatorname{conv}(W)$. The polytope $\operatorname{conv}(W)$ realizes P because it has the same vertex-facet incidence structure as P (this determines the face lattice of the polytope, see [71, Exercise 2.7]) with the correct labels. □

Our model of the realization space behaves nicely with respect to duality. Recall that the *polar polytope* P^Δ of a labeled centered d-polytope P is the polytope

$$P^\Delta := \{\mathbf{y} \in \mathbb{R}^d \mid \mathbf{y}^t\mathbf{x} \leq 1 \text{ for all } \mathbf{x} \in P\}.$$

There is an inclusion-reversing bijection between the face lattices of P and P^Δ. This bijection maps the vertices (resp. the facets) of P onto the facets (resp. the vertices) of P^Δ. We assume that the vertices (resp. the facets) of P^Δ are labeled with the labels of the facets (resp. the vertices) of P induced from the bijection.

Proposition 9.2.3. *For every labeled centered d-polytope P we have $\mathcal{R}_{\mathbf{0}}(P) \cong \mathcal{R}_{\mathbf{0}}(P^\Delta)$, where the isomorphism is given by the permutation $(V, A) \mapsto (A, V)$. In particular,* $\dim \mathcal{R}_{\mathbf{0}}(P) = \dim \mathcal{R}_{\mathbf{0}}(P^\Delta)$.

9.3. The Jacobian and the degeneracy criteria

According to Proposition 9.2.2, the centered realization space $\mathcal{R}_{\mathbf{0}}(P)$ is a semi-algebraic set defined by quadratic equations and strict quadratic inequalities, so it may be seen as an open subset (cut out by the strict inequalities) of a fiber of the characteristic map defined by the equations. This interpretation of Robertson's work on [59, p. 19] yields the setup for applying the implicit function theorem in this context.

Definition 9.3.1. Let P be a d-polytope with vertices $\mathbf{v}_1, \ldots \mathbf{v}_n$ and facets $F_1, \ldots, F_m$. Let $\mu := f_{0,d-1}(P)$ denote the number of vertex-facet incidences of P. The *characteristic map* of P, denoted Φ_P, is the map

$$\begin{aligned} \Phi_P : \mathbb{R}^{d\times(n+m)} &\to \mathbb{R}^\mu \\ (W, B) &\mapsto \left(\mathbf{w}_i^t\mathbf{b}_j - 1\right)_{[i,j]:\mathbf{v}_i\in F_j}. \end{aligned}$$

We order the entries $\mathbf{w}_i^t\mathbf{b}_j - 1$ lexicographically into the vector $\Phi_P(W, B)$. That is, the indices of that vector are pairs of the form $[i, j]$, and $\mathbf{w}_i^t\mathbf{b}_j - 1$ occupies the $[i, j]$th entry.

Clearly, this map sends (the vertex and facet description of) any centered realization of P to $\mathbf{0} \in \mathbb{R}^\mu$. Thus, $\mathcal{R}_\mathbf{0}(P)$ is an open subset of the fiber $\Phi_P^{-1}(\mathbf{0})$. The heuristic that the solution set of a system of equations has dimension "number of variables minus number of equations" suggests that $\dim \mathcal{R}_\mathbf{0}(P)$ is the number of variables $df_0(P) + df_{d-1}(P)$ minus the number of equations $f_{0,d-1}(P)$. This is what we call the "natural guess" for $\dim \mathcal{R}_\mathbf{0}(P)$ (formerly called the "naive guess" in [1, 74]).

Definition 9.3.2. Let P be a d-polytope. The *natural guess* for $\dim \mathcal{R}_\mathbf{0}(P)$, the dimension of the centered realization space of P, is

$$\mathrm{NG}(P) := d(f_0(P) + f_{d-1}(P)) - f_{0,d-1}(P).$$

From an algebraic point of view, the equations $\mathbf{w}_i^t\mathbf{b}_j = 1$ do not necessarily generate a nice ideal. It is certainly not prime in general, as we argue next.

Remark 9.3.3. For any d-polytope P with n vertices and m facets, the fiber $\Phi_P^{-1}(\mathbf{0})$ of the characteristic map contains certain subsets of "degenerate configurations." Namely, there is

- the set $S_V(P)$ where all columns of V are identical (corresponding to identical points) and the m affine hyperplanes contain that point, which has dimension

$$d + m(d-1) = (m+1)d - m = (m+1)(d-1) + 1,$$

- and the set $S_A(P)$ where all columns of A are identical (corresponding to identical affine hyperplanes) and the n points lie on that affine hyperplane, which has dimension

$$d + n(d-1) = (n+1)d - n = (n+1)(d-1) + 1.$$

These subsets are not contained in $\mathcal{R}_\mathbf{0}(P)$ because all of the strict inequalities are violated. Yet the equations defining $\mathcal{R}_\mathbf{0}(P)$ still hold.

Example 9.3.4. The 3-cube $C_3 \subset \mathbb{R}^3$ has 8 vertices, 6 facets and 24 vertex-facet incidences. We will later give a proof for the Legendre–Steinitz Theorem, which in this special case gives that $\dim(\mathcal{R}_\mathbf{0}(C_3)) = \mathrm{NG}(C_3) = 18$. However, the set of "degenerate configurations" $S_A(C_3)$ for the cube has dimension 19.

9.3.1. Examples

In the following proposition, we calculate the natural guess for special classes and common constructions of polytopes.

Proposition 9.3.5. *Let P be a d-polytope.*

(i) *If P is simplicial, then* $\mathrm{NG}(P) = df_0(P)$.

(ii) *If P is simple, then* $\mathrm{NG}(P) = df_{d-1}(P)$.

(iii) *If P is a 3-polytope, then* $\mathrm{NG}(P) = f_1(P) + 6$.

(iv) *If $P = \mathrm{pyr}(Q)$ is a pyramid over a $(d-1)$-polytope Q, then* $\mathrm{NG}(P) = \mathrm{NG}(Q) + 2d$.

(v) *If $P = \mathrm{bipyr}(Q)$ is a bipyramid over a $(d-1)$-polytope Q, then* $\mathrm{NG}(P) = 2\mathrm{NG}(Q) + (2-d)f_0(Q) + 2d$.

Proof. (i) Each facet has exactly d vertices. Therefore, $f_{0,d-1}(P) = df_{d-1}$.
(ii) This is the dual statement of (i).
(iii) Each edge of a P determines 4 vertex-facet incidences, while each vertex-facet incidence corresponds to 2 edges. Therefore, $2f_{0,2}(P) = 4f_1(P)$. Using Euler's formula for 3-polytopes, we get

$$\mathrm{NG}(P) = 3\,(f_0(P) + f_2(P)) - f_{0,2}(P) = f_1(P) + 6.$$

(iv) Here we have $f_0(P) = f_0(Q) + 1$ and $f_{d-1}(P) = f_{d-2}(Q) + 1$. Every vertex of Q lies in the facet Q of P and in a facet of P that is the pyramid over a facet F of Q if and only if it lies in F. This gives us $f_0(Q) + f_{0,d-2}(Q)$ incidences. Additionally, the new vertex of the pyramid (the apex) lies in $f_{d-2}(Q)$ many facets of P. Thus, $f_{0,d-1}(P) = f_0(Q) + f_{0,d-2}(Q) + f_{d-2}(Q)$. Therefore, the natural guess is

$$\begin{aligned}\mathrm{NG}(P) &= d\,(f_0(Q) + 1 + f_{d-2}(Q) + 1) - f_0(Q) - f_{0,d-2}(Q) - f_{d-2}(Q)\\ &= (d-1)\,(f_0(Q) + f_{d-2}(Q)) - f_{0,d-2}(Q) + 2d = \mathrm{NG}(Q) + 2d.\end{aligned}$$

(v) Here we have $f_0(P) = f_0(Q) + 2$ and $f_{d-1}(P) = 2f_{d-2}(Q)$. Let F be a facet of Q. Each vertex of Q lies in two facets of P (namely the two pyramids over a facet F of Q) if and only if it lies in F. This gives us $2f_{0,d-2}(Q)$ incidences. Finally, the new two vertices of the bipyramid (the apexes) each lie in $f_{d-2}(Q)$ facets of P. Thus, $f_{0,d-1}(P) = 2f_{0,d-2}(Q) + 2f_{d-2}(Q)$. Therefore, the natural guess is

$$\begin{aligned}\mathrm{NG}(P) &= d\,(f_0(Q) + 2 + 2f_{d-2}(Q)) - 2f_{0,d-2}(Q) - 2f_{d-2}(Q)\\ &= 2(d-1)\,(f_0(Q) + f_{d-2}(Q)) - 2f_{0,d-2}(Q) + (2-d)f_0(Q) + 2d\\ &= 2\mathrm{NG}(Q) + (2-d)f_0(Q) + 2d.\end{aligned}$$

□

As we will see later, for large, very common classes of polytopes the natural guess is equal to the dimension of the realization space. However, this is not true in general. The following examples show that the natural guess can be negative.

Example 9.3.6 (Adiprasito & Ziegler [74])**.** A d-polytope is called *cubical* if its facets are combinatorially isomorphic to the standard $(d-1)$-cube $[-1,1]^{d-1}$. A *neighborly cubical polytope* is a cubical d-polytope whose $(\lfloor \frac{d}{2} \rfloor - 1)$-skeleton is combinatorially equivalent to that of an n-cube. Such polytopes $\mathrm{NCP}_d(n)$ were constructed by Joswig and Ziegler [39] for all $n \geq d$. Their f-vectors are determined by n and d: The number of vertices of $\mathrm{NCP}_d(n)$ is 2^n, and the number of its facets is given by

$$f_{d-1}(\mathrm{NCP}_d(n)) = 2d + 4\sum_{p=0}^{n-d-1}\left(\binom{\lfloor \frac{d}{2} \rfloor + p + 1}{p+2} + \binom{\lfloor \frac{d+1}{2} \rfloor + p}{p+2}\right)2^p,$$

see [39, Corollary 18]. Each facet of $\mathrm{NCP}_d(n)$ has 2^{d-1} vertices, and thus

$$f_{0,d-1}(\mathrm{NCP}_d(n)) = 2^{d-1} f_{d-1}(\mathrm{NCP}_d(n)).$$

Now the natural guess of $\mathrm{NCP}_d(n)$ is a function of d and n, and we can compute it.

- If $d = 4$, then $f_3(\mathrm{NCP}_4(n)) = (n-2)2^{n-2}$, and thus

$$\mathrm{NG}(\mathrm{NCP}_4(n)) = (6-n)2^n < 0 \text{ for } n \geq 7.$$

- If $d \geq 5$, then $\mathrm{NG}(\mathrm{NCP}_d(n)) < 0$ for $n \geq d+1$.

Example 9.3.7. Let $Q := C_{d-1}(n)^\Delta$ be the polar of a $(d-1)$-dimensional (centered) cyclic polytope with n vertices. The number of facets of Q is n, and the number of

vertices of Q is given by

$$f_0(Q) = \binom{n - \lceil \frac{d-1}{2} \rceil}{\lfloor \frac{d-1}{2} \rfloor} + \binom{n - \lfloor \frac{d-1}{2} \rfloor - 1}{\lceil \frac{d-1}{2} \rceil - 1},$$

see [34, 4.7.3]. Since Q is simple, we have $\mathrm{NG}(Q) = (d-1)f_{d-2}(Q)$. Finally, let P be a bipyramid over Q. The natural guess of P is then given by

$$\begin{aligned}\mathrm{NG}(P) &= 2\mathrm{NG}(Q) + (2-d)f_0(Q) + 2d \\ &= 2(d-1)f_{d-2}(Q) + (2-d)f_0(Q) + 2d.\end{aligned}$$

We can easily compute $\mathrm{NG}(P)$ as a function of n and d. We see, for instance, if $d = 5$, then $\mathrm{NG}(P) < 0$ for $n \geq 10$, and if $d = 6$, then $\mathrm{NG}(P) < 0$ for $n \geq 9$.

Let us record some intuition about this example: consider the natural guess for a bipyramid: As we saw in Proposition 9.3.5(v), for a bipyramid the number of vertices enters with a negative sign to the natural guess. So for a bipyramid over a simple polytope Q, the natural guess grows with the number of facets, but it decreases with the number of vertices of Q. It is therefore natural to look at bipyramids over simple polytopes that maximize the number of vertices given the number of facets, i.e., over dual-to-neighborly polytopes.

We note that in these examples, $\mathcal{R}_{\mathbf{0}}(P)$ may still be a manifold (for the bipyramids over duals of cyclic polytopes this is indeed the case, see Proposition 9.5.6), but certainly its dimension is not $\mathrm{NG}(P)$.

9.3.2. The Jacobian criterion

Now we are ready to state our first main theorem, which is an application of the implicit function theorem.

Theorem 9.3.8 (The Jacobian Criterion; cf. Robertson [59, p. 19])**.** *Let P be a d-polytope. If the Jacobian matrix $J_{\Phi_P}(V_0, A_0)$ of the characteristic map Φ_P at some point $(V_0, A_0) \in \mathcal{R}_{\mathbf{0}}(P)$ has full row rank (that is, if it has rank $f_{0,d-1}(P)$), then $\mathcal{R}_{\mathbf{0}}(P)$ is, in a neighborhood of (V_0, A_0), a smooth manifold of dimension $\mathrm{NG}(P)$. In particular, $\dim_{(V_0,A_0)} \mathcal{R}_{\mathbf{0}}(P) = \mathrm{NG}(P)$ and $\dim \mathcal{R}_{\mathbf{0}}(P) \geq \mathrm{NG}(P) \geq 0$.*

Proof. By the implicit function theorem (see for example [43, Theorem 5.15]), $\Phi_P^{-1}(\mathbf{0})$ is, in a neighborhood of (V_0, A_0), a smooth manifold of dimension $\mathrm{NG}(P)$. The result follows since $\mathcal{R}_{\mathbf{0}}(P)$ is an open subset of $\Phi_P^{-1}(\mathbf{0})$. □

Remark 9.3.9. More generally, even if the Jacobian matrix does not have full rank, its corank still gives an upper bound for the local dimension:

$$\dim_{(V_0,A_0)} \mathcal{R}_{\mathbf{0}}(P) \leq d(n+m) - \operatorname{rank} J_{\Phi_P}(V_0, A_0).$$

Indeed, if the rank is r, we select r rows of the Jacobian that form a submatrix of full rank r, and then apply the Implicit Function Theorem to the corresponding map $\Phi_P^{(r)} : \mathbb{R}^{d\times(n+m)} \to \mathbb{R}^r$. obtained by restricting the characteristic map to the corresponding r components.

The previous theorem gives us the motivation to study the structure of the Jacobian matrix of Φ_P for a polytope P.

Notation 9.3.10. Let P be a d-polytope with n vertices, m facets and μ vertex-facet incidences. The *Jacobian matrix in compressed notation* of Φ_P at $(V_0, A_0) \in \mathbb{R}^{d\times(n+m)}$, denoted by $J^c_{\Phi_P}(V_0, A_0)$, is the matrix we get from the matrix $J_{\Phi_P}(V_0, A_0)$ by replacing

the columns indexed by $v_{i_1}, \ldots, v_{i_d}$ (resp. $a_{j_1}, \ldots, a_{j_d}$) by one column indexed by $\mathbf{v}_i$ (resp. $\mathbf{a}_j$) whose entries are the corresponding row vectors. Note that

$$J^c_{\Phi_P}(V_0, A_0) \text{ is a } (\mu \times (n+m))\text{-block-matrix whose entries are row vectors,}$$

while

$$J_{\Phi_P}(V_0, A_0) \text{ is a } (\mu \times d(n+m))\text{-matrix.}$$

Lemma 9.3.11. *$J^c_{\Phi_P}(V, A)$ has $\mathbf{a}_j^t$ in the $[i,j]$th row and the ith column, and it has $\mathbf{v}_i^t$ in the $[i,j]$th row and the $(n+j)$th column. All other entries are zero.*

Proof. This follows since, for each $k \in \{1, \ldots, d\}$ we have

$$\frac{\partial(\mathbf{v}_i^t \mathbf{a}_j - 1)}{\partial v_{i,k}} = a_{j,k} \qquad \text{and} \qquad \frac{\partial(\mathbf{v}_i^t \mathbf{a}_j - 1)}{\partial a_{j,k}} = v_{i,k}. \qquad \square$$

Example 9.3.12. Let P be the 3-polytope shown in Figure 9.1 together with a Schlegel diagram of it through the facet $F_1 = \{\mathbf{v}_1, \mathbf{v}_2, \mathbf{v}_3, \mathbf{v}_4\}$.

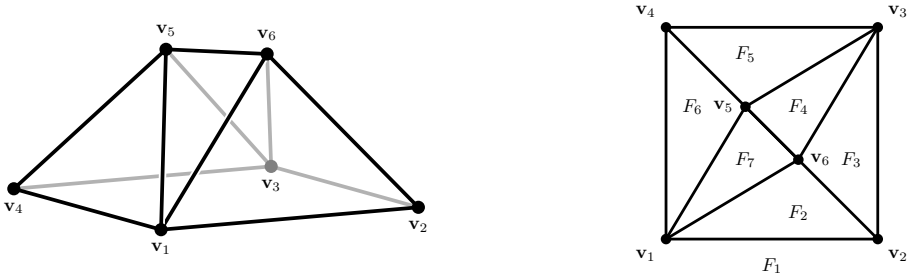

Figure 9.1.: A "tent" and a Schlegel diagram of it through the facet F_1.

Then the matrix $J^c_{\Phi_P}(V, A)$ at a point $(V, A) \in \mathbb{R}^{3\times(6+7)}$ is

$$\begin{array}{c} \\ [1,1] \\ [1,2] \\ [1,6] \\ [1,7] \\ [2,1] \\ [2,2] \\ [2,3] \\ [3,1] \\ [3,3] \\ [3,4] \\ [3,5] \\ [4,1] \\ [4,5] \\ [4,6] \\ [5,4] \\ [5,5] \\ [5,6] \\ [5,7] \\ [6,2] \\ [6,3] \\ [6,4] \\ [6,7] \end{array} \begin{array}{c} \begin{array}{ccccccccccccc} \mathbf{v}_1 & \mathbf{v}_2 & \mathbf{v}_3 & \mathbf{v}_4 & \mathbf{v}_5 & \mathbf{v}_6 & \mathbf{a}_1 & \mathbf{a}_2 & \mathbf{a}_3 & \mathbf{a}_4 & \mathbf{a}_5 & \mathbf{a}_6 & \mathbf{a}_7 \end{array} \\ \left[\begin{array}{ccccccccccccc} \mathbf{a}_1^t & \mathbf{0} & \mathbf{0} & \mathbf{0} & \mathbf{0} & \mathbf{0} & \mathbf{v}_1^t & \mathbf{0} & \mathbf{0} & \mathbf{0} & \mathbf{0} & \mathbf{0} & \mathbf{0} \\ \mathbf{a}_2^t & \mathbf{0} & \mathbf{0} & \mathbf{0} & \mathbf{0} & \mathbf{0} & \mathbf{0} & \mathbf{v}_1^t & \mathbf{0} & \mathbf{0} & \mathbf{0} & \mathbf{0} & \mathbf{0} \\ \mathbf{a}_6^t & \mathbf{0} & \mathbf{0} & \mathbf{0} & \mathbf{0} & \mathbf{0} & \mathbf{0} & \mathbf{0} & \mathbf{0} & \mathbf{0} & \mathbf{0} & \mathbf{v}_1^t & \mathbf{0} \\ \mathbf{a}_7^t & \mathbf{0} & \mathbf{0} & \mathbf{0} & \mathbf{0} & \mathbf{0} & \mathbf{0} & \mathbf{0} & \mathbf{0} & \mathbf{0} & \mathbf{0} & \mathbf{0} & \mathbf{v}_1^t \\ \mathbf{0} & \mathbf{a}_1^t & \mathbf{0} & \mathbf{0} & \mathbf{0} & \mathbf{0} & \mathbf{v}_2^t & \mathbf{0} & \mathbf{0} & \mathbf{0} & \mathbf{0} & \mathbf{0} & \mathbf{0} \\ \mathbf{0} & \mathbf{a}_2^t & \mathbf{0} & \mathbf{0} & \mathbf{0} & \mathbf{0} & \mathbf{0} & \mathbf{v}_2^t & \mathbf{0} & \mathbf{0} & \mathbf{0} & \mathbf{0} & \mathbf{0} \\ \mathbf{0} & \mathbf{a}_3^t & \mathbf{0} & \mathbf{0} & \mathbf{0} & \mathbf{0} & \mathbf{0} & \mathbf{0} & \mathbf{v}_2^t & \mathbf{0} & \mathbf{0} & \mathbf{0} & \mathbf{0} \\ \mathbf{0} & \mathbf{0} & \mathbf{a}_1^t & \mathbf{0} & \mathbf{0} & \mathbf{0} & \mathbf{v}_3^t & \mathbf{0} & \mathbf{0} & \mathbf{0} & \mathbf{0} & \mathbf{0} & \mathbf{0} \\ \mathbf{0} & \mathbf{0} & \mathbf{a}_3^t & \mathbf{0} & \mathbf{0} & \mathbf{0} & \mathbf{0} & \mathbf{0} & \mathbf{v}_3^t & \mathbf{0} & \mathbf{0} & \mathbf{0} & \mathbf{0} \\ \mathbf{0} & \mathbf{0} & \mathbf{a}_4^t & \mathbf{0} & \mathbf{0} & \mathbf{0} & \mathbf{0} & \mathbf{0} & \mathbf{0} & \mathbf{v}_3^t & \mathbf{0} & \mathbf{0} & \mathbf{0} \\ \mathbf{0} & \mathbf{0} & \mathbf{a}_5^t & \mathbf{0} & \mathbf{0} & \mathbf{0} & \mathbf{0} & \mathbf{0} & \mathbf{0} & \mathbf{0} & \mathbf{v}_3^t & \mathbf{0} & \mathbf{0} \\ \mathbf{0} & \mathbf{0} & \mathbf{0} & \mathbf{a}_1^t & \mathbf{0} & \mathbf{0} & \mathbf{v}_4^t & \mathbf{0} & \mathbf{0} & \mathbf{0} & \mathbf{0} & \mathbf{0} & \mathbf{0} \\ \mathbf{0} & \mathbf{0} & \mathbf{0} & \mathbf{a}_5^t & \mathbf{0} & \mathbf{0} & \mathbf{0} & \mathbf{0} & \mathbf{0} & \mathbf{0} & \mathbf{v}_4^t & \mathbf{0} & \mathbf{0} \\ \mathbf{0} & \mathbf{0} & \mathbf{0} & \mathbf{a}_6^t & \mathbf{0} & \mathbf{0} & \mathbf{0} & \mathbf{0} & \mathbf{0} & \mathbf{0} & \mathbf{0} & \mathbf{v}_4^t & \mathbf{0} \\ \mathbf{0} & \mathbf{0} & \mathbf{0} & \mathbf{0} & \mathbf{a}_4^t & \mathbf{0} & \mathbf{0} & \mathbf{0} & \mathbf{0} & \mathbf{v}_5^t & \mathbf{0} & \mathbf{0} & \mathbf{0} \\ \mathbf{0} & \mathbf{0} & \mathbf{0} & \mathbf{0} & \mathbf{a}_5^t & \mathbf{0} & \mathbf{0} & \mathbf{0} & \mathbf{0} & \mathbf{0} & \mathbf{v}_5^t & \mathbf{0} & \mathbf{0} \\ \mathbf{0} & \mathbf{0} & \mathbf{0} & \mathbf{0} & \mathbf{a}_6^t & \mathbf{0} & \mathbf{0} & \mathbf{0} & \mathbf{0} & \mathbf{0} & \mathbf{0} & \mathbf{v}_5^t & \mathbf{0} \\ \mathbf{0} & \mathbf{0} & \mathbf{0} & \mathbf{0} & \mathbf{a}_7^t & \mathbf{0} & \mathbf{0} & \mathbf{0} & \mathbf{0} & \mathbf{0} & \mathbf{0} & \mathbf{0} & \mathbf{v}_5^t \\ \mathbf{0} & \mathbf{0} & \mathbf{0} & \mathbf{0} & \mathbf{0} & \mathbf{a}_2^t & \mathbf{0} & \mathbf{v}_6^t & \mathbf{0} & \mathbf{0} & \mathbf{0} & \mathbf{0} & \mathbf{0} \\ \mathbf{0} & \mathbf{0} & \mathbf{0} & \mathbf{0} & \mathbf{0} & \mathbf{a}_3^t & \mathbf{0} & \mathbf{0} & \mathbf{v}_6^t & \mathbf{0} & \mathbf{0} & \mathbf{0} & \mathbf{0} \\ \mathbf{0} & \mathbf{0} & \mathbf{0} & \mathbf{0} & \mathbf{0} & \mathbf{a}_4^t & \mathbf{0} & \mathbf{0} & \mathbf{0} & \mathbf{v}_6^t & \mathbf{0} & \mathbf{0} & \mathbf{0} \\ \mathbf{0} & \mathbf{0} & \mathbf{0} & \mathbf{0} & \mathbf{0} & \mathbf{a}_7^t & \mathbf{0} & \mathbf{0} & \mathbf{0} & \mathbf{0} & \mathbf{0} & \mathbf{0} & \mathbf{v}_6^t \end{array}\right] \end{array}.$$

Notice that the columns are indexed by the vertices and the facets, while the rows are indexed by the vertex-facet incidences.

9.3.3. The degeneracy criterion

Definition 9.3.13. The *vertex-facet incidence graph* of a polytope P is the undirected graph $\Gamma_P = (\mathcal{V} \cup \mathcal{F}, E)$, where $\mathcal{V}$ is the set of all vertices of P, $\mathcal{F}$ is the set of all facets of P, and

$$E = \{\{\mathbf{v}, F\} \subset \mathcal{V} \cup \mathcal{F} \mid \mathbf{v} \in F\}.$$

Since there are no edges among the nodes in $\mathcal{V}$, nor among the nodes in $\mathcal{F}$, the graph Γ_P is bipartite.

Definition 9.3.14. An undirected graph G is *k-degenerate* if there exists an ordering of its nodes in which each node has at most k neighbors appearing after it in this ordering. Such an ordering is called *k-degenerate ordering*. The *degeneracy* of a graph is the smallest value of k for which it is k-degenerate

The degeneracy of a graph was defined by Lick & White in [45], where they established some basic results about degenerate graphs. The following proposition extends one of these results to bipartite graphs.

Proposition 9.3.15. *An n-node k-degenerate bipartite graph G with $n \geq 2k$ has at most $kn - k^2$ edges.*

Proof. We prove this statement by induction on n. Suppose that $n = 2k$. We will show that G has at most $kn - k^2 = 2k^2 - k^2 = k^2$ edges. This follows since an n-node bipartite graph can have at most $\frac{n^2}{4} = \frac{4k^2}{4} = k^2$ edges.

Now suppose that $n \geq 2k + 1$. Since G is k-degenerate, it has a node of degree at most k, say v. The graph $G - v$ is bipartite and k-degenerate. By induction, it has at most $k(n-1) - k^2 = kn - k^2 - k$ edges. Thus, G has at most $kn - k^2 - k + \deg v \leq kn - k^2 - k + k = kn - k^2$ edges. □

Remark 9.3.16. A bipartite graph $G = (A \cup B, E)$ of degeneracy k has at least $2k$ nodes. To see this, suppose that all the nodes in A have degree at most $\ell < k$, then we get an ℓ-degenerate ordering by putting the nodes of A first and then the nodes of B. This contradicts that the degeneracy of G is k. Thus, A has a node of degree at least k. Similar argument shows that B has a node of degree at least k.

Applying the previous proposition and remark on the vertex-facet incidence graph of a polytope, we immediately get the following corollary.

Corollary 9.3.17. *Let P be a d-polytope and assume that its vertex-facet incidence graph Γ_P has degeneracy k. Then the inequality*

$$f_{0,d-1}(P) \leq k\,(f_0(P) + f_{d-1}(P)) - k^2$$

holds. In particular, if Γ_P is d-degenerate, then $\mathrm{NG}(P) \geq d^2$. □

In Appendix H we investigate the degeneracy of Γ_P in more details. In particular, we show that the degeneracy is unbounded for d-polytopes when $d \geq 5$, giving a partial answer to an open question by Barnette and Grünbaum. For 4-polytopes, we relate the degeneracy with the "complexity" of that polytope, and finally we survey known 4-polytopes with high degeneracy.

The next theorem gives a lower bound for the dimension of the realization space of a d-polytope if its vertex-facet incidence graph is d-degenerate.

The following theorem is inspired by the proof for Steinitz's Theorem given by Borisov, Dickinson & Hastings [8, Lemma 2.8]. We call it the *degeneracy criterion*.

Theorem 9.3.18 (The Degeneracy Criterion)**.** *Let P be a d-polytope. If the vertex-facet incidence graph Γ_P has a d-degenerate ordering of its nodes such that the following two conditions hold.*

(i) *For each facet in this ordering, the vertices appearing after it and incident to it are linearly independent in any centered realization of P.*

(ii) *For each vertex in this ordering, the normal vectors of the facets appearing after it and incident to it are linearly independent in any centered realization of P.*

Then $\mathcal{R}_{\mathbf{0}}(P)$ is a smooth manifold of dimension $\mathrm{NG}(P)$.

Note that the requirement that Γ_P is d-degenerate is redundant since it follows from the conditions (i) and (ii).

Proof. Let $\mathbf{v}_1, \ldots, \mathbf{v}_n$ and $F_1, \ldots, F_m$ denote the vertices and the facets of P respectively. We will show that the Jacobian Criterion (Theorem 9.3.8) is satisfied at each point of $\mathcal{R}_{\mathbf{0}}(P)$ by block triangularizing the Jacobian matrix. Let $J^c := J^c_{\Phi_P}(V_0, A_0)$ denote the Jacobian matrix in compressed notation of the characteristic map Φ_P of P at some centered realization $(V_0, A_0) \in \mathcal{R}_{\mathbf{0}}(P)$. First reorder the columns of J^c in the way given by the degeneracy. Then, process these columns one by one from left to right. If the column is indexed by a vertex $\mathbf{v}_i$, move the rows indexed by

$$\{[i,j] \mid \mathbf{v}_i \in F_j, F_j \text{ appears after } \mathbf{v}_i \text{ in the ordering}\}$$

to the bottom of J^c. If the column is indexed by a normal vector $\mathbf{a}_j$, move the rows indexed by

$$\{[i,j] \mid \mathbf{v}_i \in F_j, \mathbf{v}_i \text{ appears after } F_j \text{ in the ordering}\}$$

to the bottom of J^c. After doing this for all the columns, we get an upper block-triangularized matrix. Now J^c has full rank if all of these blocks have full row rank, which is guaranteed by conditions (i) and (ii). The statement follows using the Jacobian Criterion at all centered realizations. □

Remark 9.3.19. Let G be the graph obtained from Γ_P by deleting some r edges such that G is d-degenerate and satisfies the conditions (i) and (ii) from the previous theorem. Then

$$\dim \mathcal{R}_{\mathbf{0}}(P) \leq \mathrm{NG}(P) + r.$$

This corresponds to finding a $((\mu - r) \times d(n+m))$-submatrix of the Jacobian matrix that has full rank at all centered realizations of P.

The Degeneracy Criterion is not purely combinatorial. The conditions (i) and (ii) might be satisfied for some geometric centered realizations and fail for others. However, in the next section, we will derive some purely combinatorial results from the Degeneracy Criterion.

Before moving on to applications, we set up a (scaled) homogeneous version of the results of this section, which turns out to be useful below. Let $C \subset \mathbb{R}^{d+1}$ be a closed and pointed polyhedral cone of dimension $d+1$. Analogously to the centered realization space, we define a primal-dual realization space model for C as follows

$$\mathcal{R}_h(C) = \Big\{(W,B) \in \mathbb{R}^{(d+1)\times(n+m)} \mid \mathrm{cone}(W) = \{x \in \mathbb{R}^{d+1} \mid B^t x \leq 0\} \text{ realizes } C, \\ \|\mathbf{w}_i\|2 = \|b_j\|2 = 1\Big\},$$

where n is the number of extreme rays and m is the number of facets of C. Analogously to the centered realization space, this set can be described as a semi-algebraic set. Let

$\mathbf{v}_1, \ldots, \mathbf{v}_n$ and $F_1, \ldots, F_m$ denote the extreme rays and the facets of C respectively. Then $\mathcal{R}_h(C)$ is equal to the set

$$\left\{ (W,B) \in \mathbb{R}^{(d+1)\times(n+m)} \;\middle|\; \mathbf{w}_i^t \mathbf{b}_j \begin{cases} = 0 & \text{if } \mathbf{v}_i \in F_j \\ < 0 & \text{if } \mathbf{v}_i \notin F_j \end{cases}, \sum_{k=1}^{d+1} w_{ik}^2 = \sum_{k=1}^{d+1} b_{jk}^2 = 1 \right\}.$$

Theorem 9.3.20 (The Homogeneous Degeneracy Criterion)**.** *Let C be a closed and pointed polyhedral cone of dimension $d+1$. Assume that its ray-facet incidence graph Γ_C has a d-degenerate ordering of its nodes such that the following conditions hold.*

(i) *For each facet in this ordering, the ray generators appearing after it and connected to it by an edge are linearly independent in any realization of C.*

(ii) *For every ray in this ordering, the normal vectors of the facets appearing after it and connected to it by an edge are linearly independent in any realization of C.*

Then the realization space $\mathcal{R}_h(C)$ is a smooth manifold of dimension $d(n+m)-\mu$, where n is the number of extreme rays of C, m is the number of facets of C and μ is the number of ray-facet incidences.

The proof of this theorem is analogous to the proof of Theorem 9.3.18. The rows which correspond to the norm equations can be handled as follows. The row indexed by the equation $\|\mathbf{v}_i\|^2 = 1$ (resp. $\|\mathbf{a}_j\|^2 = 1$) should be considered to move with the rows we move when processing the column indexed by $\mathbf{v}_i$ (resp. $\mathbf{a}_j$).

9.4. Applications

Definition 9.4.1 (Vertex set and facet set of a face)**.** Let P be a d-polytope and let F be a face of P. The *vertex set* of F is the set of all vertices of P contained in F. The *facet set* of F is the set of all facets of P containing F.

The following proposition is easy. However, combining it with the Degeneracy Criterion produces interesting combinatorial results.

Proposition 9.4.2. *Let $P \subset \mathbb{R}^d$ be a centered d-polytope.*

(i) *Let S be a set of $k \leq d$ vertices that lie on a facet of P. If some $k-1$ vertices from S are the vertex set of a $(k-2)$-face, then the vertices in S are linearly independent.*

(ii) *Let S be a set of $k \leq d$ facets that share a vertex of P. If some $k-1$ facets from S are the facet set of a $(d-k+1)$-face, then the normal vectors of the facets in S are linearly independent.*

Proof. The second statement (ii) is the dual of (i), so we will only prove (i). Let F be the facet of P which the vertices of S lie on. Let $\mathbf{v}_1, \ldots, \mathbf{v}_{k-1} \in S$ be the vertices of P which form a $(k-2)$-face, and $\mathbf{v}_k$ be the last vertex in S. Since $\mathbf{v}_1, \ldots, \mathbf{v}_{k-1}$ form a $(k-2)$-face (that is, a $(k-2)$-simplex), they are affinely independent. By the definition of a proper face, there is an affine hyperplane in $\mathbb{R}^d$ which contains all these vertices and does not contain $\mathbf{v}_k$. The affine hull of $\mathbf{v}_1, \ldots, \mathbf{v}_{k-1}$ is contained in this hyperplane, and thus the affine hull of $\mathbf{v}_1, \ldots, \mathbf{v}_{k-1}$ does not contain $\mathbf{v}_k$. Thus, $\mathbf{v}_1, \ldots, \mathbf{v}_k$ are affinely independent. Since the hyperplane spanned by F does not contain $\mathbf{0}$, these vertices are also linearly independent. □

If the size of S is at most 3, some of the assumptions in the previous proposition can be dropped.

Proposition 9.4.3. *Let $P \subset \mathbb{R}^d$ be a polytope containing the origin in its interior.*

(i) *Let S be a set of $k \leq 3$ vertices that lie on a facet of P. Then the vertices in S are linearly independent.*

(ii) *Let S be a set of $k \leq 3$ facets that share a vertex of P. Then the normal vectors of the facets in S are linearly independent.*

Proof. This is true since any three vertices on a facet are affinely independent and the affine span of any facet cannot contain the origin in a centered realization. Again, (ii) is the dual statement of (i). □

9.4.1. Almost 3-degenerate polytopes

Theorem 9.4.4. *Let P be a d-polytope. Let Π be the graph obtained from the vertex-facet incidence graph Γ_P by removing the nodes of degree d. If Π is 3-degenerate, then $\mathcal{R}_{\mathbf{0}}(P)$ is a smooth manifold of dimension $\mathrm{NG}(P)$.*

Proof. We will use the Degeneracy Criterion (Theorem 9.3.18) to prove this statement. The following ordering of the nodes of Γ_P is d-degenerate. First put all the nodes of Γ_P of degree d. These correspond to the simple vertices and the simplex facets. Then put the nodes of Π ordered by a 3-degenerate ordering. By Proposition 9.4.2, the conditions (i) and (ii) of the Degeneracy Criterion are satisfied at the nodes of Γ_P of degree d. By Proposition 9.4.3, the conditions (i) and (ii) of the Degeneracy Criterion are satisfied at the remaining nodes of Γ_P, which are exactly those nodes that are connected to at most 3 later nodes in the d-degenerate ordering we constructed. □

This is our main tool that we apply to special classes of polytopes to show that their realization spaces are manifolds. Before we begin with these applications, we again record a homogeneous version for later use.

Theorem 9.4.5. *Let C be a closed and pointed polyhedral cone of dimension $d+1$. Let Π be the graph obtained from its ray-facet incidence graph Γ_C by removing the nodes of degree d. If Π is 3-degenerate, then $\mathcal{R}_h(C)$ is a smooth manifold of dimension $d(m+n)-\mu$.*

The proof is the same as that of Theorem 9.4.4 with the only exception that we use Theorem 9.3.20 instead of the non-homogeneous version Theorem 9.3.18.

Corollary 9.4.6. *Let P be a d-polytope. If*

(i) *each vertex of P lies in at most 3 non-simplex facets, or*

(ii) *each facet of P contains at most 3 non-simple vertices,*

then $\mathcal{R}_{\mathbf{0}}(P)$ is a smooth manifold of dimension $\mathrm{NG}(P)$. □

This applies to simple and simplicial polytopes, of course. The corresponding natural guess is computed in Proposition 9.3.5.

Corollary 9.4.7. *Let P be a d-polytope.*

(i) *If P is simplicial, then $\mathcal{R}_{\mathbf{0}}(P)$ is a smooth manifold of dimension $df_0(P)$.*

(ii) *If P is simple, then $\mathcal{R}_{\mathbf{0}}(P)$ is a smooth manifold of dimension $df_{d-1}(P)$.* □

Polygons are always simple and simplicial, so we get that their realization spaces are always manifolds.

Corollary 9.4.8. *Let P be a 2-polytope, then $\mathcal{R}_{\mathbf{0}}(P)$ is a smooth manifold of dimension $2f_0(P) = 2f_1(P)$.* □

To get the analogue for 3-polytopes, we use the following combinatorial well-known observation for bipartite planar graphs. Planar for us means that we can draw the graph in the plane without crossing edges, but we do not insist on the edges being line segments.

Proposition 9.4.9. *Bipartite planar graphs are* 3*-degenerate.*

Proof. Let G be a bipartite planar graph with v nodes and e edges. We first show that $e \leq 2v-4$. Consider a planar drawing of G in the plane. Since the graph is bipartite, every cycle in G has length at least 4 and therefore, every connected component of the complement of G (called a face of the drawing) is bounded by at least 4 edges. On the other hand, every edge is in 2 faces. Thus, $4f \leq 2e$, where f is the number of faces of the drawing of G. Using Euler's formula for planar graphs, we get $e = v+f-2 \leq v+\frac{1}{2}e-2$. Thus, $e \leq 2v-4$.

If all nodes in G have degree ≥ 4, then by Handshaking lemma,

$$2e = \sum_{v \in G} \deg(v) \geq 4v,$$

and thus $4v-8 \geq 4v$. Thus, G has a node of degree ≤ 3. Now we get a 3-degenerate ordering of G recursively by deletion of nodes degree ≤ 3. □

Corollary 9.4.10 (see Borisov, Dickinson & Hastings [8, Lemma 2.8])**.** *Let P be a* 3*-polytope. Then $\mathcal{R}_{\mathbf{0}}(P)$ is a smooth manifold of dimension* $\mathrm{NG}(P) = f_1(P)+6$.

Proof. By Proposition 9.3.5 (iii) $\mathrm{NG}(P) = f_1(P)+6$. The vertex-facet incidence graph Γ_P of P is planar since we can draw it in the plane without crossing edges as follows. Draw one additional point on each facet of P, and connect it by edges to the vertices of that facet. Then project the vertices of P, the new points and the new edges from an interior point of P onto a sphere that contains P. Now apply a stereographic projection to the plane to get a planar graph. By Proposition 9.4.9, Γ_P is 3-degenerate. We are done by Theorem 9.4.4. □

9.4.2. Hypersimplices

The hypersimplices are key examples in polytope theory, which first appeared in the work of Gabriélov, Gel'fand & Losik [28] on characteristic classes.

Definition 9.4.11 (see [21] or [73])**.** The *standard hypersimplex* $\Delta_d(k)$ is the polytope defined by

$$\Delta_d(k) := \operatorname{conv}\left\{\mathbf{v} \in \{0,1\}^d \mid \sum_{i=1}^{d} v_i = k\right\},$$

where $1 \leq k \leq d-1$.

Note that $\Delta_d(k) \subset \mathbb{R}^d$ is a $(d-1)$-polytope since it lies in the affine hyperplane defined by $\sum_{i=1}^{d} x_i = k$. It has $\binom{d}{k}$ vertices (the number of ways to choose exactly k ones in a zero-one vector in $\mathbb{R}^d$.) Note also that $\Delta_d(k)$ is affinely isomorphic to $\Delta_d(d-k)$ under the map $\mathbf{x} \mapsto \mathbf{1}-\mathbf{x}$. For $k=1$ or $k=d-1$, we get a $(d-1)$-simplex Δ_{d-1}. Thus, we are particularly interested in the cases when k lies between 2 and $d-2$.

We first collect information about the facets of hypersimplices. See Ziegler [73, Sect. 3], De Loera, Rambau & Santos [21, Sect. 6.3.6] and Paffenholz & Ziegler [54, Sect. 3.3.1] for more information.

Proposition 9.4.12. *For $2 \leq k \leq d-2$, the following statements hold.*

(i) *$\Delta_d(k)$ has $2d$ facets: d of them are combinatorially isomorphic to $\Delta_{d-1}(k)$, and the other d facets are combinatorially isomorphic to $\Delta_{d-1}(k-1)$.*

(ii) *Each vertex of $\Delta_d(k)$ lies on d facets: $d-k$ of them are combinatorially isomorphic to $\Delta_{d-1}(k)$, and the other k facets are combinatorially isomorphic to $\Delta_{d-1}(k-1)$.*

(iii) *Each $d-3$ facets of $\Delta_d(2)$ of the form $\Delta_{d-1}(2)$ is the facet set of a triangular 2-face, that is, the set of all facets that contain a triangle face.*

Proof. Parts (i) and (ii) are also quite well-known, see for instance [21, Proposition 6.3.15] and its proof.

(i) Facets are defined by two types of hyperplanes,

$$H_i^{(0)} = \{\mathbf{x} \in \mathbb{R}^d \mid x_i = 0\} \text{ and}$$
$$H_i^{(1)} = \{\mathbf{x} \in \mathbb{R}^d \mid x_i = 1\},$$

for $1 \leq i \leq d$. The first type $H_i^{(0)}$ produces facets of the form $\Delta_{d-1}(k)$, while the second type $H_i^{(1)}$ produces facets of the form $\Delta_{d-1}(k-1)$.

(ii) Each vertex has $d-k$ zeros, and thus it lies on $d-k$ facets of the form $\Delta_{d-1}(k)$. It also has k ones, and thus it lies on k facets of the form $\Delta_{d-1}(k-1)$.

(iii) Fix $d-3$ facets of the form $\Delta_{d-1}(2)$. Without loss of generality, assume that these $d-3$ facets are defined by the first $d-3$ hyperplanes

$$H_i^{(0)} = \{\mathbf{x} \in \mathbb{R}^d \mid x_i = 0\}, \text{ for } 1 \leq i \leq d-3.$$

Thus, the face of $\Delta_d(2)$ which they define has the following vertex set.

$$\begin{aligned}&\{\mathbf{v} \in \{0,1\}^d \mid v_1 = \ldots = v_{d-3} = 0,\ v_{d-2} + v_{d-1} + v_d = 2\}\\ =&\{(\mathbf{0},1,1,0),(\mathbf{0},1,0,1),(\mathbf{0},0,1,1)\} \subset \mathbb{R}^d,\end{aligned}$$

which is a triangular 2-face. This face clearly does not lie on any of the following hyperplanes.

$$H_i^{(0)} = \{\mathbf{x} \in \mathbb{R}^d \mid x_i = 0\}, \text{ for } d-2 \leq i \leq d,$$

and

$$H_i^{(1)} = \{\mathbf{x} \in \mathbb{R}^d \mid x_i = 1\}, \text{ for } 1 \leq i \leq d. \qquad \square$$

Theorem 9.4.13. *The realization space of $\Delta_d(2)$ is a smooth manifold of dimension* $\mathrm{NG}(\Delta_d(2)) = \frac{3}{2}(d^2-d)$.

Proof. We will use the Degeneracy Criterion (Theorem 9.3.18) to prove this statement. Each vertex of $\Delta_d(2)$ lies in d facets, and we have $\binom{d}{2}$ vertices. Thus,

$$f_{0,d-2}(\Delta_d(2)) = d\binom{d}{2}.$$

In particular,

$$\mathrm{NG}(\Delta_d(2)) = (d-1)\left(\binom{d}{2} + 2d\right) - d\binom{d}{2} = \frac{3}{2}(d^2-d).$$

Let $P \subset \mathbb{R}^{d-1}$ be a centered realization of $\Delta_d(2)$. The following ordering of the nodes of the vertex-facet incidence graph Γ_P is $(d-1)$-degenerate. First put all the facets of the form $\Delta_{d-1}(1)$ at the beginning. These are $(d-2)$-simplices. Then put all the vertices, and at the end put all the facets of the form $\Delta_{d-1}(2)$. By Proposition 9.4.2 (i), condition (i) of the Degeneracy Criterion is satisfied at the simple nodes (these are the $(d-2)$-simplices). Thus, we only need to check the Degeneracy Criterion conditions

at the nodes corresponding to the vertices. Let $\mathbf{v}_i$ be a vertex of P. The corresponding node is adjacent to exactly $d-2$ later nodes $F_{i_1}, \ldots, F_{i_{d-2}}$. These nodes correspond to facets of the form $\Delta_{d-1}(2)$. By Proposition 9.4.12 (iii), any $d-3$ of them are the facet set of a 2-face. Thus, by Proposition 9.4.2 (ii), condition (ii) of the Degeneracy Criterion is satisfied at the nodes corresponding to the vertices. □

Indeed, Grande, Padrol & Sanyal [33] proved that the realization space of the hypersimplex $\Delta_d(2)$ modulo projective transformations is topologically a ball.

9.5. Negative results

In this section, we discuss negative results of various flavors. The first set of negative results shows that there are 4-polytopes with the property that their realization spaces are smooth manifolds but the dimension is not the expected one, i.e. not equal to the natural guess, providing explicit smooth counterexamples to the false claim in Robertson [59]. In the second part, we show that the realization space of the 24-cell is not a smooth manifold, at least in its natural embeddings.

9.5.1. The smallest polytopes P with $\dim \mathcal{R}_0(P) \neq \mathrm{NG}(P)$

We tested[24] the Degeneracy Criterion on the database of all 4-polytopes with at most 9 vertices [25]. The results are summarized in Table 9.1.

n	$\lvert\mathcal{P}_n^4\rvert$	$\lvert\mathcal{A}_n^4\rvert$	$\lvert\mathcal{P}_n^4 \setminus \mathcal{A}_n^4\rvert$
5	1	1	0
6	4	4	0
7	31	31	0
8	1294	1291	3
9	274148	274025	123

Table 9.1.: $\mathcal{P}_n^4$ is the set of all 4-polytopes with n vertices. $\mathcal{A}_n^4$ is the subset of $\mathcal{P}_n^4$ of those which satisfy the conditions of the Degeneracy Criterion.

In this section, we are going to look at the three 4-polytopes with 8 vertices which do not satisfy the Degeneracy Criterion. We will call them P_1, P_2 and P_3, and we will determine the dimensions of their realization spaces, which turn out to be different from the respective natural guess. Thus, we found the smallest examples (in terms of the number of vertices) where the dimensions of their realization spaces are different from their natural guesses. These three polytopes can be constructed from a pyramid over a triangular prism pyr(prism(Δ)) by adding a new point as follows:

(1) In P_1, the new point should lie beyond the triangular prism facet, on the supporting hyperplane of a simplex facet and beneath all the other facets. This polytope has 8 vertices, 9 facets and 43 vertex-facet incidences. A realization of P_1 is given by the

[24] In particular, for each of these polytopes, we use Matula & Beck algorithm [48] to find a 4-degenerate ordering satisfying the Degeneracy Criterion. The algorithm in [48] finds a degenerate ordering by repeatedly finding and deleting a node with the smallest degree. For those polytopes which do not satisfy the Degeneracy Criterion, a certificate of a realization with a deficient Jacobian matrix is already given in the database.

following vertex description.

$$\begin{array}{cccccccc} \mathbf{v}_0 & \mathbf{v}_1 & \mathbf{v}_2 & \mathbf{v}_3 & \mathbf{v}_4 & \mathbf{v}_5 & \mathbf{v}_6 & \mathbf{v}_7 \\ \left[\begin{array}{cccccccc} -1 & -1 & -1 & 1 & 1 & 1 & 1 & 1 \\ 1 & -1 & 0 & 1 & -1 & 0 & 0 & 0 \\ 1 & 1 & -1 & 1 & 1 & -1 & 0 & 0 \\ 0 & 0 & 0 & 0 & 0 & 0 & -1 & 1 \end{array}\right] \end{array}.$$

(2) In P_2, the new point should lie beyond the triangular prism facet and beneath all the other facets. In other words, P_2 is a bipyramid over the triangular prism. This polytope has 8 vertices, 10 facets and 46 vertex-facet incidences. A realization of P_2 is given by the following vertex description.

$$\begin{array}{cccccccc} \mathbf{v}_0 & \mathbf{v}_1 & \mathbf{v}_2 & \mathbf{v}_3 & \mathbf{v}_4 & \mathbf{v}_5 & \mathbf{v}_6 & \mathbf{v}_7 \\ \left[\begin{array}{cccccccc} -1 & -1 & -1 & 1 & 1 & 1 & 0 & 0 \\ 1 & -1 & 0 & 1 & -1 & 0 & 0 & 0 \\ 1 & 1 & -1 & 1 & 1 & -1 & 0 & 0 \\ 0 & 0 & 0 & 0 & 0 & 0 & -1 & 1 \end{array}\right] \end{array}.$$

(3) In P_3, the new point should lie beyond the triangular prism facet, beyond a simplex facet and beneath all the other facets. This polytope has 8 vertices, 11 facets and 50 vertex-facet incidences. A realization of P_3 is given by the following vertex description.

$$\begin{array}{cccccccc} \mathbf{v}_0 & \mathbf{v}_1 & \mathbf{v}_2 & \mathbf{v}_3 & \mathbf{v}_4 & \mathbf{v}_5 & \mathbf{v}_6 & \mathbf{v}_7 \\ \left[\begin{array}{cccccccc} -1 & -1 & -1 & 1 & 1 & 1 & 2 & 2 \\ 1 & -1 & 0 & 1 & -1 & 0 & 0 & 0 \\ 1 & 1 & -1 & 1 & 1 & -1 & 0 & 0 \\ 0 & 0 & 0 & 0 & 0 & 0 & -1 & 1 \end{array}\right] \end{array}.$$

To start, we introduce notation for a classical notion of realization spaces.

Definition 9.5.1. Let P be a labeled d-polytope with n vertices. The *realization space* of P is the set

$$\mathcal{R}(P) = \{V \in \mathbb{R}^{d\times n} \mid \operatorname{conv}(V) \text{ realizes } P\}.$$

Remark 9.5.2. Our various models of realization spaces that we considered so far fit together nicely. Let $P \subset \mathbb{R}^d$ be a d-dimensional polytope and denote by $\widehat{P} \subset \mathbb{R}^{d+1}$ the polyhedral cone generated by $\{(1, \mathbf{x}) \in \mathbb{R}^{d+1} | \, \mathbf{x} \in P\}$. The centered realization space $\mathcal{R}_{\mathbf{0}}(P)$ is diffeomorphic to an open subset of $\mathcal{R}(P)$ by the map $(V, A) \mapsto V$. The set $\mathcal{R}(P)$ is diffeomorphic to an open subset of $\mathcal{R}_h(\widehat{P})$ by the process of homogenization (with appropriate choice of scaling for the ray and facet description of the resulting cone, namely scaling the columns of these matrices to have norm 1). In particular, if we can show that $\mathcal{R}_h(\widehat{P})$ is a smooth manifold, then the spaces $\mathcal{R}(P)$ and $\mathcal{R}_{\mathbf{0}}(P)$ are smooth manifolds of dimension $\dim \mathcal{R}_h(\widehat{P})$.

Richter-Gebert introduced the following notion in [57] for polytopes that we also use in a cone version.

Definition 9.5.3. A d-polytope is *necessarily flat* if any polyhedral embedding of its boundary complex in $\mathbb{R}^n$, where $n \geq d$, has affine dimension at most d. A $(d+1)$-dimensional closed and pointed polyhedral cone is *necessarily flat* if any polyhedral embedding of its boundary fan in $\mathbb{R}^n$, where $n \geq d+1$, has affine dimension at most $d+1$.

Here a *polyhedral embedding* of a d-dimensional polyhedral complex $\mathcal{C}$ in $\mathbb{R}^n$, where $n \geq d$, is a mapping of the vertices of $\mathcal{C}$ into $\mathbb{R}^n$ such that the image of every k-face of $\mathcal{C}$ is a k-dimensional convex polyhedron combinatorially equivalent to that k-face, and for no two faces the images intersect in their relative interiors.

In dimension 2, the only necessarily flat polytope is the triangle. In dimension 3, Richter-Gebert in [57, Lemma 3.2.6] showed that pyramids, prisms and "tents" over n-gons are necessarily flat. Using the same proof provided by Richter-Gebert, one can show that the polyhedral cone that arises from a 3-dimensional prism is necessarily flat. Another related result is by Schwartz [63, Lemma 2.6] who showed that every simple d-polytope is necessarily flat, for $d \geq 3$.

Proposition 9.5.4. *The realization spaces of P_1, P_2 and P_3 are smooth manifolds of the following dimensions:*

$$\begin{aligned}\dim \mathcal{R}_{\mathbf{0}}(P_1) &= 26 > 25 = \mathrm{NG}(P_1),\\ \dim \mathcal{R}_{\mathbf{0}}(P_2) &= 27 > 26 = \mathrm{NG}(P_2),\\ \dim \mathcal{R}_{\mathbf{0}}(P_3) &= 27 > 26 = \mathrm{NG}(P_3).\end{aligned}$$

Proof. The boundary fan of each of the cones $\widehat{P_1}, \widehat{P_2}$ and $\widehat{P_3}$ contains the boundary fan of the cone over a triangular prism (with a missing simplex facet for $\widehat{P_1}$), which we call $\mathcal{F}$. The fan $\mathcal{F}$ has dimension 4 in any realization of $\widehat{P_1}, \widehat{P_2}$ and $\widehat{P_3}$ since the cone of a triangular prism is necessarily flat. Due to convexity, we know that the span of $\mathcal{F}$ has dimension 4 in any realization of $\widehat{P_1}, \widehat{P_2}$ and $\widehat{P_3}$. Thus, every realization of $\widehat{P_i}$ is obtained from a realization of C, where C is the cone of a pyramid over a triangular prism. The apex ray $\mathbf{x}$ can be chosen in an open subset of a linear space that varies differentiably with the realization of C. In P_2 and P_3, this open subset has dimension $5-1$ since $\mathbf{x}$ should have norm 1 and the only other constraints are strict inequalities which correspond to the conditions that $\mathbf{x}$ lies beneath or beyond a facet. In P_1, this open subset has dimension $5-2$ since, in addition to the constraints mentioned in P_2 and P_3, $\mathbf{x}$ should lie on the supporting hyperplane of a simplicial facet of C. We are done knowing that $\mathcal{R}_h(C)$ is a smooth manifold of dimension 23 by the Homogeneous Degeneracy Criterion Theorem 9.3.20, and using Remark 9.5.2. □

Theorem 9.5.5. *Let P be a 4-polytope with at most 8 vertices. Then the realization space $\mathcal{R}_{\mathbf{0}}(P)$ is a smooth manifold. Its dimension is equal to $\mathrm{NG}(P)$, except for the three polytopes P_1, P_2, and P_3, for which the dimension of the realization space is $\mathrm{NG}(P_i)+1$.*

Proof. This is shown by Proposition 9.5.4, combined with the enumeration that we have reported about at the beginning of Section 9.5.1. □

The following proposition provides a class of examples of polytopes where the dimension of the realization space does not equal the natural guess.

Proposition 9.5.6. *For $d \geq 3$, let Q be a simple d-polytope that is not a simplex. Then, the realization space of $P := \mathrm{bipyr}(Q)$, the bipyramid over Q, is a manifold but of dimension strictly greater than $\mathrm{NG}(P)$.*

Proof. Using Proposition 9.3.5(v), we have

$$\mathrm{NG}(P) = 2\dim \mathcal{R}_{\mathbf{0}}(Q) - (d-1)f_0(Q) + 2(d+1).$$

By Schwartz [63, Lemma 2.6], Q is necessarily flat. Thus, any realization of P can be obtained by embedding a realization of Q into a hyperplane H in $\mathbb{R}^{d+1}$ and then adding two points $\mathbf{v}$ and $\mathbf{v}'$, each in a different open half space of H, such that the segment

$[\mathbf{v}, \mathbf{v}']$ intersects the relative interior of Q. In particular,

$$\dim \mathcal{R}_{\mathbf{0}}(P) = \dim \mathcal{R}_{\mathbf{0}}(Q) + 3(d+1).$$

Thus,

$$\dim \mathcal{R}_{\mathbf{0}}(P) - \mathrm{NG}(P) = (d+1) + (d-1)f_0(Q) - \dim \mathcal{R}_{\mathbf{0}}(Q).$$

Since Q is simple,

$$\dim \mathcal{R}_{\mathbf{0}}(P) - \mathrm{NG}(P) = (d+1) + (d-1)f_0(Q) - df_{d-1}(Q).$$

We are done if we show that the right-hand-side is positive. For this we use the Lower Bound Theorem by Barnette [4] [9], to derive

$$\begin{aligned} f_0(Q) &\geq (d-1)f_{d-1}(Q) - (d+1)(d-2) \\ &= \tfrac{d}{d-1}f_{d-1}(Q) + ((d-1) - \tfrac{d}{d-1})f_{d-1}(Q) - (d+1)(d-2) \\ &> \tfrac{d}{d-1}f_{d-1}(Q) + ((d-1) - \tfrac{d}{d-1})(d+1) - (d+1)(d-2) \\ &= \tfrac{d}{d-1}f_{d-1}(Q) - \tfrac{d+1}{d-1}, \end{aligned}$$

where the strict inequality comes from the fact that Q is not a simplex. □

In particular, Proposition 9.5.6 implies that the realization space is is a manifold of dimension greater than $\mathrm{NG}(P)$ both for the bipyramid over a triangular prism P_2 of Theorem 9.5.5, as well as for the bipyramids over duals of cyclic polytopes of Example 9.3.7.

9.5.2. The 24-cell

Arguably the 24-cell $C_4^{(24)}$ is one of the most interesting and unique examples in polytope theory. It was discovered by Ludwig Schläfli around 1850, but his work was published only in 1901 [62]. For a classical discussion see e.g. Coxeter [19]. Its symmetry group is the Coxeter–Weyl group F_4 of order 1152. The 24-cell is unique in many ways. For example, it is the only centrally-symmetric self-dual regular polytope. It is also the only regular polytope that is neither simple nor simplicial. Thus, in particular, by Corollary 9.4.7 for every regular polytope P — except for possibly the 24-cell — the realization space is a smooth manifold of dimension $\mathrm{NG}(P)$.

The 24-cell has 24 vertices (and 24 facets, whence the name) and 144 vertex-facet incidences. Thus, the Jacobian Matrix has the format $f_{0,3} \times 4(f_0 + f_3) = 144 \times 192$. Full rank would mean full row rank 144, and the natural guess is

$$\mathrm{NG}(C_4^{(24)}) = 192 - 144 = 48.$$

The 24 facets of the 24-cell are octahedra (which have 6 vertices each), and each vertex of the 24-cell lies in exactly six of these octahedra. Thus, its vertex-facet incidence graph is 6-regular. So it is not 4-degenerate, and thus the Degeneracy Criterion cannot be applied. Instead, we will apply the Jacobian Criterion at specific realizations.

The following theorem gives bounds on the dimension of $\mathcal{R}_{\mathbf{0}}(C_4^{(24)})$.

Theorem 9.5.7. *The dimension of the realization space of the 24-cell satisfies the estimates*

$$48 \leq \dim \mathcal{R}_{\mathbf{0}}(C_4^{(24)}) \leq 52.$$

Proof. For the lower bound, we give a realization of the 24-cell where the Jacobian matrix has full rank: See the third item of the following proposition, Proposition 9.5.8.

For the upper bound, we find a (140×192)-submatrix of the Jacobian matrix, which has full rank at all centered realizations. Then the bound follows from Remark 9.3.19. For this, we construct an ordering of the nodes of the vertex-facet incidence graph of $C_4^{(24)}$. Start with four nodes $\mathbf{v}, \mathbf{u}, F, G$ such that $\mathbf{v}, \mathbf{u} \in F \cap G$. For two vertices in the ordering which form an edge, add the facets which contain it and are not already in the ordering. For two facets in the ordering which intersect in a ridge, add the vertices which form the ridge and are not already in the ordering. Repeat this until all the vertices and the facets are ordered. This process does not get stuck because the edge-ridge graph is connected; see Sallee [61]. If we remove the four edges between the nodes $\{\mathbf{v}, \mathbf{u}, F, G\}$, we get a 4-degenerate ordering which satisfies the degeneracy criterion: A facet in this ordering was added because an edge of it appeared before. So for each facet, there are at most 4 of its vertices appearing after it, and these four vertices are always affinely independent because they miss two vertices which form an edge of the octahedral facet. Similar argument for the vertices. We are done by Remark 9.3.19. □

The group of projective transformations on $\mathbb{R}^4$ has dimension 24. Thus, this establishes that the dimension of the realization space of $C_4^{(24)}$ modulo projective transformations satisfies

$$\dim(\mathcal{R}_{\mathbf{0}}(C_4^{(24)})/\mathrm{PGL}(\mathbb{R}, 4)) \;\geq\; 24,$$

where the best previous estimate, due to Paffenholz [52, 53], had been

$$\dim(\mathcal{R}_{\mathbf{0}}(C_4^{(24)})/\mathrm{PGL}(\mathbb{R}, 4)) \;\geq\; 4.$$

Proposition 9.5.8. *The Jacobian matrix for the 24-cell $C_4^{(24)}$ has different ranks at different realizations:*

(1) *For any realization of the 24-cell as a regular polytope, the Jacobian matrix has rank* 140 *(i.e., rank deficit* 4*).*

(2) *For the non-regular Paffenholz realizations of the 24-cell, the Jacobian matrix has rank* ≤ 142 *(i.e., rank deficit* ≥ 2*).*

(3) *For eight* 1*-parameter families of non-regular realizations of the 24-cell with a symmetry group of order* 24*, the Jacobian has rank* 144 *(i.e., full rank).*

Proof.

(1) A regular realization of $C_4^{(24)}$ is given by the following vertex description.

$$V_{\mathrm{reg}} = \mathrm{conv}\left\{\pm\mathbf{e}_i \pm \mathbf{e}_j \in \mathbb{R}^4 \mid 1 \leq i \leq j \leq 4\right\}.$$

At this realization, the Jacobian matrix has rank 140, which is not full.

(2) Paffenholz [52, Table 3.6] [53, Table 4.4] constructed a 4-parameter family of realizations of the 24-cell. One way to describe his construction is to start with the standard 4-cube $[-1, 1]^4$, and choose a point $(a, b, c, d) \in (-1, 1)^4$ in the interior of that cube. Now reflect this point through the 8 supporting hyperplanes of the facets of that cube to get 8 new points. The convex hull of the 16 vertices of the standard cube and the 8 new points gives the 4-parameter family. The rows of the following matrix describe the vertices of this 4-dimensional family of realizations.

$$\begin{bmatrix}
-1 & -1 & -1 & -1 \\
1 & 1 & -1 & -1 \\
1 & -1 & 1 & -1 \\
-1 & 1 & 1 & -1 \\
1 & -1 & -1 & 1 \\
-1 & 1 & -1 & 1 \\
-1 & -1 & 1 & 1 \\
1 & 1 & 1 & 1 \\
1 & -1 & -1 & -1 \\
-1 & 1 & -1 & -1 \\
-1 & -1 & 1 & -1 \\
1 & 1 & 1 & -1 \\
-1 & -1 & -1 & 1 \\
1 & 1 & -1 & 1 \\
1 & -1 & 1 & 1 \\
-1 & 1 & 1 & 1 \\
a & b & c & -d-2 \\
a & b & -c+2 & d \\
a & b & c & -d+2 \\
a & b & -c-2 & d \\
a & -b+2 & c & d \\
-a-2 & b & c & d \\
a & -b-2 & c & d \\
-a+2 & b & c & d
\end{bmatrix}.$$

If all the parameters are zero, we get a (different) regular realization, and the Jacobian matrix of the corresponding characteristic map at this realization has rank 140. Otherwise, using SageMath [66], we found two linear dependencies between the rows of the (symbolic) Jacobian matrix.

(3) Finally, we give a new construction of eight 1-parameter families of realizations of the 24-cell.

To get these families, start with the standard 4-cube $C_4 = [-1,1]^4$. Let $\mathbf{v}_i$ denote a point beyond the facet of C_4 defined by $\{\mathbf{x} \in \mathbb{R}^4 \mid x_i = 1\}$ and beneath all the other facets. Similarly, let $\mathbf{u}_i$ denote a point beyond the facet of C_4 defined by $\{\mathbf{x} \in \mathbb{R}^4 \mid x_i = -1\}$ and beneath all the other facets. Our goal is to construct a 24-cell whose vertex set is $\{-1,1\}^4 \cup \{\mathbf{v}_1, \ldots, \mathbf{v}_4, \mathbf{u}_1, \ldots, \mathbf{u}_4\}$ such that it has the following symmetries:

$$\begin{aligned}
\mathbf{u}_i &= -\mathbf{v}_i \quad \forall 1 \le i \le 4. \\
\mathbf{v}_i \mapsto \mathbf{v}_j \mapsto \mathbf{u}_i \mapsto \mathbf{u}_j \mapsto \mathbf{v}_i &\quad \forall 1 \le i \ne j \le 4. \\
\mathbf{v}_i \mapsto \mathbf{u}_j \mapsto \mathbf{u}_i \mapsto \mathbf{v}_j \mapsto \mathbf{v}_i &\quad \forall 1 \le i \ne j \le 4.
\end{aligned}$$

Letting $\mathbf{v}_1 = (a,b,c,d)$ and looking at the symmetries of C_4 which map the points as described above, we see that we have only two options for the coordinates of the $\mathbf{v}_i$'s.

$$\begin{array}{c} \mathbf{v}_1 \\ \mathbf{v}_2 \\ \mathbf{v}_3 \\ \mathbf{v}_4 \end{array} \begin{bmatrix} a & b & c & d \\ -b & a & -d & c \\ -c & d & a & -b \\ -d & -c & b & a \end{bmatrix}$$

and

$$\begin{array}{c} \mathbf{v}_1 \\ \mathbf{v}_2 \\ \mathbf{v}_3 \\ \mathbf{v}_4 \end{array} \begin{bmatrix} a & b & c & d \\ -b & a & d & -c \\ -c & -d & a & b \\ -d & c & -b & a \end{bmatrix}.$$

The convex hull of $\{-1,1\}^4 \cup \{\mathbf{v}_1,\ldots,\mathbf{v}_4,\mathbf{u}_1,\ldots,\mathbf{u}_4\}$ is a 24-cell if and only if each line segment between a pair $(\mathbf{v},\mathbf{v}')$ of non-opposite points of $\{\mathbf{v}_1,\ldots,\mathbf{v}_4\} \cup \{\mathbf{u}_1,\ldots,\mathbf{u}_4\}$ intersects the (relative) interior of the 2-face of C_4 defined by $F_{\mathbf{v}} \cap F_{\mathbf{v}'}$, where $F_{\mathbf{v}}$ (resp. $F_{\mathbf{v}'}$) is the facet of C_4 which $\mathbf{v}$ (resp. $\mathbf{v}'$) lies beyond. Writing up these conditions we see that they are equivalent to the following conditions.

$$b^2, c^2, d^2 = -a^2 + 2a, \quad 1 < a \leq 2.$$

The above equations can be rationally parameterized; Putting $a = \frac{2}{(x^2+1)}$ gives

$$b, c, d = \pm\frac{2x}{(x^2+1)}, \quad 0 \leq x < 1.$$

The plus-minus signs are independent, so this corresponds to $2^3 = 8$ families. The following matrix describes the vertex description of these families, where $s_1, s_2, s_3 \in \{-1,1\}^3$ and $0 \leq x < 1$.

$$\begin{bmatrix}
-1 & -1 & -1 & -1 \\
-1 & -1 & -1 & 1 \\
-1 & -1 & 1 & -1 \\
-1 & -1 & 1 & 1 \\
-1 & 1 & -1 & -1 \\
-1 & 1 & -1 & 1 \\
-1 & 1 & 1 & -1 \\
-1 & 1 & 1 & 1 \\
1 & -1 & -1 & -1 \\
1 & -1 & -1 & 1 \\
1 & -1 & 1 & -1 \\
1 & -1 & 1 & 1 \\
1 & 1 & -1 & -1 \\
1 & 1 & -1 & 1 \\
1 & 1 & 1 & -1 \\
1 & 1 & 1 & 1 \\
-\frac{2}{x^2+1} & -\frac{2\,s_1x}{x^2+1} & -\frac{2\,s_2x}{x^2+1} & -\frac{2\,s_3x}{x^2+1} \\
\frac{2}{x^2+1} & \frac{2\,s_1x}{x^2+1} & \frac{2\,s_2x}{x^2+1} & \frac{2\,s_3x}{x^2+1} \\
\frac{2\,s_1x}{x^2+1} & -\frac{2}{x^2+1} & \frac{2\,s_3x}{x^2+1} & -\frac{2\,s_2x}{x^2+1} \\
-\frac{2\,s_1x}{x^2+1} & \frac{2}{x^2+1} & -\frac{2\,s_3x}{x^2+1} & \frac{2\,s_2x}{x^2+1} \\
\frac{2\,s_2x}{x^2+1} & -\frac{2\,s_3x}{x^2+1} & -\frac{2}{x^2+1} & \frac{2\,s_1x}{x^2+1} \\
-\frac{2\,s_2x}{x^2+1} & \frac{2\,s_3x}{x^2+1} & \frac{2}{x^2+1} & -\frac{2\,s_1x}{x^2+1} \\
\frac{2\,s_3x}{x^2+1} & \frac{2\,s_2x}{x^2+1} & -\frac{2\,s_1x}{x^2+1} & -\frac{2}{x^2+1} \\
-\frac{2\,s_3x}{x^2+1} & -\frac{2\,s_2x}{x^2+1} & \frac{2\,s_1x}{x^2+1} & \frac{2}{x^2+1}
\end{bmatrix}$$

If $x = 0$, we get a regular realization, and the Jacobian matrix of the corresponding characteristic map at this realization has rank 140. Otherwise, when $0 < x < 1$, we get a non-regular realization. Using SageMath, we were able to show that the Jacobian matrices at the open interval $0 < x < 1$ have full rank. We did that by finding (144×144)-submatrices which have non-vanishing determinants on $0 < x < 1$.

□

Corollary 9.5.9. *There is an open subset of the realization space $\mathcal{R}_{\mathbf{0}}(C_4^{(24)})$ that is a smooth manifold of dimension* 48*.*

Proof. This holds in the neighborhood of the new realizations of Proposition 9.5.8 (3), where the Jacobian has full rank. □

However, in contrast to the local situation announced by Corollary 9.5.9, there are other points (e.g. at the regular realization) where the Jacobian property fails. The following theorem shows that $\mathcal{R}_{\mathbf{0}}(C_4^{(24)})$ contains points at which it is not smooth.

Theorem 9.5.10. *The realization space $\mathcal{R}_{\mathbf{0}}(C_4^{(24)}) \subset \mathbb{R}^{192}$ is not smooth at any point that corresponds to a realization of the 24-cell as a regular polytope.*

Proof. For each of the 8 families we constructed in Proposition 9.5.8 (3) above, we construct the corresponding Jacobian matrix J_{s_1,s_2,s_3} as a function of x. These Jacobian matrices have full rank in the interval $0 < x < 1$. Thus, their kernels define (48-dimensional) tangent spaces along these families. We computed the limits of these 8 (symbolic) tangent spaces at $x = 0$, and we noticed that these limits give four different

48-dimensional subspaces. Thus, the regular realization, given by $x = 0$, is not a smooth point in $\mathcal{R}_{\mathbf{0}}(C_4^{(24)})$.

These computations were done using SageMath [66]. To be able to compute the limits, we did the following. We computed the bases for the kernels in an echelon form, and then we orthogonalized (but not normalized!) the rows of these bases using Gram-Schmidt process. The entries of this echelon form are now rational functions in x. This produced rows with entries that go to infinity as x goes to 0. Those rows, we multiplied by x, after which the entries all became convergent. □

Remark 9.5.11. Bates, Hauenstein, Peterson & Sommese [6] and Wampler, Hauenstein & Sommese [69] introduced a local dimension numerical test based on the growth rate of the corank of the Macaulay matrix of the given variety after adding to it some number of random linear equations passing through the point at which we want to compute the local dimension. We used this test and we got the following numerical results.

- the local dimension of the realization space of the 24-cell at the regular realization is at most 50, and
- the local dimension of the realization space of the 24-cell at a Paffenholz realization is at most 49.

9.6. Comparison to other models

In what follows, we discuss various other models for realization spaces of polytopes and how they compare to the centered realization space. In particular, we argue that the results from Section 9.5.2 translate to these other models.

The simplest and most obvious model is to record the vertex coordinates of the realization; this leads to the set $\mathcal{R}(P) = \{V \in \mathbb{R}^{d \times f_0(P)} \colon \operatorname{conv}(V) \text{ realizes } P\}$, see Definition 9.5.1. This was, for example, used in Mnëv's original statement of the Universality Theorem for polytopes [50]. The centered realization space is diffeomorphic to an open subset of the naive model. Thus, the naive model is essentially the same as the centered realization space model. One might want to factor out the action of the affine group (which acts transitively on the naive model) or related transformation group actions. Several different ways to do this have been proposed in the literature, and they lead to slightly different models for the realization space of a polytope; see Gouveia, Macchia & Wiebe [32].

9.6.1. Realization spaces modulo transformation group actions

We begin with the model favored by Richter-Gebert in his work on the universality theorem for 4-polytopes [57, 58]. Here, we factor out affine transformations by fixing vertices, which by the combinatorial structure of the polytope have to be affinely independent in every realization, to be the origin and the standard basis vectors. The following proposition tells us how we can identify this model explicitly with a subset of the centered realization space (of lower dimension).

Proposition 9.6.1. *Let P be a d-dimensional polytope. Let $\mathcal{RG}(P)$ be the realization space of P in Richter-Gebert's model, which fixes vertices $\mathbf{v}_0, \mathbf{v}_1, \ldots, \mathbf{v}_d$ of P to be $\mathbf{e}_0 = \mathbf{0}$, $\mathbf{e}_1, \ldots, \mathbf{e}_d$. Let $\mathbf{x}_0, \mathbf{x}_1, \ldots, \mathbf{x}_d$ be affinely independent vectors in $\mathbb{R}^d$. Richter-Gebert's model is diffeomorphic to the space of realizations of P with $\mathbf{v}_i = \mathbf{x}_i$.*

Proof. Let A be the linear map that maps $\mathbf{e}_i$ to $\mathbf{x}_i - \mathbf{x}_0$. This linear transformation has full rank. Therefore, the affine transformation $\mathbf{x} \mapsto A\mathbf{x} + \mathbf{x}_0$ that maps $\mathbf{e}_i$ to $\mathbf{x}_i$ is invertible. This map induces a diffeomorphism of the described realization spaces. □

A recent way to encode realizations of a polytope is the *slack realization space* introduced by Gouveia, Macchia, Thomas & Wiebe [31]. Essentially, the authors show that realizations of a polytope correspond to $f_0 \times f_{d-1}$ matrices of rank $d+1$ (whose rows are indexed by vertices and columns by facets) with nonnegative entries, where zero entries appear only at the positions that correspond to vertex-facet incidences. In this model it is particularly easy to interpret and analyze the quotients modulo transformation groups. The connection of the slack model to Richter-Gebert's model discussed above as well as to the point of view of chirotopes (or oriented matroids with the same face lattice as the polytope) are explored in Gouveia, Macchia & Wiebe [32]. All different models modulo transformation groups are at least *birational*, which is to say isomorphic on an open subset (as subsets of algebraic varieties, so in particular also locally diffeomorphic wherever the map is defined).

For instance, if $P \subset \mathbb{R}^d$ is a d-dimensional polytope whose first $d+1$ vertices are affinely independent in any realization of P, Richter-Gebert's model fixes the first $d+1$ vertices of the polytope to be $\mathbf{0}, \mathbf{e}_1, \ldots, \mathbf{e}_d$. In the Grassmannian model of the realization space, a realization V of $P = \operatorname{conv}(V)$ is mapped to the column space of $\widehat{V}$. By the choice of the first $d+1$ columns of V, the Plücker vector of such a realization always ends up in the same canonical affine chart of the Grassmannian given by the first $(d+1) \times (d+1)$ block of $\widehat{V}$ having full rank (so that the corresponding entry in the Plücker vector is non-zero, more precisely 1). So Richter-Gebert's model is naturally a subset of the Grassmannian model of realizations of $\widehat{P}$. The slack realization space is birational to the Grassmannian model by [32, Theorem 4.7].

We discuss how to translate smoothness results from the centered realization space model to these quotient models exemplarily for the 24-cell in the following section.

9.6.2. The 24-cell in other models for the realization space

Proposition 9.6.2. *There is an open neighborhood of the regular realization of the 24-cell in $\mathcal{RG}(C_4^{(24)})$ that is diffeomorphic to a transversal affine section of $\mathcal{R}_{\mathbf{0}}(C_4^{(24)})$. In particular, the regular realization is also a singular point in $\mathcal{RG}(C_4^{(24)})$.*

Proof. Choose the vectors $\mathbf{x}_0 = (-1,1,1,1)$, $\mathbf{x}_1 = (1,1,1,1)$, $\mathbf{x}_2 = (0,2,0,0)$, $\mathbf{x}_3 = (0,0,2,0)$, $\mathbf{x}_4 = (0,0,0,2)$. These are affinely independent so that Proposition 9.6.1 implies that $\mathcal{RG}(C_4^{(24)})$ is diffeomorphic to all realizations of the 24-cell such that 5 vertices have the above coordinates, which we call $\mathcal{RG}'(C_4^{(24)})$. These are chosen as they are vertices of a regular realization. There is an open neighborhood of this regular realization in $\mathcal{RG}'(C_4^{(24)})$ that lies in $\mathcal{R}_{\mathbf{0}}(C_4^{(24)})$. This neighborhood is an affine section $\mathcal{R}_{\mathbf{0}}(C_4^{(24)}) \cap L$ of the centered realization space determined by the affine conditions that the 5 vertices $\mathbf{v}_7, \mathbf{v}_{15}, \mathbf{v}_{19}, \mathbf{v}_{21}, \mathbf{v}_{23}$ are equal to $\mathbf{x}_0, \ldots, \mathbf{x}_4$ respectively. We can now show that claim by a computation. We consider the same four curves as in Theorem 9.5.10 in $\mathcal{R}_{\mathbf{0}}(C_4^{(24)})$ that approach the regular realization. We transform them into curves in $\mathcal{RG}'(C_4^{(24)})$ by the affine transformation moving the five chosen vertices to the fixed x_i. Sufficiently close to the regular realization (given by the parameter value 0), these transformed curves in $\mathcal{RG}'(C_4^{(24)})$ pass through smooth points in $\mathcal{RG}'(C_4^{(24)})$ by generic smoothness of the quotient map. The tangent space to $\mathcal{RG}'(C_4^{(24)})$ is a 28-dimensional linear space depending on a parameter x. The limit for $x = 0$ can be computed by intersecting the limits of the tangent spaces of the original curves inside $\mathcal{R}_{\mathbf{0}}(C_4^{(24)})$ with the linear space $lin(L)$ corresponding to the affine subspace L, which we compute to be a 28-dimensional subspace. In fact, as in the proof of Theorem 9.5.10, we obtain four different 28-dimensional subspaces, which shows that $\mathcal{RG}'(C_4^{(24)})$, and therefore $\mathcal{RG}(C_4^{(24)})$, is not smooth at the regular realization. □

The fact that the realization space of the 24-cell is not a smooth manifold in Richter-Gebert's model locally around a regular realization also shows that it is not a smooth manifold in the Grassmannian model and therefore neither in the slack model (see [32]), as the transition maps between the models are defined locally around the regular realizations.

Bibliography

[1] Karim Adiprasito and Günter M. Ziegler. Many projectively unique polytopes. *Inventiones mathematicae*, 199:581–652, 2015.

[2] Simon L. Altmann. Hamilton, Rodrigues, and the quaternion scandal. *Mathematics Magazine*, 62(5):291–308, 1989. doi:10.1080/0025570X.1989.11977459.

[3] Thomas F. Banchoff. Torus decompositions of regular polytopes in 4-space. In Marjorie Senechal, editor, *Shaping Space*, pages 257–266. Springer, 2013. doi:10.1007/978-0-387-92714-5_20.

[4] David W. Barnette. The minimum number of vertices of a simple polytope. *Israel J. Math.*, 10:121–125, 1971.

[5] David W. Barnette and Branko Grünbaum. On Steinitz's theorem concerning convex 3-polytopes and on some properties of planar graphs. In *The many facets of graph theory*, pages 27–40. Springer, 1969.

[6] Daniel J. Bates, Jonathan D. Hauenstein, Chris Peterson, and Andrew J. Sommese. A numerical local dimensions test for points on the solution set of a system of polynomial equations. *SIAM J. Numer. Anal.*, 47(5):3608–3623, 2009. doi:10.1137/08073264X.

[7] Marcel Berger. *Geometry II*. Springer Science & Business Media, 2009.

[8] Alexander Borisov, Mark Dickinson, and Stuart Hastings. A congruence problem for polyhedra. *The American Mathematical Monthly*, 117(3):232–249, 2010.

[9] Arne Brøndsted. *An Introduction to Convex Polytopes*, volume 90 of *Graduate Texts in Mathematics*. Springer-Verlag, New York Berlin, 1983.

[10] Harold Brown, Rolf Bülow, Joachim Neubüser, Hans Wondratschek, and Hans Zassenhaus. *Crystallographic Groups of Four-Dimensional Space*. Wiley, New York, 1978.

[11] Christopher Cashen. Quasi-isometries between tubular groups. *Groups, Geometry, and Dynamics*, 4(3):473–516, 2010. doi:10.4171/GGD.

[12] John H. Conway, Heidi Burgiel, and Chaim Goodman-Strauss. *The Symmetries of Things*. A K Peters, 2008.

[13] John H. Conway, Ronald H. Hardin, and Neil J. A. Sloane. Packing lines, planes, etc.: packings in Grassmannian spaces. *Experimental Mathematics*, 5(2):139–159, 1996. doi:em/1047565645.

[14] John H. Conway and Derek A. Smith. *On Quaternions and Octonions*. CRC Press, 2003.

[15] H. S. M. Coxeter. Symmetrical definitions for the binary polyhedral groups. In *Finite Groups*, volume 1 of *Proc. Sympos. Pure Math.*, pages 64–87. Amer. Math. Soc., 1959.

[16] H. S. M. Coxeter. *Regular Polytopes*. Dover, 3rd edition, 1973.

[17] H. S. M. Coxeter. Regular and semi-regular polytopes. II. *Math. Z.*, 188:559–591, 1985. doi:10.1007/BF01161657.

[18] H. S. M. Coxeter. *Regular Complex Polytopes*. Cambridge Univ. Press, 2nd edition, 1991.

[19] Harold Scott Macdonald Coxeter. *Regular Polytopes*. Macmillan, New York, second edition, 1963. Corrected reprint, Dover, New York 1973.

[20] James Cruickshank and Seamus Kelly. Rearrangement inequalities and the alternahedron. *Discrete & Computational Geometry*, 35(2):241–254, 2006. doi:10.1007/s00454-005-1199-6.

[21] Jesús A. De Loera, Jörg Rambau, and Francisco Santos. *Triangulations*, volume 25 of *Algorithms and Computation in Mathematics*. Springer, Berlin Heidelberg, 2010.

[22] Paul de Medeiros and José Figueroa-O'Farrill. Half-BPS M2-brane orbifolds. *Advances in Theoretical and Mathematical Physics*, 16(5):1349–1408, 2012. doi:10.4310/ATMP.2012.v16.n5.a1.

[23] Patrick Du Val. *Homographies, Quaternions and Rotations*. Clarendon Press, 1964.

[24] William D. Dunbar. Nonfibering spherical 3-orbifolds. *Transactions of the American Mathematical Society*, 341(1):121–142, 1994. doi:10.2307/2154616.

[25] Moritz Firsching. The complete enumeration of 4-polytopes and 3-spheres with nine vertices. *Israel Journal of Mathematics*, 240(1):417–441, 2020. doi:10.1007/s11856-020-2070-4.

[26] Erik Friese and Frieder Ladisch. Affine symmetries of orbit polytopes. *Advances in Mathematics*, 288:386–425, 2016.

[27] Erik Friese and Frieder Ladisch. Classification of affine symmetry groups of orbit polytopes. *Journal of Algebraic Combinatorics*, 48(3):481–509, 2018. URL: https://rdcu.be/cDHw3, doi:10.1007/s10801-017-0804-0.

[28] Andrei M. Gabriélov, Izrail M. Gel'fand, and Mark V. Losik. Combinatorial computation of characteristic classes. *Functional Analysis and Applications*, 9:103–115, 1975.

[29] The GAP Group. *GAP – Groups, Algorithms, and Programming, Version 4.11.1*, 2021. URL: https://www.gap-system.org.

[30] Edouard Goursat. Sur les substitutions orthogonales et les divisions régulières de l'espace. *Annales scientifiques de l'É.N.S. 3^e série*, 6:9–102, 1889. doi:10.24033/asens.317.

[31] João Gouveia, Antonio Macchia, Rekha R. Thomas, and Amy Wiebe. The slack realization space of a polytope. *SIAM J. Discrete Math.*, 33(3):1637–1653, 2019.

[32] João Gouveia, Antonio Macchia, and Amy Wiebe. Combining realization space models of polytopes, 2020. Preprint, 32 pages, March 2020, arXiv:2001.11999. arXiv:2001.11999.

[33] Francesco Grande, Arnau Padrol, and Raman Sanyal. Extension complexity and realization spaces of hypersimplices. *Discrete & Computational Geometry*, 59(3):621–642, 2018.

[34] Branko Grünbaum. *Convex Polytopes*, volume 221 of *Graduate Texts in Mathematics*. Springer-Verlag, New York, 2003. Second edition prepared by V. Kaibel, V. Klee and G. M. Ziegler (original edition: Interscience, London 1967).

[35] Norman F. M. Henry, editor. *International tables for X-ray crystallography, Vol. 1, Symmetry Groups*. Kynoch Press, Birmingham, 2nd edition, 1952.

[36] C. Hermann. Translationsgruppen in n Dimensionen. In H. O'Daniel, editor, *Zur Struktur und Materie der Festkörper*, pages 24–33. Springer-Verlag, Berlin, Göttingen, Heidelberg, 1952. doi:10.1007/978-3-662-29427-7_2.

[37] A. C. Hurley. Finite rotation groups and crystal classes in four dimensions. *Mathematical Proceedings of the Cambridge Philosophical Society*, 47(4):650–661, 1951. doi:10.1017/S0305004100027109.

[38] A. C. Hurley. Finite rotation groups and crystal classes in four dimensions: II. revised tables and projection of groups of antisymmetry in three dimensions. In Per Olov Löwdin, editor, *Quantum Theory of Atoms, Molecules, and the Solid State: A Tribute to John C. Slater*, pages 571–586. Academic Press, 1966.

[39] Michael Joswig and Günter M. Ziegler. Neighborly cubical polytopes. *Discrete & Computational Geometry (Grünbaum Festschrift: G. Kalai, V. Klee, eds.)*, (2-3)24:325–344, 2000.

[40] Heuna Kim and Günter Rote. Congruence testing of point sets in 4 dimensions, March 2016. arXiv:1603.07269.

[41] Heuna Kim and Günter Rote. Congruence testing of point sets in 4-space. In Sándor Fekete and Anna Lubiw, editors, *32st International Symposium on Computational Geometry (SoCG 2016)*, volume 51 of *Leibniz International Proceedings in Informatics (LIPIcs)*, pages 48:1–48:16. Schloss Dagstuhl–Leibniz-Zentrum für Informatik, 2016. doi:10.4230/LIPIcs.SOCG.2016.48.

[42] Christian Lange and Marina A. Mikhaîlova. Classification of finite groups generated by reflections and rotations. *Transformation Groups*, 21:1155–1201, 2016. doi:10.1007/s00031-016-9385-6.

[43] John M. Lee. *Introduction to Smooth Manifolds*, volume 218 of *Graduate Texts in Mathematics*. Springer-Verlag, New York, 2001.

[44] Adrien-Marie Legendre. *Eléments de Géométrie*. Firmin Diderot, père et fils, Paris, 1794. twelfth ed. 1823.

[45] Don R. Lick and Arthur T. White. k-degenerate graphs. *Canadian Journal of Mathematics*, 22:1082–1096, 1970. doi:10.4153/CJM-1970-125-1.

[46] David W. Lyons. An elementary introduction to the Hopf fibration. *Mathematics Magazine*, 76(2):87–98, 2003. doi:10.2307/3219300.

[47] M. A. Maerchik. Finite groups generated by pseudoreflections in four-dimensional Euclidean space. *Trudy Kirgiz Gos. Univ. Ser. Mat. Nauk*, 11:66–72, 1976. (in Russian).

[48] David W. Matula and Leland L. Beck. Smallest-last ordering and clustering and graph coloring algorithms. *Journal of the ACM (JACM)*, 30(3):417–427, 1983.

[49] Mattia Mecchia and Bruno Zimmermann. On finite groups acting on homology 4-spheres and finite subgroups of SO(5). *Topology and its Applications*, 158(6):741–747, 2011. doi:10.1016/j.topol.2011.01.017.

[50] Nikolai E. Mnëv. The universality theorems on the classification problem of configuration varieties and convex polytopes varieties. In *Topology and geometry—Rohlin Seminar*, volume 1346 of *Lecture Notes in Mathematics*, pages 527–543. Springer, Berlin, 1988. doi:10.1007/BFb0082792.

[51] J. L. Nicolas and G. Robin. Majorations explicites pour le nombre de diviseurs de n. *Canadian Mathematical Bulletin*, 26(4):485–492, 1983. doi:10.4153/CMB-1983-078-5.

[52] Andreas Paffenholz. *Constructions for Posets, Lattices, and Polytopes*. PhD thesis, TU Berlin, Berlin, 2005. v+202 pages; dx.doi.org/10.14279/depositonce-1150.

[53] Andreas Paffenholz. New polytopes from products. *Journal of Combinatorial Theory, Ser. A*, 113:1396–1418, 2006.

[54] Andreas Paffenholz and Günter M. Ziegler. The E_t-construction for lattices, spheres and polytopes. *Discrete Comput. Geometry (Billera Festschrift: M. Bayer, C. Lee, B. Sturmfels, eds.)*, 32:601–624, 2004.

[55] Laith Rastanawi and Günter Rote. Towards a geometric understanding of the 4-dimensional point groups, 2022. URL: https://arxiv.org/abs/2205.04965, doi:10.48550/ARXIV.2205.04965.

[56] Laith Rastanawi, Rainer Sinn, and Günter M Ziegler. On the dimensions of the realization spaces of polytopes. *Mathematika*, 67(2):342–365, 2021. doi:10.1112/mtk.12075.

[57] Jürgen Richter-Gebert. *Realization Spaces of Polytopes*, volume 1643 of *Lecture Notes in Mathematics*. Springer-Verlag, Berlin Heidelberg, 1996.

[58] Jürgen Richter-Gebert and Günter M. Ziegler. Realization spaces of 4-polytopes are universal. *Bulletin of the American Mathematical Society*, 32:403–412, 1995.

[59] Stewart A. Robertson. *Polytopes and symmetry*, volume 90 of *London Mathematical Society Lecture Note Series*. Cambridge University Press, Cambridge, 1984.

[60] G. de B. Robinson. On the orthogonal groups in four dimensions. *Mathematical Proceedings of the Cambridge Philosophical Society*, 27(1):37–48, 1931. doi:10.1017/S0305004100009312.

[61] George Thomas Sallee. Incidence graphs of convex polytopes. *Journal of Combinatorial Theory*, 2(4):466–506, 1967.

[62] Ludwig Schläfli. *Theorie der vielfachen Kontinuität*. Denkschriften der Schweizerischen naturforschenden Gesellschaft, Vol. 38, pp. 1–237. Zürcher und Furrer, Zürich, 1901. Written 1850-1852. Reprinted in: Ludwig Schläfli, 1814-1895, Gesammelte Mathematische Abhandlungen Vol. I, Birkhäuser, Basel 1950, pp. 167–387.

[63] Alexander Schwartz. *Constructions of Cubical Polytopes*. PhD thesis, TU Berlin, Berlin, October 2003. 159 pages; dx.doi.org/10.14279/depositonce-920.

[64] Henry Segerman and Saul Schleimer. Puzzling the 120-cell. *Notices of the AMS*, 62(11):1309–1316, 2015. doi:10.1090/noti1297.

[65] Ernst Steinitz and Hans Rademacher. *Vorlesungen über die Theorie der Polyeder unter Einschluss der Elemente der Topologie*. Springer-Verlag, Berlin-New York, 1976. Reprint der 1934 Auflage, Grundlehren der Mathematischen Wissenschaften, No. 41.

[66] The Sage Developers. *SageMath, the Sage Mathematics Software System (Version 9.5)*, 2022. URL: https://www.sagemath.org.

[67] W. Threlfall and H. Seifert. Topologische Untersuchung der Diskontinuitätsbereiche endlicher Bewegungsgruppen des dreidimensionalen sphärischen Raumes. *Math. Annalen*, 104:1–70, 1931. doi:10.1007/BF01457920.

[68] W. Threlfall and H. Seifert. Topologische Untersuchung der Diskontinuitätsbereiche endlicher Bewegungsgruppen des dreidimensionalen sphärischen Raumes (Schluß). *Math. Annalen*, 107:543–586, 1933. doi:10.1007/BF01448910.

[69] Charles W. Wampler, Jonathan D. Hauenstein, and Andrew J. Sommese. Mechanism mobility and a local dimension test. *Mechanism and machine theory*, 46(9):1193–1206, 2011.

[70] Günter Ziegler. Projected products of polygons. *Electronic research announcements of the american mathematical society*, 10(14):122–134, 2004.

[71] Günter M. Ziegler. *Lectures on Polytopes*, volume 152 of *Graduate Texts in Mathematics*. Springer-Verlag, New York, 1995. Revised edition, 1998; seventh updated printing 2007.

[72] Günter M Ziegler. Face numbers of 4-polytopes and 3-spheres. *arXiv preprint math/0208073*, 2002.

[73] Günter M. Ziegler. Convex polytopes: Extremal constructions and f-vector shapes. In E. Miller, V. Reiner, and B. Sturmfels, editors, *"Geometric Combinatorics", Proc. Park City Mathematical Institute (PCMI) 2004*, volume 13 of *IAS/Park City Math. Ser.*, pages 617–691, Providence, RI, 2007. Amer. Math. Society.

[74] Günter M. Ziegler. Polytopes with low-dimensional realization spaces (joint work with Karim Adiprasito). *Oberwolfach Reports*, 8(3):2522–2525, 2011.

[75] Bruno P. Zimmermann. On finite groups acting on spheres and finite subgroups of orthogonal groups. *Sib. Èlektron. Mat. Izv.*, 9:1–12, 2012. URL: http://mi.mathnet.ru/eng/semr/v9/p1, arXiv:1108.2602.

Appendix

A Generators for the polyhedral and axial groups

Table A.1 gives a complete summary of the polyhedral (Table 5.1) and axial groups (Table 6.3), following the numbering by Goursat [30], as extended to the haploid groups by Du Val [23], together with a set of generators for each group. The axial groups can be recognized as having only two numbers different from 2 in their Coxeter name. Our adaptations of Du Val's names was explained in Table 6.3 and footnote 19 on p. 77. The top part contains the chiral groups (#20–#32) and the bottom part the achiral ones (#39–#51).[25]

Where appropriate, we include a reference to the numbering of crystallographic point groups according to Brown, Bülow, Neubüser, Wondratschek, Zassenhaus (BBNWZ) [10], see also Appendix D.

In addition to the quaternions defined in (1.6) in Section 1.11, the following elements are used for generating the groups:

$$\bar\omega = \tfrac12(-1-i-j-k) \qquad \text{(order 3)}$$

$$i_I^\dagger = \tfrac12(i + \tfrac{-\sqrt5-1}{2}j + \tfrac{-\sqrt5+1}{2}k) \qquad \text{(order 4)} \qquad \text{(A.1)}$$

$$i_I' = \tfrac12(-\tfrac{\sqrt5-1}{2}i - \tfrac{\sqrt5+1}{2}j + k) \qquad \text{(order 4)} \qquad \text{(A.2)}$$

$\bar\omega$ is simply the conjugate quaternion of ω. We tried to reduce the number of generators by trial and error, confirming by computer whether the generated groups did not change.

For a few groups, the groups given by Conway and Smith are not identical to the groups of Du Val, and our table lists both possibilities.

Conway and Smith [14, Tables 4.2–4.3] specified the five groups of type $[I \times \bar I]$ (#32, #32′ and #51–#51″) by the generating set "$[\omega,\omega], [i_I, \pm i_I']$", possibly extended by $*$ or $-*$ for the achiral groups, but they did not define what i_I' is.[26] We tried all 120 elements of $2I$, and it turned out that (A.2) is the only value that works in this way. We don't see how we could have predicted precisely this element, and we have no explanation for it.

Du Val [23], on the other hand, specifies generators for these five groups in terms of the quaternion $i_I^\dagger$ defined in (A.1), which is obtained by flipping the sign of $\sqrt5$ in the expression for $i_I = \frac12(i + \frac{\sqrt5-1}{2}j + \frac{\sqrt5+1}{2}k)$. This alternative choice generates a group $2I^\dagger$ that is different from $2I$. With this setup, it is not possible to use the simple extending elements $*$ and $-*$ for the three achiral extensions #51–#51″: For example, the square of the element $*[i_I^\dagger, i_I]$ is $[i_I i_I^\dagger, i_I^\dagger i_I]$ with $i_I i_I^\dagger = \frac14 + \frac{\sqrt5}{4}(i+j-k)$, and this element is in

[25] A similar table, containing some four-dimensional reflection groups and their subgroups, appears in Coxeter [17, p. 571], with correspondences between Coxeter's own notation and Du Val's names. The very first entry in that table, $[3,3,2]^+$, mistakenly refers to Du Val's group #21 $(T/C_2; T/C_2) = \pm\frac{1}{12}[T\times T]$, while it is actually #26″ $(O/C_1; O/C_1)'' = +\frac{1}{24}[O\times\overline{O}]$. The fifth entry, $[3,3,2]$, refers to Du Val's group $(O/C_1; O/C_1)^*$, while it should actually be $(O/C_1; O/C_1)^*_-$, or more precisely #44″ $(O/C_1; O/C_1)^{*\prime\prime}_- = +\frac{1}{24}[O\times\overline{O}]\cdot 2_1$. The confusing ambiguity of Du Val's names for the groups 44′ and 44″ mentioned in the caption of Table 6.3 was apparently not realized by Coxeter.

[26] Five years later, the tables were almost literally reproduced in another book [12, Chapter 26], still without a definition of i_I'.

Du Val # & name	CS name	generators	Cox. name	order	BBNWZ
20. $(T/T;T/T)$	$\pm[T\times T]$	$[i,\omega],[\omega,i]$	$[^+3,4,3^+]$	288	33/13
21. $(T/C_2;T/C_2)$	$\pm\frac{1}{12}[T\times T]$	$[\omega,-\omega],[i,i]$	$2.[3,3]^+$	24	24/02
21′. $(T/C_1;T/C_1)$	$+\frac{1}{12}[T\times T]$	$[\omega,\omega],[i,i]$	$[3,3]^+$	12	24/01
22. $(T/V;T/V)$	$\pm\frac{1}{3}[T\times T]$	$[i,1],[1,i],[\omega,\omega]$	$[^+3,3,4^+]$	96	32/16
23. $(O/O;T/T)$	$\pm[O\times T]$	$[i_O,\omega],[\omega,i]$	$[[^+3,4,3^+]]_L$	576	not cryst.
23. $(T/T;O/O)$	$\pm[T\times O]$	$[i,\omega],[\omega,i_O]$	$[[^+3,4,3^+]]_R$	576	not cryst.
24. $(I/I;T/T)$	$\pm[I\times T]$	$[i_I,\omega],[\omega,i]$	$[3,3,5]^+_{\frac{1}{5}L}$	1440	not cryst.
24. $(T/T;I/I)$	$\pm[T\times I]$	$[i,\omega],[\omega,i_I]$	$[3,3,5]^+_{\frac{1}{5}R}$	1440	not cryst.
25. $(O/O;O/O)$	$\pm[O\times O]$	$[i_O,\omega],[\omega,i_O]$	$[[3,4,3]]^+$	1152	not cryst.
26. $(O/C_2;O/C_2)$	$\pm\frac{1}{24}[O\times O]$	$[\omega,-\omega],[i_O,i_O]$	$2.[3,4]^+$	48	25/06
26′. $(O/C_1;O/C_1)'$	$+\frac{1}{24}[O\times O]$	$[\omega,\omega],[i_O,i_O]$	$[3,4]^+$	24	25/03
26″. $(O/C_1;O/C_1)''$	$+\frac{1}{24}[O\times \overline{O}]$	$[\omega,\omega],[i_O,-i_O]$	$[2,3,3]^+$	24	25/04
27. $(O/V;O/V)$	$\pm\frac{1}{6}[O\times O]$	$[i,j],[\omega,\omega],[i_O,i_O]$	$[3,3,4]^+$	192	32/20
28. $(O/T;O/T)$	$\pm\frac{1}{2}[O\times O]$	$[\omega,1],[1,\omega],[i_O,i_O]$	$[3,4,3]^+$	576	33/15
29. $(I/I;O/O)$	$\pm[I\times O]$	$[i_I,\omega],[\omega,i_O]$	$[[3,3,5]^+_{\frac{1}{5}L}]$	2880	not cryst.
29. $(O/O;I/I)$	$\pm[O\times I]$	$[i_O,\omega],[\omega,i_I]$	$[[3,3,5]^+_{\frac{1}{5}R}]$	2880	not cryst.
30. $(I/I;I/I)$	$\pm[I\times I]$	$[i_I,\omega],[\omega,i_I]$	$[3,3,5]^+$	7200	not cryst.
31. $(I/C_2;I/C_2)$	$\pm\frac{1}{60}[I\times I]$	$[\omega,\omega],[i_I,-i_I]$	$2.[3,5]^+$	120	not cryst.
31′. $(I/C_1;I/C_1)$	$+\frac{1}{60}[I\times I]$	$[\omega,\omega],[i_I,i_I]$	$[3,5]^+$	60	not cryst.
32. $(I^\dagger/C_2;I/C_2)^\dagger$	$\pm\frac{1}{60}[I\times \overline{I}]$	$[\omega,\omega],[i_I,-i_I^\dagger]$ $[\omega,\omega],[i_I,-i_I']$	$[[3,3,3]]^+$	120	31/06
32′. $(I^\dagger/C_1;I/C_1)^\dagger$	$+\frac{1}{60}[I\times \overline{I}]$	$[\omega,\omega],[i_I,i_I^\dagger]$ $[\omega,\omega],[i_I,i_I']$	$[3,3,3]^+$	60	31/03
39. $(T/C_2;T/C_2)^*_c$	$\pm\frac{1}{12}[T\times T]\cdot 2$	$[\omega,-\omega],*[i,-i]$	$2.[^+3,4]$	48	25/05
39′. $(T/C_1;T/C_1)^*_c$	$+\frac{1}{12}[T\times T]\cdot 2_3$	$[\omega,\omega],*[i,i]$	$[^+3,4]$	24	25/02
39′. $(T/C_1;T/C_1)^*_{c-}$	$+\frac{1}{12}[T\times T]\cdot 2_1$	$[\omega,\omega],*[i,-i]$	$[^+3,4]^\circ$	24	25/01
40. $(T/C_2;T/C_2)^*$	$\pm\frac{1}{12}[T\times \overline{T}]\cdot 2$	$[\omega,-\omega],*[i_O,-i_O]$ $[\omega,-\overline{\omega}],*[i,-i]$	$2.[3,3]$	48	24/05
40′. $(T/C_1;T/C_1)^*$	$+\frac{1}{12}[T\times \overline{T}]\cdot 2_1$	$[\omega,\omega],*[i_O,i_O]$ $[\omega,\overline{\omega}],*[i,i]$	$[3,3]$	24	24/04
40′. $(T/C_1;T/C_1)^*_-$	$+\frac{1}{12}[T\times \overline{T}]\cdot 2_3$	$[\omega,\omega],*[i_O,-i_O]$ $[\omega,\overline{\omega}],*[i,-i]$	$[3,3]^\circ$	24	24/03
41. $(T/V;T/V)^*$	$\pm\frac{1}{3}[T\times T]\cdot 2$	$*[i,1],[\omega,\omega]$	$[^+3,3,4]$	192	32/18
42. $(T/V;T/V)^*_-$	$\pm\frac{1}{3}[T\times \overline{T}]\cdot 2$	$*[i,1],[\omega,\overline{\omega}]$	$[3,3,4^+]$	192	32/19
43. $(T/T;T/T)^*$	$\pm[T\times T]\cdot 2$	$[i,\omega],*[\omega,i]$	$[3,4,3^+]$	576	33/14
44. $(O/C_2;O/C_2)^*$	$\pm\frac{1}{24}[O\times O]\cdot 2$	$[\omega,-\omega],[i_O,i_O],-*$	$2.[3,4]$	96	25/11
44′. $(O/C_1;O/C_1)^{*\prime}$	$+\frac{1}{24}[O\times O]\cdot 2_3$	$[\omega,\omega],[i_O,i_O],*$	$[3,4]$	48	25/10
44′. $(O/C_1;O/C_1)^{*\prime}_-$	$+\frac{1}{24}[O\times O]\cdot 2_1$	$[\omega,\omega],[i_O,i_O],-*$	$[3,4]^\circ$	48	25/07
44″. $(O/C_1;O/C_1)^{*\prime\prime}$	$+\frac{1}{24}[O\times \overline{O}]\cdot 2_3$	$[\omega,\omega],[i_O,-i_O],*$	$[2,3,3]^\circ$	48	25/09
44″. $(O/C_1;O/C_1)^{*\prime\prime}_-$	$+\frac{1}{24}[O\times \overline{O}]\cdot 2_1$	$[\omega,\omega],[i_O,-i_O],-*$	$[2,3,3]$	48	25/08
45. $(O/T;O/T)^*$	$\pm\frac{1}{2}[O\times O]\cdot 2$	$*[\omega,1],[i_O,i_O]$	$[3,4,3]$	1152	33/16
46. $(O/T;O/T)^*_-$	$\pm\frac{1}{2}[O\times O]\cdot \bar{2}$	$[\omega,1],*[1,i_O]$	$[[3,4,3]^+]$	1152	not cryst.
47. $(O/V;O/V)^*$	$\pm\frac{1}{6}[O\times O]\cdot 2$	$*[i\omega,\omega],[i_O,i_O]$	$[3,3,4]$	384	32/21
48. $(O/O;O/O)^*$	$\pm[O\times O]\cdot 2$	$*[1,\omega],[\omega,i_O]$	$[[3,4,3]]$	2304	not cryst.
49. $(I/C_2;I/C_2)^*$	$\pm\frac{1}{60}[I\times I]\cdot 2$	$[\omega,-\omega],*[i_I,-i_I]$	$2.[3,5]$	240	not cryst.
49′. $(I/C_1;I/C_1)^*$	$+\frac{1}{60}[I\times I]\cdot 2_3$	$[\omega,\omega],*[i_I,i_I]$	$[3,5]$	120	not cryst.
49′. $(I/C_1;I/C_1)^*_-$	$+\frac{1}{60}[I\times I]\cdot 2_1$	$[\omega,\omega],*[i_I,-i_I]$	$[3,5]^\circ$	120	not cryst.
50. $(I/I;I/I)^*$	$\pm[I\times I]\cdot 2$	$[i_I,\omega],[\omega,i_I],*$	$[3,3,5]$	14400	not cryst.
51. $(I^\dagger/C_2;I/C_2)^{\dagger *}$	$\pm\frac{1}{60}[I\times \overline{I}]\cdot 2$	$[\omega,-\omega],*[i_Ii_Oi,i_I^\dagger i_Oi]$ $[\omega,-\omega],*[i_I,i_I']$	$[[3,3,3]]$	240	31/07
51′. $(I^\dagger/C_1;I/C_1)^{\dagger *}$	$+\frac{1}{60}[I\times \overline{I}]\cdot 2_1$	$[\omega,\omega],*[i_Ii_Oi,i_I^\dagger i_Oi]$ $[\omega,\omega],[i_I,i_I'],-*$	$[3,3,3]$	120	31/05
51′. $(I^\dagger/C_1;I/C_1)^{\dagger *}_-$	$+\frac{1}{60}[I\times \overline{I}]\cdot 2_3$	$[\omega,\omega],*[i_Ii_Oi,-i_I^\dagger i_Oi]$ $[\omega,\omega],*[i_I,i_I']$	$[[3,3,3]^+]$	120	31/04

Table A.1.: Polyhedral and axial groups with generators

neither of the groups $2I$ or $2I^\dagger$. Du Val [23, p. 55–56] gives a thorough and transparent exposition of these groups and explains why they represent the symmetries of the 4-simplex.

For the axial groups of type $\frac{1}{12}[T \times \bar{T}]$ (#40 and #40′), the natural generators from an algebraic viewpoint involve the quaternion $\bar{\omega}$, and these were chosen by Conway and Smith. However, the axis that is kept invariant by the groups is then spanned by the quaternion $j - k$. With $*[i_O, \pm i_O]$ as the orientation-reversing generator, the invariant axis becomes the real axis, and only in this representation, the groups are subgroups of the larger axial group $\pm\frac{1}{24}[O \times O]$ (#44).

B

Orbit polytopes for tubical groups with special starting points

We show polar orbit polytopes for the tubical groups of cyclic type with all choices of special starting points.

Each subsection considers a left tubical group G together with a representative f-fold rotation center p of G^h, corresponding to an entry in Table 3.2. The particular data are given in the caption. In addition, we indicate the subgroup H of G of elements that preserve K_p. An *alternate group* refers to an index-2 dihedral-type supergroup of G that, for an appropriate starting point on K_p, produces the same orbit as G.

Two of these groups were already illustrated in the main text (Figures 3.7 and 3.8), and we follow the same conventions as in these figures: On the top left, we show the G^h-orbit polytope of p, and on the top right the spherical Voronoi diagram of that orbit. Then we show the cells of the polar G-orbit polytopes of a starting point on K_p, for different values of n, in increasing order of the size of the orbit. For each cell, we indicate the values of n, and in addition, the counterclockwise angle (as seen from the top) by which the group rotates the cell as it proceeds to the next cell above. A blue vertical line indicates the cell axis, the direction towards the next cell along K_p. For small values of n, this axis sometimes exits through a vertex or an edge of the cell, but for large enough n it goes through the top face where the next cell is attached.

When the same orbit arises for several values of n, then the specified rotation angle is the unique valid angle only for the smallest value n_0 that is given. For a larger value $n = n_0 f$, this can be combined with arbitrary multiples of an f-fold rotation. For example, in Figure B.1, we have the same cell for $n = 5$ and $n = 15$. The specified rotation angle $(\frac{1}{3} + \frac{1}{30}) \cdot 2\pi$ is the unique valid angle between consecutive cells in the group $\pm[I \times C_5]$, but in the larger group $\pm[I \times C_{15}]$, it can be combined with all multiples of $\frac{2}{3}\pi$. That is, all three rotation angles $\frac{1}{15}\pi$, $(\frac{2}{3} + \frac{1}{15})\pi$, and $(\frac{4}{3} + \frac{1}{15})\pi$ are valid. In some cases, such as $n = 18$, the angle is never unique, and this is indicated by a free parameter k in the angle specification, which can take any integer value.

By observing the rotation angles for the successive cells in the figures, one can recognize the pattern that they follow.

B.1. $\pm[I \times C_n]$

B.1.1. $\pm[I \times C_n]$, 3-fold rotation center

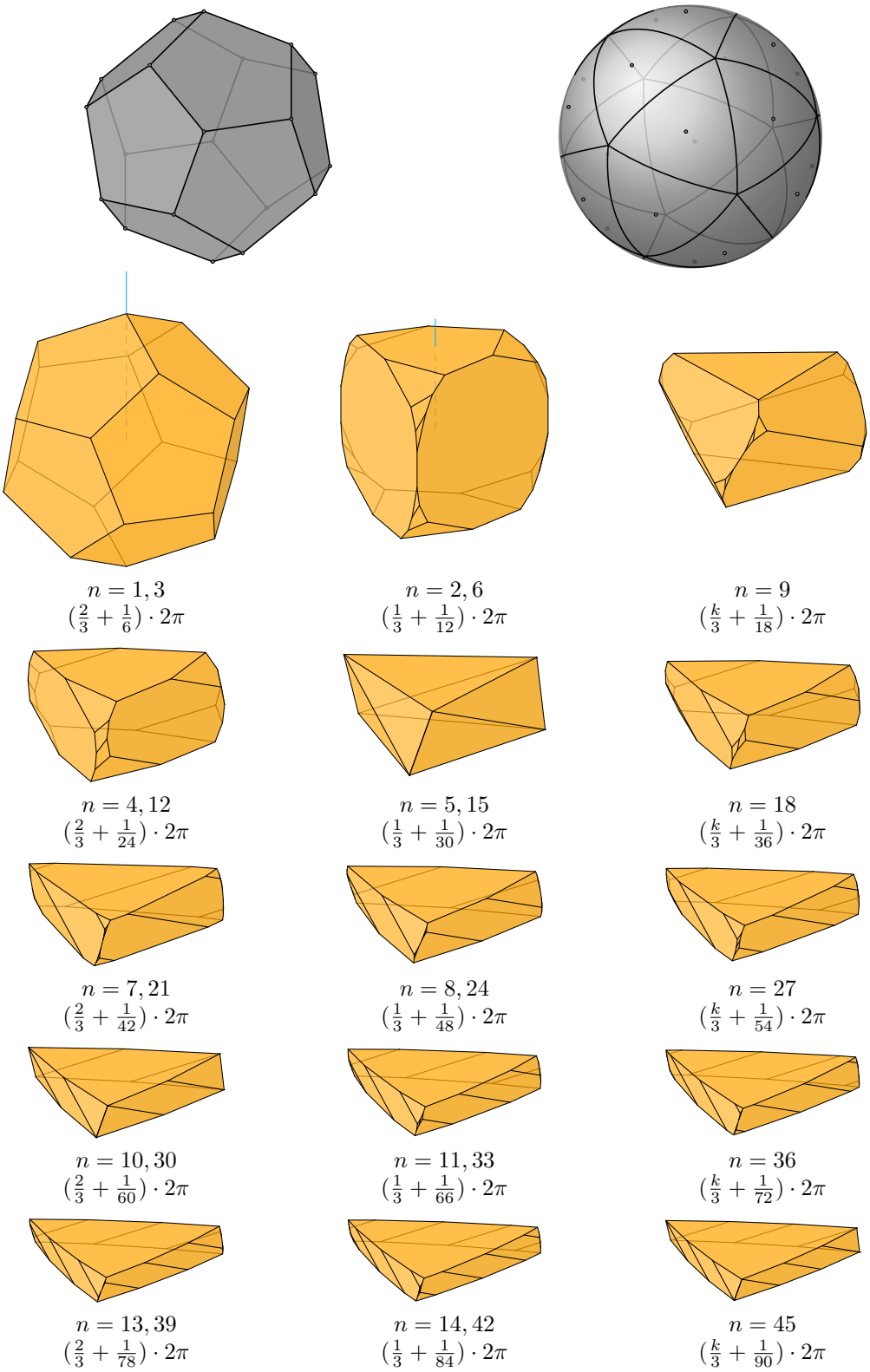

Figure B.1.: $G = \pm[I \times C_n]$, $G^h = +I$, 3-fold rotation center $p = \frac{1}{\sqrt{3}}(-1, -1, -1)$. $H = \langle[-\omega, 1], [1, e_n]\rangle$. 20 tubes, each with $\mathrm{lcm}(2n, 6)$ cells. Alternate group: $\pm[I \times D_{2n}]$. When $n = 1$ or $n = 3$, the cells of a tube are disconnected from each other.

B.1.2. $\pm[I \times C_n]$, 2-fold rotation center

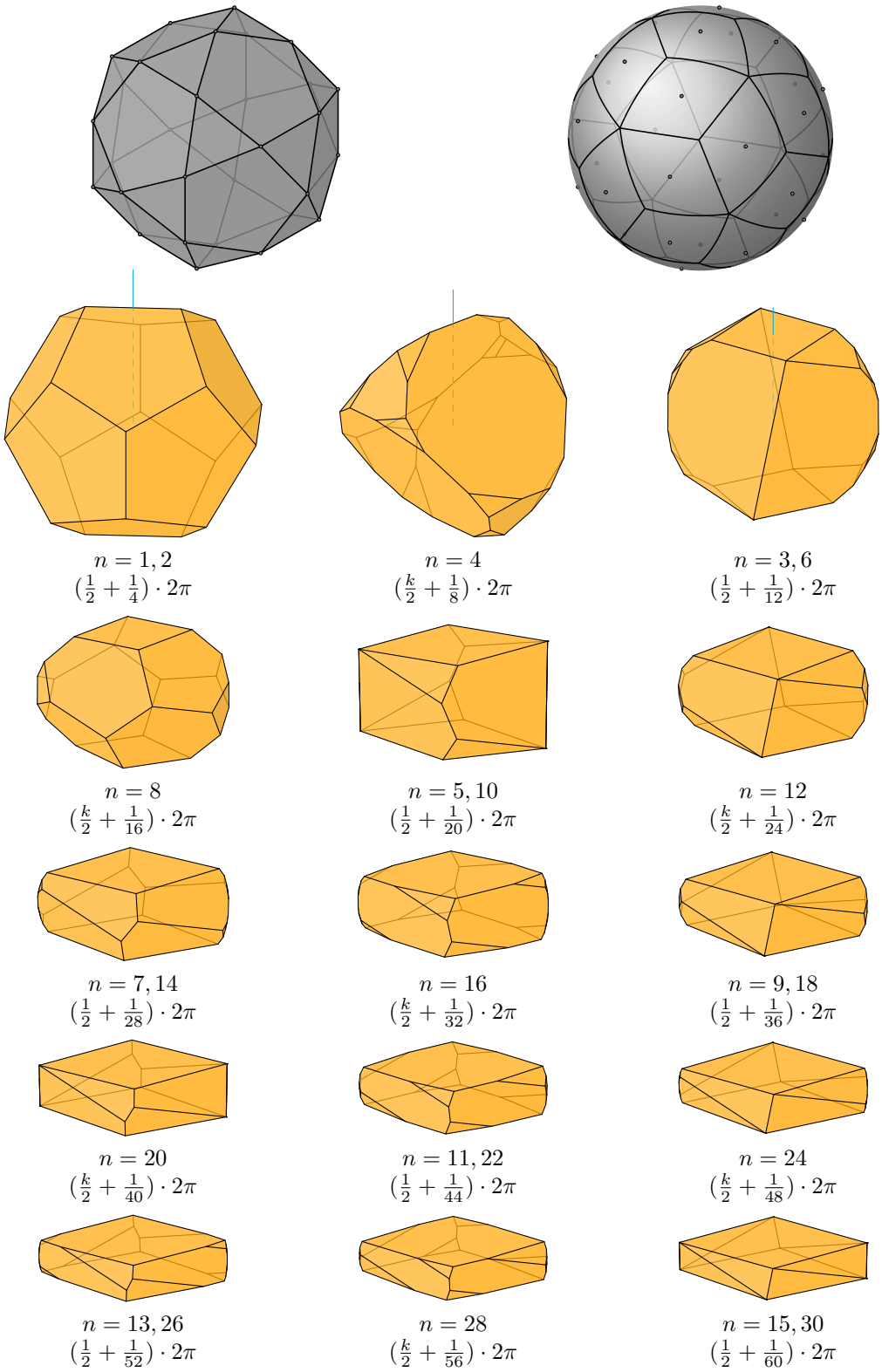

Figure B.2.: $G = \pm[I \times C_n]$, $G^h = +I$, 2-fold rotation center $p = \frac{1}{2}(1, \frac{1}{\varphi}, \varphi)$, where $\varphi = \frac{1+\sqrt{5}}{2}$. The G^h-orbit polytope is an icosidodecahedron. The corresponding Voronoi diagram on the 2-sphere has the structure of a rhombic triacontahedron. $H = \langle [i_I, 1], [1, e_n] \rangle$. 30 tubes, each with $\mathrm{lcm}(2n, 4)$ cells. Alternate group: $\pm[I \times D_{2n}]$. When $n = 1$, 2, or 4, the cells of a tube are disconnected from each other.

B.2. $\pm[O \times C_n]$

B.2.1. $\pm[O \times C_n]$, 4-fold rotation center

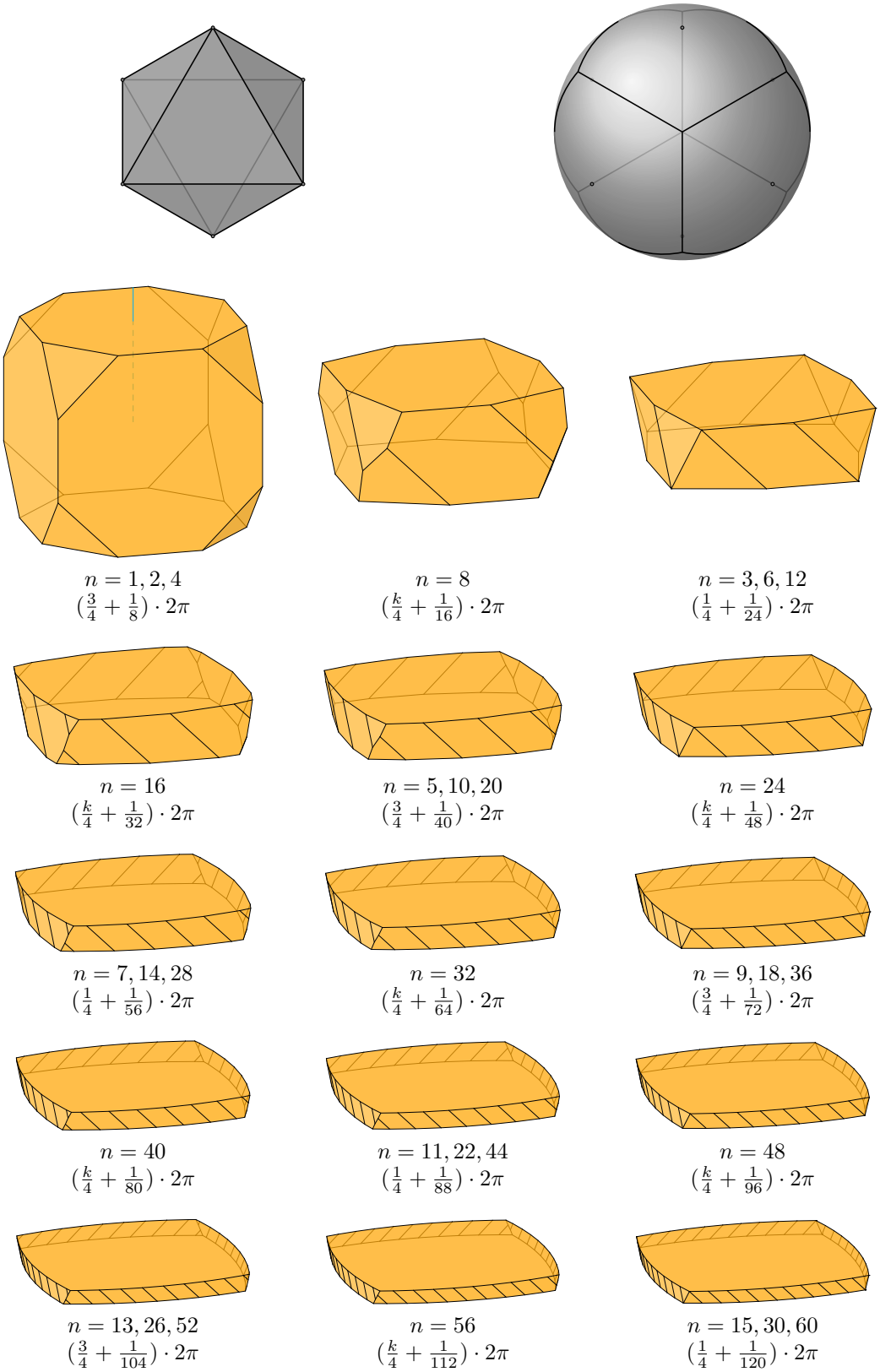

Figure B.3.: $G = \pm[O \times C_n]$, $G^h = +O$, 4-fold rotation center $p = (0, 1, 0)$. $H = \langle[-\omega i_O, 1], [1, e_n]\rangle$. 6 tubes, each with $\mathrm{lcm}(2n, 8)$ cells. Alternate group: $\pm[O \times D_{2n}]$.

B.2.2. $\pm[O \times C_n]$, 3-fold rotation center

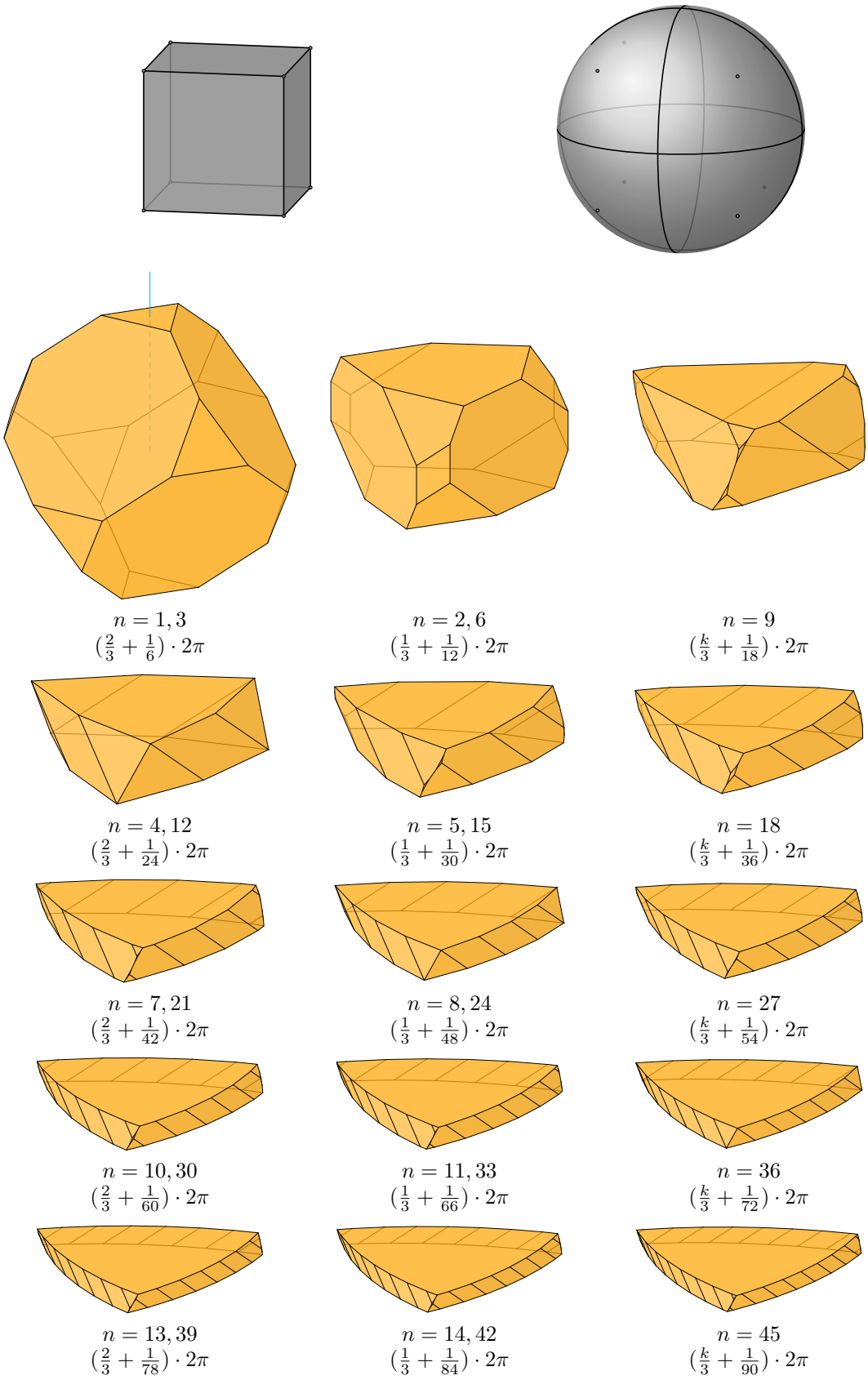

Figure B.4.: $G = \pm[O \times C_n]$, $G^h = +O$, 3-fold rotation center $p = \frac{1}{\sqrt{3}}(-1, -1, -1)$. $H = \langle [-\omega, 1], [1, e_n] \rangle$. 8 tubes, each with $\mathrm{lcm}(2n, 4)$ cells. Alternate group: $\pm[O \times D_{2n}]$.

B.2.3. $\pm[O \times C_n]$, 2-fold rotation center

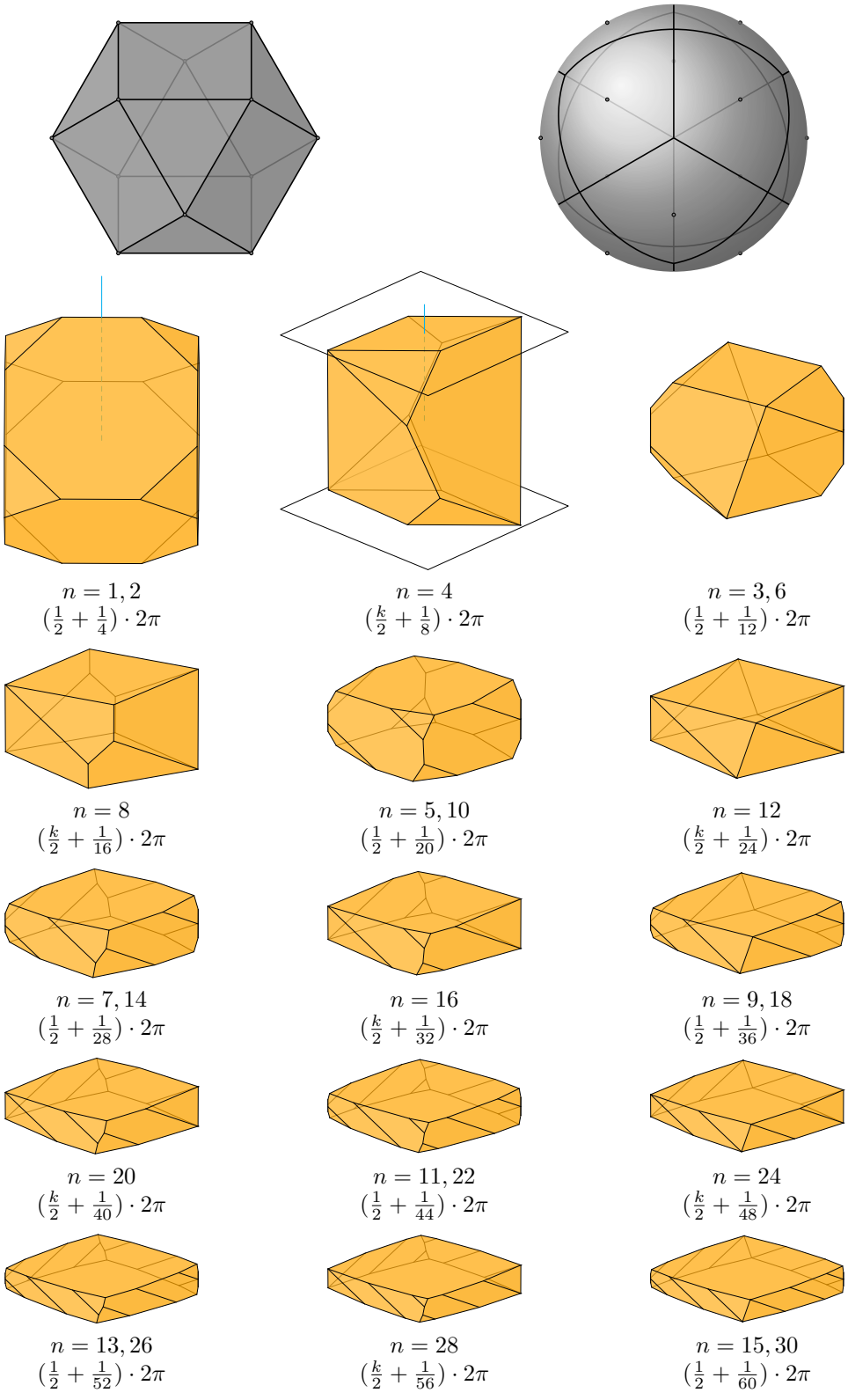

Figure B.5.: $G = \pm[O \times C_n]$, $G^h = +O$, 2-fold rotation center $p = \frac{1}{\sqrt{2}}(0, 1, 1)$. $H = \langle [i_O, 1], [1, e_n] \rangle$. 12 tubes, each with $\mathrm{lcm}(2n, 4)$ cells. Alternate group: $\pm[O \times D_{2n}]$. When $n = 1$ or $n = 2$, the cells of a tube are disconnected from each other. For $n = 4$, we have drawn squares in the planes around the top and bottom face, to indicate that these faces are horizontal and parallel.

B.3. $\pm\frac{1}{2}[O \times C_{2n}]$

B.3.1. $\pm\frac{1}{2}[O \times C_{2n}]$, 3-fold rotation center

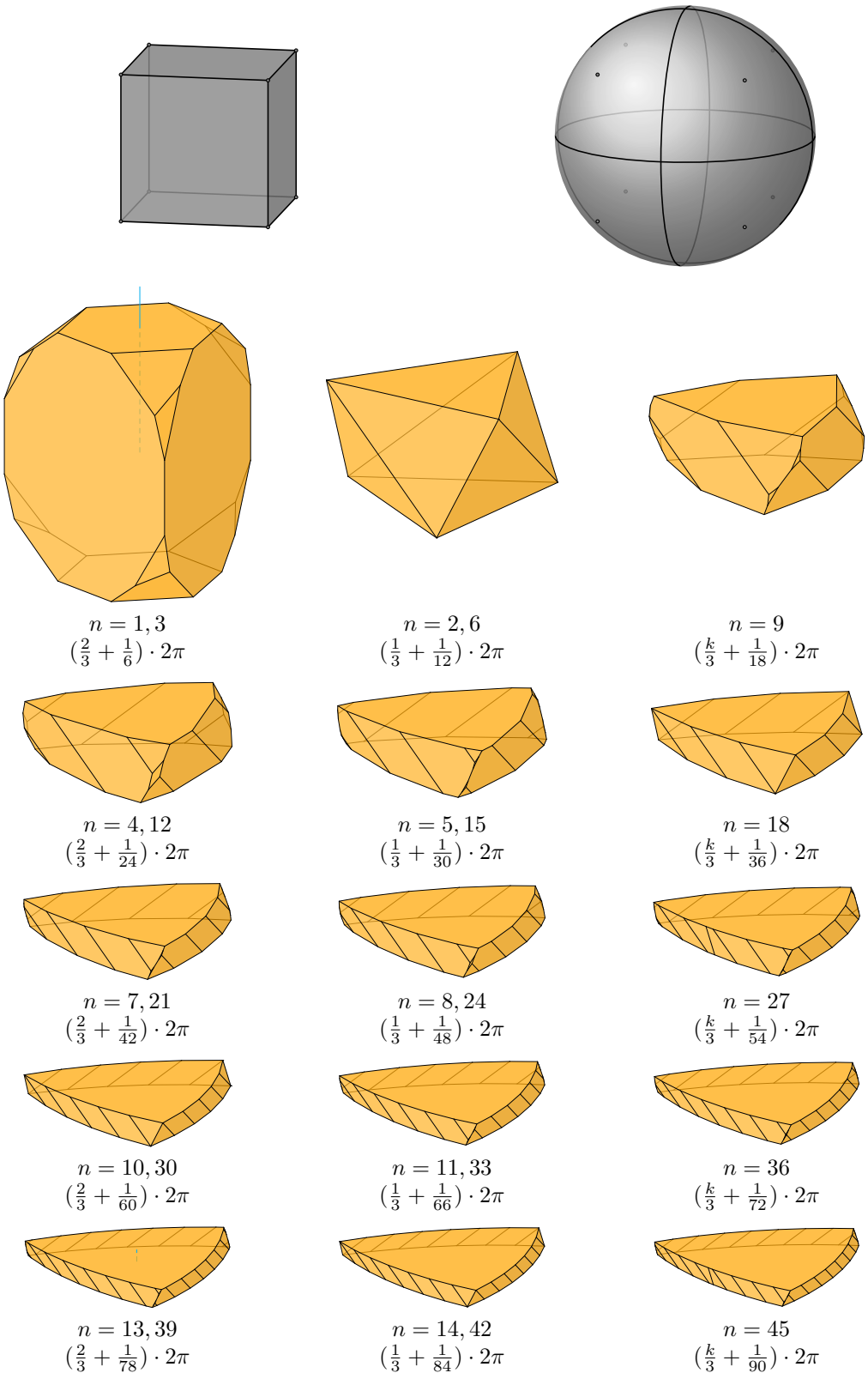

Figure B.6.: $G = \pm\frac{1}{2}[O \times C_{2n}]$, $G^h = +O$, 3-fold rotation center $p = \frac{1}{\sqrt{3}}(-1, -1, -1)$. $H = \langle[-\omega, 1], [1, e_n]\rangle$. 8 tubes, each with $\mathrm{lcm}(2n, 6)$ cells. Alternate group: $\pm\frac{1}{2}[O \times \overline{D}_{4n}]$.

B.3.2. $\pm\frac{1}{2}[O \times C_{2n}]$, 2-fold rotation center

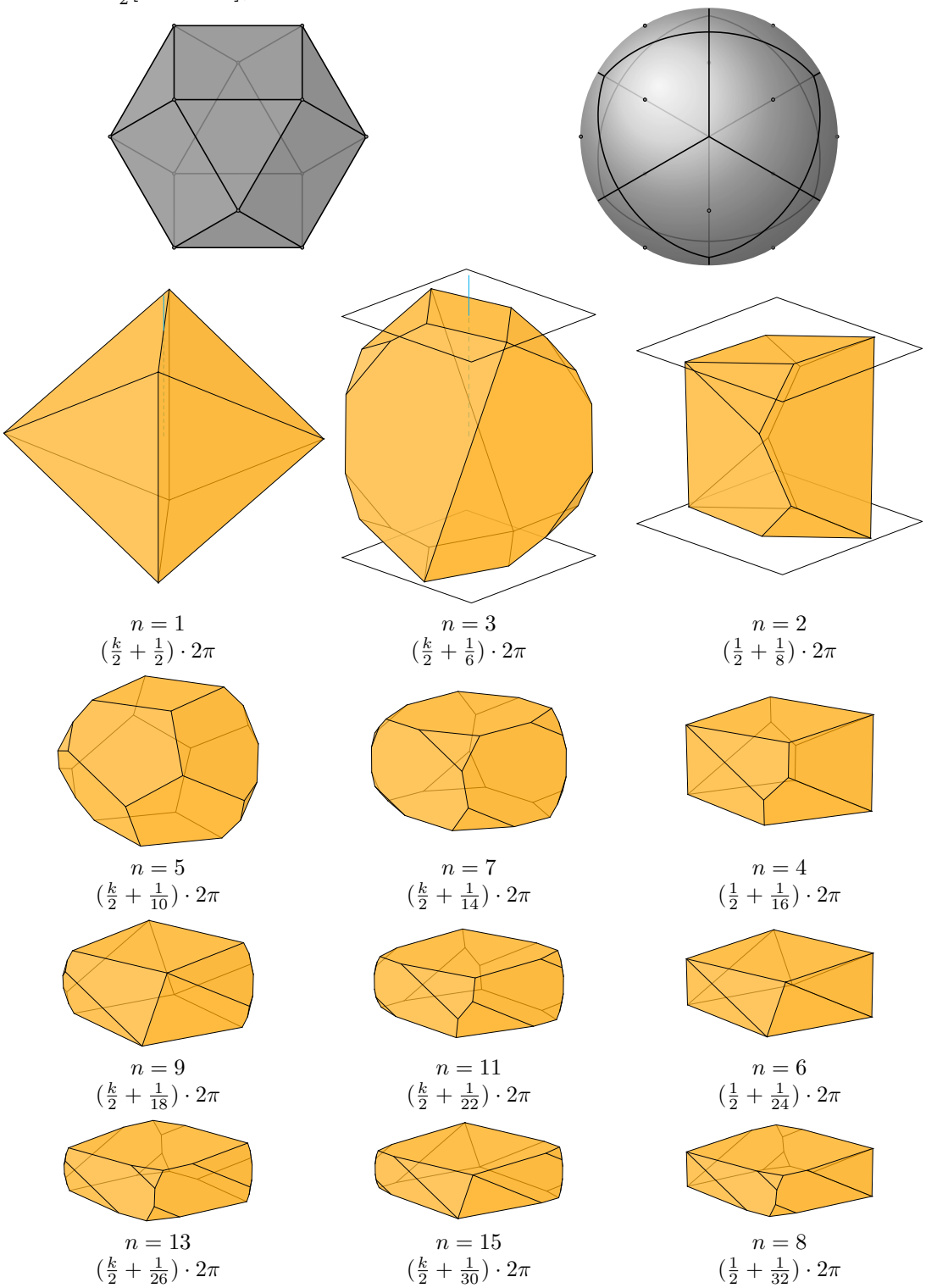

Figure B.7.: $G = \pm\frac{1}{2}[O \times C_{2n}]$, $G^h = +O$, 2-fold rotation center $p = \frac{1}{\sqrt{2}}(0, 1, 1)$. The G^h-orbit polytope is a cuboctahedron. The corresponding Voronoi diagram on the 2-sphere has the structure of a rhombic dodecahedron. $H = \langle [i_O, e_{2n}], [1, e_n] \rangle$. 12 tubes, each with $\frac{4n}{\gcd(n-1,2)}$ cells. Alternate group: $\pm\frac{1}{2}[O \times \overline{D}_{4n}]$. When $n = 1$, the cells of a tube are disconnected from each other. For $n = 2$ and $n = 3$, we have drawn squares in the planes around the top and bottom face, to indicate that these faces are horizontal and parallel.

B.4. $\pm[T \times C_n]$

B.4.1. $\pm[T \times C_n]$, 3-fold rotation center

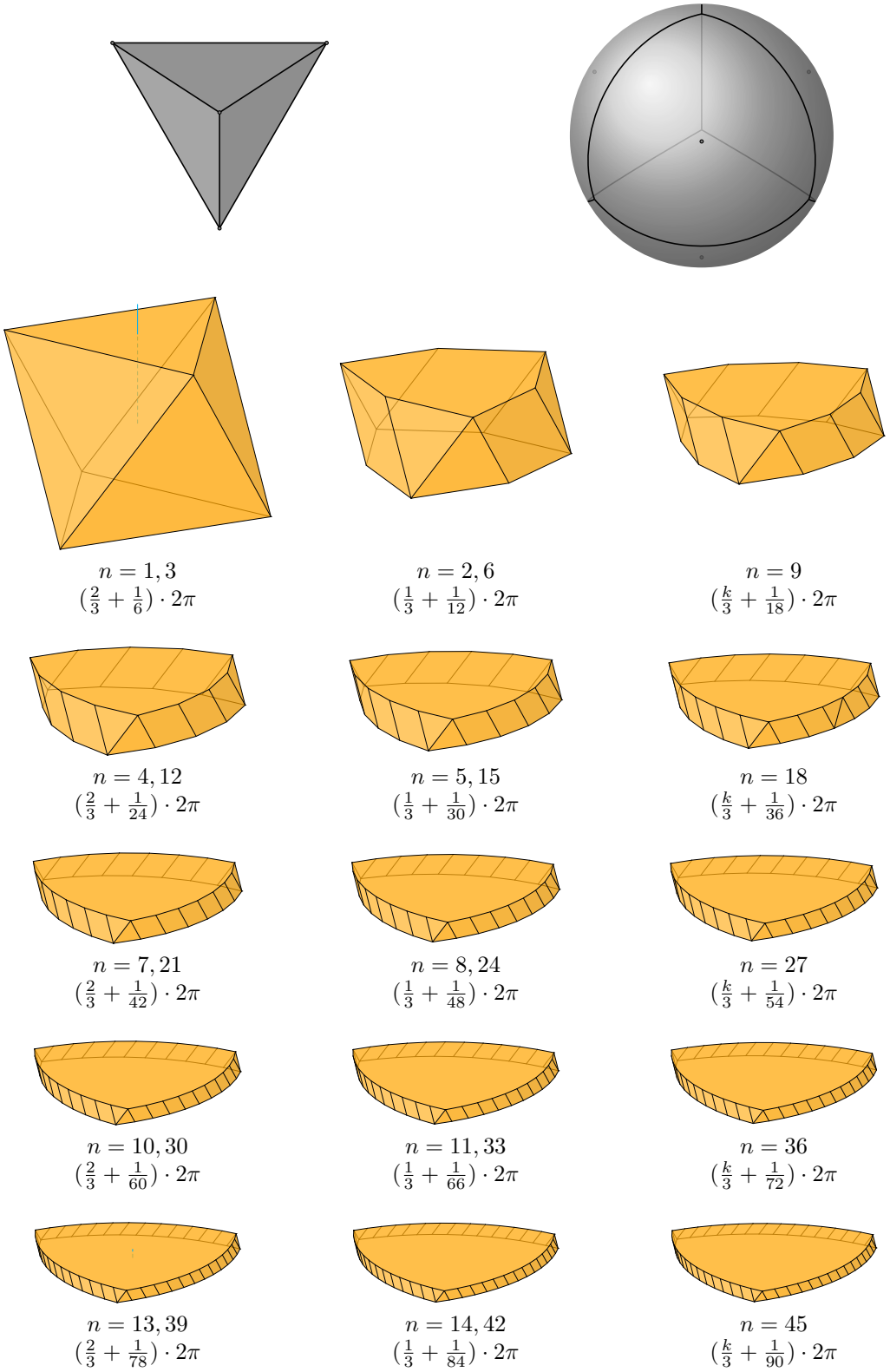

Figure B.8.: $G = \pm[T \times C_n]$, $G^h = +T$, 3-fold (type I) rotation center $p = \frac{1}{\sqrt{3}}(-1, -1, -1)$. $H = \langle [-\omega, 1], [1, e_n] \rangle$. 4 tubes, each with $\mathrm{lcm}(2n, 6)$ cells. Alternate group: $\pm\frac{1}{2}[O \times D_{2n}]$.

B.4.2. $\pm[T \times C_n]$, 2-fold rotation center

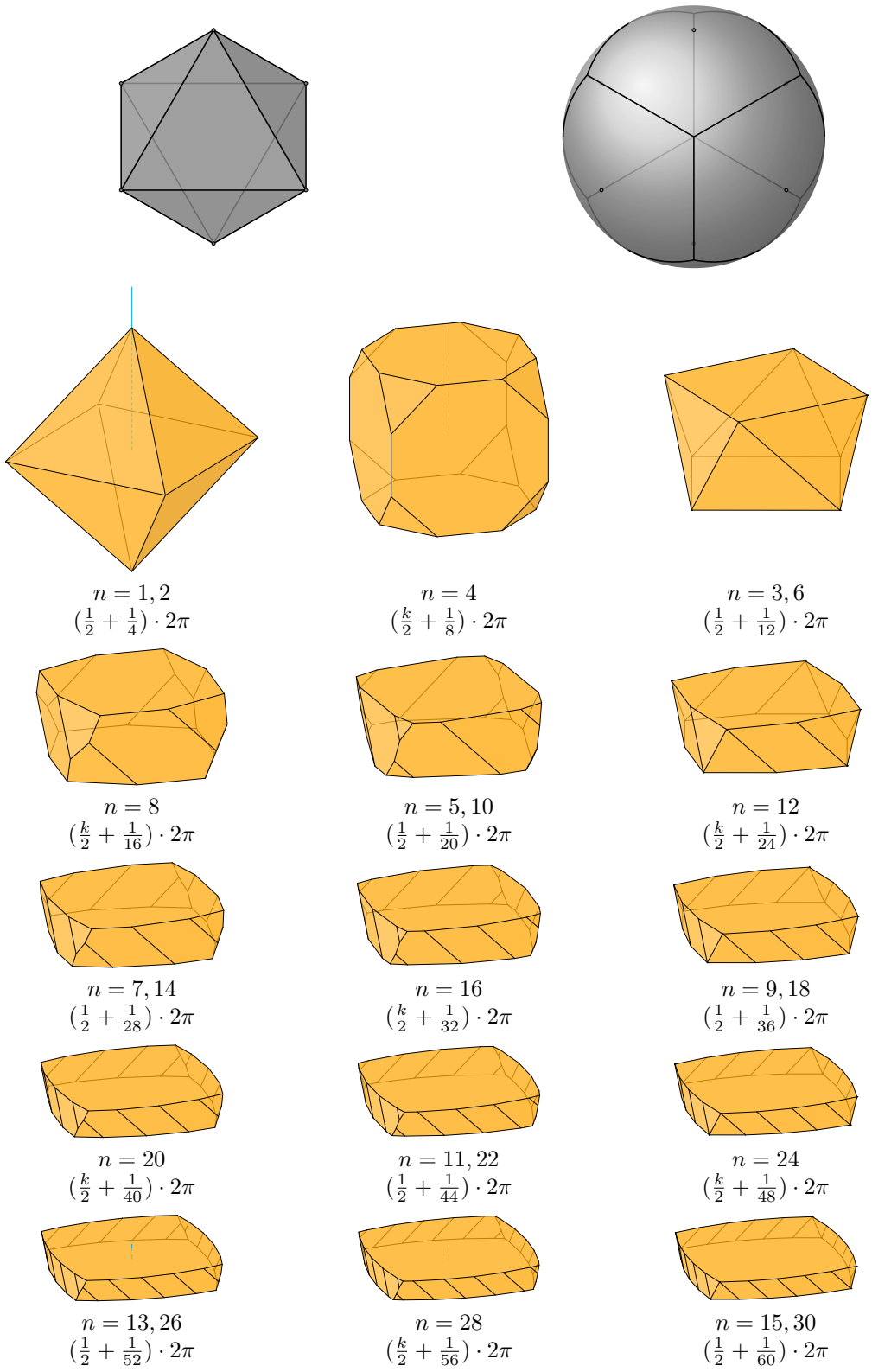

Figure B.9.: $G = \pm[T \times C_n]$, $G^h = +T$, 2-fold rotation center $p = (1, 0, 0)$. $H = \langle [i, 1], [1, e_n] \rangle$. 6 tubes, each with $\mathrm{lcm}(2n, 4)$ cells. Alternate groups: $\pm[T \times D_{2n}]$ and $\pm\frac{1}{2}[O \times D_{2n}]$ (also their common supergroup $\pm[O \times D_{2n}]$) if $n \equiv 0 \mod 4$, else $\pm[T \times D_{2n}]$ (and its supergroup $\pm\frac{1}{2}[O \times \overline{D}_{4n}]$). When $n = 1$ or $n = 2$, consecutive cells of a tube touch only via vertices.

B.5. $\pm\frac{1}{3}[T \times C_{3n}]$

B.5.1. $\pm\frac{1}{3}[T \times C_{3n}]$, 3-fold (type I) rotation center

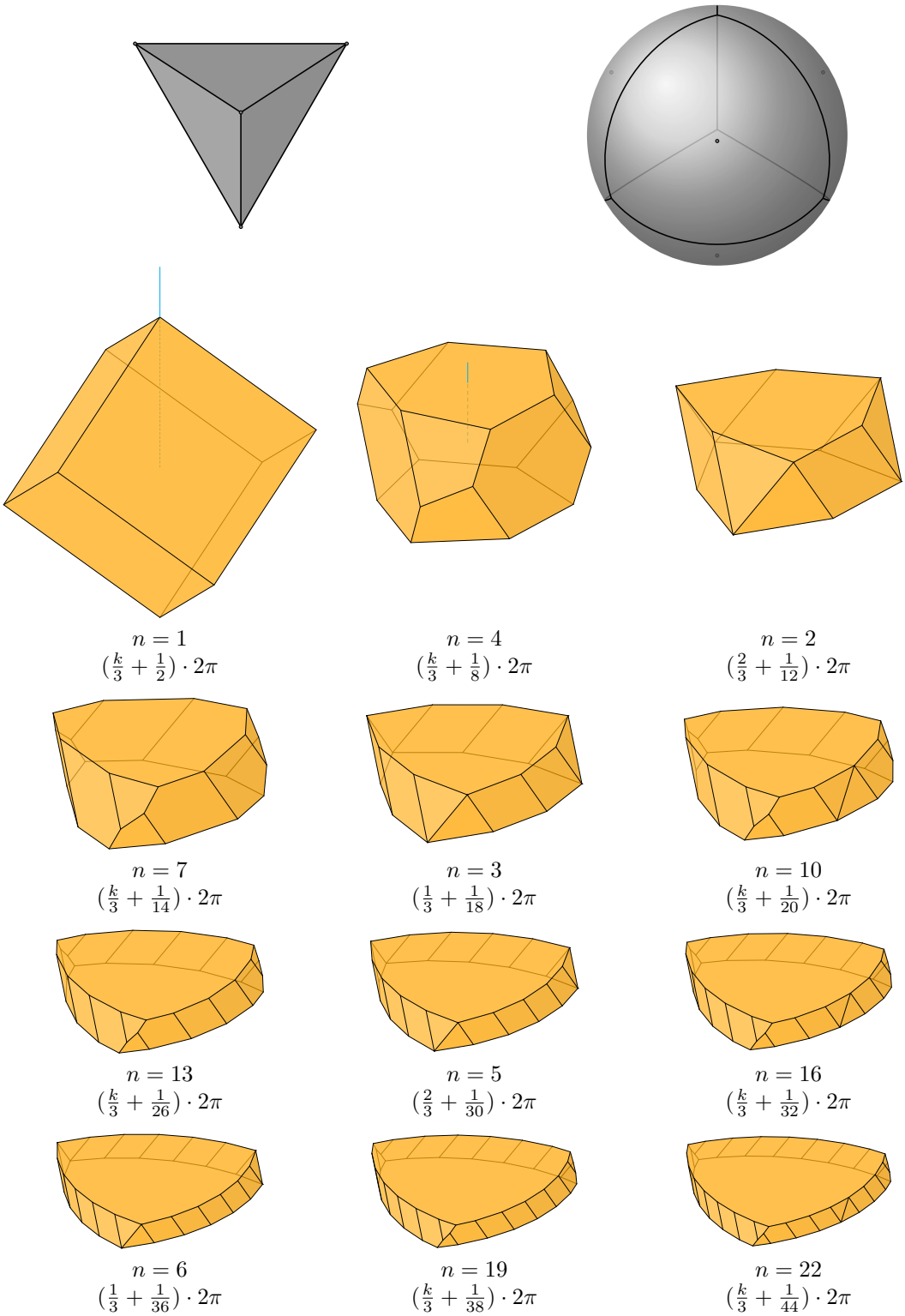

Figure B.10.: $G = \pm\frac{1}{3}[T \times C_{3n}]$, $G^h = +T$, 3-fold (type I) rotation center $p = \frac{1}{\sqrt{3}}(-1,-1,-1)$. $H = \langle[-\omega, e_{3n}], [1, e_n]\rangle$. 4 tubes, each with $\frac{6n}{\gcd(n-1,3)}$ cells. Alternate groups: $\pm\frac{1}{6}[O \times D_{6n}]$ (and its supergroup $\pm\frac{1}{2}[O \times D_{6n}]$ if $n \not\equiv 1 \mod 3$). When $n = 1$, the cells of a tube are disconnected from each other.

B.5.2. $\pm\frac{1}{3}[T \times C_{3n}]$, 3-fold (type II) rotation center

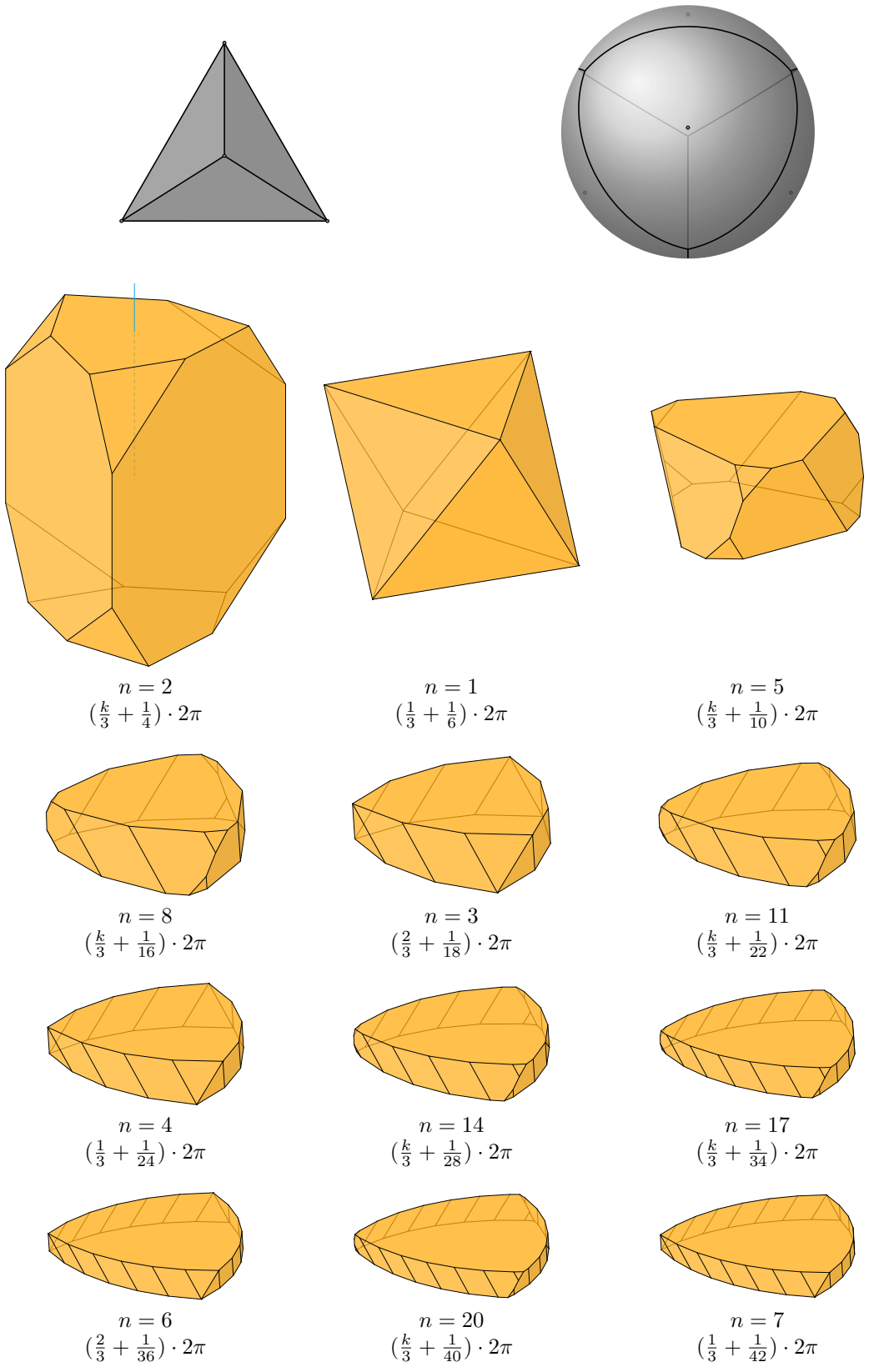

Figure B.11.: $G = \pm\frac{1}{3}[T \times C_{3n}]$, $G^h = +T$, 3-fold (type II) rotation center $p = \frac{1}{\sqrt{3}}(1, 1, 1)$. $H = \langle[-\omega^2, e_{3n}^2], [1, e_n]\rangle$. 4 tubes, each with $\frac{6n}{\gcd(n-2,3)}$ cells. Alternate groups: $\pm\frac{1}{6}[O \times D_{6n}]$ (and its supergroup $\pm\frac{1}{2}[O \times D_{6n}]$ if $n \not\equiv 2 \mod 3$).

B.5.3. $\pm\frac{1}{3}[T \times C_{3n}]$, 2-fold rotation center

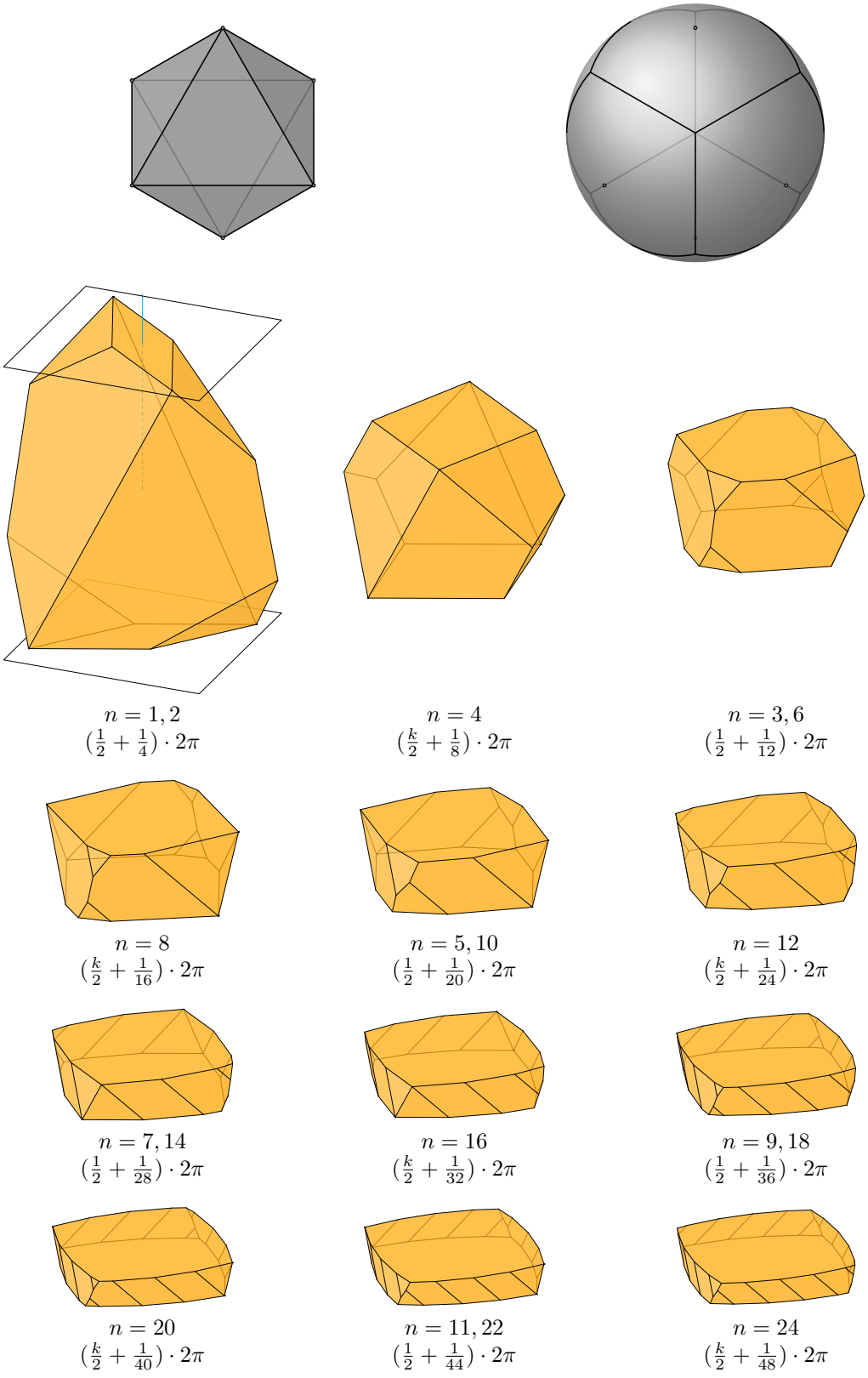

Figure B.12.: $G = \pm\frac{1}{3}[T \times C_{3n}]$, $G^h = +T$, 2-fold rotation center $p = (1, 0, 0)$. $H = \langle [i, 1], [1, e_n] \rangle$. 6 tubes, each with $\mathrm{lcm}(2n, 4)$ cells. Alternate group: $\pm\frac{1}{6}[O \times D_{6n}]$. For $n = 1$ and $n = 2$, we have drawn squares in the planes around the top and bottom face, to indicate that these faces are horizontal and parallel.

C

The number of groups of given order

We will see that the number of groups of order N is always at least $N/2$, and less than $O(N^2)$. If N is an odd prime, there are exactly $(N+3)/2$ groups, namely the torus translation groups $\square^{(s)}_{1,N}$ for $0 \le s \le (N-1)/2$ and $\square^{((1-N)/2)}_{N,1}$.

The richest class of groups are the toroidal groups, and among them, the most numerous groups are the torus translation groups, of type $\square$: For each divisor m of N, there are $\sim n/2$ groups $\square^{(s)}_{m,n}$, where $n = N/m$. Thus, the number of groups is about 1/2 times the sum $\sigma(N)$ of divisors of N, which is bounded by $N^{1+\frac{1+O(1/\log\log n)}{\log_2 \ln N}} \le N^2$ [51]. The upper bound of $O(N^2)$ is very weak; the actual bound is slightly superlinear.

The number of groups of type $\boxdot$ is of similar magnitude, provided that N is even. For all the other types, there is at most one group for every divisor of N, except for the swapturn groups, whose number is related to the number of integer points on the circle $a^2 + b^2 = N/4$, and this number is at most N.

From all the remaining classes of groups (tubical, polyhedral, or axial), there can be only a constant number of groups of a given order.

The number of groups of order 100. As an exercise, let us compute the number of point groups of order $N = 100$.

We proceed through the toroidal classes of groups in Table 4.3 one by one. For the pure translation groups of type $\square$, we can write $100 = mn = 1\cdot 100 = 2\cdot 50 = 4\cdot 25 = 5\cdot 20 = 10\cdot 10 = 20\cdot 5 = 25\cdot 4 = 50\cdot 2 = 100\cdot 1$ with accordingly $50+26+13+10+6+3+2+2+1 = 113$ choices of s, see the remark after (4.5) in Section 4.5. For the flip groups of type $\boxdot$ of order $100 = 2mn$, we have to factor 50 instead of 100. The possibilities are $50 = 1\cdot 50 = 2\cdot 25 = 5\cdot 10 = 10\cdot 5 = 25\cdot 2 = 50\cdot 1$ with $25+13+5+3+1+1 = 48$ choices of s.

For the swap groups $\boxslash^{\mathbf{pm}}_{m,n}$ of order $4mn$, we have to split $25 = mn$ into two factors mn larger than 1. There is one possibility: $25 = 5\times 5$. For the groups $\boxslash^{\mathbf{pg}}_{m,n}$, only the first factor m must be larger than 1. This gives 2 choices. For $\boxslash^{\mathbf{cm}}_{m,n}$ of order $2mn$, $mn = 50$ must be split into two factors of the same parity. This is impossible since $mn \equiv 2 \pmod 4$. Thus, in total we have 3 swap groups of type $\boxslash$. Clearly, there is the same number of 3 swap groups of type $\boxbslash$.

Finally, for the full torus swap groups, almost all types have order $8mn$, which cannot equal 100. We only need to consider the groups of type $\boxtimes^{\mathbf{c2mm}}_{m,n}$, of order $4mn$, We have to split $100/4 = 25$ into two factors ≥ 3 of the same parity. There is one possibility: $25 = 5\times 5$.

In total, we get $113+48+3+3+1 = 168$ chiral toroidal groups of order 100.

Let us turn to the achiral groups: For the reflection groups $\boxminus$, we have to consider all factorizations $100 = 2mn$ (types **pm** and **pg**) or $100 = 4mn$ (type **cm**). This gives $2\times\sigma_0(50) + \sigma_0(25) = 2\times 6 + 3 = 15$ groups, where σ_0 denotes the number of divisors of a number.

For the full reflection groups $\boxplus$, we have to consider all factorizations $100 = 4mn$ or $100 = 8mn$, respectively, where in one case (**p2mg**), we distinguish the order of the factors. We get $2+3+2+0 = 7$ possibilities. For general N, there are $2\lceil\sigma_0(\frac{N}{4})/2\rceil +$

$\sigma_0(\frac{N}{4}) + \lceil \sigma_0(\frac{N}{8})/2 \rceil$ full reflection groups of order N, where $\sigma_0(x) = 0$ if x is not an integer.

For ◻, we must have $100 = 4(a^2 + b^2)$ with $a \geq b \geq 0$. There are two possibilities: $(a, b) = (5, 0)$ or $(4, 3)$.

For the full torus groups ⊠, the order would have to be a multiple of 8; so there are no such groups of order 100.

In total, we get $15 + 7 + 2 = 24$ achiral toroidal groups of order 100, and 192 toroidal groups altogether.

$N = 100$ does not occur as the order of any of the other types of groups. So 192 is the total number of 4-dimensional point groups of order 100.

Enantiomorphic pairs. As an advanced exercise, we can ask, how many of the 168 chiral groups or order 100 are their own mirror image?

For the groups of type □, we are looking for a lattice of translations of size 100 that has an orientation-reversing symmetry. If it is symmetric with respect to a horizontal axis, then, according to Lemma 4.7.1, the possibilities are an $m \times n$ rectangular grid of mn points or a rhombic grid of $2mn$ points. In this case, it is also symmetric with respect to a vertical axis.

Thus, we have to split $100 = mn$ and $50 = mn$ into two factors m and n. The order of the factors plays no role, because the reflection ◿ swaps the factors. We have 5 possibilities for $100 = 1 \cdot 100 = 2 \cdot 50 = 4 \cdot 25 = 5 \cdot 20 = 10 \cdot 10$ and 3 possibilities for $50 = 1 \cdot 50 = 2 \cdot 25 = 5 \cdot 10$, which gives $5 + 3 = 8$ possibilities in total. (Alternatively, adding a vertical and horizontal mirror to such a translational subgroup will produce a group of type ⊞ **p2mm** or ⊞ **c2mm**. So we can equivalently count the groups of these types of order $4N = 400$.)

There is also the possibility that the lattice is symmetric with respect to a swapturn operation ◻. The number of these groups equals the number of groups of type ◻ of order $4N = 400$. It can be computed as the number of integer points (a, b) on the circle $100 = a^2 + b^2$ with $a \geq b \geq 0$. There are two possibilities: $(10, 0)$ and $(8, 6)$.

We have overcounted the lattices that are symmetric with respect to both ⊞ and ◻, in other words, the upright or slanted square lattices. There is one lattice of this type: the 10×10 upright lattice.

In total, $8 + 2 - 1 = 9$ groups among the 113 groups of type □ are equal to their own mirror.

For the groups of type ⊡, we can repeat the same game, except that we are looking for a translation lattice of half the size, 50. For the lattices with ⊞ symmetry, we have 3 possibilities for $50 = 1 \cdot 50 = 2 \cdot 25 = 5 \cdot 10$, and 2 possibilities for $25 = 1 \cdot 25 = 5 \cdot 5$, giving $3 + 2 = 5$ possibilities in total. There are two possibilities for $50 = a^2 + b^2$ with $a \geq b \geq 0$: $(7, 1)$ and $(5, 5)$. We have to subtract 1 for the slanted 5×5 grid, for a total of $5 + 2 - 1 = 6$ groups among the 48 flip groups.

The mirrors of the groups of type ◿ are the groups of type ◺, and hence none of them is its own mirror. The groups of type ⊠ are easy to handle: The two parameters m and n must be equal. We have one such group, $\boxtimes^{\mathbf{c2mm}}_{5,5}$. In total, $9 + 6 + 1 = 16$ chiral groups are their own mirror images. The remaining $168 - 16 = 152$ chiral groups consist of enantiomorphic pairs.

The number of groups of order 7200. To look at a more interesting example, let us count the groups of order 7200. The count of toroidal groups follows the same calculation as above, and it amounts to 19,319 chiral and 216 achiral groups. In addition, we have 22 tubical groups: $\pm[I \times C_{60}], \pm[I \times D_{60}], \pm[O \times C_{150}], \pm[O \times D_{150}], \pm[T \times C_{300}], \pm[T \times D_{300}], \pm\frac{1}{2}[O \times D_{300}], \pm\frac{1}{2}[O \times \overline{D}_{300}], \pm\frac{1}{2}[O \times C_{300}], \pm\frac{1}{6}[O \times D_{900}], \pm\frac{1}{3}[T \times C_{900}]$,

and their mirrors. Finally, there is one polyhedral group $\pm[I \times I]$. In total, we have $19{,}319 + 22 + 1 = 19{,}342$ chiral groups and 216 achiral ones.

The number of groups of order at most M. While the number of groups of a given order N fluctuates between a linear lower bound and a slightly superlinear upper bound, the "average number" can be estimated quite precisely: We have seen that the number of groups of order N is of order $\Theta(\sigma(N))$, where $\sigma(N)$ is the sum of divisors of N. If we look at all groups of order at most M, we can sum over all potential divisors d and get

$$\sum_{N=1}^{M} \sigma(N) = \sum_{d=1}^{M} d\lfloor M/d \rfloor = \Theta(M^2).$$

Thus, the number of four-dimensional groups of order at most M is $\Theta(M^2)$. The majority of these groups is chiral, but the achiral ones alone are already of the order $\Theta(M^2)$: There is essentially one swapturn group for each integer point (a, b) in the disk $a^2 + b^2 \leq M/4$, with roughly a factor 8 of overcounting of symmetric points, and this gives $\Theta(M^2)$ chiral groups.

The crystallographic point groups

D

Brown, Bülow, Neubüser, Wondratschek, Zassenhaus classified the four-dimensional crystallographic space groups in 1978 [10]. They grouped them by the underlying point groups (geometric crystal classes, or $\mathbb{Q}$-classes), and assigned numbers to these groups. The crystallographic point groups are characterized as having some lattice that they leave invariant.

There are 227 crystallographic points groups, sorted into 33 crystal systems according to the holohedry, i.e., the symmetry group of the underlying lattice. Tables D.1–D.2 give a reference from the 227 groups in the list of [10, Table 1C, pp. 79–260] to our notation (for the toroidal groups) or Conway and Smith's notation (for the remaining groups). When appropriate, we list two enantiomorphic groups.

The first classification of the four-dimensional crystallographic point groups was obtained by Hurley in 1951 [37], see Section 7.2. A few mistakes were later corrected [38].

All these groups are subgroups of only four maximal groups:

- $31/07 = \pm\frac{1}{60}[I \times \bar{I}] \cdot 2 = [[3,3,3]]$ (the simplex and its polar, order 240)
- $33/16 = \pm\frac{1}{2}[O \times O] \cdot 2 = [3,4,3]$ (the 24-cell, order 1152). Taking the permutations of $(\pm1, \pm1, 0, 0)$ as the vertices of a 24-cell, this set generates a lattice, and this lattice is invariant under the group. The symmetries of the hypercube/cross-polytope, $32/21 = \pm\frac{1}{6}[O \times O] \cdot 2 = [3,3,4]$, are contained in this group as a subgroup.
- $30/13 = \boxtimes_6^{\mathbf{p4mm}^{\mathrm{U}}} = \pm\frac{1}{2}[\bar{D}_{12} \times \bar{D}_{12}] \cdot 2$, order 288. The invariant lattice is the Cartesian product of two hexagonal plane lattices.
- $20/22 = \boxplus_{6,4}^{\mathbf{p2mm}} = \pm\frac{1}{24}[D_{24} \times D_{24}^{(5)}] \cdot 2^{(0,0)}$, order 96. The invariant lattice is the Cartesian product of a hexagonal lattice and a square lattice.

The last three items in Table D.2 are the "pseudo crystal groups" of Hurley [38]: Each such group consists of transformations that can individually occur in crystallographic groups, but as a whole, it is not a crystallographic group. All its proper subgroups are crystallographic groups.

		order
01/01	$\square_{1,1}$	1
01/02	$\square_{2,1}$	2
02/01	$\square^{\mathbf{pg}}_{1,1}$	2
02/02	$\square^{\mathbf{pm}}_{1,1}$	2
02/03	$\square^{\mathbf{cm}}_{1,1}$	4
03/01	$\square^{\mathbf{cm}}_{1,1}$	2
03/02	$\square^{\mathbf{pm}}_{2,2}$	4
04/01	$\square^{\mathbf{p2gg}}_{1,1}$	4
04/02	$\square^{\mathbf{p2mg}}_{1,1}$	4
04/03	$\square^{\mathbf{p2mm}}_{1,1}$	4
04/04	$\square^{\mathbf{c2mm}}_{1,1}$	8
05/01	$\square^{\mathbf{c2mm}}_{1,1}$	4
05/02	$\square^{\mathbf{p2mm}}_{2,2}$	8
06/01	$\square^{\mathbf{p2mg}}_{2,1}$	8
06/02	$\square^{\mathbf{p2mm}}_{2,1}$	8
06/03	$\square^{\mathbf{p2mm}}_{2,2}$	16
07/01	$\square^{(1)}_{1,4}$	4
07/02	$\square^{(0)}_{1,4}$	4
07/03	$\square^{(0)}_{2,4}$	8
07/04	$\square^{\mathbf{cm}}_{1,2}$	8
07/05	$\square^{\mathbf{pm}}_{1,4}$	8
07/06	$\square^{\mathbf{pg}}_{1,4}$	8
07/07	$\square^{\mathbf{pm}}_{2,4}$	16
08/01	$\square^{(0)}_{1,3}$	3
08/02	$\square^{(0)}_{2,3}$	6
08/03	$\square^{\mathbf{pg}}_{1,3}$	6
08/04	$\square^{\mathbf{pm}}_{1,3}$	6
08/05	$\square^{\mathbf{cm}}_{1,3}$	12
09/01	$\square^{(0)}_{1,6}$	6
09/02	$\square^{(2)}_{1,6}$	6
09/03	$\square^{(0)}_{2,6}$	12
09/04	$\square^{\mathbf{pg}}_{1,6}$	12
09/05	$\square^{\mathbf{pm}}_{1,6}$	12
09/06	$\square^{\mathbf{pm}}_{2,3}$	12
09/07	$\square^{\mathbf{pm}}_{2,6}$	24
10/01	$\square^{\mathbf{pg}}_{2,2} \mid \square^{\mathbf{pg}}_{2,2}$	4
11/01	$\square^{(1)}_{1,3} \mid \square_{3,1}$	3
11/02	$\square^{(-1)}_{2,3} \mid \square_{6,1}$	6
12/01	$\square_{1,0}$	4
12/02	$\square_{1,1}$	8
12/03	$\square^{\mathbf{p4gm}\mathrm{U}}_{1}$	8
12/04	$\square^{\mathbf{p4mm}\mathrm{U}}_{1}$	8
12/05	$\square^{\mathbf{p4mm}\mathrm{S}}_{1}$	16

		order
13/01	$\square^{\mathbf{pm}}_{4,1}$	8
13/02	$\square^{\mathbf{cm}}_{2,1}$	8
13/03	$\square^{(1)}_{1,4}$	8
13/04	$\square^{(0)}_{1,4}$	8
13/05	$\square^{\mathbf{pm}}_{4,2}$	16
13/06	$\square^{\mathbf{p2mg}}_{4,1}$	16
13/07	$\square^{\mathbf{c2mm}}_{2,1}$	16
13/08	$\square^{\mathbf{p2mm}}_{4,1}$	16
13/09	$\square^{(0)}_{2,4}$	16
13/10	$\square^{\mathbf{p2mm}}_{4,2}$	32
14/01	$\square^{\mathbf{pm}}_{3,1}$	6
14/02	$\square^{\mathbf{pg}}_{3,1}$	6
14/03	$\square^{(0)}_{1,3}$	6
14/04	$\square^{\mathbf{cm}}_{3,1}$	12
14/05	$\square^{(0)}_{2,3}$	12
14/06	$\square^{\mathbf{p2mg}}_{3,1}$	12
14/07	$\square^{\mathbf{p2mm}}_{3,1}$	12
14/08	$\square^{\mathbf{p2gg}}_{3,1}$	12
14/09	$\square^{\mathbf{p2mg}}_{1,3}$	12
14/10	$\square^{\mathbf{c2mm}}_{3,1}$	24
15/01	$\square^{\mathbf{pm}}_{6,1}$	12
15/02	$\square^{\mathbf{pg}}_{3,2}$	12
15/03	$\square^{\mathbf{pm}}_{3,2}$	12
15/04	$\square^{(0)}_{1,6}$	12
15/05	$\square^{(2)}_{1,6}$	12
15/06	$\square^{\mathbf{p2mg}}_{6,1}$	24
15/07	$\square^{\mathbf{p2mg}}_{2,3}$	24
15/08	$\square^{\mathbf{pm}}_{6,2}$	24
15/09	$\square^{\mathbf{p2mm}}_{6,1}$	24
15/10	$\square^{\mathbf{p2mm}}_{3,2}$	24
15/11	$\square^{(0)}_{2,6}$	24
15/12	$\square^{\mathbf{p2mm}}_{6,2}$	48
16/01	$\square^{\mathbf{p2gm}}_{2,2} \mid \square^{\mathbf{p2mg}}_{2,2}$	8
17/01	$\square^{\mathbf{cm}}_{1,3} \mid \square^{\mathbf{cm}}_{3,1}$	6
17/02	$\square^{\mathbf{pm}}_{2,6} \mid \square^{\mathbf{pm}}_{6,2}$	12
18/01	$\square^{\mathbf{p2gg}}_{2,2}$	8
18/02	$\square^{\mathbf{p4gm}\mathrm{S}}_{1}$	16
18/03	$\square_{2,0}$	16
18/04	$\square^{\mathbf{c2mm}}_{2,2}$	16
18/05	$\square^{\mathbf{p4mm}\mathrm{U}}_{2}$	32
19/01	$\square^{\mathbf{pg}}_{2,4}$	16
19/02	$\square^{(0)}_{4,4}$	16
19/03	$\square^{\mathbf{pm}}_{4,4}$	32
19/04	$\square^{\mathbf{p2mg}}_{4,2}$	32
19/05	$\square^{(0)}_{4,4}$	32
19/06	$\square^{\mathbf{p2mm}}_{4,4}$	64

		order
20/01	$\square^{(3)}_{1,12}$	12
20/02	$\square^{(2)}_{1,12}$	12
20/03	$\square^{\mathbf{pg}}_{2,3}$	12
20/04	$\square^{\mathbf{pm}}_{4,3}$	24
20/05	$\square^{(4)}_{2,12}$	24
20/06	$\square^{\mathbf{pm}}_{3,4}$	24
20/07	$\square^{(3)}_{1,12}$	24
20/08	$\square^{\mathbf{pg}}_{3,4}$	24
20/09	$\square^{\mathbf{cm}}_{2,3}$	24
20/10	$\square^{\mathbf{cm}}_{3,2}$	24
20/11	$\square^{(2)}_{1,12}$	24
20/12	$\square^{\mathbf{p2gg}}_{3,2}$	24
20/13	$\square^{\mathbf{p2mg}}_{3,2}$	24
20/14	$\square^{\mathbf{pg}}_{2,6}$	24
20/15	$\square^{\mathbf{pm}}_{4,6}$	48
20/16	$\square^{\mathbf{p2mm}}_{4,3}$	48
20/17	$\square^{\mathbf{p2mg}}_{4,3}$	48
20/18	$\square^{\mathbf{pm}}_{6,4}$	48
20/19	$\square^{(4)}_{2,12}$	48
20/20	$\square^{\mathbf{c2mm}}_{3,2}$	48
20/21	$\square^{\mathbf{p2mg}}_{6,2}$	48
20/22	$\square^{\mathbf{p2mm}}_{6,4}$	96
21/01	$\square^{\mathbf{cm}}_{1,3} \mid \square^{\mathbf{cm}}_{3,1}$	6
21/02	$\square^{\mathbf{pm}}_{2,6} \mid \square^{\mathbf{pm}}_{6,2}$	12
21/03	$\square^{\mathbf{c2mm}}_{1,3} \mid \square^{\mathbf{c2mm}}_{3,1}$	12
21/04	$\square^{\mathbf{p2mm}}_{2,6} \mid \square^{\mathbf{p2mm}}_{6,2}$	24
22/01	$\square^{(0)}_{3,3}$	9
22/02	$\square^{(-3)}_{6,3}$	18
22/03	$\square^{\mathbf{pg}}_{3,3}$	18
22/04	$\square^{\mathbf{pm}}_{3,3}$	18
22/05	$\square^{(0)}_{3,3}$	18
22/06	$\square^{\mathbf{cm}}_{3,3}$	36
22/07	$\square^{(-3)}_{6,3}$	36
22/08	$\square^{\mathbf{p2gg}}_{3,3}$	36
22/09	$\square^{\mathbf{p2mg}}_{3,3}$	36
22/10	$\square^{\mathbf{p2mm}}_{3,3}$	36
22/11	$\square^{\mathbf{c2mm}}_{3,3}$	72
23/01	$\square^{(0)}_{3,6}$	18
23/02	$\square^{(0)}_{6,6}$	36
23/03	$\square^{\mathbf{pm}}_{3,6}$	36
23/04	$\square^{\mathbf{pg}}_{3,6}$	36
23/05	$\square^{(0)}_{3,6}$	36
23/06	$\square^{\mathbf{pm}}_{6,3}$	36
23/07	$\square^{\mathbf{pm}}_{6,6}$	72
23/08	$\square^{(0)}_{6,6}$	72
23/09	$\square^{\mathbf{p2mm}}_{6,3}$	72
23/10	$\square^{\mathbf{p2mg}}_{6,3}$	72
23/11	$\square^{\mathbf{p2mm}}_{6,6}$	144

Table D.1.: The 227 crystallographic point groups in four dimensions, part 1

		order
24/01	$+\frac{1}{12}[T \times T]$	12
24/02	$\pm\frac{1}{12}[T \times T]$	24
24/03	$+\frac{1}{12}[T \times \bar{T}] \cdot 2_3$	24
24/04	$+\frac{1}{12}[T \times \bar{T}] \cdot 2_1$	24
24/05	$\pm\frac{1}{12}[T \times \bar{T}] \cdot 2$	48
25/01	$+\frac{1}{12}[T \times T] \cdot 2_1$	24
25/02	$+\frac{1}{12}[T \times T] \cdot 2_3$	24
25/03	$+\frac{1}{24}[O \times O]$	24
25/04	$+\frac{1}{24}[O \times \bar{O}]$	24
25/05	$\pm\frac{1}{12}[T \times T] \cdot 2$	48
25/06	$\pm\frac{1}{24}[O \times O]$	48
25/07	$+\frac{1}{24}[O \times O] \cdot 2_1$	48
25/08	$+\frac{1}{24}[O \times \bar{O}] \cdot 2_1$	48
25/09	$+\frac{1}{24}[O \times \bar{O}] \cdot 2_3$	48
25/10	$+\frac{1}{24}[O \times O] \cdot 2_3$	48
25/11	$\pm\frac{1}{24}[O \times O] \cdot 2$	96
26/01	$\boxslash^{\mathbf{pg}}_{2,4} \mid \boxdiagup^{\mathbf{pg}}_{4,2}$	8
26/02	$\boxtimes^{\mathbf{p2mg}}_{2,4} \mid \boxtimes^{\mathbf{p2gm}}_{4,2}$	16
27/01	$\square^{(1)}_{1,5}$	5
27/02	$\square^{(1)}_{2,5}$	10
27/03	$\boxdot^{(1)}_{1,5}$	10
27/04	$\boxdot^{(1)}_{2,5}$	20
28/01	$\boxslash^{\mathbf{pg}}_{2,6} \mid \boxdiagup^{\mathbf{pg}}_{6,2}$	12
28/02	$\boxtimes^{\mathbf{p2mg}}_{2,6} \mid \boxtimes^{\mathbf{p2gm}}_{6,2}$	24
29/01	$\boxslash^{\mathbf{cm}}_{3,3} \mid \boxdiagup^{\mathbf{cm}}_{3,3}$	18
29/02	$\boxslash^{\mathbf{pm}}_{6,6} \mid \boxdiagup^{\mathbf{pm}}_{6,6}$	36
29/03	$\boxtimes^{\mathbf{c2mm}}_{3,3}$	36
29/04	$\boxcircle_{3,0}$	36
29/05	$\boxtimes^{\mathbf{p2mm}}_{6,6}$	72
29/06	$\boxcircle_{3,3}$	72
29/07	$\circledast^{\mathbf{p4gm}\mathrm{U}}_{3}$	72
29/08	$\circledast^{\mathbf{p4mm}\mathrm{U}}_{3}$	72
29/09	$\circledast^{\mathbf{p4mm}\mathrm{S}}_{3}$	144
30/01	$\boxdiagup^{\mathbf{pg}}_{2,6} \mid \boxslash^{\mathbf{pg}}_{6,2}$	12
30/02	$\boxtimes^{\mathbf{p2gg}}_{2,6} \mid \boxtimes^{\mathbf{p2gg}}_{6,2}$	24
30/03	$\boxslash^{\mathbf{cm}}_{2,6} \mid \boxdiagup^{\mathbf{cm}}_{6,2}$	24
30/04	$\boxtimes^{\mathbf{p2gm}}_{2,6} \mid \boxtimes^{\mathbf{p2mg}}_{6,2}$	24
30/05	$\boxslash^{\mathbf{pg}}_{6,6} \mid \boxdiagup^{\mathbf{pg}}_{6,6}$	36
30/06	$\boxtimes^{\mathbf{c2mm}}_{2,6} \mid \boxtimes^{\mathbf{c2mm}}_{6,2}$	48
30/07	$\boxslash^{\mathbf{cm}}_{6,6} \mid \boxdiagup^{\mathbf{cm}}_{6,6}$	72
30/08	$\boxtimes^{\mathbf{p2mg}}_{6,6} \mid \boxtimes^{\mathbf{p2gm}}_{6,6}$	72
30/09	$\boxtimes^{\mathbf{p2gg}}_{6,6}$	72
30/10	$\boxtimes^{\mathbf{c2mm}}_{6,6}$	144
30/11	$\boxcircle_{6,0}$	144
30/12	$\circledast^{\mathbf{p4gm}\mathrm{S}}_{3}$	144
30/13	$\circledast^{\mathbf{p4mm}\mathrm{U}}_{6}$	288

		order
31/01	$\boxcircle_{2,1}$	20
31/02	$\boxcircle_{3,1}$	40
31/03	$+\frac{1}{60}[I \times \bar{I}]$	60
31/04	$+\frac{1}{60}[I \times \bar{I}] \cdot 2_3$	120
31/05	$+\frac{1}{60}[I \times \bar{I}] \cdot 2_1$	120
31/06	$\pm\frac{1}{60}[I \times \bar{I}]$	120
31/07	$\pm\frac{1}{60}[I \times \bar{I}] \cdot 2$	240
32/01	$\boxdiagup^{\mathbf{pg}}_{2,4} \mid \boxslash^{\mathbf{pg}}_{4,2}$	8
32/02	$\boxslash^{\mathbf{cm}}_{2,4} \mid \boxdiagup^{\mathbf{cm}}_{4,2}$	16
32/03	$\boxtimes^{\mathbf{p2gg}}_{2,4} \mid \boxtimes^{\mathbf{p2gg}}_{4,2}$	16
32/04	$\boxtimes^{\mathbf{p2mg}}_{4,2} \mid \boxtimes^{\mathbf{p2gm}}_{2,4}$	16
32/05	$\pm\frac{1}{3}[T \times C_3] \mid \pm\frac{1}{3}[C_3 \times T]$	24
32/06	$\boxtimes^{\mathbf{c2mm}}_{2,4} \mid \boxtimes^{\mathbf{c2mm}}_{4,2}$	32
32/07	$\boxtimes^{\mathbf{p2gg}}_{4,4}$	32
32/08	$\boxslash^{\mathbf{cm}}_{4,4} \mid \boxdiagup^{\mathbf{cm}}_{4,4}$	32
32/09	$\circledast^{\mathbf{p4gm}\mathrm{U}}_{2}$	32
32/10	$\boxtimes^{\mathbf{p2mm}}_{4,4}$	32
32/11	$\pm\frac{1}{6}[O \times D_6] \mid \pm\frac{1}{6}[D_6 \times O]$	48
32/12	$\boxtimes^{\mathbf{c2mm}}_{4,4}$	64
32/13	$\circledast^{\mathbf{p4gm}\mathrm{S}}_{2}$	64
32/14	$\circledast^{\mathbf{p4mm}\mathrm{S}}_{2}$	64
32/15	$\boxcircle_{4,0}$	64
32/16	$\pm\frac{1}{3}[T \times T]$	96
32/17	$\circledast^{\mathbf{p4mm}\mathrm{U}}_{4}$	128
32/18	$\pm\frac{1}{3}[T \times T] \cdot 2$	192
32/19	$\pm\frac{1}{3}[T \times \bar{T}] \cdot 2$	192
32/20	$\pm\frac{1}{6}[O \times O]$	192
32/21	$\pm\frac{1}{6}[O \times O] \cdot 2$	384
33/01	$\boxslash^{\mathbf{pg}}_{4,6} \mid \boxdiagup^{\mathbf{pg}}_{6,4}$	24
33/02	$\boxdiagup^{\mathbf{pg}}_{4,6} \mid \boxslash^{\mathbf{pg}}_{6,4}$	24
33/03	$\pm[C_1 \times T] \mid \pm[T \times C_1]$	24
33/04	$\boxtimes^{\mathbf{p2gg}}_{4,6} \mid \boxtimes^{\mathbf{p2gg}}_{6,4}$	48
33/05	$\pm[C_2 \times T] \mid \pm[T \times C_2]$	48
33/06	$\pm\frac{1}{2}[O \times C_2] \mid \pm\frac{1}{2}[C_2 \times O]$	48
33/07	$\pm[C_3 \times T] \mid \pm[T \times C_3]$	72
33/08	$\pm[D_4 \times T] \mid \pm[T \times D_4]$	96
33/09	$\pm\frac{1}{2}[O \times D_4] \mid \pm\frac{1}{2}[D_4 \times O]$	96
33/10	$\pm\frac{1}{2}[O \times C_4] \mid \pm\frac{1}{2}[C_4 \times O]$	96
33/11	$\pm\frac{1}{2}[O \times D_6] \mid \pm\frac{1}{2}[D_6 \times O]$	144
33/12	$\pm\frac{1}{2}[O \times \bar{D}_8] \mid \pm\frac{1}{2}[\bar{D}_8 \times O]$	192
33/13	$\pm[T \times T]$	288
33/14	$\pm[T \times T] \cdot 2$	576
33/15	$\pm\frac{1}{2}[O \times O]$	576
33/16	$\pm\frac{1}{2}[O \times O] \cdot 2$	1152
—	$\boxtimes^{\mathbf{p2gm}}_{4,6} \mid \boxtimes^{\mathbf{p2mg}}_{6,4}$	48
—	$\boxtimes^{\mathbf{p2mg}}_{4,6} \mid \boxtimes^{\mathbf{p2gm}}_{6,4}$	48
—	$\pm[D_6 \times T] \mid \pm[T \times D_6]$	144

Table D.2.: The 227 crystallographic point groups, part 2, and 3 pseudo-crystal groups

E

Geometric interpretation of oriented great circles

Section 2.1.2 introduced the notation $\vec{K}_p^q$ to denote oriented great circles on S^3. Here we give a geometric interpretation of the orientation. In fact, we will give two equivalent geometric interpretations. However, at the boundary cases $p = q$ and $q = -p$, one or the other of the interpretations loses its meaning, and only by combining both interpretations we get a consistent definition that covers all cases.

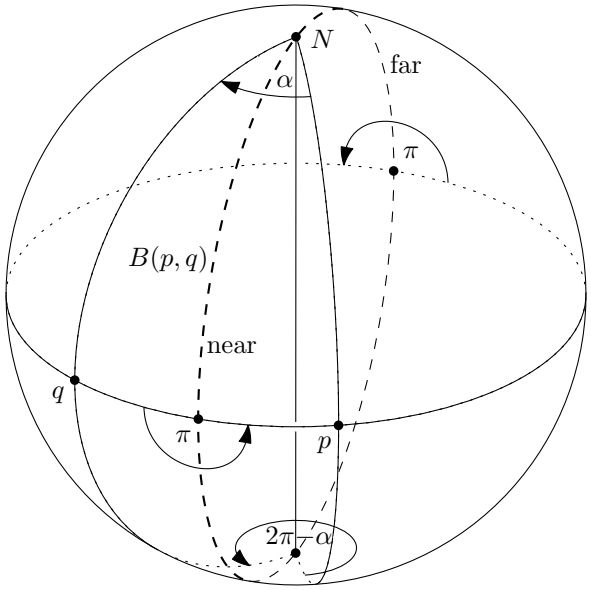

Figure E.1.: The centers of the rotations mapping p to q lie on the bisecting circle $B(p, q)$.

We start from the definition (2.1) of K_p^q as the set of rotations $[x]$ that map p to q in S^2. The centers r of these rotations lie on the bisecting circle $B(p, q)$ between p and q. In Figure E.1, we have drawn p and q on the equator, with p east of q. If we observe the clockwise rotation angle φ as r moves along $B(p, q)$, we see that φ has two extrema: If the angular distance between p and q is α, the minimum clockwise angle $\varphi = \alpha$ is achieved when r is at the North Pole. The maximum $2\pi - \alpha$ is achieved at the South Pole. The poles bisect $B(p, q)$ into two semicircles, the *near semicircle* and the *far semicircle*, according to the distance from p and q.

To define an orientation, we let r move continuously on $B(p, q)$, see Figure E.2 for an illustration on a small patch of S^2. We make the movement in such a way that

(i) the rotation center r moves in counterclockwise direction around p;
(ii) simultaneously, the clockwise rotation angle φ increases when r is on the near semicircle and decreases when r is on the far semicircle.

In Figure E.2, as r moves from r_1 to r_2 along the thick arrow, the angle φ increases from φ_1 to φ_2. These rules define an orientation of $B(p, q)$.

When we want to transfer this orientation to K_p^q, we must be aware of the $2 : 1$ relation between quaternions $x = \cos\frac{\varphi}{2} + r \cdot \sin\frac{\varphi}{2}$ and rotations $[x]$ of S^2. The angle φ

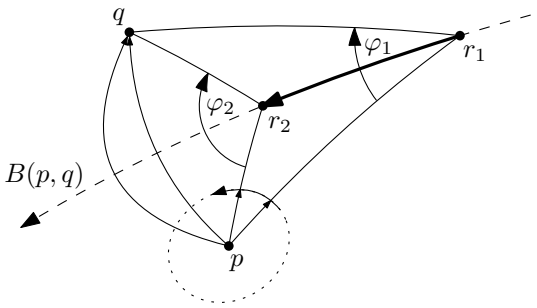

Figure E.2.: Orienting the great circle K_p^q

is defined only up to multiples of 2π, and hence a rotation corresponds to two opposite quaternions x and $-x$. Thus, there are two ways of defining a continuous dependence from r via φ to x. Both possibilities lead to the same orientation of K_p^q, but we can select one of them by restricting φ to the interval $0 \leq \varphi < 2\pi$. Once this mapping is chosen, two opposite points r and $-r$ on $B(p,q)$, which define the same rotation $[r]$ of S^2, correspond to opposite quaternions x and $-x$ on K_p^q. (The easiest way to check this is for the midpoint of p and q in Figure E.1 and the opposite point. Both have the same rotation angle $\varphi = \pi$. Generally, the transition from φ to $2\pi - \varphi$ changes the sign of $\cos\frac{\varphi}{2}$ and leaves $\sin\frac{\varphi}{2}$ unchanged.) Thus, as r traverses $B(p,q)$, x traverses K_p^q once, and this traversal defines the orientation $\vec{K}_p^q$.

The rules break down in the degenerate situations when $q = \pm p$. Luckily, in each situation, there is one rule that works.

- When $p = q$, the only rotations centers are $r = p$ and $r = -p$. In this case, we can maintain rule (ii): We consider increasing rotation angles around $r = p$ (or decreasing rotation angles around $r = -p$, which corresponds to the far semicircle).
- When $p = -q$, the rotation angle $\varphi = 180°$ is constant, but we can stick to rule (i): The rotation centers r lie on the circle $B(p,-p)$ that has p and $-p$ as poles, and we let them move counterclockwise around p.

Considering the definition (2.1) of K_p^q, it is actually surprising that K_p^q makes a smooth transition when q approaches p: The locus $B(p,q)$ of rotation centers changes discontinuously from a circle to a set of opposite points.

When p and q are exchanged with $-p$ and $-q$, the circle K_p^q of rotations remains the same, but everything changes its direction: A counterclockwise movement of r around p becomes a clockwise movement when seen from $-p$, and r is on the near semicircle of p and q if it is on the far semicircle of $-p$ and $-q$. Thus, $\vec{K}_{-p}^{-q}$ has the opposite orientation.

F

Subgroup relations between tubical groups

Figure F.1 shows the subgroup structure between different tubical groups. Some types are included multiple times with different parameters to indicate common supergroups. However, all the types appear at least once with the parameter "n". (Those are the ones in red.)

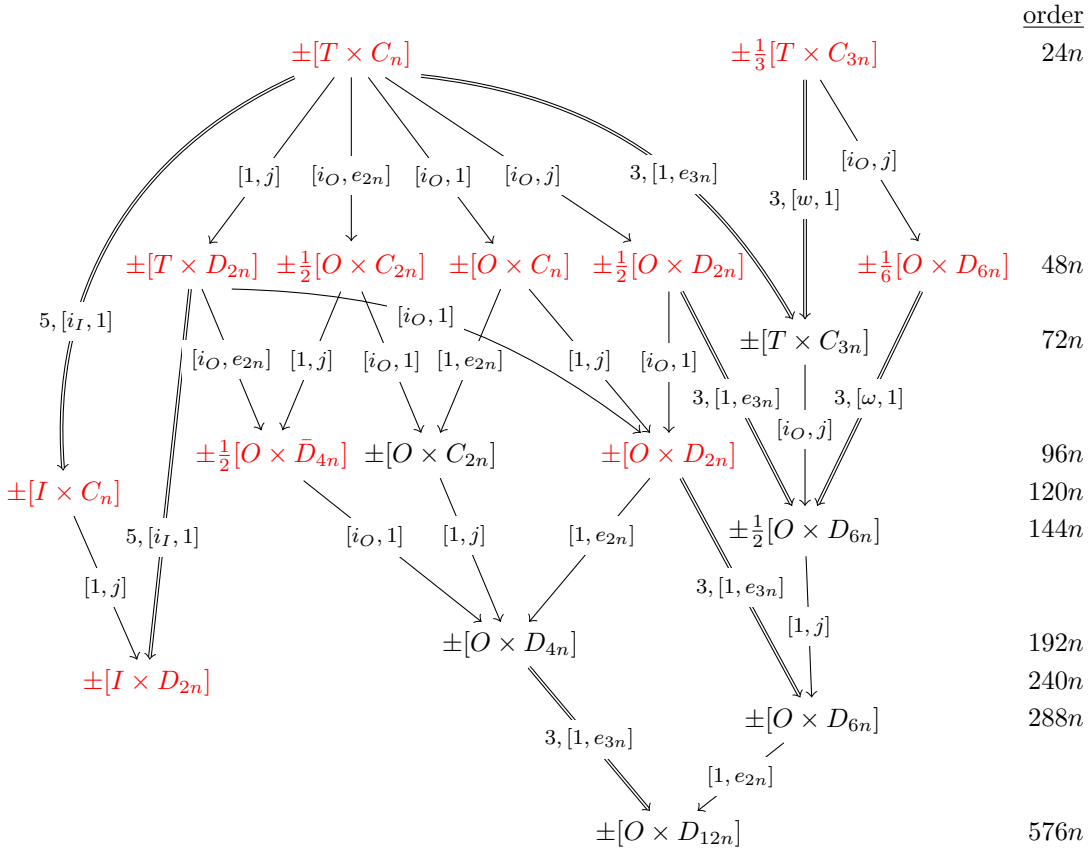

Figure F.1.: Small-index containments between left tubical groups. Each arrow is marked with an extending element. Single arrows indicate index-2 containments. Double arrows denote index-3 or index-5 containments, as specified with the extending element. The red groups have the "natural" parameter n (as in Table 3.1). Groups at the same horizontal level have the same order, which is given in the rightmost column.

G

Conway and Smith's classification of the toroidal groups

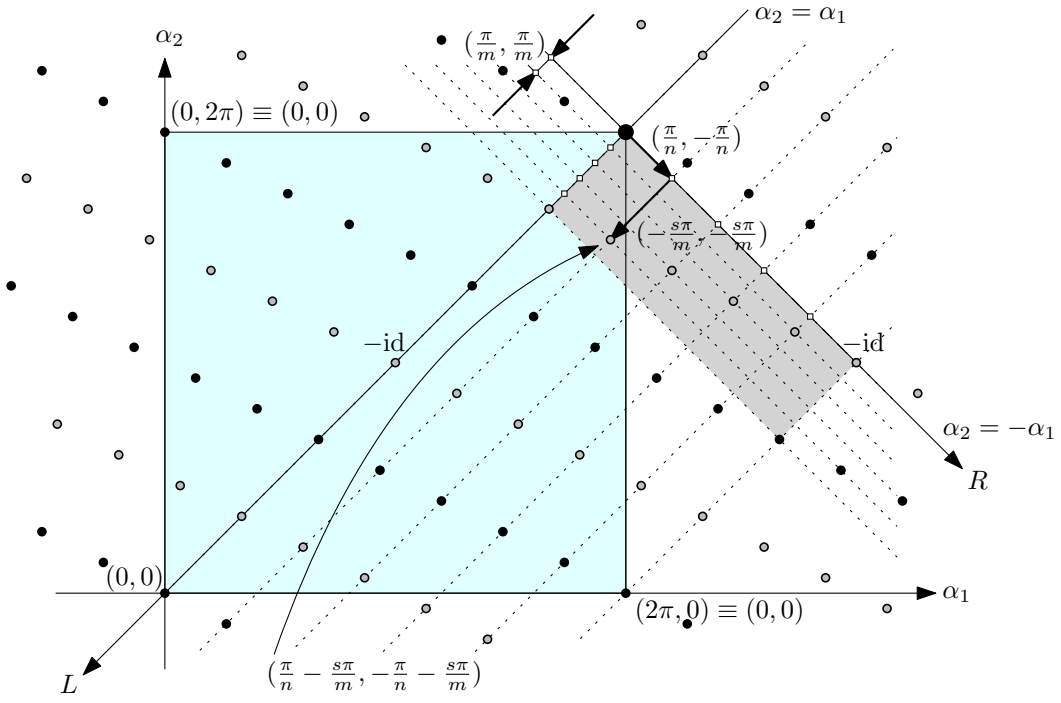

Figure G.1.: Parameterization of the translation groups in Conway and Smith. The black and gray points together form the diploid group $\pm\frac{1}{5}[C_{15}^{(4)} \times C_5] = \square_{6,5}^{(-2)}$ of order 30. The black points alone form the haploid group $+\frac{1}{5}[C_{15}^{(9)} \times C_5] = \square_{3,5}^{(-1)}$ of order 15.

We describe the parameterization of the lattice translations for the Conway–Smith classification of the groups of types $\pm[C \times C]$ and $+[C \times C]$ in geometric terms and relate them to our torus translations groups (type $\square$). This might be interesting for readers who want to study the classic classification for the toroidal groups and understand the connections.

As before, we describe the groups in terms of the lattice of torus translations in the (α_1, α_2) coordinate system, see Figure G.1. We put the origin at the top right corner $(2\pi, 2\pi)$ because the left rotations $[e_m, 1]$ is a shift by π/m along the negative $\alpha_1 = \alpha_2$ axis. This is the axis for the left rotations, and we call it the L-axis. The right rotations move on the $\alpha_2 = -\alpha_1$ axis in the southeast direction, and we call this the R-axis.

We first describe the diploid groups $\pm\frac{1}{f}[C_m^{(s)} \times C_n]$, and we related them to our groups $\square_{m',n}^{(s')}$. The left and right groups are determined by the grid formed by drawing $\pm 45°$ lines through all points. If $2m$ grid lines cross the L-axis between $(0, 0)$ and $(2\pi, 2\pi)$, then the left group is C_m. Similarly, if there are $2n$ grid intervals on the R-axis between $(2\pi, 2\pi)$ and $(4\pi, 0)$, (or equivalently, on the $-45°$ diagonal of the square), the right group is C_n. The translation vectors on these diagonals form the left kernel $C_{m/f}$ and the right

kernel $C_{n/f}$. The factor f is determined by the number of grid steps along the diagonal from one point to the next. In the picture, these are $f = 5$ steps. The parameter m' for our parameterization is hence $2m/f$. The kernels span a slanted rectangular grid; one rectangular box of this grid is shaded in the picture. In terms of grid lines, the diagonal is an $f \times f$ square, and it contains exactly one point per grid line of either direction, for a total of f points (counting the four corners only once). In geometric terms, Conway and Smith parameterize the lattice by looking at the first grid line below the L-axis, as in our parameterization. They measure s as the number of grid steps to the first lattice point, starting from the R-axis in southwest direction. The number s must be relatively prime to f, because otherwise, additional points on the R-axis would be generated.

By contrast, the parameter s' in our setup (Figure 4.4) is effectively measured in the same units along the same diagonal line, but starting from the intersection with the α_1-axis, in the northeast direction. Our parameterization is simpler because we don't specify in advance the number of points on the R-axis. This allows us to freely choose s' within some range.

The group $\pm\frac{1}{f}[C_m^{(s)} \times C_n]$ is therefore generated by the translation vectors $[e_m^f, 1]$ along the L-axis, $[1, e_n^f]$ along the R-axis, and the additional vector $[e_m^s, e_n]$. (The second generator $[1, e_n^f]$ is actually redundant because $[e_m^s, e_n]^f [e_m^f, 1]^{-s} = [1, e_n^f]$.)

For our group $\square_{m',n}^{(s')}$, the parameter n is the same, and $m' = 2m/f$. The parameter s' can be computed as follows. Choose generators for $\pm\frac{1}{f}[C_m^{(s)} \times C_n]$ as in Figure 4.4. These generators are then $t_1 = (\frac{f\pi}{m}, \frac{f\pi}{m})$ and $t_2 = (\frac{\pi}{n} - \frac{s\pi}{m} + \frac{f\pi}{m}, -\frac{\pi}{n} - \frac{s\pi}{m} + \frac{f\pi}{m})$. Comparing them with the generators in Proposition 4.5.1, we get $s' = \frac{-m+(f-s)n}{f}$.

As mentioned in footnote 14 on p. 60, we have swapped the roles of the left and right groups with respect to Conway and Smith's convention, to get a closer correspondence. In the original convention of Conway and Smith, the group $\pm\frac{1}{f}[C_m \times C_n^{(s)}]$ is considered, whose third generator is $[e_m, e_n^s]$. This group is the mirror of the group $\pm\frac{1}{f}[C_n^{(s)} \times C_m]$.

A haploid group $+\frac{1}{f}[C_m^{(s)} \times C_n]$ exists if both m/f and n/f are odd. We modify the first generator to $[e_m^{2f}, 1]$. This omits every other point on the L-axis (and on every line parallel to it) and thus avoids the point $(\pi, \pi) = -\mathrm{id}$. In addition to being relatively prime to f, s must be odd, because otherwise, since $[e_m^s, e_n]^n [e_m^{2f}, 1]^{-n/f \cdot s/2} = [1, e_n^n] = [1, -1]$, we would nevertheless generate the point $(\pi, \pi) = -\mathrm{id}$.

Reflection in the L-axis gives the same group. Hence $\pm\frac{1}{5}[C_{15}^{(4)} \times C_5] \doteq \pm\frac{1}{5}[C_{15}^{(1)} \times C_5] = \square_{6,5}^{(1)}$, and $+\frac{1}{5}[C_{15}^{(9)} \times C_5] \doteq +\frac{1}{5}[C_{15}^{(1)} \times C_5] = \square_{3,5}^{(2)}$. This reflection changes the parameter s to $f - s$ for the diploid groups and to $2f - s$ for the haploid groups. To eliminate these duplications, the parameter s should be constrained to the interval $0 \le s \le f/2$ for the diploid groups and $0 \le s \le f$ for the haploid groups. As mentioned in footnote 15 on p. 63, these constraints are not stated in Conway and Smith. This concerns the last four entries of [14, Table 4.2], see Figure G.3.

With the help of the geometric picture of Figure G.1 for the parameterization of Conway and Smith, one can give a geometric interpretation to the conditions $s = fg \pm 1$ of [14, pp. 52–53] for the last 4 lines of Table 4.3: The condition $s = fg - 1$ expresses the fact that a square lattice is generated, as is necessary for the torus swapturn groups $\boxed{\circlearrowleft}$ (type $[D \times D] \cdot \bar{2}$). The condition $s = fg + 1$ characterizes a rectangular lattice, as required for the groups of type $\boxed{\square}$ and $\boxed{\boxplus}$. (Accordingly, for the two types of groups $\pm[C \times C] \cdot 2^{(\gamma)}$ and $+[C \times C] \cdot 2^{(\gamma)}$ in the upper half of [14, pp. 53], the condition $s = fg - 1$ must be corrected to $s = fg + 1$, see Figure G.6.)

G.1. Index-4 subgroups of D_{4m}

There is one ambiguity that is notorious for causing oversights and omissions. It arises when the group C_m is used as an index-4 subgroup of D_{4m}.

D_{4m} is the chiral symmetry group of a regular $2m$-gon P_{2m} in space. In Figure G.2 we show such a $2m$-gon with an alternating 2-coloring of its vertices. C_m is the normal subgroup of rotations around the principal axis, perpendicular to the polygon, by multiples of $2\pi/m$ (those that respect the coloring). C_m has three cosets in D_{4m}: The "cyclic coset" C'_m of rotations by odd multiples of π/m (those that swap the coloring), and two "half-turn cosets" C^0_m and C^1_m. One of these contains the half-turns through the vertices of P_{2m} (the dashed axes, keeping the colors), and the other the half-turns through the edge midpoints of P_{2m} (the dotted axes, swapping colors). However, when we rotate P_{2m} by $\pi/(2m)$, the involved groups and subgroups don't change, and hence we see that C^0_m and C^1_m are geometrically the same, whereas C'_m is clearly distinguishable (unless $m = 1$).

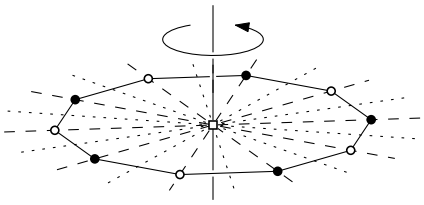

Figure G.2.: The operations of D_{20} on a regular 10-gon P_{10}

The case of the index-4 subgroups C_m and C_n of D_{4m} and D_{4n} is denoted in Conway and Smith [14] by the notation $\frac{1}{4}[D_{4m} \times D_{4n}]$, possibly with some decoration to distinguish different cases.

The actual group is determined by an isomorphism between the cosets of D_{4m}/C_m and D_{4n}/C_n. For this there are two possibilities.

(a) The cyclic coset C'_m is matched with the cyclic coset C'_n.

(b) The cyclic coset C'_m and the cyclic coset C'_n are not matched to each other.

Goursat's omission. In the earliest enumeration by Goursat from 1889, the less natural possibility (b) has been overlooked. This was noted by Threlfall and Seifert in 1931, [67, footnote 9 on p. 14][27] and by Hurley in 1951 [37, bottom of p. 652],[28] who consequently extended the classification by adding an additional class XIII′ of groups to Goursat's list. Du Val [23] followed Goursat and omitted case (b) again.

A missed duplication in Conway and Smith. Conway and Smith [14] denote case (b) by adding a bar to the second factor as follows:

$$\pm\tfrac{1}{4}[D_{4m} \times \bar{D}_{4n}] \text{ or } +\tfrac{1}{4}[D_{4m} \times \bar{D}_{4n}]$$

[27] Referring to Goursat's work: "Gruppen dieser Substitutionen – mit unseren Paargruppen 1-isomorph – sind mit einer Ausnahme (§ 4 S. 18 Fußnote und § 4 S. 22) vollständig angegeben." (Groups of these substitutions – which are 1-isomorphic to our pair groups – are completely specified with one exception, see § 4 p. 18 footnote 13 and § 4 p. 22.) In fact, in footnote 13 on p. 18, they use two such groups as an example of groups with equal normal subgroups L_0 and R_0 that are different already as abstract groups. It is curious that Threlfall and Seifert, in the same paper, when they came to the actual classification, overlooked this class of groups again. They noted the gap themselves and filled it in part II [68, pp. 585–586, Appendix II, Note 5].

[28] "In the course of this calculation we find that Goursat has omitted one family of groups. This omission appears to have passed unnoticed by subsequent writers."

When $n = 1$, the distinction between case (a) and (b) disappears. D_4 is the Vierergruppe, whose nontrivial operations are half-turns around three perpendicular axes, and these elements are geometrically indistinguishable.

Conway and Smith express this succinctly in the concluding sentence of their classification (see Figure G.6): "In the last eight lines, it is always permissible to replace D_2 by C_2 and $\bar{D}_4$ by D_4." However, this formulation in connection with the choice of notation might lead an unwary reader into a trap:[29] The choice (b) of an alternative mapping between the index-4 cosets in $\frac{1}{4}[D_{4m} \times D_{4n}]$ is not a property associated to D_{4n} and its chosen normal subgroup, and it would more appropriate to add the bar to the $\times$ operator or the whole expression. The distinction disappears when at least *one* of D_{4m} and D_{4n} is D_4, and hence, the bar can also be removed in a case like $[D_4 \times \bar{D}_{4n}]$ when the first factor is D_4. This duplication example has been treated in detail in Section 4.11.2.

Conway and Smith use the bar notation $\bar{D}_{4n}$ also for something different, namely in the index-2 case, for example in $\pm\frac{1}{2}[O \times \bar{D}_{4n}]$, see Table 3.1. It indicates that, as the kernel R_0 (or L_0) of D_{4n}, the normal subgroup D_{2n} is used, as opposed to C_{2n}. Also in this case, the distinction disappears for $n = 1$, but this time, it is a property of the group D_{4n} and its normal subgroup, and hence the notation of attaching the bar to D_{4n} causes no confusion.

Another duplication in Conway and Smith. Our computer check unveiled another duplication in Conway and Smith's classification. It concerns the groups $\boxplus^{\mathbf{p2mg}}_{m,n}$ for $m = n$:

$$\boxplus^{\mathbf{p2mg}}_{n,n} \doteq \pm\tfrac{1}{4}[D_{2n} \times D^{(1)}_{2n}] \cdot 2^{(1,0)} \doteq \pm\tfrac{1}{4}[D_{2n} \times D^{(1)}_{2n}] \cdot 2^{(1,1)} \qquad \text{for even } n$$
$$\boxplus^{\mathbf{p2mg}}_{n,n} \doteq +\tfrac{1}{2}[D_{2n} \times D^{(1)}_{2n}] \cdot 2^{(0,0)} \doteq +\tfrac{1}{2}[D_{2n} \times D^{(1)}_{2n}] \cdot 2^{(0,2)} \qquad \text{for odd } n$$

Neither of these duplications is warranted according to the equalities listed in [14, pp. 52–53]. For example, for $\pm\frac{1}{4}[D_{2n} \times D^{(s)}_{2n}] \cdot 2^{(\alpha,\beta)}$ in the first line, we need a transition from $(\alpha, \beta) = (1, 0)$ to $(\alpha, \beta) = (1, 1)$. In this example, $f = 2$ and $g = 0$. The only rule according to [14, bottom of p. 52] that allows this change is the transition from $\langle s, \alpha, \beta\rangle$ to $\langle s + f, \alpha, \beta - \alpha\rangle$ (see Figure G.5), but it comes with a simultaneous change of s from $s = 1$ to $s + f = 3$. The parameter s is regarded modulo $2f = 4$.

We did not investigate the reason for this duplication. Since $f = 2$ in both cases, it may have to do with "... the easy cases when $f \leq 2$, which we exclude" [14, p. 52, line 2], see Figure G.5.

The book of Conway and Smith [14] is otherwise a very nice book on topics related to quaternions and octonions, but it suffers from a concentration of mistakes near the end of Chapter 4, in particular, concerning the achiral groups. As an "erratum" to [14, §4], we attach in Figures G.3–G.6 the Tables 4.1–4.2 and the last three pages of Chapter 4 of [14] with our additional explanations and corrections, as far as we could ascertain them, but we certainly did not fix all problems.

[29] Besides, the rule should also apply to entries that are not in the last eight lines of the tables. Accordingly, the constraint $n \geq 2$, which is stated for five of the eleven tubical groups in Table 3.1, should also be applied to the corresponding groups in [14, Table 4.1]. For the group $+\frac{1}{2}[D_{2m} \times C_{2n}]$ in the penultimate line of Table 4.1, the obvious condition that m and n should be odd was forgotten. This omission has already been noted by Medeiros and Figueroa-O'Farrill [22, p. 1405].

Group	Generators	
$\pm[I\times O]$	$[i_I,1],[\omega,1],[1,i_O],[1,\omega]$;	
$\pm[I\times T]$	$[i_I,1],[\omega,1],[1,i],[1,\omega]$;	
$\pm[I\times D_{2n}]$	$[i_I,1],[\omega,1],[1,e_n],[1,j]$;	$(n\geq 2)$
$\pm[I\times C_n]$	$[i_I,1],[\omega,1],[1,e_n]$;	
$\pm[O\times T]$	$[i_O,1],[\omega,1],[1,i],[1,\omega]$;	
$\pm[O\times D_{2n}]$	$[i_O,1],[\omega,1],[1,e_n],[1,j]$;	$(n\geq 2)$
$\pm\frac{1}{2}[O\times D_{2n}]$	$[i,1],[\omega,1],[1,e_n]$;$[i_O,j]$	$(n\geq 2)$
$\pm\frac{1}{2}[O\times \overline{D}_{4n}]$	$[i,1],[\omega,1],[1,e_n],[1,j]$;$[i_O,e_{2n}]$	$(n\geq 2)$
$\pm\frac{1}{6}[O\times D_{6n}]$	$[i,1],[j,1],[1,e_n]$;$[i_O,j],[\omega,e_{3n}]$	
$\pm[O\times C_n]$	$[i_O,1],[\omega,1],[1,e_n]$;	
$\pm\frac{1}{2}[O\times C_{2n}]$	$[i,1],[\omega,1],[1,e_n]$;$[i_O,e_{2n}]$	
$\pm[T\times D_{2n}]$	$[i,1],[\omega,1],[1,e_n],[1,j]$;	$(n\geq 2)$
$\pm[T\times C_n]$	$[i,1],[\omega,1],[1,e_n]$;	
$\pm\frac{1}{3}[T\times C_{3n}]$	$[i,1],[1,e_n]$;$[\omega,e_{3n}]$	
$\pm\frac{1}{2}[D_{2m}\times \overline{D}_{4n}]$	$[e_m,1],[1,e_n],[1,j]$;$[j,e_{2n}]$	$(m\geq 2, n\geq 2)$
$\pm[D_{2m}\times C_n]$	$[e_m,1],[j,1],[1,e_n]$;	$(m\geq 2)$
$\pm\frac{1}{2}[D_{2m}\times C_{2n}]$	$[e_m,1],[1,e_n]$;$[j,e_{2n}]$	$(m\geq 2, n\geq 2)$
$+\frac{1}{2}[D_{2m}\times C_{2n}]$	$-\ ,\ -\ ;\ +$	m and n odd $(m\geq 2, n\geq 2)$
$\pm\frac{1}{2}[\overline{D}_{4m}\times C_{2n}]$	$[e_m,1],[j,1],[1,e_n]$;$[e_{2m},e_{2n}]$	$(m\geq 2)$

Table 4.1. Chiral groups, I. These are most of the "metachiral" groups—see section 4.6—some others appear in the last few lines of Table 4.2.

Group	Generators	Coxeter Name	
$\pm[I\times I]$	$[i_I,1],[\omega,1],[1,i_I],[1,\omega]$;	$[3,3,5]^+$	
$\pm\frac{1}{60}[I\times I]$	;$[\omega,\omega],[i_I,i_I]$	$2.[3,5]^+$	
$+\frac{1}{60}[I\times I]$	; + , +	$[3,5]^+$	
$\pm\frac{1}{60}[I\times \overline{I}]$	;$[\omega,\omega],[i_I,i_I']$ MISSING DEFINITION	$2.[3,3,3]^+$	
$+\frac{1}{60}[I\times \overline{I}]$	; + , +	$[3,3,3]^+$	
$\pm[O\times O]$	$[i_O,1],[\omega,1],[1,i_O],[1,\omega]$;	$[3,4,3]^+:2$	
$\pm\frac{1}{2}[O\times O]$	$[i,1],[\omega,1],[1,i],[1,\omega]$;$[i_O,i_O]$	$[3,4,3]^+$	
$\pm\frac{1}{6}[O\times O]$	$[i,1],[j,1],[1,i],[1,j]$;$[\omega,\omega],[i_O,i_O]$	$[3,3,4]^+$	
$\pm\frac{1}{24}[O\times O]$	;$[\omega,\omega],[i_O,i_O]$	$2.[3,4]^+$	
$+\frac{1}{24}[O\times O]$	; + , +	$[3,4]^+$	
$+\frac{1}{24}[O\times \overline{O}]$	; + , −	$[2,3,3]^+$	
$\pm[T\times T]$	$[i,1],[\omega,1],[1,i],[1,\omega]$;	$[^+3,4,3^+]$	
$\pm\frac{1}{3}[T\times T]$	$[i,1],[j,1],[1,i],[1,j]$;$[\omega,\omega]$	$[^+3,3,4^+]$	
$\cong\pm\frac{1}{3}[T\times \overline{T}]$	$[i,1],[j,1],[1,i],[1,j]$;$[\omega,\overline{\omega}]$	"	
$\pm\frac{1}{12}[T\times T]$	;$[\omega,\omega],[i,i]$	$2.[3,3]^+$	
$\cong\pm\frac{1}{12}[T\times \overline{T}]$	;$[\omega,\overline{\omega}],[i,-i]$	"	
$+\frac{1}{12}[T\times T]$	; + , +	$[3,3]^+$	
$\cong+\frac{1}{12}[T\times \overline{T}]$	; + , +	"	
$\pm[D_{2m}\times D_{2n}]$	$[e_m,1],[j,1],[1,e_n],[1,j]$;		$(m\geq 2, n\geq 2)$
$\pm\frac{1}{2}[\overline{D}_{4m}\times \overline{D}_{4n}]$	$[e_m,1],[j,1],[1,e_n],[1,j]$;$[e_{2m},e_{2n}]$		
$\pm\frac{1}{4}[D_{4m}\times \overline{D}_{4n}]$	$[e_m,1],[1,e_n]$;$[e_{2m},j],[j,e_{2n}]$	Conditions	
$+\frac{1}{4}[D_{4m}\times \overline{D}_{4n}]$	$-\ ,\ -\ ;\ +\ ,\ +$	m,n odd	
$\pm\frac{1}{2f}[D_{2mf}\times D^{(s)}_{2nf}]$	$[e_m,1],[1,e_n]$;$[e_{mf},e^s_{nf}],[j,j]$	$(s,f)=1$	$0\leq s\leq f/2$
$+\frac{1}{2f}[D_{2mf}\times D^{(s)}_{2nf}]$	$-\ ,\ -\ ;\ +\ ,\ +$	m,n odd, $(s,2f)=1$	$0\leq s\leq f$
$\pm\frac{1}{f}[C_{mf}\times C^{(s)}_{nf}]$	$[e_m,1],[1,e_n]$;$[e_{mf},e^s_{nf}]$	$(s,f)=1$	$0\leq s\leq f/2$
$+\frac{1}{f}[C_{mf}\times C^{(s)}_{nf}]$	$-\ ,\ -\ ;\ +$	m,n odd, $(s,2f)=1$	$0\leq s\leq f$

Table 4.2. Chiral groups, II. These groups are mostly "orthochiral," with a few "parachiral" groups in the last few lines. The generators should be taken with both signs except in the haploid cases, for which we just indicate the proper choice of sign. The "Coxeter names" are explained in Section 4.4.

Figure G.3.: Corrections and remarks for [14, Tables 4.1 and 4.2, p. 44 and 46].

The Completeness of Table 4.3

Here we obtain G from the "half-group" H corresponding to some isomorphism $L/L_0 \cong R/R_0$ by adjoining an extending element $*[a,b]$, which must normalize H. We shall show that (at some cost) the extending element may be reduced to the form $*[1,c]$, and also that (at no cost) c can be multiplied by any element of R_0, or altered by any inner automorphism of R, while finally c must be in the part of R that is fixed (mod R_0) by the isomorphism (since $(*[1,c])^2 = [c,c]$ must be in H).

For, conjugation by $[1,a]$ replaces $*[a,b]$ by

$$(*[a,b])^{[1,a]} = [1,\overline{a}] * [a,b][1,a] = *[\overline{a}a, ba] = *[1,c], \text{ say,}$$

at the cost of replacing $[l,r]$ by $[l,\overline{a}ra]$, which changes the isomorphism to a geometrically equivalent one. If $r_0 \in R_0$, $*[1,cr_0]$ defines the same group as does $*[l_1,cr_1]$ for any $[l_1,r_1] \in H$, and this reduces to $*[1,cr_1l_1]$ on conjugation by $[1,l_1]$, which replaces the r in $[l,r]$ by $\overline{l_1}rl_1$, its image under an arbitrary inner automorphism of R.

These considerations almost always suffice to restrict the extending element to

$$*[1,\pm 1] = * \text{ or } -*,$$

notated respectively by $\cdot 2_3$ or $\cdot 2_1$ (the subscript being the dimension of the negated space). The exceptions are the "$D \times D$" and "$C \times C$" cases, for which Table 4.3 lists every c, and just two more cases, denoted

$$\pm\frac{1}{2}[O \times O] \cdot \overline{2} \quad \text{and} \quad \pm\frac{1}{2}[\overline{D}_{4n} \times \overline{D}_{4n}] \cdot \overline{2}$$

in which we can take $c = i_O$ and e_{2n}, respectively.

As we remarked, the reduction to the form $*[1,c]$ comes at the cost of replacing the isomorphism by a geometrically equivalent one, and in the "$T \times T$" case, this sometimes replaces the identity isomorphism by the one we indicate by $\overline{T}$, namely

$$\omega \to \overline{\omega} \quad \text{and} \quad i \to \overline{i} = -i.$$

The Last Eight Lines of Table 4.3

For $\pm[D \times D] \cdot 2$, we start from the fact that the extending element $*[a,b]$ may be reduced (mod H) and must normalize H, and therefore also E, the

Figure G.4.: Corrections for [14, p. 51].

subgroup of elements of the form $[e^\gamma, e^\delta]$, in H, since E is a characteristic subgroup of H (except in the easy cases when $f \le 2$, which we exclude). MISSING This puts a and b in $e^{\mathbb{R}}(1 \text{ or } j)$, and so (since $[j,j] \in H$) we can take $*[a,b] = *[e^\lambda, e^\mu]$ (leading to $\pm[D\times D]\cdot 2^{(\alpha,\beta)}$) or $*[a,b] = *[e^\lambda, e^\mu j]$ (leading to $\pm[D \times D] \cdot \overline{2}$—see footnote 4.) In the first case, we must have

$$[j,j]^{*[e^\lambda,e^\mu]} = [j,j]^{[e^\lambda,e^\mu]} = [je^{2\lambda}, je^{2\mu}] \in H,$$

which forces $\lambda = \frac{\alpha}{2}$ and $\mu = \frac{\alpha s+\beta f}{s\,2}$, where $\alpha, \beta \in \mathbb{Z}$. The fact that the square of this is in H imposes the condition $\alpha g + \beta f \equiv 0 \pmod 2$.

G is unaltered when we increase α or β by 2 since $[e, e^s]$, $[1, e^f] \in H$. For a similar reason, s is initially only defined (mod f), but the equation

$$*[e^{\frac{\alpha}{2}}, e^{\frac{\alpha s+\beta f}{2}}] = *[e^{\frac{\alpha}{2}}, e^{\frac{\alpha(s+f)+(\beta-\alpha)f}{2}}]$$ DEFINED HERE

shows that

$$\langle s, \alpha, \beta\rangle \approx \langle s+f, \alpha, \beta-\alpha\rangle,$$

so from now on it is better to regard s as defined mod $2f$. Since $[e^s, e^{\beta}]$ = $[e, e^s]^{*[a,b]}$ and $[e, e^{s^2}]$ are both in H, we must have $s^2 = fg + 1$ for some integer $g \in \mathbb{Z}$.

To discuss equalities, we must consider all possibilities for an element that transforms this group $\langle s, \alpha, \beta\rangle$ to a similar one $\langle s', \alpha', \beta'\rangle$. The transforming element can also be reduced mod H and after taking account of $*$ and $[1, j]$ (which takes $\langle s, \alpha, \beta\rangle$ to itself or $\langle -s, \alpha, -\beta\rangle$), can be supposed to normalize H and therefore have the form $[e^{\frac{a}{2}}, e^{\frac{as+bf}{2}}]$, with $a, b \in \mathbb{Z}$. We find that transforming by this adds some multiple (which can be odd) of (f, g) to (α, β), so the only further relation is $\langle s, \alpha, \beta\rangle \approx \langle s, \alpha+f, \beta+g\rangle$.

To summarize, we have for this group

Variables	Conditions	Equalities
$\alpha \pmod 2$	$s^2 = fg + 1$	$\langle s, \alpha, \beta\rangle$
$\beta \pmod 2$	$\alpha g + \beta f \equiv 0 \pmod 2$	$\approx \langle -s, \alpha, -\beta\rangle$
$s \pmod{2f}$		$\approx \langle s+f, \alpha, \beta-\alpha\rangle$
		$\approx \langle s, \alpha+f, \beta+g\rangle$,

[4] In the second case we can choose new generators to simplify the group; namely, conjugation by $[1, e^\lambda]$ fixes E and replaces $*[e^\lambda, e^\mu j]$ by $*[1, e^{\mu-\lambda} j] = *[1, J]$, and then J can replace j, since $(*[1, J])^2 = [J, J]$ must be in H.

Figure G.5.: Corrections and remarks for [14, p. 52].

Appendix: Completeness of the Tables 53

while for $\pm[D \times D^{(s)}] \cdot \overline{2}$ we have

Variables	Conditions	Equalities
$s \pmod f$	$s^2 = fg - 1$	$\langle s \rangle \approx \langle -s \rangle$.

Equalities in the other cases are summarized as:

Group	Variables	Conditions	Equalities
$+[D \times D^{(s)}] \cdot 2^{(\alpha,\beta)}$	$\alpha \pmod 2$ $\beta \pmod 4$ $s \pmod{4f}$	$s^2 = fg + 1$ $\alpha g \equiv 0 \pmod 4$ n odd, g even	$\langle s, \alpha, \beta \rangle$ $\approx \langle -s, \alpha, -\beta \rangle$ $\approx \langle s + 2f, \alpha, \beta - 2\alpha \rangle$ $\approx \langle s, \alpha, \beta + 2h \rangle$
$+[D \times D] \cdot \overline{2}$	$s \pmod{2f}$	$s^2 = fg - 1, g = 2h$ even	$\langle s \rangle \approx \langle -s \rangle$
$\pm[C \times C] \cdot 2^{(\gamma)}$	$s \pmod f$ $\gamma \pmod 2$ $*[1, e^{\frac{\gamma(f,s+1)}{2}}]$	$s^2 = fg - 1$ $(g, s-1)\gamma \equiv 0 \pmod 2$ $(f, s+1)\gamma \equiv 0 \pmod 2$ g even	$\langle s, \gamma \rangle$ $\approx \langle s, -\gamma \rangle$
$+[C \times C] \cdot 2^{(\gamma)}$	$s \pmod{2f}$ $\gamma \pmod{2d}$ $*[1, e^{\frac{\gamma(f,s+1)}{2}}]$ $d = \frac{(2f,s+1)}{(f,s+1)}$	$s^2 = fg - 1$ $(g, s-1)\gamma \equiv 0 \pmod 4$ $(f, s+1)\gamma \equiv 0 \pmod 2$ n odd, $g = 2h$ even	$\langle s, \gamma \rangle$ $\approx \langle s, -\gamma \rangle$

Table 4.4 summarizes the different achiral groups among the last four lines of Table 4.3. In the last eight lines, it is always permissible to replace D_2 by C_2 and $\overline{D_4}$ by D_4.

f, g even	:	$\cdot 2^{(0,0)}, \cdot 2^{(0,1)}, \cdot 2^{(1,0)}, \cdot 2^{(1,1)}$ and $\cdot \overline{2}$
else		$\cdot 2$ and $\cdot \overline{2}$
f, h even	:	$\cdot 2^{(0,0)}, \cdot 2^{(0,2)}, \cdot 2^{(1,0)}, \cdot 2^{(1,2)}$ and $\cdot \overline{2}$
else		$\cdot 2$ and $\cdot \overline{2}$
g even	:	$\cdot 2^{(0)}, \cdot 2^{(1)}$ and $\cdot \overline{2}$
else		$\cdot 2$ and $\cdot \overline{2}$
h even	:	$\cdot 2^{(0)}, \cdot 2^{(d)}$ and $\cdot \overline{2}$
else		$\cdot 2$ and $\cdot \overline{2}$

Table 4.4. Different achiral groups.

Figure G.6.: Corrections and remarks for [14, p. 53].

Degeneracy of a polytope

H

We define the *degeneracy of a polytope* P as the degeneracy of its vertex-facet incidence graph Γ_P (see Definitions 9.3.13 and 9.3.14), and we denote it by degen(P). Barnette and Grünbaum in [5], asked the following question about the degeneracy (with slight change of notation):

> " Is it always possible to order the vertices of Γ_P in a sequence in such a fashion that each is joined by an edge to at most $c(d)$ vertices preceding it, where $c(d)$ depends on the dimension d of P but not on the particular d-polytope P. Lemma 2 may be interpreted as saying that $n(3) = 3$. It may be conjectured that $c(d) < \infty$ for all d, though the question is open already for $d = 4$. "

In particular, they showed that degen(P) $= 3$ if P is a 3-polytope (see Proposition 9.4.9), and they conjectured that for all d, there is a constant $c(d)$, which depends on d, such that every d-polytope P has degen(P) $\leq c(d)$. However, the following example shows that the conjecture does not hold for $d \geq 5$.

Example H.0.1. The join[30] of two n-gons is a self-dual 5-polyope. Each facet of P (and its dual) is a 2-fold pyramid over one of the two base n-gons. In particular, the graph Γ_P is $(n+2)$-regular, and thus it has degeneracy $n+2$.

Moreover, building pyramids over a polytope cannot decrease its degeneracy. Thus, this example shows that degen(P) is not bounded for $d \geq 5$.

This leaves only one case open $d = 4$. So the natural question to ask:

Question H.0.2. Does there exist a constant c such that every 4-polytope P has degeneracy at most c.

This question remains open. Next we will show that the degeneracy of a 4-polytope is bounded from below by its complexity. The *complexity*, see Ziegler [72], of a 4-polytope P is defined as

$$C(P) = \frac{f_{0,3} - 20}{f_0 + f_3 - 10}.$$

It is an open question to decide if $C(P)$ is bounded from above.

The following proposition is a stronger version of Proposition 9.3.15.

Proposition H.0.3. *Let $G = (A \cup B, E)$ be k-degenerate bipartite graph with $|A|, |B| \geq k+1$ and $k \geq 3$. If G is $K_{3,k-1}$-free[31], then G has $\leq k(|A| + |B|) - k^2 - k$ edges.*

Proof. We prove this by induction on the number of nodes in G.

Suppose that G has $2k+2$ nodes. Thus, $|A| = |B| = k+1$. Suppose that G has $\geq k(2k+2) - k^2 - k + 1 = k(k+1) + 1$ edges. We will find three nodes in A which

[30] The join $P \star P'$, of the d-polytope $P \subset \mathbb{R}^d$ and the d'-polytope $P' \subset \mathbb{R}^{d'}$, is the convex hull of P and P' after embeddings them in $\mathbb{R}^{d+d'+1}$ where their affine hulls are skew.

[31] We say that the graph G is *H-free* if G does not contain a subgraph isomorphic to the graph H.

form a $K_{3,k-1}$ with their neighbors in B. If all nodes in A have degree $\leq k$, then G has $\leq k(k+1)$ edges, which is less than $k(k+1)+1$. Thus, A has a node v of degree $k+1$. Now $G-\{v\}$ has $\geq k(k+1)+1-\deg(v) = k^2+k+1-k-1 = k^2$ edges. If all nodes in $A-\{v\}$ have degree $\leq k-1$, then $G-\{v\}$ has $\leq k(k-1)$ edges, which is less than k^2. Thus, A has a node u of degree $\geq k$. Since $|B| = k+1$, we have two options.

- If degree of u is k, then $G-\{v,u\}$ has $\geq k(k+1)+1-\deg v-\deg(u) = k(k+1)+1-k-1-k = k^2-k$ edges. If all nodes in $A-\{v,u\}$ have degree $\leq k-1$, then $G-\{v,u\}$ has $\leq (k-1)(k-1) = k^2-2k+1$ edges, which is less than k^2-k for $k \geq 3$. Thus, A has a node w of degree $\geq k$.
- If degree of u is $k+1$, then $G-\{v,u\}$ has $\geq k(k+1)+1-\deg v-\deg(u) = k(k+1)+1-k-1-k-1 = k^2-k-1$ edges. If all nodes in $A-\{v,u\}$ have degree $\leq k-1$, then $G-\{v,u\}$ has $\leq (k-1)(k-1) = k^2-2k+1$ edges, which is less than k^2-k-1 for $k \geq 3$. Thus, A has a node w of degree $\geq k$.

The vertices v,u,w with their neighbors in B form a $K_{3,k-1}$ subgraph. This concludes the base case.

Now suppose that G has $\geq 2k+2$ nodes, say $|A| \geq k+2$ and $|B| \geq k+1$. Removing a node of degree $\leq k$ from G will result in a bipartite k-degenerate graph which is $K_{3,3}$-free. Thus, to apply the induction hypothesis, we only need to check that the size of the new partitions is $\geq k+1$. Since G is k-degenerate, it has a node v of degree $\leq k$. If $v \in A$, we are done. So suppose that $v \in B$. If $|B| > k+1$, we are done. So suppose that $|B| = k+1$. Since $|A| \geq k+2$ and the degree of v is $\leq k$, there is a vertex v' in A which is not adjacent to v, and thus its degree is $\leq k$. Replace the labels of v and v' (that is, we will remove v' from G instead of v.)

Now $G-\{v\}$ satisfies the conditions in the statement. Thus, it has $\leq k(|A|+|B|-1)-k^2-k$ edges. Thus, G has $\leq k(|A|+|B|-1)-k^2-k+\deg v \leq k(|A|+|B|-1)-k^2-k+k = k(|A|+|B|)-k^2-k$.

□

Theorem H.0.4. *For a 4-polytope P, we have $C(P) \leq \operatorname{degen}(P)$.*

Proof. In a 4-polytope P, a 2-face is defined by exactly two facets. Thus, three facets can share at most two vertices (an edge), and three vertices can share at most two facets. Thus, Γ_P is $K_{3,3}$-free. In particular, it is $K_{3,k-1}$-free for $k \geq 4$. Thus, if Γ_P is k-degenerate, then by the Proposition H.0.3, $f_{0,3} \leq k(f_0+f_3)-k^2-k$. In particular,

$$\begin{aligned} f_{0,3}-20 &\leq k(f_0+f_3)-k^2-k-20 \\ f_{0,3}-20 &\leq k(f_0+f_3-10)-k^2+9k-20 \end{aligned}$$

We have $-k^2+9k-20 \leq 0$ on the integers $k \geq 4$. Thus,

$$\begin{aligned} f_{0,3}-20 &\leq k(f_0+f_3-10) \\ \frac{f_{0,3}-20}{f_0+f_3-10} &\leq \frac{k(f_0+f_3-10)}{f_0+f_3-10} \\ C(P) &\leq k. \end{aligned}$$

□

Various construction were made to produce polytopes with high complexity. Ziegler in [70] lists these polytopes in a table. We take some entries from that table and add to them the complexity we get from Theorem H.0.4. See Table H.1. We also include some polytopes with high degeneracy.

4-polytope	degeneracy	complexity	reference
24-cell	6	3.26	Schläfli [62]
orbit$\big((0,1,1,1),\pm[O\times O]\big)$	8	4.05347	See Example H.0.5
neighborly cubical 4-polytopes	$\geq 8-\epsilon$	$8-\epsilon$	Joswig and Ziegler [39]
projected products of polygons	$\geq 16-\epsilon$	$16-\epsilon$	Ziegler [70]

Table H.1.: Polytopes with highly degenerate vertex-facet incidence graphs.

Example H.0.5. The orbit polytope P of $\pm[O\times O]$ (See Section 5.1) with $(0,1,1,1)$ as a starting point has $C(P)\approx 4.05347$ and $\operatorname{degen}(P)=8$. Its f-vector is $(192,864,864,192)$. It is not self-dual. Its facets are 48 cubes and 144 twisted cubes. The facets of the polar polytopes are 192 stacked triangular prisms (that is, a triangular prism with two new points stacked on the triangular faces).

Zusammenfassung

Diese Dissertation befasst sich mit zwei verschiedenen Themen, von denen jedes seinen eigenen Teil hat.

Der erste Teil befasst sich mit 4-dimensionalen Punktgruppen. Wir schlagen eine neue Klassifizierung für diese Gruppen vor (siehe Theorem A), die im Gegensatz zu früheren Klassifizierungen eine geometrische Sichtweise betont und versucht, die Aktionen dieser Gruppen zu visualisieren und zu verstehen.

Im Folgenden werden diese Gruppen kurz beschrieben. Die polyedrischen Gruppen (Kapitel 5) sind mit den regelmäßigen Polytopen verwandt. Die axialen Gruppen (Kapitel 6) sind diejenigen, die eine Achse festhalten. Die schlauchartigen Gruppen (Kapitel 3) werden als solche charakterisiert, die genau eine invariantes Hopf-Bündel haben. Sie entstehen bei einer Zerlegung der 3-Sphäre in schlauchartige Strukturen (diskrete Hopf-Faserungen). Die toroidalen Gruppen (Kapitel 4) sind dadurch gekennzeichnet, dass sie einen invarianten Torus haben. Wir schlagen eine neue, geometrische Klassifizierung dieser Gruppen vor. Im Wesentlichen läuft sie darauf hinaus, die Isometriegruppen des zweidimensionalen quadratischen flachen Torus zu klassifizieren.

Nebenbei geben wir eine in sich geschlossene Darstellung der Hopf-Faserungen (Kapitel 2). Als Hilfsmittel für die Arbeit mit ihnen führen wir eine Parametrisierung für Großkreise in S^3 ein, die an anderer Stelle nützlich sein könnte.

Der zweite Teil befasst sich mit Realisierungsräumen von Polytopen. Wir bauen auf Robertsons Modell und Ansatz [59] auf, um die Realisierungsräume von Polytopen zu untersuchen.

Wir stellen kombinatorische Kriterien auf (Abschnitte 9.3.3 und 9.4.1), um zu entscheiden, ob der Realisierungsraum des betrachteten Polytops eine glatte Mannigfaltigkeit der durch die "natürliche Vermutung" gegebenen Dimension ist. Als weitere Anwendung, untersuchen wir die Realisierungsräume der zweiten Hypersimplices (Abschnitt 9.4.2).

Nebenbei identifizieren wir die kleinsten Beispiele von 4-Polytopen, für die dieser Ansatz versagt (Abschnitt 9.5).

Schließlich untersuchen wir den Realisierungsraum der 24-Zelle (Abschnitt 9.5.2). Wir zeigen, dass es Punkte gibt, an denen sie keine glatte Mannigfaltigkeit ist. Zuletzt zeigen wir, dass seine Dimension mindestens 48 und höchstens 52 beträgt.

Selbstständigkeitserklärung

Gemäß §7 (4) der Promotionsordnung des Fachbereichs Mathematik und Informatik der Freien Universität Berlin vom 8. Januar 2007 versichere ich hiermit, dass ich alle Hilfsmittel und Hilfen angegeben und auf dieser Grundlage die Arbeit selbständig verfasst habe. Zudem wurde die Arbeit auch noch nicht in einem früheren Promotionsverfahren eingereicht.

Berlin, May 2022

Laith Rastanawi